THE ROLE OF BINDING DETERMINANTS IN GROUND STATE AND TRANSITION STATE STABILIZATION BY MANDELATE RACEMASE

by

Martin St.-Maurice

Submitted in partial fulfillment of the requirements
for the degree of Doctor of Philosophy

at

Dalhousie University
Halifax, Nova Scotia
March, 2003

Canada

DALHOUSIE UNIVERSITY

FACULTY OF GRADUATE STUDIES

The undersigned hereby certify that they have read and recommend to the Faculty of

Graduate Studies for acceptance a thesis entitled "The Role of Binding Determinants In

Ground State And Transition State Stabilization By Mandelate Racemase" by Martin St.-

Maurice in partial fulfillment for the degree of Doctor of Philosophy.

Dated: February 28, 2003

External Examiner:

Research Supervisor:

Examining Committee:
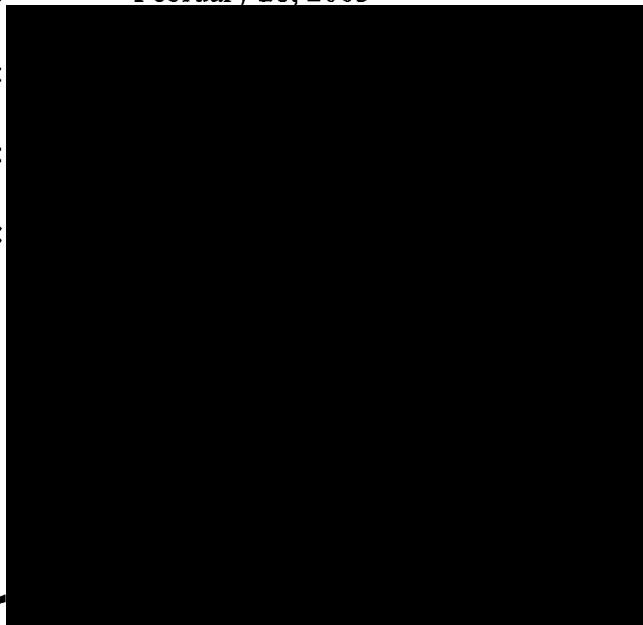
DALHOUSIE UNIVERSITY

DATE: March 20, 2003

AUTHOR: Martin St.-Maurice

TITLE: The Role of Binding Determinants in Ground State and Transition State

Stabilization by Mandelate Racemase

DEPARTMENT OR SCHOOL: Biochemistry and Molecular Biology

DEGREE: Ph. D.   CONVOCATION: May   YEAR: 2003

Permission is herewith granted to Dalhousie University to circulate and to have copied for non-commercial purposes, at its discretion, the above title upon the request of individuals or institutions.

Signature of Author

The author reserves other publication rights, and neither the thesis nor extensive extracts from it may be printed or otherwise reproduced without the author's written permission.

The author attests that permission has been obtained for the use of any copyrighted material appearing in the thesis (other than the brief excerpts requiring only proper acknowledgement in scholarly writing), and that all such use is clearly acknowledged.

TABLE OF CONTENTS

LIST OF FIGURES

x

surface areas of the hydroxamic acid inhibitor molecules

LIST OF TABLES

LIST OF SCHEMES

ABSTRACT

Mandelate racemase (MR) (E.C. 5.1.2.2.) from *Pseudomonas putida* catalyzes the interconversion of the two enantiomers of mandelic acid. The enzyme is remarkable in its ability to catalyze rapid carbon–hydrogen bond cleavage from a carbon acid with a high pK_a, making it a useful paradigm for understanding enzyme–catalyzed proton abstraction from carbon acids. The proficiency of an enzyme catalyst is a function of its ability to provide greater stabilizing interactions with the altered substrate in the transition state than with the substrate in the ground state. To better understand the molecular origins of the high proficiency of MR, the relative contributions from enzyme binding determinants to the stabilization of the substrate in the ground state and the altered substrate in the transition state have been investigated. The rates of the forward and reverse reactions catalyzed by MR were dependent on the concentration of viscosogenic agents, demonstrating that both substrate binding and product dissociation are partially rate-determining in both directions. Using these viscosity studies over a range of temperatures, the enthalpic and entropic contributions to MR–catalyzed racemization of (*R*)-mandelate at 25 °C were estimated. The high proficiency of MR was shown to be achieved principally through 23 kcal/mol of enthalpic reduction, suggesting that enzyme residues play a critical role in transition state stabilization by providing specific interactions with the altered substrate in the transition state. Investigation of the molecular origins of these interactions required the identification of a high affinity, intermediate analogue inhibitor to act as a stable probe for the enzyme-transition state complex. A fixed–time, high–performance liquid chromatography assay for MR activity was developed and validated. Using this assay and a circular dichroism–based assay, a series of carboxylate-, phosphonate- and hydroxamate-containing substrate and intermediate analogues were examined for their ability to inhibit MR. Two intermediate analogues, α-hydroxybenzylphosphonate and benzohydroxamate, were bound with affinities approximately 100-fold greater than that observed for the substrate. Inhibition by these intermediate analogues suggested that the substrate's α-hydroxyl function is preferentially stabilized in the transition state relative to the ground state. Kinetic studies with truncated and modified substrate and intermediate analogues further revealed a contribution to transition state stabilization from a hydrophobic cavity in the enzyme active site. Finally, benzohydroxamate was assessed to be a reasonable mimic of the transition state and contributions from the active site, hydrophobic cavity and the residues Glu 317, Lys 164 and Asn 197 to both ground state and transition state stabilization by MR were determined. The proficiency of MR does not appear to originate from any single, dominant interaction in the transition state but, rather, it is a function of strengthened molecular interactions over the entire surface of the altered substrate molecule.

LIST OF ABBREVIATIONS AND SYMBOLS

α selectivity factor: $\alpha = \dfrac{(t_R)_B - t_M}{(t_R)_A - t_M}$; where $(t_R)_B$ and $(t_R)_A$ are the retention times for the more strongly and less strongly retained species, respectively and t_M is the retention time for the solvent front.

R_S resolution: $R_S = \dfrac{2[(t_R)_B - (t_R)_A]}{W_A + W_B}$; where $(t_R)_B$ and $(t_R)_A$ are the retention times and W_A and W_B the peak widths for the more strongly and less strongly retained species, respectively.

t_R retention time

α,α-F$_2$BP	α,α-difluorobenzylphosphonate
α-FBP	α-fluorobenzylphosphonate
α-HBP	α-hydroxybenzylphosphonate
BHA	benzohydroxamate
BSA	bovine serum albumin
CD	circular dichroism
Da	Dalton
DFBP	difluorobenzylphosphonate
DMSO	dimethylsulfoxide
(His)$_6$-MR	N-terminal hexahistidine-tagged mandelate racemase
HEPES	4-(2-hydroxyethyl)piperazine-1-ethanesulfonic acid
HPLC	high-performance liquid chromatography
IPTG	Isopropyl β-D-thiogalactopyranoside
LB	Luria-Bertani
MES	2-(N-morpholino)ethanesulfonic acid
MOPS	3-[N-morpholino]propanesulfonic acid
MR	mandelate racemase (EC 5.1.1.2)
Mr	molecular mass (in Da)
NMR	nuclear magnetic resonance

PEG	poly(ethylene glycol)
PIPES	piperazine-N,N'-bis[2-ethanesulfonic acid]
PMSF	phenylmethylsulfonyl fluoride
PAGE	polyacrylamide gel electrophoresis
SDS	sodium dodecyl sulfate
SSHB	short, strong hydrogen bond
TAPS	N-[tris(hydroxymethyl)methyl]-3-aminopropanesulfonic acid
THF	tetrahydrofuran
A	adenine
T	thymine
G	guanine
C	cytosine
Ala (A)	alanine
Asn (N)	asparagine
Arg (R)	arginine
Gln (Q)	glutamine
Glu (E)	glutamate
Gly (G)	glycine
His (H)	histidine
Leu (L)	leucine
Lys (K)	lysine
Met (M)	methionine
Pro (P)	proline
Ser (S)	serine
Val (V)	valine

ACKNOWLEDGEMENTS

I thank Dr. Stephen Bearne for his excellent guidance and supervision throughout my graduate studies. I admire his strong dedication to research through which I have learned much of how to conduct quality scientific investigation. I have very much enjoyed our discussions, both scientific and otherwise, over the past years. He has always been extremely approachable and open-minded and he has encouraged me to explore new directions as my research has progressed. I also credit him with eliminating *some* of my "bleeding-heart" liberalism, though I can say with confidence that I will assuredly always remain to his left on the political spectrum.

I thank Anathea Flaman and Mark Vaughan for conducting preliminary experiments on the purification and HPLC assay of mandelate racemase. I also thank Dr. John Gerlt (U. Illinois) for providing the laboratory with the mandelate racemase clone, Dr. Scott Taylor (U. Waterloo) for supplying the α-fluorobenzylphosphonates, Dr. Alex Jurgens (Sepracor, Inc.) for supplying the (*S*)-cyclohexylphenylglycolic acid, Dr. Stephen Bearne for synthesizing (*R,S*)-1-naphthylglycolic acid, Dr. Christian Blouin (Dalhousie U.) for his assistance with the molecular modelling of benzilate, Anathea Flaman for synthesizing α-hydroxybenzylphosphonate and methyl α-hydroxybenzylphosphonate, and Shauna Drover for synthesizing and resolving (*S*)-*p*-nitromandelate and constructing the V29D mutant. Thanks also to Dr. Carmichael Wallace, Dr. Peter Dolphin, Dr. Roger McLeod and Dr. David Jakeman for serving on my thesis supervisory committee. I am grateful to the Natural Sciences and Engineering Research Council of Canada as well as the Izaak Walton Killam Memorial Foundation for financial support over the course of my graduate studies.

The Bearne Lab has always been an environment where research is taken seriously but where the atmosphere remains friendly and enjoyable and I thank all members of the lab, past and present, who have made the daily frustrations of conducting research far

more bearable. I particularly thank Mark Vaughan, Travis MacLeod, Akshai Iyengar, and Jenn MacDonnell for their friendship over the past several years. Thanks also to the faculty, staff and students of the department of Biochemistry and Molecular Biology for creating a pleasant working environment (as well as the occasional excuse for a raucous party).

I also thank Darren, Will and Doug for having absolutely nothing to do with this thesis. They are extremely talented musicians and playing alongside them has helped me forget many frustrating days of research and writing. One of my greatest joys and fondest memories from the time that I have spent in Halifax will be of the evenings and early mornings spent playing excellent music in the company of good friends.

I thank my parents, Monique and Jean-Pierre, for giving me the confidence to pursue my interests. They have shown me that a successful and productive career, including one in research, need not come at the expense of a healthy and happy family life. I am indebted to Jean-Pierre St.-Maurice for reminding me of the logarithm rules essential for deriving equation 4.1 and curve-fitting the data in figures 4.4 and 4.5.

Finally, I thank Sam for her love, patience and support. She has sacrificed much of her own research in order to allow me to complete this thesis and, for that, I am deeply grateful. And to my daughter Danika, my hopes and dreams are for your future... may you never be foolish enough to stay in school into your thirties. Go out and get a real job for heaven's sake.

CHAPTER 1

INTRODUCTION

1.1 Mandelate Racemase

1.1.1 Expression and Characterization of Mandelate Racemase

Mandelate racemase from *Pseudomonas putida* A.3.12 (MR; EC 5.1.1.2) catalyzes a 1,1-proton transfer reaction that interconverts the two stereoisomers of mandelic acid (**scheme 1.1**). The enzyme was initially identified by Stanier and coworkers (Gunsalus *et al.*, 1953a; Gunsalus *et al.*, 1953b) following the observation that *P. putida* strain A.3.12 was uniquely capable of growing on media containing *either* D- or L-mandelic acid as the sole carbon source. While several microrganisms have been shown to be capable of using mandelic acid as a sole source of carbon (Hegeman *et al.*, 1970), *P. putida* A.3.12 remains, at present, the only identified organism capable of utilizing both the D- and L-enantiomers of mandelic acid. Stanier and coworkers identified the metabolic pathway responsible for mandelic acid catabolism in *P. putida* A.3.12 and identified MR as the first enzyme in this pathway (Gunsalus *et al.*, 1953a; Gunsalus *et al.*, 1953b). It was later determined that MR is expressed in an inducible operon that includes five enzymes involved in converting (*R,S*)-mandelic acid into benzoic acid; the so–called "mandelate group" of enzymes (Hegeman, 1966a, b, c). The operon can be induced by either (*R*)- or (*S*)-mandelic acid as well as by benzoylformic acid, the third intermediate of the pathway (Hegeman, 1966a, b). The sequentially inducible enzymes of the β-ketoadipate group subsequently convert benzoic acid into succinate and acetyl coenzyme A (Ornston & Stanier, 1966) (**figure 1.1**). Subsequent cloning and sequencing of the gene for MR from *P. putida* revealed that it is located immediately downstream of the promoter, suggesting

1

Scheme 1.1 Interconversion of (*R*)- and (*S*)-mandelic acid.

(*R*)-mandelic acid   (*S*)-mandelic acid
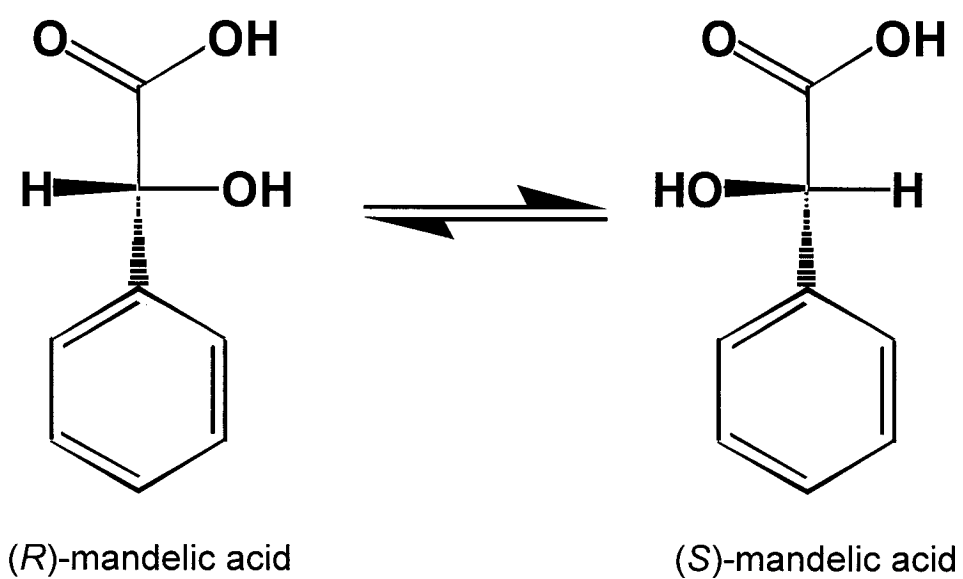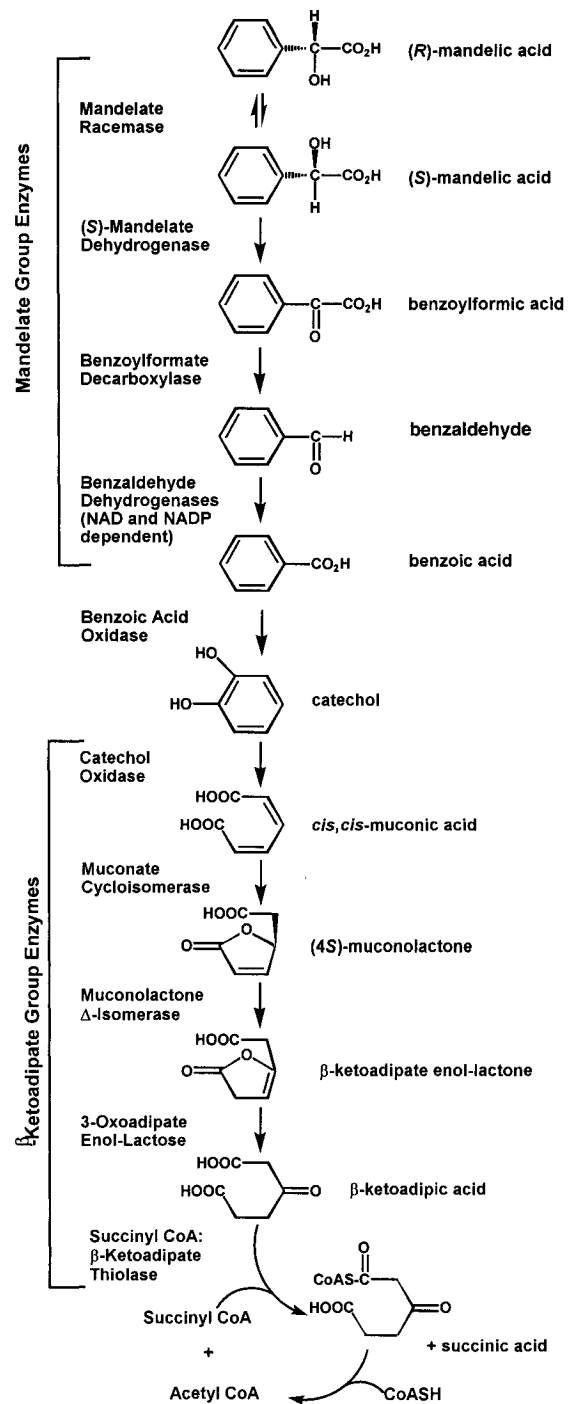
Figure 1.1 Metabolic pathway for the oxidation of (R)- and (S)-mandelic acid by Pseudomonas putida A.3.12 (Hegeman et al., 1970).

that it is the first gene in the operon (Ransom *et al.*, 1988).

Gunsalas *et al.* (1953a) initially characterized a crude preparation of MR from *P. putida* and determined that the enzyme was both soluble and cofactor–independent. Partially purified MR was further characterized by Weil–Malherbe (1966) who used a coupled assay with L-mandelate dehydrogenase to identify Mg^{2+} as an activator in the reaction. Weil–Malherbe also determined the pH optimum for MR (~7.8) and the relative rates of racemization for the D- and L-enantiomers (equivalent to (*R*)- and (*S*)-mandelate, respectively). Using rigorous dialysis conditions and a pure enzyme preparation, Fee *et al.* (1974b) later confirmed an absolute dependence for MR on divalent cations and established Mg^{2+} as the most effective cation for restoring MR activity. Hegeman *et al.* (1970) described the purification of MR from *P. putida* and investigated the kinetics of the purified enzyme using several electron–withdrawing and electron–donating *para*-substituted mandelic acid substrates. This work confirmed that purified MR does not contain pyridine nucleotide or flavin cofactors. Furthermore, the kinetics with the *para*-substituted mandelic acid substrates indicated that a carbanion intermediate was likely involved in the reaction mechanism. In a contemporary study, Kenyon and Hegeman (1970) examined the MR–catalyzed exchange of solvent and substrate derived deuterium and reported a significant primary deuterium isotope effect (V_H/V_D = 5.1 – 5.6), suggesting that the α-carbon–hydrogen bond of the substrate is broken in the transition state. The absence of any detectable exchange with ^{18}O-enriched H_2O and with externally supplied benzoylformic acid indicated that the mechanism probably did not involve a carbonium ion. The combined evidence from these investigations implied a mechanism for MR involving carbon–hydrogen bond cleavage and the generation of a carbanion intermediate. (As will be discussed in subsequent sections of this chapter, the lifetime of

unstable carbanion intermediates are too short to account for the rates of enzyme–catalyzed reactions (Thibblin & Jencks, 1979). Thus, the term "carbanion intermediate" is used here only to assist the description of the general reaction mechanism and does not make inferences to the protonation state or the degree of stabilization of the intermediate in the enzyme active site.)

1.1.2   General Mechanisms of Epimerases and Racemases

The overall reaction catalyzed by racemases and epimerases is very simple, involving only the inversion of configuration about an asymmetrically substituted carbon atom.   However, the chemistry required for these transformations is often not so straightforward.   Substrates of racemases and epimerases are very stable and epimerisations and racemisations do not occur spontaneously (Allard *et al.*, 2001). Epimerases and racemases have evolved diverse mechanistic strategies to catalyze these difficult chemical reactions (**figure 1.2**) (Allard *et al.*, 2001; Tanner, 2002).

The most common mechanism for racemases and epimerases is the abstraction of a proton from a carbon center adjacent to a carbonyl group, generating an enol or enediol intermediate (**figure 1.2A**).   All known amino acid racemases function in this way (Tanner, 2002). The presence of a carbonyl group adjacent to the carbon center assists in reducing the pK_a of the α-carbon acid by resonance stabilization of the resulting carbanion intermediate (Gerlt, 1994; Tanner, 2002).   Nevertheless, the pK_a of the α-carbons remain quite high (≥ 21 for amino acids), making proton abstraction difficult. Racemases overcome the barrier to these unfavourable reactions by stabilizing
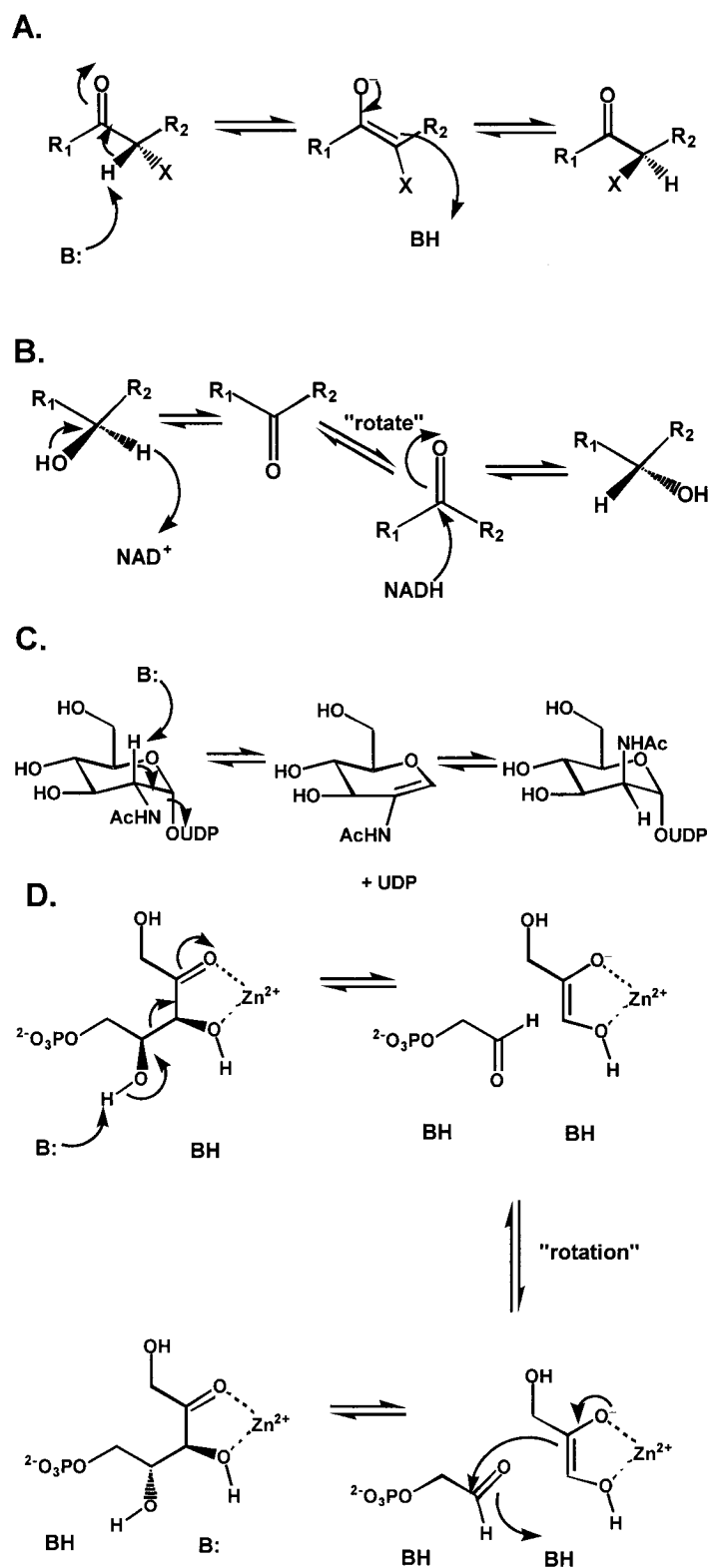
Figure 1.2 Mechanistic strategies for inversion of stereochemistry by racemases and epimerases. Specific reference is made to the reaction catalyzed by UDP-*N*-acetylglucosamine 2-epimerase (**C**) and L-ribulose-5-phosphate 4-epimerase (**D**).

the reaction intermediate(s). Alanine racemase, for example, forms an imine linkage with a pyridoxal phosphate cofactor (PLP) to improve the resonance stabilization of the carbanion intermediate (Shaw *et al.*, 1997). Many other racemases, such as glutamate racemase and proline racemase, are cofactor–independent and must rely on active site residues to stabilize the intermediate (Glavas & Tanner, 2001).

Several epimerases use a hydride transfer mechanism with a redox active cofactor (NAD(P)) to generate a transiently stable keto intermediate (**figure 1.2B**). The hydride is redelivered to the opposite face of the intermediate to generate a product with the opposite stereochemistry at the carbon atom of concern. For example, UDP-galactose-4-epimerase uses an enzymic base to abstract a proton from the 4-hydroxyl of UDP-galactose. This is followed by a hydride transfer to NAD^+ to generate a keto sugar intermediate which remains bound to the enzyme (Frey, 1996). The carbohydrate of the intermediate subsequently rotates, allowing NADH to transfer the hydride back to the opposite face, generating the product (Allard *et al.*, 2001).

The enzymes UDP-*N*-acetylglucosamine 2-epimerase (**figure 1.2C**) and L-ribulose-5-phosphate 4-epimerase (**figure 1.2D**) use unique mechanisms to catalyze inversions of configuration about the C2 and C4 stereocenters of their respective substrates. Not only do these enzymes demonstrate the mechanistic diversity with which enzymes catalyze epimerisation reactions but they also illustrate that epimerases may have evolved from diverse enzymatic families. UDP-*N*-acetylglucosamine 2-epimerase catalyzes the *anti*–elimination of the C2 proton and UDP from UDP-*N*-glucosamine to generate the stable intermediates 2-acetamidoglucol and UDP (**figure 1.2C**) (Sala *et al.*, 1996). The proton and UDP are subsequently returned through a *syn*–addition across the double bond of the intermediate, inverting the stereochemistry at C2 and generating the product, UDP-*N*-

acetylmannosamine. Interestingly, there is structural and mechanistic evidence that this epimerase is distantly related to a group of phosphoglycosyltransferases which all catalyze substitution reactions involving the displacement of UDP or phosphate from a carbon stereocenter on the sugar (Campbell *et al.*, 2000). Using a different strategy, L-ribulose-5-phosphate 4-epimerase catalyzes the cofactor–independent, divalent metal ion–dependent interconversion of L-ribulose 5-phosphate and D-xylulose 5-phosphate (**figure 1.2D**). The reaction proceeds, not by breaking a carbon–hydrogen bond, but rather by cleaving the C3–C4 carbon–carbon bond, generating glycoaldehyde phosphate and the stabilized enolate of dihydroxyacetone (Deupree & Wood, 1972; Lee *et al.*, 2000). Following reorientation of the two intermediates, an aldol addition reaction reforms the carbon–carbon bond, generating a product with inverted stereochemistry at the C4 carbon center. There is strong evidence for an evolutionary relationship between this epimerase and L-fucolose 1-phosphate aldolase, a class II metal ion–dependent aldolase (Johnson & Tanner, 1998).

The mechanistic diversity with which racemases and epimerases catalyze their reactions is a testament to the power of evolution in creating enzymatic solutions to promote unfavourable chemical reactions. Nevertheless, the overriding theme for catalysis by *all* epimerases and racemases is intermediate stabilization: while many tactics are available, all reactions proceed through a stabilized intermediate. Bearing this in mind, the central focus of my thesis will address what mechanism MR uses to stabilize the transition states and the intermediate formed during catalysis.

1.1.3 Mechanism of the Reaction Catalyzed by MR

Early investigations into catalysis by MR revealed that the reaction mechanism involves cofactor–independent, carbon–hydrogen bond cleavage adjacent to a carboxylate group and likely proceeds through a carbanion intermediate (Hegeman *et al.*, 1970; Kenyon & Hegeman, 1970). It was later shown that MR catalyzes the elimination of bromide from *p*-(bromomethyl)mandelate, a reaction which strongly supports the argument for a carbanion intermediate (Lin *et al.*, 1988).

With compelling evidence for a transiently stable intermediate, it remained to be determined whether MR uses a one–acceptor (one–base) or two–acceptor (two–base) mechanism to catalyze the racemization of mandelic acid. These two mechanisms may be distinguished kinetically by following the exchange of solvent with the substrate–derived hydrogen (Rose, 1966). In a one–base mechanism, the product should retain the substrate derived hydrogen at a high rate (a process called "internal return"). Low or negligible rates of internal return are also possible with a one–base mechanism if the conjugate acid of the general base catalyst exchanges its substrate derived hydrogen at a rate greater than or equal to the rate of proton transfer with the substrate. In this case, the relative rate of solvent exchange should be equal in the product and the remaining substrate pool. Alternatively, in a two–base mechanism, there should be no internal return in the product and, if the general base catalyst is monoprotic, no solvent hydrogen should be incorporated into the remaining substrate pool.

Sharp *et al.* (1977) reported a one–base mechanism for MR based on tracer experiments with racemic mixtures of isotopically labelled mandelic acid. The results from three separate tracer experiments demonstrated internal return and appeared to favour a one–base mechanism. However, Powers *et al.* (1991) revisited this question and

reported compelling kinetic evidence for a two–base mechanism. Using enantiomerically pure substrates, a chiral derivatizing agent, and working under initial velocity conditions, they were able to accurately separate and determine the relative incorporation of solvent derived hydrogen into both the substrate and product. In the $R \rightarrow S$ direction, no internal return was observed in the product and no incorporation of solvent hydrogen was detected in the remaining substrate pool, consistent with a two–base mechanism with an (R)-specific monoprotic base. In the $S \rightarrow R$ direction, no internal return was observed in the product but ~66% incorporation of solvent hydrogen in the remaining substrate pool was detected, consistent with a two–base mechanism with an (S)-specific *polyprotic* base. Overshoot experiments in D_2O also indicated a two–base mechanism with a polyprotic base abstracting the proton in the $S \rightarrow R$ direction and a monoprotic base abstracting the proton in the $R \rightarrow S$ direction. The accepted two–base mechanism of MR is summarized in **scheme 1.2**.

Thibblin and Jencks (1979) have cautioned that the lifetime of high–energy carbanion intermediates is very short such that many enzyme–catalyzed reactions thought to proceed through a carbanion intermediate can not support such a mechanism and, rather, may ultimately proceed through a concerted mechanism. Assuming that the activation energy barrier for the reaction catalyzed by MR is determined only by the thermodynamic barrier associated with proton transfer from the substrate carbon acid to the general base catalyst, the formation of an isolated enolate anion intermediate is inconsistent with the observed rates of catalysis by MR (Gerlt & Gassman, 1993a, b) (see section 1.2). This analysis, however, does not imply that MR must proceed by a concerted mechanism (Gerlt, 1994). Despite the high energy of the proposed

Scheme 1.2 The accepted two–base mechanism of MR.

(where B_1 is monoprotic and B_2 is polyprotic)
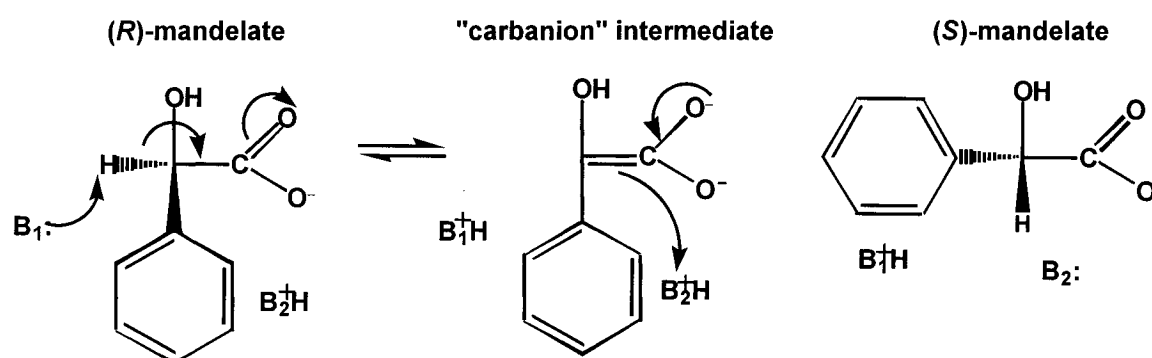
intermediate(s) (Chiang *et al.*, 1990; Gerlt *et al.*, 1991; Kresge, 1991), the kinetic

evidence for a stabilized intermediate in the reaction catalyzed by MR is overwhelming

(Hegeman *et al.*, 1970; Kenyon & Hegeman, 1970; Landro *et al.*, 1991; Lin *et al.*, 1988;

Mitra *et al.*, 1995; Neidhart *et al.*, 1991). The most compelling evidence for a stepwise

mechanism comes from the kinetics of the H297N mutant of MR, where the (*R*)-specific

base, His 297, is rendered inactive by substitution with Asn (Landro *et al.*, 1991)

(discussed in section 1.1.5). While this mutant is unable to catalyze the racemization of

either substrate enantiomer, it catalyzes bromide elimination from (*S*)-*p*-

(bromomethyl)mandelate and deuterium exchange with (*S*)-mandelate at rates comparable

to the wild–type enzyme. Thus, proton abstraction by the H297N mutant of MR

generates an intermediate with a lifetime long enough to at least allow rotation about the

bond of the polyprotic conjugate acid of the (*S*)-specific general base. It is extremely

likely, therefore, that the reaction catalyzed by the wild–type enzyme proceeds by a

stepwise mechanism, generating a transiently stable intermediate that is reprotonated by

the conjugate acid of either general base to generate the product or regenerate the

substrate. *Ab initio* calculations on a model reaction of MR–catalyzed racemization of

mandelate also predict a stepwise mechanism for the reaction (Alagano *et al.*, 1997).

1.1.4 The Structure of MR

The subunit molecular mass of MR from *P. putida* was initially determined by

SDS–PAGE to be approximately 69 000 Da (Fee *et al.*, 1974b). Cross–linking studies

further predicted that the MR quaternary structure consists of four identical subunits with

a total molecular mass of approximately 280 000 Da (Fee *et al.*, 1974b). Ransom *et al.*

(1988) later redetermined the subunit molecular mass of purified, homogeneous MR from

P. putida using SDS–PAGE and reported a molecular mass of 41 000 Da, contradicting the value originally reported by Fee *et al.* (1974b). Sequencing of the gene for MR predicted a protein consisting of 359 amino acid residues with a molecular mass of 38 570 Da, in excellent agreement with the revised molecular mass determined by SDS–PAGE (Ransom *et al.*, 1988). Edman degradation of the *P. putida* enzyme revealed that the *N*-terminal formylmethionine residue is removed from the enzyme, resulting in an *N*-terminal Ser residue in the mature enzyme (Ransom *et al.*, 1988). When MR is cloned and expressed in *Escherichia coli*, no processing of the enzyme occurs and the *N*-terminal formylmethionine remains intact (Ransom *et al.*, 1988).

A more complete understanding of MR catalysis awaited a detailed structural description of the enzyme. Crystals diffracting to beyond 3.0 Å resolution were first reported for MR in 1988 (Neidhart *et al.*, 1988) and, a few years later, the first crystal structure of MR was solved (Neidhart *et al.*, 1991). This crystal structure of MR, refined to 2.5 Å resolution, revealed a quaternary enzyme structure composed of an octamer of identical subunits. The octamer was described as a "tetramer of dimers" based on the apparent tight association between the two–fold related subunits and the fact that the enzyme active site includes residues from a neighbouring two–fold related subunit. This tight association of dimers within the MR octamer may explain the discrepancy in the results reported by Fee *et al.* (1974b).

MR is composed of three distinct structural domains (Neidhart *et al.*, 1991): an *N*-terminal domain made up of a three–stranded antiparallel β-sheet and an antiparallel four–α-helix bundle, a central domain consisting of an eight–stranded α,β-barrel similar in

structure to that first described in triosephosphate isomerase (Banner *et al.*, 1975), and a short *C*-terminal domain composed of extended β-strands.

The location of the active site was determined from the position of the metal ions europium and manganese in the crystallized enzyme (Neidhart *et al.*, 1991). As with all α,β-barrel enzymes, the active site is located at the mouth of the barrel, at the *C*-terminal ends of the β-strands. Crystals soaked in mother liquor containing (*R*,*S*)-*p*-iodomandelate permitted the substrate binding site to be modeled from the electron density of the iodine substituent (Neidhart *et al.*, 1991). The position of the substrate in the active site has since been confirmed by crystal structures of wild–type and mutant MR enzymes complexed with various substrates and inhibitors (Kallarakal *et al.*, 1995; Landro *et al.*, 1994; Schafer *et al.*, 1996). The structure of MR is shown in **figure 1.3** with the competitive inhibitor, (*S*)-atrolactate, bound at the active site of the enzyme (Landro *et al.*, 1994). The active site includes three residues (Asp 195, Glu 221 and Glu 247) which participate directly in coordinating the metal ion (the active site metal ion is also coordinated by a carboxylate oxygen of the substrate, the α-hydroxyl of the substrate and a bound water molecule). There is also a large hydrophobic cavity which binds the phenyl group of the substrate. This cavity is made up, in part, by a mobile, β-meander flap from the *N*-terminal domain of the enzyme.

The identities of the general base catalytic residues were, at first, tentatively assigned based on the modeled position of (*S*)-*p*-iodomandelate in the active site of MR (Neidhart *et al.*, 1991). His 297 was assigned as the (*R*)-specific base while Lys 166 was predicted to be the (*S*)-specific base. These assignments agreed with the prediction that
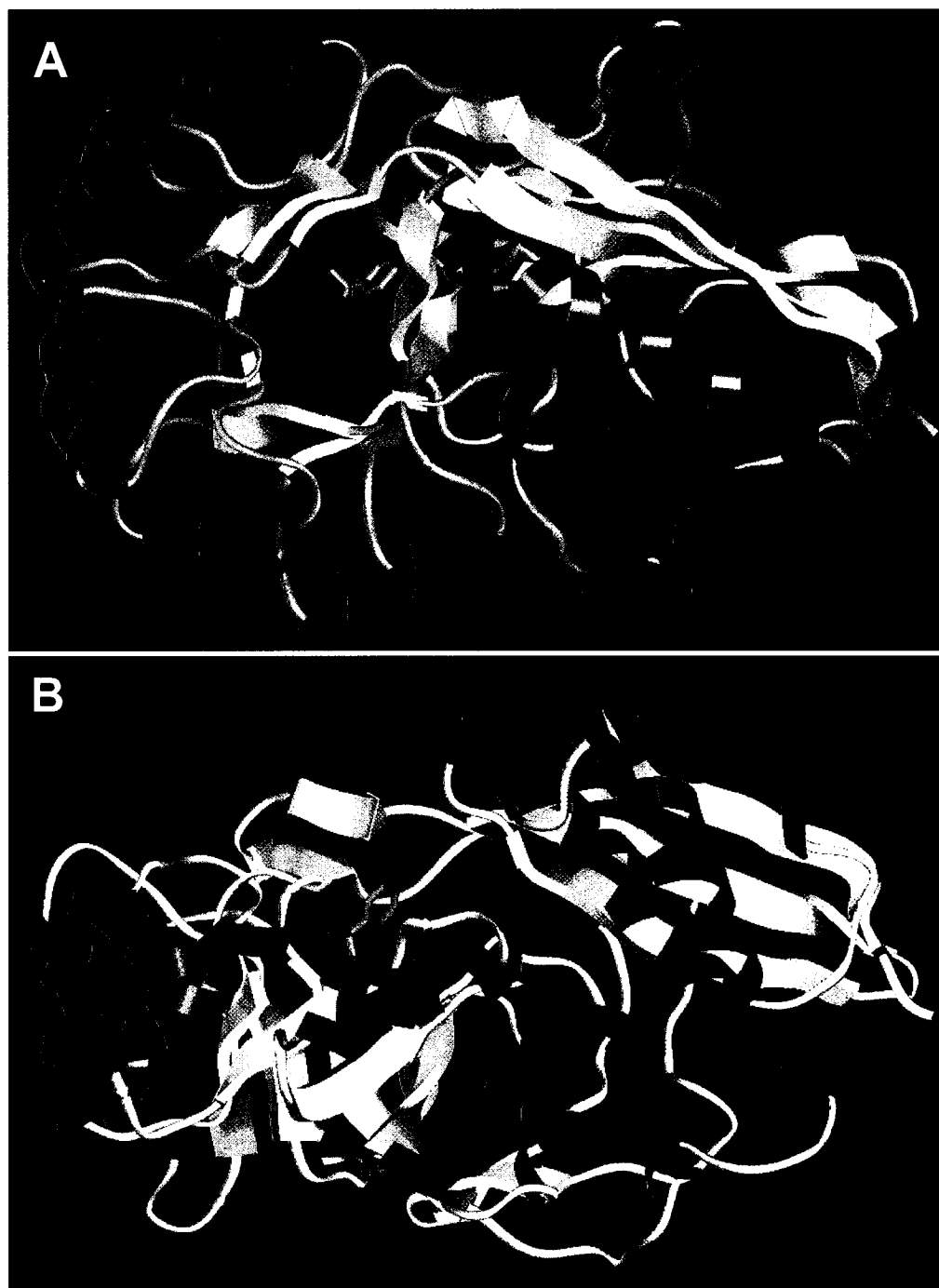
Figure 1.3   X-ray crystal structure of MR with the substrate analogue (*S*)-atrolactate [pdb key = 1MDR (Landro *et al.*, 1994)]. The active site is located at the mouth of the central α,β-barrel and includes a flexible, hinged loop from the *N*-terminal domain. The illustration in (**B**) is rotated 90° in the plane of the z-axis relative to (**A**).

the conjugate acid of the (R)-specific base is monoprotic while the conjugate acid of the (S)-specific base is polyprotic (Powers *et al.*, 1991). All residues involved in ligand binding, metal ion coordination and catalysis extend from the β-strands of the α,β-barrel (Neidhart *et al.*, 1991). This design strategy facilitates the evolution of new catalytic function within the enolase enzyme superfamily to which MR belongs (Babbitt & Gerlt, 1997; Babbitt *et al.*, 1996; Gerlt & Babbitt, 1998). A magnified structure of the active site of MR with the bound substrate analogue, (S)-atrolactate, is shown in **figure 1.4** highlighting the relative positions of the essential Mg^{2+}, the proposed general base catalysts, Lys 166 and His 297, as well as two residues, Glu 317 and Lys 164, positioned in close proximity to the substrate carboxylate oxygens.

1.1.5 The General Base Catalysts: Lys 166 and His 297

Confirmation of His 297 as the (R)-specific general base catalyst was obtained by constructing and characterizating the H297N mutant of MR (Landro *et al.*, 1991). The structure of this mutant, determined by X-ray crystallography, revealed no significant structural perturbations in the enzyme active site relative to the wild–type enzyme. The H297N mutant was unable to racemize either enantiomer of mandelic acid but catalyzed enantioselective bromide elimination from (S)-p-(bromomethyl)mandelate and exchanged solvent–derived deuterium with the α-proton of (S)- but not (R)-mandelate. Thus, the H297N mutation abolished the function of the (R)-specific base while the function of the (S)-specific base remained intact, demonstrating conclusively that His 297 functions as the (R)-specific general base catalyst in MR. From the rate of the deuterium exchange reaction catalyzed by H297N MR, the pK_a for the α-carbon acid of (S)-mandelate in the
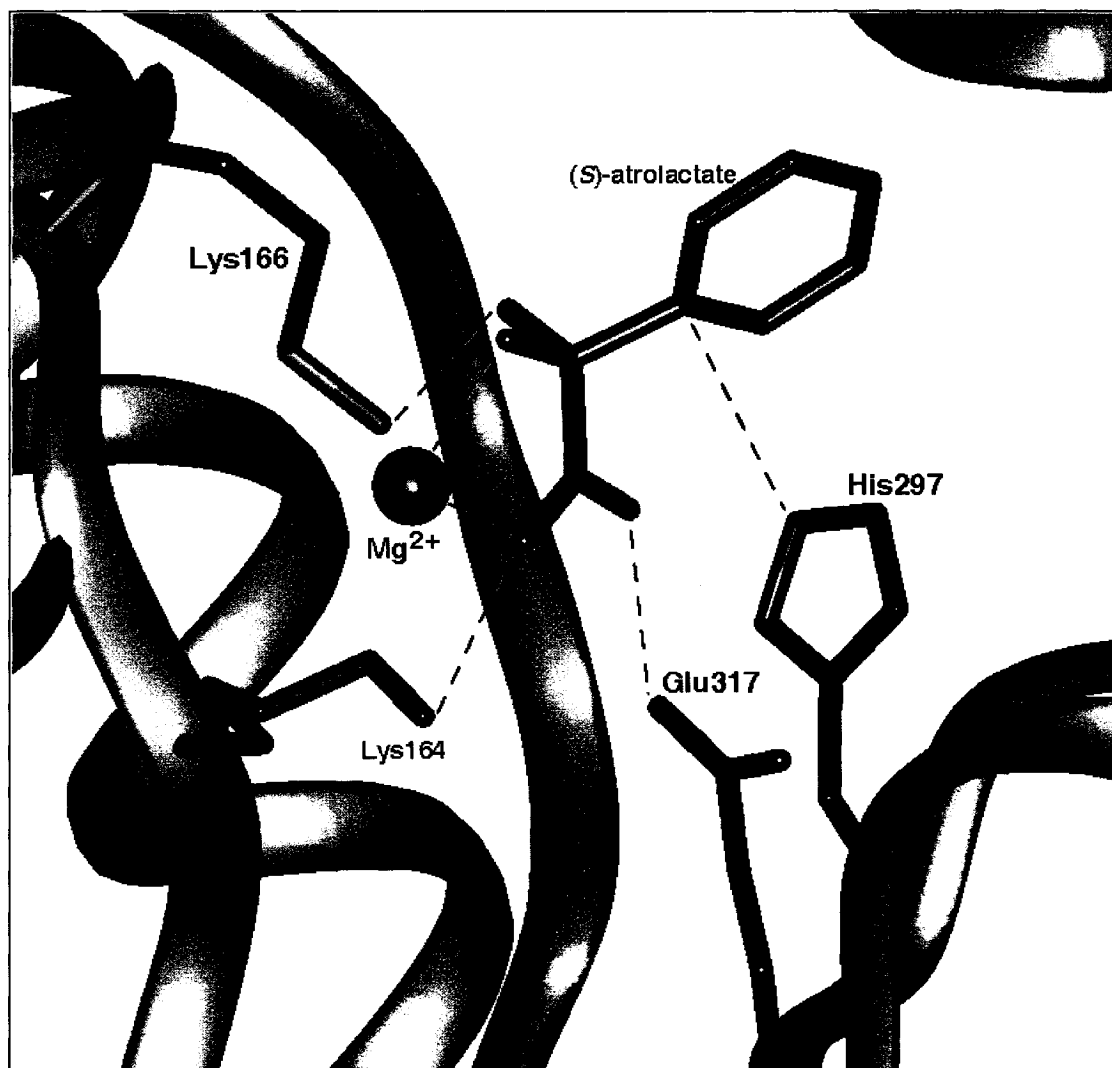
Figure 1.4 **X-ray crystal structure of the active site of MR with the substrate analogue (S)-atrolactate** [pdb key = 1MDR (Landro *et al.*, 1994)]. Oxygen, nitrogen and carbon atoms are red, blue and green, respectively. The α-carbon backbone is gold.

active site of MR was calculated to be ≤ 15 (Landro *et al.*, 1991). This pK_a for the α-carbon acid in the active site of MR represents a significant reduction in the pK_a of both mandelate ion (estimated pK_a ~ 29 (Gerlt *et al.*, 1991)) and mandelic acid (pK_a = 22 (Chiang *et al.*, 1990)) in solution. Thus, functional groups on the enzyme afford a substantial reduction in the pK_a for the α-carbon acid of the substrate by stabilizing the reaction intermediate (discussed in section 1.2).

The identity of Lys 166 as the (*S*)-specific general base catalyst was established using affinity labeling and site–directed mutagenesis experiments. Landro *et al.* (1994) synthesized both (*R*)- and (*S*)-α-phenylglycidate (an epoxide based derivative of mandelate) and determined that only (*R*)-α-phenylglycidate inactivated the enzyme. The crystal structure of the inactivated enzyme revealed that the covalent adduct is formed by nucleophilic attack from the ϵ-ammonium of Lys 166 to the distal endocyclic carbon of (*R*)-α-phenylglycidate (**scheme 1.3**). This carbon atom in (*R*)-α-phenylglycidate occupies the same position in the enzyme active site as is normally occupied by the α-proton of the (*S*)-mandelate substrate (Landro *et al.*, 1994), indicating that Lys 166 is ideally poised to abstract the α-proton from the (*S*)-enantiomer of the substrate. Further evidence for Lys 166 as the (*S*)-specific general base catalyst was revealed by the kinetic characterization of a K166R mutant of MR (Kallarakal *et al.*, 1995). Crystallographic studies showed that this mutant was structurally equivalent to the wild–type enzyme, with the exception of the positions of the side chains of residue 166. Unlike the H297N mutant, the K166R mutant retained a low level of racemase activity where k_{cat} was substantially reduced (≥ 1000-fold) in both reaction directions and k_{cat}/K_m was reduced approximately 5000-fold. As

Scheme 1.3 Inactivation of MR by (*R*)-phenylglycidate.

(*R*)-α-phenylglycidate
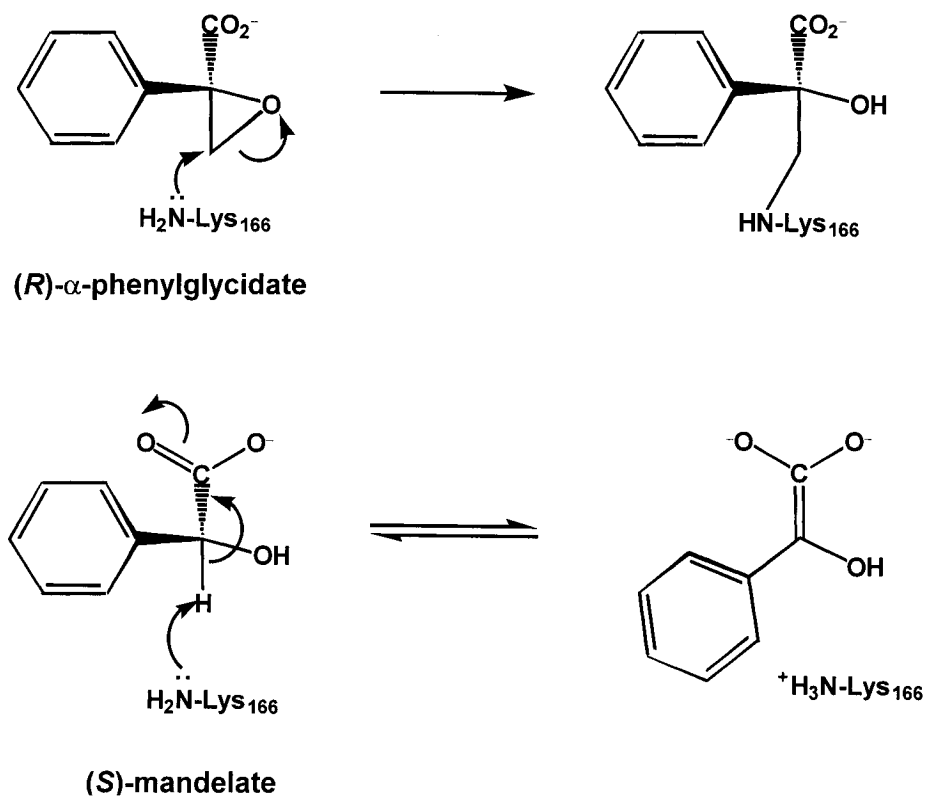
(*S*)-mandelate

with the H297N mutant, K166R catalyzed the stereoselective elimination of bromide ion

from p-(bromomethyl)mandelate. In this case, however, the reaction was specific for the

(R)-enantiomer of p-(bromomethyl)mandelate. Despite the low level of racemase activity

retained by the K166R mutant, these results provided convincing evidence that Lys 166

is, indeed, the (S)-specific general base catalyst of MR.

Dixon–Webb log plots (Dixon & Webb, 1964) for the dependencies of k_{cat} on pH

for MR revealed pK_a values of 6 and 10 from the ascending and descending limbs of the

plot, respectively (Kallarakal et $al.$, 1995; Landro et $al.$, 1991). These pK_a values were

the same in both the $R{\rightarrow}S$ and $S{\rightarrow}R$ directions. The pK_a values obtained from these plots

may represent pK_a values for enzyme ionizable groups in the enzyme–substrate complex.

Indeed, in order to function both as a general base catalyst to abstract the proton from the

substrate and a general acid catalyst to reprotonate the intermediate, both Lys 166 and His

297 must be subject to substantial fluctuations in the pK_a values of their ionizable side–

chain groups, perhaps as much as 4 pK_a units, depending on whether the (R)- or (S)-

substrate is bound in the active site (Neidhart et $al.$, 1991; Schafer et $al.$, 1996). For

example, in order to function as a general base catalyst to abstract a proton from the α-

carbon of (S)-mandelate, the pK_a of Lys 166 must be ~6, representing a substantial

perturbation from the "normal" Lys pK_a of ~10. This perturbation could result from the

close proximity of the positive charges of Mg^{2+} and Lys 164 to the ε-amino group of Lys

166 (Neidhart et $al.$, 1991). However, to function as a general acid catalyst in the reverse

reaction direction, the pK_a of Lys 166 must shift to a value of ~10. The same problem

exists for His 297, which must function at a "normal" pK_a of ~6 when it is acting as the

general base catalyst with the (R)-mandelate substrate but must subsequently shift to a

perturbed pK_a of ~10 to act as the general acid catalyst. His 297 functions as part of a catalytic diad with Asp 270 in order to maintain its "normal" pK_a in the positively charged environment of the active site (Schafer *et al.*, 1996).

The pH–rate profile for the K166R mutant suggests that only the pK_a determined from the ascending limb of the plots (pK_a ~ 6) is associated with a catalytic residue and that the descending limb (pK_a ~ 10) is *not* representative of the conjugate acid of the general base catalyst (Kallarakal *et al.*, 1995). Obviously, estimating pK_a values from pH–rate profiles is subject to problems of interpretation and a more direct measure of the pK_a of Lys 166 and His 297 would be preferred. Nevertheless, in order for catalysis to proceed in both directions at neutral pH, the stereochemistry of the substrate must influence the pK_a for the conjugate acid of the general base, allowing it be protonated in the presence of one substrate enantiomer and deprotonated in the presence of the other. This pK_a "shift" likely originates from conformational changes in the active site of MR induced by the stereochemistry of the substrate.

1.6 The General Acid Catalyst: Glu 317

The mechanism of the reaction catalyzed by MR proceeds via a transiently stable intermediate (Hegeman *et al.*, 1970; Kenyon & Hegeman, 1970; Landro *et al.*, 1991; Lin *et al.*, 1988; Mitra *et al.*, 1995; Neidhart *et al.*, 1991). This poses a mechanistic problem for the enzyme since the proposed enolate anion intermediate would be too unstable to account for the rates of reaction observed with MR (Thibblin & Jencks, 1979). Gerlt and Gassman (1993a; 1993b) proposed a mechanism for overcoming this problem involving concerted general acid–general base catalysis such that a proton is partially transferred from a general acid catalyst to stabilize the intermediate (see section 2.1). The crystal

structures of MR with bound ligand reveal the presence of Glu 317 within hydrogen bonding distance to one of the carboxylate oxygens of the substrate (**figure 1.4**). This residue is ideally situated to act as a general acid catalyst and could, therefore, play a critical role in stabilizing the intermediate. To test the role of Glu 317 in catalysis, the E317Q mutant was constructed and characterized (Mitra *et al.*, 1995). This mutant was designed to maintain the hydrogen bond with the carboxylate of the substrate but, because of the increased pK_a of the carboxamide of Gln relative to the carboxylate of Glu, proton transfer to the intermediate was expected to be significantly reduced. If proton transfer from Glu 317 is an important factor in catalysis then activity of the E317Q enzyme would be severely impaired. The crystal structure of the E317Q enzyme with the bound substrate analogue, (*S*)-atrolactate, indicated no significant perturbations to the structure of the active site relative to the wild–type enzyme. The K_m values for both (*R*)- and (*S*)-mandelate were only mildly affected by the mutation whereas k_{cat} values were reduced by a factor 5×10^3 and 3×10^4 in the $R{\rightarrow}S$ and $S{\rightarrow}R$ directions, respectively. E317Q MR also showed a significantly reduced rate of catalyzed elimination of the bromide ion from (*R,S*)-*p*-(bromomethyl)mandelate relative to the wild–type enzyme. These results indicated that proton transfer from Glu 317 plays an important role in stabilizing the enolic intermediate. Unlike the MR–catalyzed elimination reaction with (*R,S*)-*p*-(bromomethyl)mandelate, the inactivation of MR by (*R*)-α-phenylglycidate uses the conjugate acid of the general base His 297 to assist the nucleophilic attack on the oxirane ring by Lys 166 (Landro *et al.*, 1994) and does not proceed through a transiently stable intermediate. Thus, the general acid catalyst is not expected to be implicated in this reaction and the E317Q mutation should not significantly influence the rate of

inactivation. Indeed, the rate of inactivation of the E317Q enzyme by (R)-α-phenylglycidate was nearly equivalent to the rate of inactivation of the wild type enzyme (Mitra *et al.*, 1995). In addition to the proposed role for Glu 317 in MR catalysis, Lys 164 and Mg^{2+} may also contribute to catalysis by neutralizing the negative charge of the substrate anion in the active site, allowing mandelate to react as the neutral mandelic acid in the active site, thus lowering the pK_a of the α-proton by ~7 units. The accepted mechanism of the reaction catalyzed by MR is summarized in **scheme 1.4**. The theory behind the proposal for general acid assisted proton abstraction from the α-carbon of mandelic acid is discussed in the following section.

1.2 Enzyme–Catalyzed Carbon–Hydrogen Bond Cleavage

1.2.1 Proton Abstraction from Carbon Acids: A Mechanistic Problem

Many cofactor–independent enzymes, including MR, catalyze reactions which cleave a carbon–hydrogen bond adjacent to a carbonyl/carboxylic acid/carboxylate group of the substrate. These include enzymes catalyzing 1,1-, 1,2- and 1,3- proton transfer reactions, β-elimination reactions, and Claisen condensation reactions (Gerlt, 1994; Tanner, 2002). In most cases, these reactions occur via a stepwise mechanism which results in the formation of a transiently stable enolate anion intermediate (Gerlt, 1994).

A carbonyl/carboxyl group adjacent to the α-carbon lowers the pK_a for the α-carbon acid by resonance stabilization of the intermediate. This effectively reduces the pK_a of the α-proton from ≥ 50 for alkanes to 29–32 for carboxylate anions, 22–25 for carboxylic acids, and 18–20 for aldehydes, ketones and thioesters (Gerlt *et al.*, 1991). While the

Scheme 1.4 The accepted mechanism of the reaction catalyzed by MR.

(R)-mandelate

enolic intermediate

(S)-mandelate
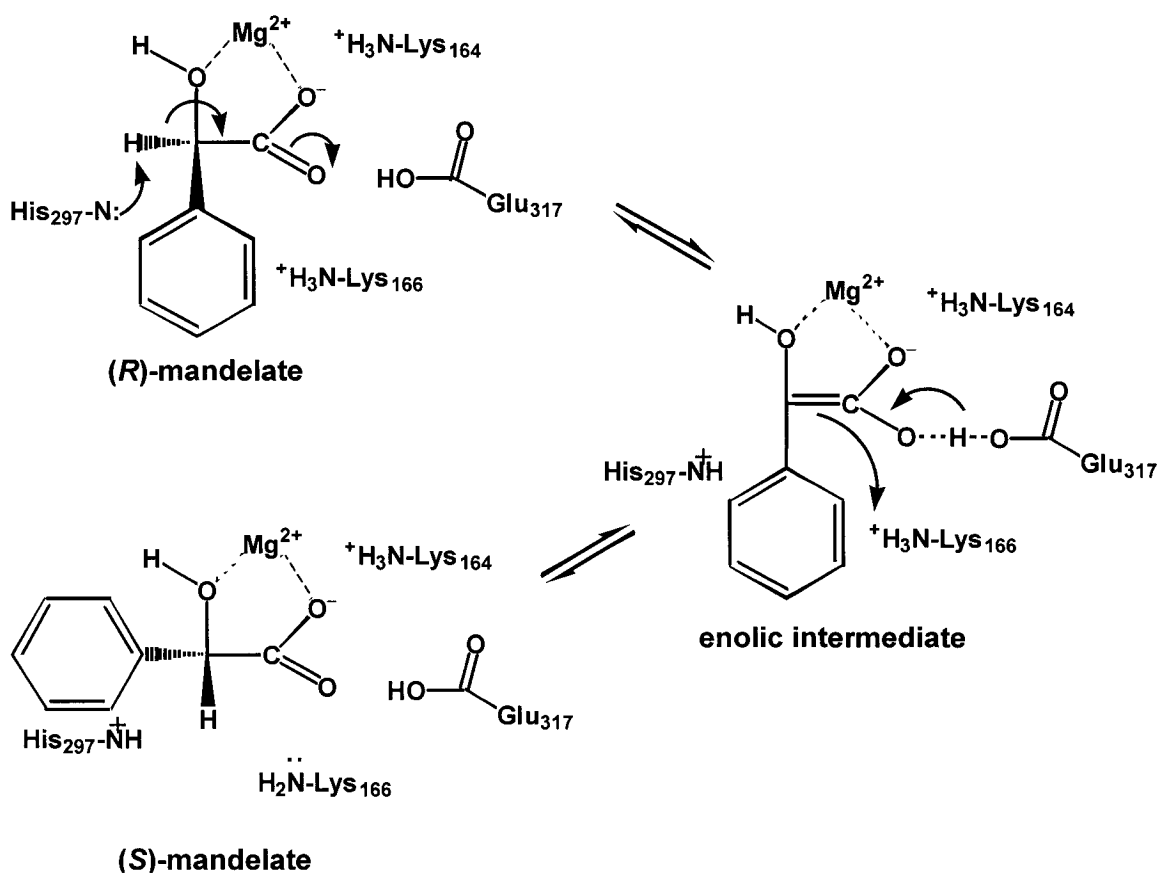
reduction in the pK_a afforded by the adjacent carbonyl/carboxylic acid/carboxylate group is significant, it is not sufficient to account for the rapid rates observed in enzyme catalysis. The problem encountered by enzymes in catalyzing proton abstraction from carbon acids is that enzyme–catalyzed reactions are typically performed under physiological conditions. These enzymes, therefore, must use general base catalysts with pK_a values ≤ 7 in order to function effectively at neutral pH. Thus, the difference in pK_a values between the conjugate acid of the general base catalyst and the α-proton of the substrate is often very large. In MR, for example, the pK_a of the conjugate acid of the general base catalyst is 6.4 in both reaction directions (Kallarakal *et al.*, 1995; Landro *et al.*, 1991). The pK_a of the α-proton of mandelic acid is 22–23 (Chiang *et al.*, 1997; Chiang *et al.*, 1990). This latter value was determined by generating the enol of mandelic acid by flash photolysis and measuring the equilibrium constant for its ionization to the enolate (pK_a^E = 6.6 (Chiang *et al.*, 1990); pK_a^E = 6.4 (Chiang *et al.*, 1997)). By relating this value to the measured keto–enol equilibrium constant (pK_E = 15.4 (Chiang *et al.*, 1990)), the pK_a of the α-carbon acid of mandelic acid was determined. The pK_a of the α-proton of mandelate anion has been estimated to be ~30, based on the pK_a of the phenylacetate anion (Gerlt *et al.*, 1991).

Assuming that formation of the intermediate is limited only by the thermodynamics of proton transfer from the substrate to the general base catalyst (*vide infra*), the activation free energy barrier for the reaction may be related to the difference in the pK_a of the general base catalyst and the α-proton of the substrate (i.e., $\Delta G^{\ddagger}$ = $\Delta G°$ = $-2.303RT\Delta pK_a$) (Gerlt, 1994; Gerlt & Gassman, 1993a, b; Gerlt *et al.*, 1991). Applying this analysis to MR, using a pK_a of 6.4 for the general base catalyst and 30 for

the mandelate anion, $\Delta G^{\circ} = \Delta G^{\ddagger} = 32$ kcal/mol. This value is 18 kcal/mol greater than the observed activation free energy barrier for the enzyme–catalyzed reaction ($\Delta G^{\ddagger} = 14$ kcal/mol (Mitra *et al.*, 1995)). Thus, a mechanism involving an *isolated* carbanion intermediate can not account for the rapid rates of reaction catalyzed by MR (Gerlt, 1994; Gerlt & Gassman, 1993a, b; Gerlt *et al.*, 1991; Thibblin & Jencks, 1979). MR must, therefore, proceed either via a concerted mechanism which avoids formation of a transient carbanion intermediate or must stabilize this species (Thibblin & Jencks, 1979). Because overwhelming kinetic evidence for a stepwise mechanism proceeding through a transiently stable intermediate has been presented (section 1.1.3), MR must provide substantial stabilization of the intermediate in the active site. The following sections present two alternative proposals for intermediate stabilization by MR that are sufficient to account for the rapid rates of MR catalysis.

1.2.2 Electrophilic Catalysis

If an isolated carbanion intermediate can not exist and a concerted mechanism is dismissed, enzymes which abstract protons from activated carbon acids must generate a *stabilized* enolic intermediate. Gerlt and Gassman (1993a; 1993b) proposed a critical role for concerted general acid–general base catalysis in generating this stabilized intermediate. According to their proposal, electrophilic catalysis by a general acid catalyst is sufficient to explain the high rates of reactions achieved by enzymes catalyzing proton abstraction from carbon acids (Gerlt, 1994; Gerlt & Gassman, 1992, 1993a, b; Gerlt *et al.*, 1991). X-Ray crystal studies of these enzymes indicate, without exception, the presence of a potential electrophilic catalyst proximal to the carbonyl/carboxylic acid/carboxylate group of the substrate (Gerlt *et al.*, 1991), implying a conserved role for

the general acid catalyst in reactions involving proton abstraction from carbon acids. Indeed, Glu 317 is located 2.6 Å from the substrate carboxylate oxygen in MR (Landro *et al.*, 1994) and concerted proton transfer from Glu 317 to the substrate carboxylate group has been demonstrated by measuring both a solvent and substrate deuterium isotope effect in formation of the enolic intermediate by the K166R mutant (Kallarakal *et al.*, 1995).

The pK_a of the neutral enol of mandelic acid is 6.4–6.6 (Chiang *et al.*, 1997; Chiang *et al.*, 1990). The pK_a for Glu 317 is also likely to be ~6 (Gerlt & Gassman, 1993b). (Support for this pK_a assigment comes from crystal structures of MR showing that Glu 317 is ~2.7 Å from the carboxylate oxygen of mandelate, suggesting that it is protonated in the enzyme–substrate complex (Landro *et al.*, 1994).) Thus, the pK_a values of the enolic intermediate and the general acid catalyst appear to be closely matched. These matched pK_a values may promote the formation of a short, strong hydrogen bond (SSHB) between the general acid catalyst and the enolic intermediate (Gerlt & Gassman, 1993b).

The properties of SSHBs in the gas phase and in solution and their role in enzyme catalysis has been the subject of many recent reviews and some controversy (Cleland, 2000; Guthrie, 1996; Perrin & Nielsen, 1997). In a SSHB, the proton is shared equally between the two heteroatoms (i.e., $A^- \cdots H^+ \cdots B$). Thus, for a SSHB bond to form, the two resonance forms of the bond (i.e., $A\text{-}H\cdots B^-$ and $A^-\cdots H\text{-}B$) must be close in energy which, in terms of acidities, means that AH and BH must have approximately the same pK_a value. In addition, the two heteroatoms must come closer together than the sum of their van der Waals radii (< 2.55 Å for O-H-O) so that the electrons can be delocalized across the entire bond distance. While "normal" hydrogen bonds have enthalpies of formation of 5 kcal/mol or less, SSHBs have values of 25–30 kcal/mol in the gas phase

and could have values as high as 21–22 kcal/mol in high dielectric media such as water (Cleland, 2000). Cleland and Kreevoy (1994) postulated that a weak hydrogen bond between the enzyme and the substrate can subsequently become a SSHB with the altered substrate in the transition state. On this basis, SSHBs have been invoked in several enzyme systems to explain the energetics of transition state stabilization, including triose phosphate isomerase (Gerlt & Gassman, 1993a), chymotrypsin (Frey et al., 1994), and staphylococcal nuclease (Loh & Markley, 1994).

The formation of a SSHB between the intermediate and the general acid catalyst could contribute more than 20 kcal/mol to the stabilization of the intermediate and substantially lower the thermodynamic barrier for catalysis. Such a SSHB will form only with the intermediate and not with the substrate since the pK_a of mandelic acid with a protonated carbonyl group is estimated to be approximately –8 (Gerlt et al., 1991). Thus, a SSHB between Glu 317 and the intermediate is sufficient to account for the rapid rates of catalysis by MR. In this proposed mechanism, it is important to note that the intermediate exists neither as a negatively charged enolate nor as a neutral enol, since both of these species are too unstable. Rather, the enolic intermediate equally shares a proton with Glu 317 through a SSHB. As a consequence of this sharing, the intermediate is not referred to as a carbanion, an enol or an enolate since this can be misleading for reactions that use electrophilic catalysis to catalyze proton abstraction from carbon acids.

Gerlt and Gassman (1993a; 1993b) have suggested that enzymes must not only overcome a thermodynamic barrier to proton abstraction from carbon acids, but they also face an intrinsic kinetic barrier resulting from the fact that protons dissociate more slowly from carbon acids than they do from "normal" heteroatom acids of equal pK_a. The slow rate of dissociation likely results from the negative entropic contribution associated with

solvent ordering about the developing negative charge of the carbonyl oxygen (Gerlt & Gassman, 1993b). The increased intrinsic kinetic barrier further raises the activation energy barrier ($\Delta G^{\ddagger}$) for the reaction. This barrier may be reduced, however, by neutralizing the developing negative charge on the carbonyl oxygen and avoiding the need for solvent reorganization. Once again, the general acid catalyst is ideally poised to overcome this difficulty, in this case by stabilizing the developing negative charge on the carbonyl oxygen by concerted proton transfer. Because of the preorientation of the substrate and enzyme functional groups in the active site, there should be little entropic cost associated with this charge neutralization. Thus, the general acid catalyst functions to reduce the intrinsic barrier to approximately zero such that $\Delta G^{\ddagger}$ can be approximated by ΔG° (Gerlt, 1994; Gerlt & Gassman, 1993a, b).

Electrophilic catalysis by Glu 317 is proposed to reduce both the intrinsic kinetic free energy barrier and the thermodynamic free energy barrier for catalysis by MR. The kinetic free energy barrier is reduced by concerted proton transfer from Glu 317 to neutralize the developing negative charge on the carbonyl oxygen. The thermodynamic barrier is reduced as much as 20 kcal/mol by formation of a SSHB between the enolic intermediate and Glu 317. Recent computer simulations performed on the MR–catalyzed racemization of vinylglycolate also reveal an essential role for concerted proton transfer from Glu 317 in stabilizing the enolic intermediate (Garcia-Viloca et al., 2001). Thus, electrophilic catalysis can account for the rates of reaction catalyzed by MR and provides a general solution to the mechanistic difficulties described in the previous section.

1.2.3 Electrostatic Stabilization

Guthrie and Kluger (1993) calculated the energies of the *O*-protonated acid, the enol and the enolate of mandelic acid and found them all to be of similar energy. On this basis, they argued that proton transfer to the enolate from a general acid catalyst provides no significant stabilization of the intermediate. In an argument completely contrary to that described above, they contend that the enolate is the *preferred* ionization state for the intermediate because it allows for electrostatic stabilization. Although the authors incorrectly assigned the active site metal ion to bridge the carboxylate oxygens of the substrate, their overall conclusion was that, in a medium of reduced polarity, electrostatic stabilization is sufficient to stabilize the intermediate and account for the reduction in the activation free energy barrier for the reaction. The proximity of several positively charged residues and the catalytically essential metal ion to the substrate carboxylate group can certainly account for the electrostatic stabilization invoked by Guthrie and Kluger. Chiang *et al.* (1997) have since reported the measured energies of the neutral enol and enolate anion of mandelic acid and have shown that, at neutral pH, these species do indeed have very similar energies. These results very much support the calculations of Guthrie and Kluger and further substantiate that either species could be generated during the enzymatic reaction.

Evidence for SSHBs in biological systems has typically come from highly perturbed chemical shifts in the NMR spectra or from characteristic deuterium fractionation factors (Frey *et al.*, 1994; Harris *et al.*, 1997). No such evidence has yet been presented for a SSHB between Glu 317 and the enolic intermediate, though the short lifetime of the intermediate may render this task difficult. The mere existence of SSHBs in biological systems continues to be the subject of considerable debate (Ash *et al.*, 1997; Guthrie,

1996; Kato *et al.*, 1996). Warshel *et al.* (1995) concluded that electrostatic effects are sufficient to account for enzyme catalysis, without the need to invoke a SSHB. Although computer simulations performed on the MR–catalyzed racemization of vinylglycolate suggest a role for concerted proton transfer from Glu 317, they do not support the existence of a SSHB between the substrate and Glu 317 (Garcia-Viloca *et al.*, 2001).

Despite the debate over the SSHB in MR catalysis, both proposals (electrophilic catalysis and electrostatic stabilization) identify important contributions to intermediate stabilization by MR. Calculations of the effective molarities of Lys 166, His 297 and Glu 317 have suggested that Glu 317 interacts more strongly with the altered substrate in the transition state than either of the two general base catalysts (Bearne & Wolfenden, 1997). In addition, the kinetic results with the E317Q mutant (Mitra *et al.*, 1995) and solvent/substrate isotope effects with the K166R mutant (Kallarakal *et al.*, 1995) confirm the importance of proton transfer from Glu 317, though they do not prove the existence of a SSHB. The $\Delta\Delta G^{\ddagger}$ for the E317Q mutant relative to the wild–type enzyme is approximately 5 kcal/mol (Mitra *et al.*, 1995). This value is much lower than that which would be expected from replacing a SSHB with a normal hydrogen bond (~15 kcal/mol). Thus, electrostatic stabilization of the intermediate may well play an important role in catalysis by MR.

Although it is not yet clear by which mechanism MR stabilizes the intermediate (i.e., electrophilic catalysis vs. electrostatic stabilization), it is evident that MR *must* provide substantial stabilization to the intermediate in order to effect catalysis. In accord with the Hammond postulate (Hammond, 1955) the high energy of the intermediate relative to the substrate necessitates that its energy be similar to the energy of the transition states for its formation. Thus, MR is an excellent example of an enzyme which

rapidly catalyzes a very difficult chemical reaction by preferentially stabilizing the reaction intermediate and, analogously, the altered substrate in the transition state.

1.3 Transition State Stabilization in Enzyme Catalysis

1.3.1 A Brief Description of Transition State Theory

According to the most basic description of transition state theory, a reactant or reactants must have sufficient energy to overcome a potential energy barrier in order to react to form product(s). The transition state for a given reaction is the highest energy species along the reaction coordinate and represents an activated complex consisting of distorted orientations and weakened and partially formed bonds. In the standard derivation of transition state theory ('quasi–equilibrium' approach) (i.e., see Thornton & Thornton, 1978), the transition state is treated as being in equilibrium with the reactant(s). For example, a unimolecular conversion of the reactant, S, to the product, P, proceeds through a transition state, $S^{\ddagger}$, which is in equilibrium with the reactant (equation 1.1).

$$K^{\ddagger} = \frac{[S^{\ddagger}]}{[S]} \tag{1.1}$$

The rate of the reaction is governed by the rate of decomposition of the transition state, $S^{\ddagger}$, to form the product, P. Thus, the rate of product formation (d[P]/dt) is proportional to the concentration of the transition state. This proportionality constant can be derived (Johnston, 1966) and is approximately equal to the rate of a slow molecular vibration (10^{13} s^{-1}) according to the relationship described in equation 1.2, where k is the first–order rate constant, k_B is the Boltzmann constant, h is Planck's constant and T is the absolute temperature (Thornton & Thornton, 1978).

$$\frac{d[P]}{dt} = \frac{k_B T}{h}[S^{\ddagger}] = \frac{k_B T}{h}K^{\ddagger}[S] = k[S] \tag{1.2}$$

From equation 1.2, the measurable first–order rate constant (k) for the reaction can be related to the equilibrium constant between the reactant and transition state ($K^{\ddagger}$) and the universal frequency factor (k_BT/h) (equation 1.3).

$$k = \left(\frac{k_BT}{h}\right)K^{\ddagger} \qquad (1.3)$$

This expression can be written in thermodynamic terms using the relationship $\Delta G^{\ddagger} = -RT\ln K^{\ddagger}$ (equation 1.4).

$$k = \left(\frac{k_BT}{h}\right)\exp\left(\frac{-\Delta G^{\ddagger}}{RT}\right) \qquad (1.4)$$

From equation 1.4, the rate of a chemical reaction can be related to the free energy of activation ($\Delta G^{\ddagger}$), such that the rate depends on the difference in energy between the reactant(s) and the transition state for the formation of product(s).

1.3.2 Transition State Stabilization

Enzymes are remarkable catalysts, capable of astonishing rate enhancements. Enzyme–catalyzed reactions occur at rates that are 10^7 to 10^{19} times faster than the corresponding uncatalyzed reactions (Wolfenden & Snider, 2001). In the most extreme example, the spontaneous decarboxylation of glycine at 25 °C in neutral solution has a half–life of 1.1 *billion* years as compared with a half–life of 0.5 *milliseconds* for the enzyme–catalyzed decarboxylation of arginine (Snider & Wolfenden, 2000). How do enzymes achieve such remarkable rate enhancements? According to transition state theory, the rate of a reaction may be increased by reducing the activation energy barrier for the reaction. Pauling (1948) first proposed that enzymes function by providing

stabilizing interactions to the altered substrate in the transition state, thus lowering the activation energy barrier for the reaction. This idea was further developed by Jencks (Jencks, 1966), Wolfenden (Wolfenden, 1969, 1972) and Lienhard (Lienhard, 1973). The free energy diagram in **figure 1.5** illustrates this concept using the reaction coordinates for a hypothetical unimolecular reaction proceeding in the presence and absence of an enzyme catalyst.

The degree to which an enzyme stabilizes a substrate in the transition state is defined as its proficiency. More specifically, enzyme proficiency is defined as the reciprocal of the virtual dissociation constant for the enzyme–substrate complex in the transition state (K_{Tx}) (Radzicka & Wolfenden, 1995). For a one–substrate reaction, an expression relating K_{Tx} to the rate constant for the nonenzymatic reaction (k_{non}) and the second order rate constant for the enzymatic reaction (k_{cat}/K_m) can be derived from the thermodynamic cycle shown in **scheme 1.5**, as originally described by Kurz for acid catalysis (Kurz, 1963). Using this thermodynamic cycle, the equilibrium constants for the enzyme–catalyzed and uncatalyzed reactions can be related according to equation 1.5.

$$\frac{K_{Tx}}{K_S} = \frac{K^{\ddagger}_{non}}{K^{\ddagger}_{cat}} \tag{1.5}$$

The equilibrium constants between the reactants and the transition state can be expressed in terms of the Eyring equation (i.e. $k = \kappa \nu K^{\ddagger}$) to give equation 1.6 (Kraut, 1988).

$$\frac{K_{Tx}}{K_S} = \frac{k_{non}}{k_{cat}} \left(\frac{(\kappa \nu)_{cat}}{(\kappa \nu)_{non}} \right) \tag{1.6}$$

Assuming that the values of κ and ν are the same in both the enzyme–catalyzed reaction and the uncatalyzed reaction, equation 1.6 can be rewritten as equation 1.7
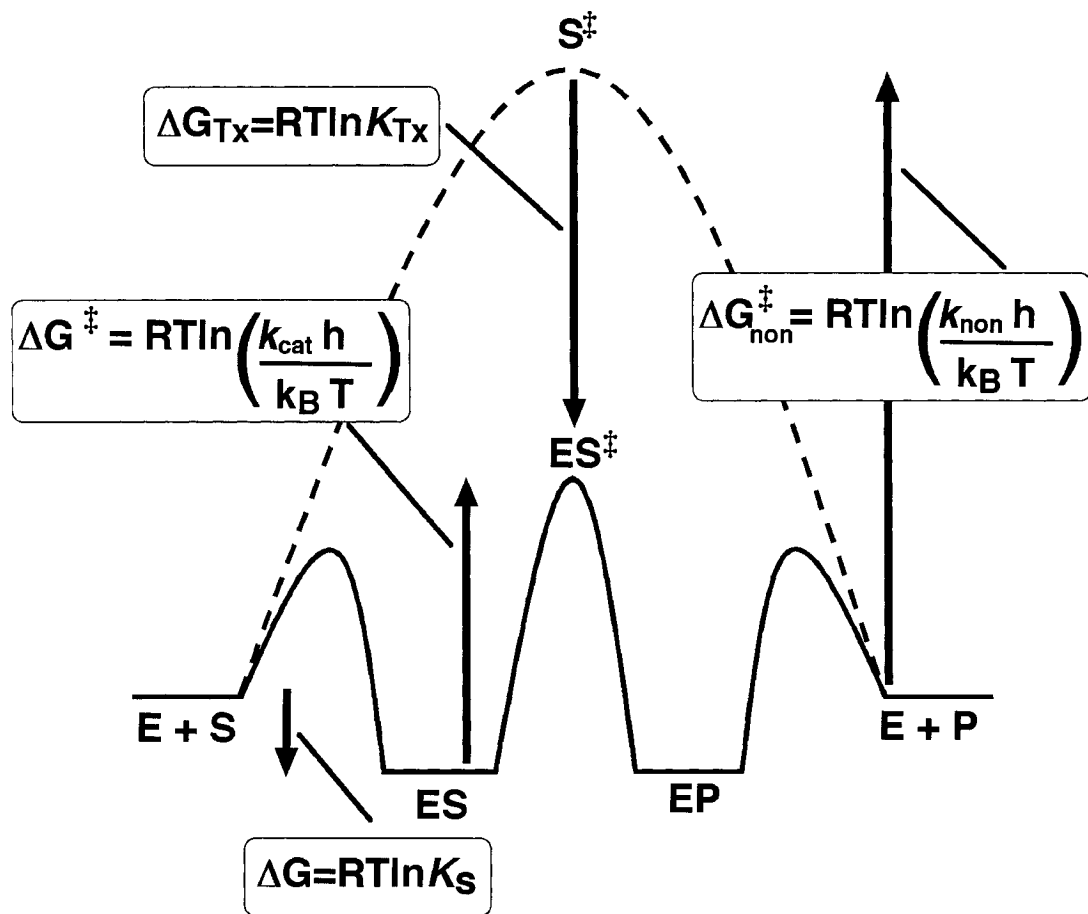
Figure 1.5 Relative free energy profiles for a hypothetical uncatalyzed (dashed line) and enzyme–catalyzed (solid line) reaction. The free energy difference between the activation barriers for the uncatalyzed and enzyme–catalyzed reactions represents the free energy of transition state stabilization provided by the enzyme (ΔG_{Tx}).

Scheme 1.5 Thermodynamic cycle describing the enzyme–catalyzed and non enzymatic conversion of substrate into product

$$E + S \xrightleftharpoons[\quad]{K_{non}^{\ddagger}} E + S^{\ddagger} \longrightarrow E + P$$

$$\begin{array}{ccc}
E + S & \xrightleftharpoons{K_{non}^{\ddagger}} & E + S^{\ddagger} \\
\Big\updownarrow K_S & & \Big\updownarrow K_{Tx} \\
ES & \xrightleftharpoons{K_{cat}^{\ddagger}} & ES^{\ddagger}
\end{array} \qquad E + P$$
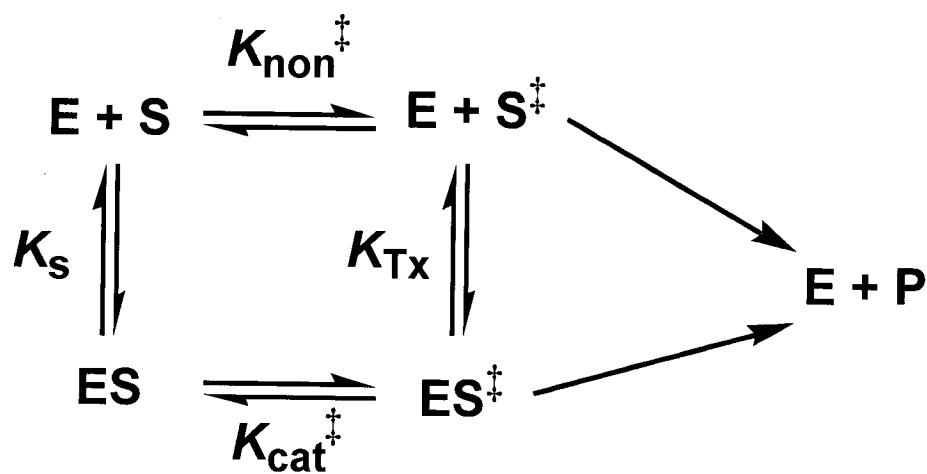
$$K_{Tx} = \frac{k_{non}}{\left(k_{cat} / K_S\right)} \qquad (1.7)$$

A similar relationship has been derived for multisubstrate enzymes (Byers, 1978; Lienhard, 1973). A recent survey of enzymes with known proficiencies reveals values ranging from 10^8 to 10^{23} M^{-1}, the equivalent of 10 to 31 kcal/mol of stabilization free energy provided by the enzyme at 25 °C (Wolfenden & Snider, 2001). Measurements of enzyme proficiencies are limited by the difficulties in measuring nonenzymatic reaction rates for very slow reactions. Consequently, the magnitude of transition state stabilization provided by enzymes has been described for relatively few cases.

The above analysis relies on two central assumptions in comparing the rates of enzyme–catalyzed and uncatalyzed reactions (Wolfenden, 1976). First, it is assumed that the catalyzed and uncatalyzed reactions proceed through identical transition states. This situation seems quite improbable since enzyme active sites differ substantially from bulk solvent and, consequently, their transition states are likely to follow different paths from those in solution. If this assumption is invalid, the result is an *underestimation* of transition state stabilization. This is because a spontaneous reaction must proceed through a pathway with the lowest possible free energy of activation; the uncatalyzed transition state matching the enzyme–catalyzed transition state can be of no lower energy than that for the spontaneous reaction and is likely to be of higher energy. This results in an underestimation of transition state stabilization. The second assumption is that the chemical step is rate–limiting for the enzyme–catalyzed reaction. Again, if this assumption is shown to be invalid, the result is an *underestimation* of the transition state

stabilization energy. This situation is described in detail for MR in Chapter 3 of this thesis.

How do enzymes bind tightly to the altered substrate in the transition state while avoiding tight binding interactions with substrates and products? It seems likely that enzymes undergo conformational changes as the reaction proceeds from the substrate through the transition state. For example, many transition state analogues are slow onset inhibitors such that the initial rapid, weak binding is followed by a slow tight–binding interaction (Morrison & Walsh, 1988). Since free enzyme is assumed to be in a conformation suited to recognize the substrate (Britt, 1993), the slow binding nature of these inhibitors is attributed to the time required for the enzyme to change from a ground state to a transition state conformation (Frieden et al., 1980). Thus, the structural rearrangements in both the substrate and the enzyme permit increased interaction energies with the transition state relative to the ground state through new and strengthened hydrogen bonds and electrostatic interactions (Shan & Herschlag, 1996; Warshel, 1998).

1.3.3 Transition State Analogues

The affinity of an enzyme for the altered substrate in the transition state is substantially greater than its affinity for the substrate in the ground state. It stands to reason, therefore, that inhibitors which mimic structural and electronic features of the transition state should be very potent inhibitors of the enzyme (Lienhard, 1973; Wolfenden, 1972). Of course, an exact mimic of the transition state using stable compounds is impossible since the partial bonds and distorted geometries in the transition state result in a species with a lifetime of less than a typical bond vibration (10^{-13} s) (Truhlar et al., 1983). However, since the affinity of an enzyme for the transition state is

so large, an inhibitor designed to capture only a small portion of the interactions that stabilize the transition state could be bound by the enzyme with a very high affinity relative to the substrate. On this basis, Wolfenden has defined a transition state analogue as an inhibitor "designed to exploit and make manifest the special interactions that distinguish the substrate in the transition state from the substrate in the ground state" (Wolfenden, 1976).

Designing a transition state analogue inhibitor requires a knowledge or an estimate of the transition state structure in the enzyme active site. Typically, a hypothetical transition state structure may be assigned based on the postulated reaction mechanism. However, a more systematic approach to discerning the structure of the transition state for an enzyme–catalyzed reaction can be achieved using kinetic isotope effects to provide a quantitative measure of the extent to which individual bonds are changing as the reaction approaches the transition state (reviewed by Schramm, 1998). In either case, there are numerous examples of transition state analogues which are bound by their respective enzymes with an affinity far exceeding the apparent affinity of the enzyme for the substrate in the ground state (Morrison & Walsh, 1988; Wolfenden, 1976; Wolfenden & Frick, 1987). In a few cases, the inhibitor is bound with such high affinity as to begin to approach the affinity of the enzyme for the transition state itself. The inhibition of adenosine deaminase by 6-hydroxy-1,6-dihydropurine ribonucleoside (Kati & Wolfenden, 1989) and cytidine deaminase by 3,4-dihydrouridine (Frick et al., 1989) are two such examples. These examples offer convincing experimental evidence that the theory of transition state stabilization in enzyme catalysis is sound. However, the exact mechanisms that enzymes use to achieve transition state stabilization and promote enzyme catalysis remain a subject of debate.

1.3.4 Ground State Effects

Is transition state stabilization sufficient to account for enzymatic catalysis? Concepts such as ground state destabilization and proximity effects have been proposed to explain enzyme catalysis without the need to invoke transition state stabilization (Jencks, 1975). One extreme stance has been to reinterpret these concepts in terms of transition state stabilization, suggesting that enzymes achieve catalysis solely by stabilizing the altered substrate in the transition state and that ground state species are inhibitory and waste catalytic power (Kraut, 1988; Schowen, 1978). According to this viewpoint, an increase in ground state binding affinity can only be detrimental to catalysis, as it leads to a greater activation energy barrier for the reaction. This so–called "fundamentalist position" of enzyme catalysis has sparked considerable debate and many proposals suggesting contributions from ground state binding to enzyme catalysis have since been advanced (Britt, 1993; Cannon *et al.*, 1996; Menger, 1992; Murphy, 1995).

The proximity of reacting groups in the enzyme–substrate ground state complex has been invoked as a major factor in catalysis, with proximity effects enhancing the rate of enzyme–catalyzed reactions by a factor of 10^8 (Page & Jencks, 1971). According to this proposal, the entropic component of the activation energy barrier is reduced by restricting the motions of the reacting groups in the enzyme active site. The unfavourable entropy associated with this process is offset by the favourable enthalpy of substrate binding. While the entropic contribution to catalysis has been widely accepted, recent computer simulations have shown that assumptions implicit in this analysis may be invalid and indicate that entropic contributions to catalysis may be much smaller than earlier predictions indicated (Villa *et al.*, 2000).

The theory of transition state stabilization has been criticized on the grounds that there are insufficient electronic and structural differences between the ground state and the transition state to account for the enormous difference in stabilization energies between these two species (Bruice & Benkovic, 2000; Cannon *et al.*, 1996). Cannon *et al.* (1996) concede that rate enhancements are reduced at high substrate concentrations (Schowen, 1978), but they do not take this to imply that the enzyme–substrate complex is inhibitory. Using computer–assisted calculations, it has been shown that the ground state complex does not decrease or inhibit the reaction at either high or low substrate concentrations (Cannon *et al.*, 1996). Rather, it is suggested that ground state binding interactions promote catalysis by maximizing the distance, orientation and conformation of the substrate relative to enzyme functional groups (and cofactors) in the active site (Cannon *et al.*, 1996). Bruice and Lightstone (1999) define this pre-oriented substrate as a "near attack complex": a substrate in the ground state which is in a conformation closely resembling that of the transition state. The altered conformation of the near attack complex is not necessarily higher in energy than the average energy for all of the enzyme–substrate conformations and, therefore, a near attack complex is still considered to be in the ground state (Bruice & Benkovic, 2000; Bruice & Lightsone, 1999). Using computer–assisted calculations to determine the fraction of species present as near attack complexes, Lightstone and Bruice (1996) determined that the rate constants for cyclic anhydride formation from dicarboxylic acid monoesters are directly proportional to the relative fraction of species present as near attack complexes. Near attack complexes may also play a role in enzyme catalysis. In a recent review, Bruice and Benkovic (2000) presented examples of computer–assisted calculations showing that near attack complexes and transition state complexes are equally stabilized by the enzyme, thereby

downplaying the overall importance of transition state stabilization in enzyme catalysis. The formation of near attack complexes in an enzyme–substrate complex is likely to be assisted by dynamic motions of the enzyme (Bruice & Benkovic, 2000; Cannon et al., 1996). Thus, there may be a role for preorganized active sites stabilizing ground state species in a near attack conformation (Bruice & Benkovic, 2000; Snider et al., 2000). It is likely that a combination of entropic factors, transition state stabilization and ground state preorientation are important in enzyme–catalyzed reactions, and that the relative contribution of each of these effects depends on the specific reaction being catalyzed.

1.4 Overview

MR catalyzes the interconversion of the two enantiomers of mandelic acid by abstracting a proton from the substrate α-carbon in a stepwise reaction mechanism proceeding through a carbanion–like intermediate (Kenyon & Hegeman, 1979). Two proposals have been advanced to explain the rapid rates of racemization. According to the first proposal, concerted general acid–general base catalysis reduces the intrinsic kinetic barrier to activation by neutralizing the developing negative charge in the transition state and reduces the thermodynamic barrier by stabilizing the enolic intermediate through the formation of a short, strong hydrogen bond (Gerlt & Gassman, 1993a, b). In the second proposal, protonation of the intermediate is not considered to be significant and, rather, electrostatic stabilization of the intermediate is sufficient to reduce the activation energy barrier for the reaction (Guthrie & Kluger, 1993). While the relative contribution to catalysis from these two effects is uncertain, it is clear that MR is an extremely proficient enzyme, binding the altered substrate in the transition state with

extremely high affinity ($K_{Tx} \leq 2 \times 10^{-19}$ M) and reducing the activation free energy barrier by at least 26 kcal/mol relative to the uncatalyzed reaction (Bearne & Wolfenden, 1997).

It is of critical importance in furthering our understanding of MR catalysis to clarify *how* the enzyme is able to achieve this astounding 26 kcal/mol of free energy to stabilize the altered substrate in the transition state while providing only approximately 5 kcal/mol to stabilize the substrate in the ground state (from $K_m = 0.2$ mM (Whitman *et al.*, 1985)). What is the molecular origin of this remarkable discrimination? Preferential binding of the altered substrate in the transition state could originate from the proposed short, strong hydrogen bond with Glu 317 (Gerlt & Gassman, 1993a, b; Mitra *et al.*, 1995) and/or from electrostatic stabilization of the intermediate (Guthrie & Kluger, 1993). Are there other factors which might contribute to preferential binding of the altered substrate in the transition state? A deeper understanding of the factors contributing to differential binding in MR would be greatly facilitated by the use of stable analogues of the transition states or intermediate. However, no transition state analogue inhibitors have yet been reported for MR. The central focus of this work, then, is to further clarify the contributions from active site residues of MR to both ground state and transition state binding by probing these interactions using substrates and intermediate analogue inhibitors.

The following chapters of this thesis further characterize the contributions from ground state and transition state binding energies to catalysis by MR and reveal previously unrecognized interactions that serve to preferentially stabilize the altered subtrate in the transition state relative to the substrate in the ground state. Chapter 2 describes the development and validation of a fixed–time, high–performance liquid chromatography assay for MR activity. Chapter 3 describes the enthalpic and entropic contributions to catalysis by MR and demonstrates that transition state stabilization in

MR is achieved principally by enthalpy reduction. Chapter 4 characterizes the inhibition of MR by two intermediate analogue inhibitors, α-hydroxybenzylphosphonate and benzohydroxamate, which are bound by the enzyme with affinities approximately 100-fold greater than that observed for the substrate. In Chapter 5, the contribution to MR catalysis from an active site, hydrophobic cavity is investigated using truncated and modified substrate and intermediate analogues, revealing an apparent binding preference in the hydrophobic cavity for the transition states and intermediate relative to the substrates. Chapter 6 describes the contributions from the active site residues Glu 317, Lys 164 and Asn 197 to both ground state and transition state stabilization by MR and assesses the degree to which benzohydroxamate acts as a mimic of the altered substrate in the transition state. The work presented here shows that the proficiency of MR does not originate from any single, dominant interaction but, rather, it is a function of strengthened interactions over the entire surface of the altered substrate molecule.

An improved understanding of the factors contributing to catalysis by MR can be extrapolated to a great number of enzymes catalyzing proton abstraction from carbon acids, particularly the growing number of enzymes in the enolase superfamily (Babbitt *et al.*, 1996). In addition, strategies used for effective inhibition of MR may be applied to other enzymes stabilizing enolic intermediates. Understanding the relative contribution of various active site residues to both ground state and transition state stabilization in MR may ultimately assist reengineering efforts aimed at designing racemases with altered substrate specificities and increased efficiencies, for use in dynamic kinetic resolutions (El Gihani & Williams, 1999; Strauss & Faber, 1999).

CHAPTER 2

AN ASSAY FOR MR USING
HIGH–PERFORMANCE LIQUID CHROMATOGRAPHY

2.1 Introduction

The assay of racemase enzymes presents a unique problem since both the substrate and the product are enantiomers and, therefore, share all physical properties with the exception of their interaction with plane polarized light. To assay a racemase, the assay must be sensitive to stereochemical configuration in order to distinguish between the enantiomers. Alternatively, in the case of racemases which catalyze the cleavage of a carbon–hydrogen bond, the reaction may be monitored by conducting the assay in D_2O and following the incorporation of deuterium into the product using NMR spectroscopy (Babu et al., 1975; Gallo et al., 1993). The deuterium exchange assay, however, does not permit one to readily distinguish between enantiomers and introduces the added complication of a solvent isotope effect.

Currently, there exist three principal methods for assaying MR activity - a coupled assay, a polarimetric assay, and a circular dichroism–based (CD) assay. The coupled assay exploits the stereospecificity of (S)-mandelate dehydrogenase, the enzyme following MR in the mandelic acid pathway of P. putida (figure 1.1). This membrane–bound, flavin mononucleotide–dependent enzyme catalyzes the oxidation of (S)-mandelate to benzoylformate with the concomitant reduction of 2,6-dichlorophenolindophenol (DCPIP) (Hegeman, 1970). The conversion of (R)-mandelate to (S)-mandelate is followed by monitoring the absorbance at 600 nm where only the oxidized form of the DCPIP chromaphore absorbs. The coupled assay suffers from a number of problems, the most significant being high turbidities of assay mixtures due to light scattering by the dehydrogenase–containing vesicles (Kenyon & Hegeman, 1979; Sharp et al., 1979). Several variations of the coupled assay have been reported. Weil–Malherbe (1966) originally assayed MR using two auxiliary enzymes, (S)-mandelate

dehydrogenase and benzoylformate decarboxylase. These enzymes converted (S)-mandelate to benzaldehyde which was measured spectrophotometrically. In another variation of the coupled assay, yeast L-lactate dehydrogenase (cytochrome b_2, EC 1.1.2.3) was used in place of (S)-mandelate dehydrogenase (Appleby & Morton, 1959; Hegeman et al., 1970). MR has also been assayed in the $S \rightarrow R$ direction using an (R)-specific mandelate dehydrogenase isolated from another strain of P. putida (Hegeman et al., 1970).

To overcome the problems associated with the coupled assay, Sharp et al. (1979) developed a CD–based assay. Since the two enantiomers of mandelic acid have molar ellipticities equal in magnitude but opposite in sign, the interconversion of (R)- and (S)-mandelate was followed directly by monitoring the CD spectral changes at 262 nm. The major advantage of this method is that it can be used to continuously assay the enzyme in either the forward or reverse directions. Polarimetry has also been used to monitor the enzyme–catalyzed racemization reaction (Hegeman et al., 1970; Landro et al., 1991; Mitra et al., 1995; Stecher et al., 1998; Weil-Malherbe, 1966). Both the CD– and polarimetry–based assays, however, are limited in their sensitivity at concentrations near or below the estimated K_m value (approximately 0.3 mM at pH 7.5 for (R)-mandelate) (Landro et al., 1991; Stecher et al., 1998; Whitman et al., 1985). The HPLC–based assay described in the present chapter is more universal than those previously described since it permits the facile and sensitive determination of MR activity in both reaction directions without any special modification of equipment available in most laboratories or the need to purify additional enzymes.

2.2 Materials and Methods

2.2.1 General

Racemic, (*R*)-, and (*S*)-mandelic acid were purchased from Sigma–Aldrich Canada Ltd. (Oakville, ON). (*R*)-Atrolactate was purchased from Lancaster Synthesis Inc. (Windham, NH, USA). Acetonitrile (HPLC–grade) was purchased from Fisher Scientific. All other chemicals were reagent grade or better.

2.2.2 Expression and Purification of Recombinant (His)$_6$–MR

A clone of recombinant, *N*-terminal hexahistidine–tagged MR ((His)$_6$-MR) from *Pseudomonas putida* was obtained from Professor John Gerlt (University of Illinois). The gene for wild–type MR, cloned into a pET15b plasmid vector (Novagen, Madison, WI), yields a construct which encodes the MR gene product with an *N*-terminal polyhistidine tag (MGSS(H)$_6$SSGLVPRGSHM$_1$...MR). The recombinant enzyme was overexpressed in and purified from *Escherichia coli* strain BL21(DE3) using standard techniques (Novagen, 1995). Luria–Bertani (LB) broth (5 mL) containing ampicillin (100 μg/mL) was inoculated with a single colony from a LB agar plate containing ampicillin (100 μg/mL). After 7 – 10 h of continual shaking at 37 °C, a 1 mL starter culture was used to inoculate each of two flasks of LB broth (750 mL) containing ampicillin (100 μg/mL). The flasks were incubated with shaking at 37 °C for 12 – 16 h (no IPTG was added), the cells were harvested by centrifugation (5000 × g, 10 min, 4 °C) and the cell pellets were frozen and stored at –20 °C. The frozen pellets were thawed and resuspended in ice cold 1× Binding Buffer (5 mM imidazole, 0.5 M NaCl, 20 mM Tris-HCl, pH 7.9) (Novagen, 1995) containing protease inhibitors (PMSF (1 mM) and

pepstatin A (1 μM)). The cells were broken by sonication and centrifuged (39,000 × g, 20 min, 4 °C). Following centrifugation, the supernatant was collected, filtered through a 0.45 μm filter and applied to a Ni^{2+}–charged His-Bind column prepared according to the manufacturer's instructions (Novagen, 1995). The loaded column was washed with 10 column volumes of 1× Binding Buffer containing protease inhibitors, 6 column volumes of 60 mM imidazole Wash Buffer (60 mM imidazole, 500 mM NaCl, 20 mM Tris-HCl, pH 7.9) and 6 column volumes of 100 mM imidazole Wash Buffer (100 mM imidazole, 500 mM NaCl, 20 mM Tris-HCl, pH 7.9). The recombinant enzyme was eluted from the column using Strip Buffer (100 mM EDTA, 500 mM NaCl, 20 mM Tris-HCl, pH 7.9) and was dialyzed overnight against MR Assay Buffer (100 mM Tris-HCl, 3.3 mM $MgCl_2$, pH 7.5) at 4 °C. Sample purity was confirmed by SDS–PAGE. The purified MR enzyme was aliquoted and stored at –80 °C for future use. Typically, 1.5 L of culture yielded approximately 5 – 10 mg of pure, recombinant, wild–type MR. The relatively low yields result from the strong tendency of MR to remain in the insoluble pellet following sonication (**figure 2.1A**), perhaps a result of the formation of inclusion bodies. Expression levels of recombinant MR were relatively high, even in the absence of IPTG (**figure 2.1B**). Therefore, cultures were not routinely induced with IPTG so that the lower rate of protein expression would limit the formation of inclusion bodies.

2.2.3 MR Assay

The enzymatic reaction was initiated by addition of MR (50 μL, 0.33 ± 0.01 μg protein/mL) to a solution (950 μL) containing $MgCl_2$ (3.3 mM), (R)-mandelate or (S)-
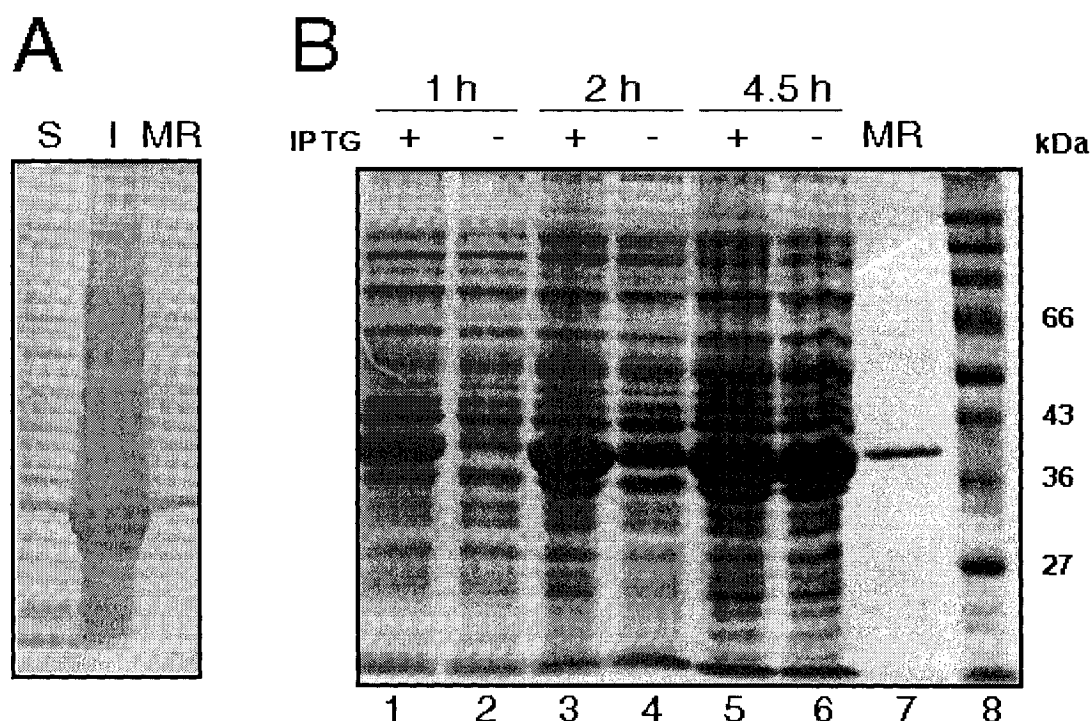
Figure 2.1 Characterization of MR expression and purification by SDS-PAGE. (A) The partitioning between the supernatant and insoluble pellet of overexpressed, (His)$_6$-MR from *E. coli* BL21(DE3) cells following sonication and ultracentrifugation (39 000 × g). Equal volumes were loaded from the soluble fraction (S) and the insoluble fraction (I). The purified enzyme (MR) was obtained by passing the soluble fraction through a Ni^{2+} affinity column as described in section 2.2.2. **(B)** Induction of *E. coli* BL21(DE3) cells expressing (His)$_6$-MR. Broth cultures (5 mL) were induced (± 1 mM IPTG; final concentration) after reaching an OD$_{600}$ = 0.7 and were harvested after incubating with shaking at 37 °C for the times indicated. The harvested pellets were resuspended in equal volumes prior to analysis by SDS-PAGE. The purified enzyme (MR) is included for comparison. Molecular weight markers are included in lane 8.

mandelate ranging in concentration between 0.1 mM and 5.0 mM, and Tris-HCl (0.10 M, pH 7.5). Both the coupled and CD assays are routinely conducted in HEPES buffer at pH 7.5, the pH optimum of the enzyme (Weil-Malherbe, 1966; Whitman *et al.*, 1985). However, HEPES buffer caused splitting of the peaks in the chromatogram and could not be used in the HPLC–based assay (see **figure 2.2 inset**). In addition, tricine, glycinamide, cholamine, MOPS, PIPES, and imidazole buffers also gave unsatisfactory chromatograms. The use of Tris buffer eliminated peak splitting in the chromatogram at all concentrations of product formed. Several other laboratories have reported the use of Tris buffer in place of HEPES and found that the substitution had no effect on the rate of racemization of (*R*)-mandelate (Hegeman *et al.*, 1970; Li *et al.*, 1995). Phosphate and pyrophosphate were not used as buffers since both are weak inhibitors of racemase activity (Hegeman *et al.*, 1970; Weil-Malherbe, 1966) and are incompatible with the HPLC column.

For the time course experiments, the reaction mixture was incubated for 0–15 min at 25 °C. The reaction was then terminated by boiling for 3 min. For routine assays, the reaction mixture was incubated for 4 min and 12 min at 25 °C and then terminated by boiling for 3 min. These two time points were then used to determine the initial velocities. The extent to which the (*R*)-mandelate (or (*S*)-mandelate) had racemized was then determined by injection of 50 μL of the reaction mixture onto the HPLC column. All buffers and solutions used in the assay were filtered through a 0.45 μm filter prior to use. No attempt was made to remove the small amount of protein present prior to injection. For inhibition studies, the reaction conditions were similar except (*R*)-atrolactate was present in the assay solution at concentrations ranging between 0 and 2.38 mM and Tris-HCl (0.05 M, pH 7.5) was used as the buffer.

2.2.4 Chromatographic Conditions

Separation of the enantiomers of mandelic acid was achieved on a Sumichiral OA-6100 reversed–phase column (4.6 mm × 150 mm, Phenomenex, Torrance, CA) which had a Sumichiral OA-6100 guard column (4 × 10 mm) connected. (R)- and (S)-Mandelate were eluted under isocratic conditions using 10% acetonitrile in 2 mM CuSO4 at a flow rate of 1.25 mL/min over a period of 25 min. The solvent was degassed prior to use. A Waters 510 pump and 680 controller were used for solvent delivery. Injections were made using a Rheodyne 7725i sample injector fitted with a 50 μL-injection loop. The eluted enantiomers of mandelic acid and inhibitors were detected by monitoring the absorbance at 254 nm using a Waters 486 tuneable absorbance detector. Chromatographic data were processed using the *PeakSimple* Chromatography Data System (SRI Instruments, Torrance, CA).

2.2.5 Data Analysis

The values of V_{max} and K_m were determined from plots of the initial velocity (v_i) versus substrate concentration ([S]) by fitting the data to equation 2.1 using nonlinear regression analysis and the program *EnzymeKinetics* v1.5b5 (Trinity Software; Plymouth, NH). Kinetic constants were determined in triplicate. The reported errors are the standard deviations. Protein concentrations were determined using the Bio-Rad Protein Assay (Bio-Rad Laboratories; Mississauga, ON) with bovine serum albumin (BSA) standards and k_{cat} values were obtained by dividing V_{max} values by the total enzyme concentration using M_r 40 728 (from the molecular weight of (His)6-MR calculated from the primary amino acid sequence (Ransom *et al.*, 1988)).

$$v_i = \frac{V_{max}[S]}{K_m + [S]} \tag{2.1}$$

52

2.3 Results

The chromatographic system efficiently resolves the enantiomers of mandelic acid (α = 3.10, R_S = 3.88 for 1 mM (R,S)-mandelate). Concentrations of either (R)- or (S)-mandelate ranging from 5 μM to 500 μM could be measured accurately ($\pm \leq 5\%$) and gave a linear absorbance response at 254 nm. Although the present method may be used to assay the enzyme–catalyzed racemization of either (R)- or (S)-mandelate, it has been used routinely to follow racemization of (R)-mandelate and the data presented are for assays in that direction (**figure 2.2**).

The production of (S)-mandelate from (R)-mandelate varied linearly with time over 15 min at all substrate concentrations (**figure 2.3**). In addition, using 5 mM (R)-mandelate as the substrate, production of (S)-mandelate was found to vary linearly with increasing enzyme concentration over the range of 1.7 to 16.3 ng/mL (**figure 2.4**). A typical Michaelis–Menten plot for MR operating in the $R \rightarrow S$ direction is shown in **figure 2.3 (inset)**. The observed values of k_{cat} and K_m are 676 $\pm$ 26 s^{-1} and 0.79 $\pm$ 0.09 mM respectively. In the $S \rightarrow R$ direction, the values of k_{cat} and K_m are 690 $\pm$ 49 s^{-1} and 0.74 $\pm$ 0.16 mM, respectively. Removal of the histidine tag by thrombin cleavage (Novagen, 1995) did not alter the observed k_{cat} and K_m values.

To demonstrate that the assay may be utilized for inhibition studies, the inhibition constant for (R)-atrolactate, a known competitive inhibitor of MR (Landro et al., 1994), was determined. The observed inhibition was competitive with respect to (R)-mandelate and the inhibition constant (K_i) was equal to 0.53 $\pm$ 0.02 mM (**figure 2.5**). This value agrees well with the K_i value of 0.41 reported by Landro et al. (1994) for (R)-atrolactate when (R)-mandelate is the substrate.
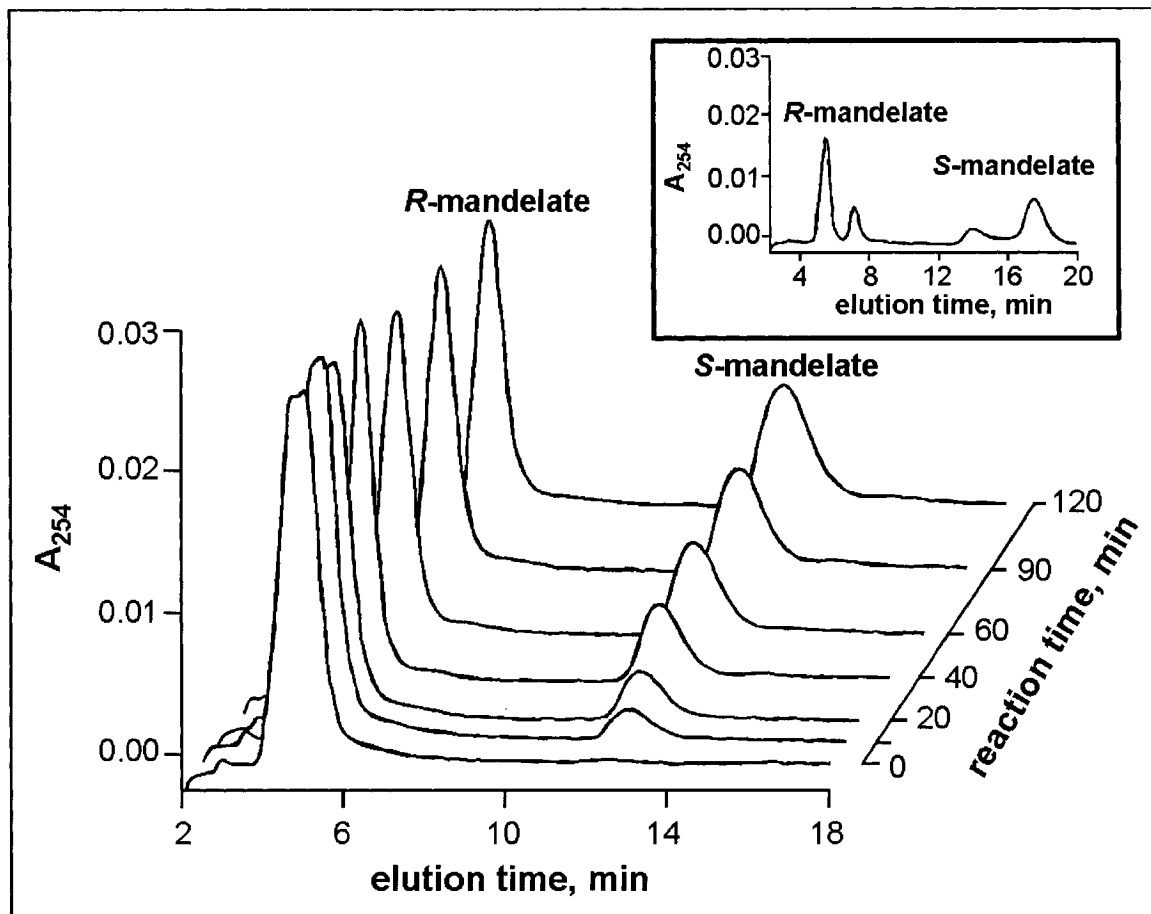
Figure 2.2 HPLC chromatograms showing the separation of (*R*)- and (*S*)-mandelate on a Sumichiral OA-6100 column. Chromatography conditions and the assay protocol were as described in section 2.2. The chromatograms shown are for samples taken from enzyme reactions containing Tris-HCl buffer (100 mM, pH 7.5) containing $MgCl_2$ (3.3 mM), and an initial (*R*)-mandelate concentration equal to 1 mM. Reactions were initiated by the addition of MR (15 ng/mL) and were then terminated by boiling at the times indicated. Inset. HPLC chromatogram of 1 mM (*R,S*)-mandelate in HEPES buffer (50 mM, pH 7.5) containing $MgCl_2$ (3.3 mM). This chromatogram shows the splitting of peaks that was commonly observed in buffers other than Tris-HCl.
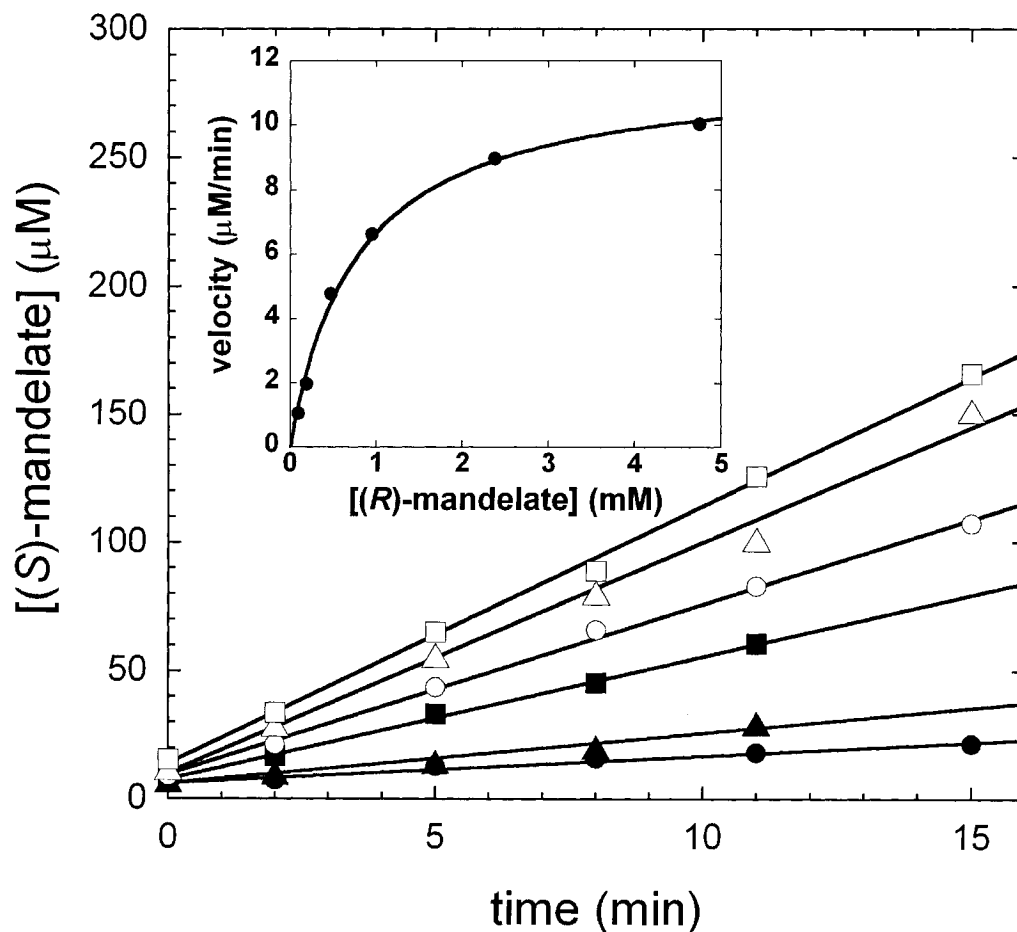
Figure 2.3 Representative time-courses for the production of (S)-mandelate by MR at initial concentrations of (R)-mandelate equal to 0.095 mM (●), 0.190 mM (▲), 0.475 mM (■), 0.950 mM (○), 2.375 mM (△) and 4.50 mM (□). Assay conditions were as described in section 2.2. **Inset.** Michaelis-Menten plot for the conversion of (R)-mandelate to (S)-mandelate catalyzed by MR. The curve shown is that determined by fitting the Michaelis-Menten equation using non-linear regression analysis. The values of K_m and V_{max} are equal to 0.71 ± 0.05 mM and 12.7 ± 0.3 μM/min, respectively.
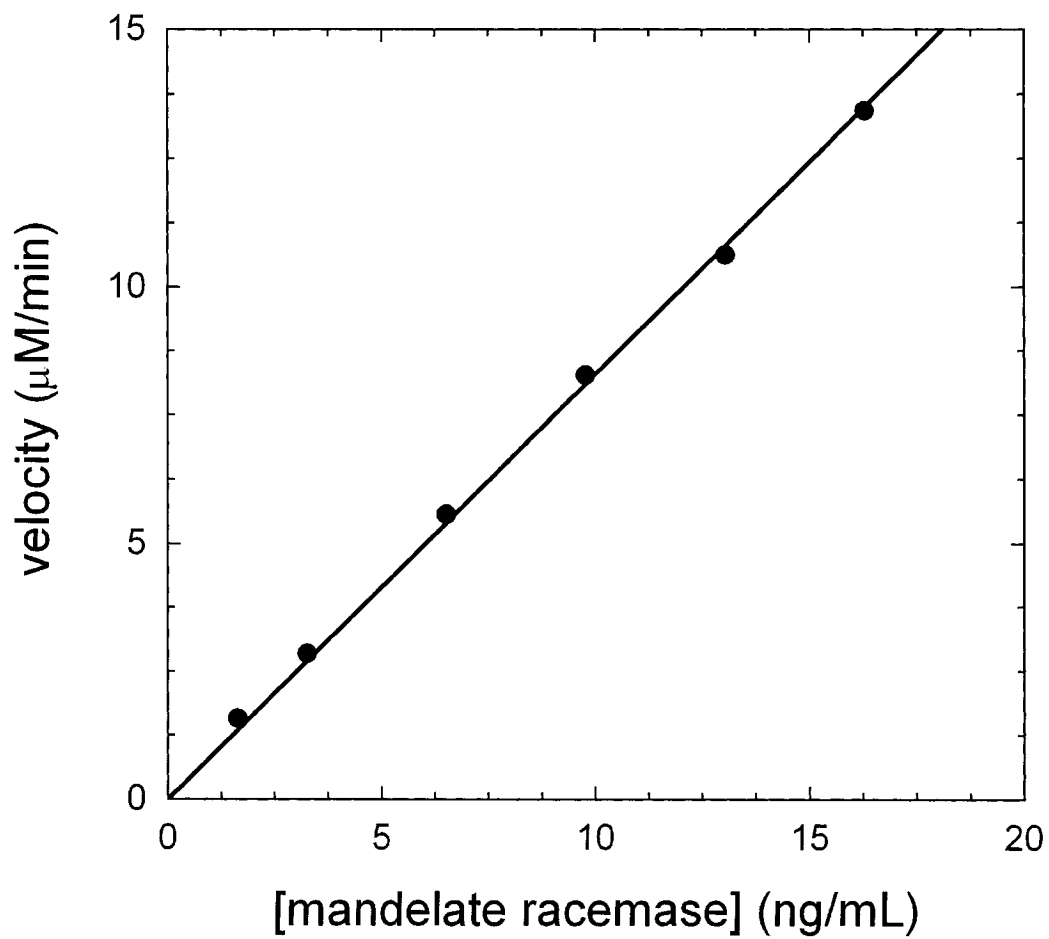
Figure 2.4 Initial rates as a function of enzyme concentration. The concentration of (*R*)-mandelate was 4.75 mM and the other assay conditions are as described in section 2.2.
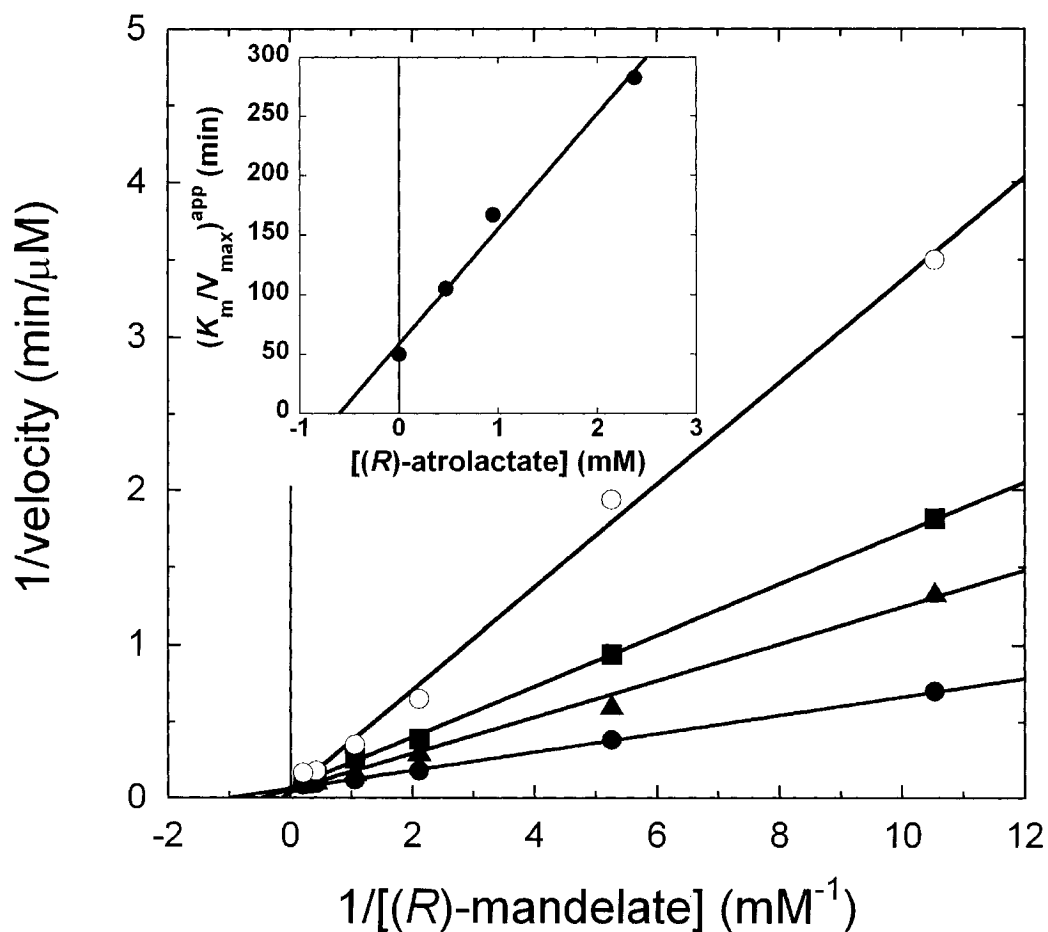
Figure 2.5 Lineweaver-Burk plot for the competitive inhibition of MR activity by (R)-atrolactate. Initial concentrations of (R)-mandelate ranged between values of 0.095 mM and 4.75 mM. (R)-Atrolactate concentrations were 0 mM (●), 0.475 mM (▲), 0.950 mM (■), and 2.375 mM (○). Assay conditions were as described in section 2.2. **Inset.** Replot of $((K_m/V_{max})^{app})$ as a function of (R)-atrolactate concentration. The K_i value for (R)-atrolactate is equal to 0.53 ± 0.02 mM.

2.4 Discussion

The application of HPLC techniques to enzyme assays is now relatively widespread (Syed, 1993). Such techniques are particularly useful when the enzymes are racemases which catalyze the interconversion of stereoisomers for which there are few techniques that permit one to distinguish between reactant and product. HPLC–based assays offer several advantages in that they are sensitive, relatively rapid and usually no modification of standard HPLC equipment is required. Major disadvantages include the length of time required for samples to elute from the column and the use of a fixed time assay.

Methods for estimating the enantiomers of mandelic acid by HPLC include both determinations of derivatized forms of mandelic acid (Drummond *et al.*, 1989) and direct determinations. The latter method is more desirable for enzyme assays because it avoids the additional derivatization step. A number of columns are commercially available that separate the enantiomers of mandelic acid. Some of these have cyclodextrins as the chiral stationary phase while others have enantiomers of amino acids as the chiral stationary phase. In an ideal assay, the enantiomers should be resolved rapidly (e.g., elution times < 15–20 min) and the peaks corresponding to the enantiomers should be well resolved. Generally, cyclodextrin–based chiral stationary phases provide rapid separation but poor resolution. For example, Armstrong and co-workers (Armstrong *et al.*, 1988) reported a value of α = 1.07 and R_S = 1.4 for mandelic acid using a β-cyclodextrin bonded phase. Enhanced resolution (α = 2.54 and R_S = 3.33) was reported by Li and Purdy (1992) using a methylbenzylamine–modified β-cyclodextrin chiral stationary phase. Unfortunately, this modified cyclodextrin stationary phase is not available commercially. Of the commercially available columns, the Sumichiral OA-6100 column, with an adsorbed L-tartaric acid-mono-L-valine-(S)-1-(α-naphthyl)ethylamide stationary phase, provided efficient resolution of the enantiomers of mandelic acid in a convenient time period. A

similar column has been employed by Takahashi *et al.* (1995) to study the asymmetric degradation of (*S*)-mandelate by various microorganisms.

The validity of the fixed–time assay was established by demonstrating that the production of (*S*)-mandelate from (*R*)-mandelate varied linearly with time over 15 min at all substrate concentrations (**figure 2.3**). The non–zero intercepts in figure 2.2 result from the inactivation of MR by boiling: enzyme inactivation in the boiling water bath is not immediate and, consequently, the apparent zero time point is offset from the true zero time point by nearly a minute. Since the initial velocity rate is a reflection of the slope of the line, and is independent of the y-intercept, the non–zero intercepts in the initial velocity curves do not interfere with the interpretation of the initial velocity kinetics. In addition, production of (*S*)-mandelate was found to vary linearly with increasing enzyme concentration (**figure 2.4**). At low enzyme concentrations, velocities can deviate from linearity. For example, at low concentrations, CTP synthetase deviates from linearity as a result of changes in equilibrium between the oligomerization states of the enzyme (Anderson, 1983; Van Kuilenburg *et al.*, 1994). Such deviations can complicate the interpretation of initial velocity kinetics, particularly in the presence of inhibitors which effectively lower the concentration of free enzyme in solution. An enzyme concentration of 16.5 ng/mL was chosen for all subsequent assays to ensure that initial velocities were within the linear range of the free enzyme concentration.

The values of k_{cat} are in good agreement with the value of 700 s^{-1} reported for pure wild–type MR (Powers *et al.*, 1991) while the values of K_m are slightly larger than those reported. Several assay conditions were modified to be consistent with those reported, including ionic strength, Mg^{2+} concentration, and removal of the *N*-terminal poly–histidine tag from the recombinant enzyme by thrombin cleavage. None of these conditions affected the kinetics for wild-type MR observed using the HPLC assay. It is likely that the discrepancy in K_m values arises from the difficulties associated with measuring MR initial velocities below substrate concentrations of 1 mM when using the

other, less sensitive assay techniques. It should be noted that the values of both k_{cat} and K_m obtained using the HPLC assay are in excellent agreement with values later obtained with the CD–based assay (i.e., see Chapters 3 & 4).

To demonstrate that the assay may be utilized for inhibition studies, the inhibition of MR activity by (R)-atrolactate, a known competitive inhibitor of the enzyme (Landro *et al.*, 1994), was investigated. The observed inhibition was competitive with respect to (R)-mandelate and the inhibition constant (K_i) was equal to 0.53 ± 0.02 mM (**figure 2.5**). This value agrees well with the K_i value of 0.41 mM reported by Landro *et al.* (1994) for (R)-atrolactate when (R)-mandelate is the substrate. (R)-Atrolactate has a retention time (t_r) equal to 11.54 min and, when a new column is employed, its peak in the chromatogram does not overlap with the peaks corresponding to either (R)-mandelate (t_r = 6.48 min) or (S)-mandelate (t_r = 16.15). However, as a column receives multiple injections, the retention times for (R)-mandelate and (S)-mandelate are reduced (e.g., to values of t_r = 4.89 min and t_r = 12.80 min, respectively). Thus, with an older column, an inhibitor may co-elute with the product enantiomer. This problem might be overcome by changing the mandelate enantiomer being used as the substrate, provided that it is well resolved from the inhibitor peak in the chromatogram. The problem may be more significant, however, when racemic inhibitors are being employed since two additional peaks will be present in the chromatogram, increasing the potential for overlap with the peaks corresponding to either (R)- or (S)-mandelate. Finally, for inhibitors which are strongly retained by the HPLC column, relative to (R)- and (S)-mandelate, the time required to analyze the reaction mixtures may be substantially increased.

This chapter has described a fixed–time assay for the quantification of MR activity. The assay involves enzymatic conversion of (R)-mandelate to (S)-mandelate (or the reverse reaction) followed by separation and detection of the substrate and product using isocratic reversed–phase high performance liquid chromatography on a Sumichiral OA-6100 column and absorbance detection at 254 nm. This method offers a more

sensitive alternative to the existing CD–based and polarimetric assays for MR and can be used to follow the reaction in either direction. The method is applicable, in principle, to the assay of many other racemases. This newly developed assay method will be used to assess the inhibition of MR by a series of intermediate analogue inhibitors (Chapter 4).

CHAPTER 3

KINETICS AND THERMODYNAMICS OF MR CATALYSIS

3.1 Introduction

The proficiency of an enzyme catalyst is a function of its ability to stabilize the altered substrate in the transition state and may be defined as the reciprocal of the virtual dissociation constant of the enzyme–substrate complex in the transition state (K_{tx}) (equation 3.1) (Radzicka & Wolfenden, 1995). MR is extremely proficient at discriminating between the substrate in the ground state and the altered substrate in the transition state, binding the latter with an apparent association constant equal to 5×10^{18} M^{-1}, and reducing the free energy of activation for the reaction by 26 kcal/mol (Bearne & Wolfenden, 1997). To develop a more detailed understanding of transition state stabilization by MR, it is of interest to determine both the enthalpic and entropic contributions to the free energy of transition state stabilization by investigating the effect of temperature on MR proficiency. Such studies have been conducted with only a limited number of enzymes including fumarase, ribonuclease A, and carbonic anhydrase (Bearne & Wolfenden, 1995), and most thoroughly for cytidine deaminase (Snider et al., 2000). For these enzymes, transition state stabilization is largely enthalpy–based (Wolfenden et al., 1999).

$$K_{tx} = k_{non} / \left(k_{cat} / K_S \right) \qquad (3.1)$$

To obtain a meaningful value of K_{tx}, either the dissociation constant for the enzyme–substrate complex in the ground state (K_S) must be determined or the Michaelis constant (K_m) must be shown to approximate K_S. In addition, k_{cat} *must* describe the chemical step for which the rate constant of the corresponding nonenzymatic reaction (k_{non}) has been determined. This is often not the case, however, when substrate binding or product release is partially rate–determining (Wolfenden, 1972; 1974), or when the

enzyme–catalyzed and nonenzymatic reactions do not proceed via the same mechanism. For example, if the rate of product release for an enzyme–catalyzed reaction is kinetically significant, k_{cat} will overestimate the activation energy barrier for the enzyme–catalyzed chemical step and the free energy of transition state stabilization will, consequently, be underestimated. Wolfenden has discussed these caveats in detail (Wolfenden, 1972; 1974).

For MR, the substrate kinetic deuterium isotope effect (k_{cat}^{H}/k_{cat}^{D}) for proton abstraction from (R)-mandelate is ~3.2 (Mitra et al., 1995; Whitman et al., 1985) and the solvent deuterium isotope effect on k_{cat} is ~2.3 (Mitra et al., 1995). These observations led Gerlt and co-workers (Mitra et al., 1995) to suggest that both proton abstraction from the substrate and proton delivery to form the product are each partially rate–determining and that substrate association and product dissociation are faster than the proton transfer reactions. The possibility remains, however, that diffusive processes such as substrate association or product dissociation are also partially rate–determining. Indeed, partial diffusion control has been observed for several enzymes including β-glucosidase (Dale et al., 1986), alkaline phosphatase (Simopoulos & Jencks, 1994), 1-aminocyclopropane-1-caboxylate synthase (Li et al., 1997), ribonuclease T_1 (Steyaert et al., 1991), subtilisin BPN' (Stratton et al., 2001), and chorismate mutase (Mattei et al., 1999) for which the values of k_{cat}/K_m are on the order of 10^5–10^6 (cf. k_{cat}/K_m for MR $\approx 10^6$ $M^{-1}s^{-1}$), well below the theoretical limit of 10^8–10^{10} $M^{-1}s^{-1}$ for a diffusion–limited enzyme–catalyzed reaction (Alberty & Hammes, 1958).

The dependence of an enzyme–catalyzed reaction on solvent viscosity offers a useful means of determining whether or not a reaction is completely or partially limited by the rates of substrate association and/or product dissociation (Brouwer & Kirsch, 1982). An increase in the solution viscosity through the addition of monomeric, polyhydroxylated molecules such as glycerol or sucrose decreases the rates for diffusive processes involving small molecules in solution without perturbing the energy barrier for

the enzyme–catalyzed chemical step. Thus, as the solution viscosity is increased, the energy barriers on the enzyme for substrate association and product dissociation are raised and, if these energy barriers are kinetically significant, the rate of the enzyme–catalyzed reaction is decreased. MR is ideally suited for study using the viscosity variation method as it involves the conversion of a single substrate to a single product and can easily be assayed in both reaction directions. The dependence on viscosity of the kinetic constants for the reaction catalyzed by MR can, therefore, yield the individual rate constants for the major steps along the reaction coordinate and can clearly establish the extent to which the reaction is limited by substrate association and/or product dissociation.

In the present chapter, it is shown that MR displays a partial viscosity dependence, indicating that the chemical step is not completely rate–determining. Using kinetic measurements obtained at various solvent viscosities, the values of the rate constants that comprise k_{cat} and k_{cat}/K_m in both reaction directions are determined. In addition, the alternative substrate, (S)-p-nitromandelate, is used in combination with (R,S)-mandelate to demonstrate that $K_m \approx K_S$ for both (R)- and (S)-mandelate. This information, combined with measurements of the temperature dependence of both the catalytic efficiency of the enzyme–catalyzed chemical step and the rate constant for the corresponding nonenzymatic reaction, permit the determination of the temperature dependence of K_{tx}. This chapter reports the enthalpy and entropy changes associated with substrate binding, the activation barrier for conversion of bound substrate to bound product, and transition state stabilization during MR–catalyzed racemization of (R)-mandelate. Although the high proficiency of MR is achieved principally by enthalpy reduction, there is also a favorable and significant entropic contribution.

3.2 Materials and Methods

3.2.1 General

Acetonitrile (HPLC–grade) and poly(ethylene glycol) (PEG; M_r 6000 – 7500) were purchased from Fisher Scientific (Nepean, ON). Sucrose and glycerol were purchased from BDH, Inc. (Toronto, ON). Racemic-, (R)-, and (S)-mandelic acid, 4-nitrobenzaldehyde, (R)-(+)-α-methylbenzylamine, D-(+)-trehalose, ficoll 400, and all other reagents were purchased from Sigma–Aldrich Canada Ltd. (Oakville, ON). (R,S)-p-Nitromandelic acid was synthesized in the Bearne laboratory by Shauna Drover according to the protocol described by Westkaemper and Hanzlik (1981). (S)-p-Nitromandelic acid was resolved by Shauna Drover to 99% enantiomeric excess from the racemic mixture (Newman, 1981). CD assays were conducted using a JASCO J-810 spectropolarimeter. The CD spectrum (200 – 260 nm) of MR obtained in the presence of sucrose (35%) was corrected by subtracting the CD spectrum arising solely from the sucrose (35%).

3.2.2 Expression and Purification of Recombinant (His)$_6$–MR

Recombinant wild–type MR from *Pseudomonas putida* was overexpressed and purified according to the protocol described in section 2.2.2. The N197A mutant of MR was generated as described in section 6.2.2 and was overexpressed and purified as described in section 2.2.2. Once eluted from the Ni^{2+} affinity columns, the enzyme solutions were dialyzed into HEPES buffer (0.1 M, pH 7.5) containing $MgCl_2$ (3.3 mM) and NaCl (0.2 M).

3.2.3 Viscosity Effects

Both monomeric viscosogens (sucrose, trehalose, and glycerol) and polymeric viscosogens (PEG and ficoll 400) were used in the present study. Stock solutions of these viscosogenic reagents were prepared at twice the desired final concentration, diluted 1:1 with HEPES buffer (0.2 M, pH 7.5) containing $MgCl_2$ (6.6 mM), and passed through a

sintered glass filter to remove any suspended material. The kinematic viscosities were subsequently measured in triplicate using a Cannon–Fenske viscometer at 25 °C and using HEPES buffer (0.1 M, pH 7.5) containing $MgCl_2$ (3.3 mM) as the reference. Solution densities were determined gravimetrically at 25 °C and the relative solvent viscosities ($\eta_{rel} = \eta/\eta^{o}$, where the superscript refers to the viscosity of HEPES buffer in the absence of added viscosogen) of the viscosogen–containing buffer solutions were calculated from the product of these densities (ρ) and the measured kinematic viscosities (η/ρ). Relative viscosities were approximately 1.32, 1.88, 2.48, 3.06, and 3.42 for 10, 20, 27.5, 32.5, and 35% (w/v) sucrose solutions, respectively; η_{rel} = 1.73, 2.10, 2.73, and 3.43 for 20, 25, 30, and 35% (w/v) trehalose solutions, respectively; η_{rel} = 1.44, 1.69, 2.09, 2.73, 3.20, and 4.01 for 10, 15, 20, 25, 27.5, and 30% (w/v) glycerol solutions, respectively; η_{rel} = 1.22, 1.89, 2.81, and 4.03 for 1.5, 3, 6, and 8% (w/v) ficoll 400 solutions, respectively; η_{rel} = 1.61, 2.50, 5.37, and 8.49 for 2.5, 5, 6, and 7.5% (w/v) PEG solutions, respectively.

Kinetic measurements were conducted using the CD assay at 262 nm described by Sharp et al. (Sharp et al., 1979). Reaction mixtures were prepared in rectangular quartz cuvettes with a 1 cm light path. Typically, 950 μL of (R)- or (S)-mandelate (0.5 to 20.0 mM) in HEPES buffer (0.2 M, pH 7.5) containing $MgCl_2$ (6.6 mM) was mixed with 950 μL of the viscosogen–containing stock solution (prepared at twice the desired final concentration). The reaction was initiated by addition of 100 μL of either wild–type MR (5 μg/mL) or the N197A mutant (468 μg/mL) in HEPES buffer (0.1 M, pH 7.5) containing $MgCl_2$ (3.3 mM) and BSA (0.1%). All kinetic experiments were conducted in the plateau region of the pH–log k_{cat} (Landro et al., 1991) and pH–log K_m (St. Maurice & Bearne, 2000) profiles for the enzyme–catalyzed racemization reaction, and well above the pK_a value of 3.41 for mandelic acid (Jencks & Regenstein, 1968). Hence, the effect of both the viscosogenic cosolutes and changes in temperature (vide infra) on the pH–profiles of the enzyme–catalyzed reaction are expected to be negligible.

3.2.4 Temperature Effects

For each reaction conducted at a given temperature, a stock solution of (*R*)-mandelate (20 mM) was prepared in HEPES buffer (0.2 M, pH 7.5) containing $MgCl_2$ (6.6 mM). The pH of both the buffer and the (*R*)-mandelate stock solution was adjusted at each assay temperature to pH 7.5 relative to thermostatted standards. The relative viscosities for the sucrose solutions at 10, 15, 20, 25, 30, 35, 40, and 45 °C, were calculated from the product of the kinematic viscosities measured at each of these temperatures and the densities of the sucrose solutions at each temperature (calculated using the equation reported by Bubnik *et al.* (1995)). MR activity was assayed at each of these temperatures using the CD assay. The molar ellipticity for (*R*)-mandelate did not change over this temperature range. All assays were conducted in rectangular quartz cuvettes with a 1.0 cm light path. Additional stock solutions of (*R*)-mandelate (0.5 to 20 mM) were prepared by dilution of the stock 20 mM solution with HEPES buffer (0.2 M, pH 7.5) containing $MgCl_2$ (6.6 mM). Substrate solutions (1.900 mL) were prepared by mixing 950 µL of the stock (*R*)-mandelate solutions with 950 µL of the desired sucrose–containing stock solution to yield (*R*)-mandelate assay concentrations ranging between 0.25 and 10.0 mM in HEPES buffer (0.1 M, pH 7.5) containing $MgCl_2$ (3.3 mM). Each substrate solution was incubated for 5 min in a water bath at the desired temperature prior to initiation of the reaction by addition of MR (100 µL, 1.0 to 12.0 µg/mL) in HEPES buffer (0.1 M, pH 7.5) containing $MgCl_2$ (3.3 mM) and BSA (0.1%). The progress of the reaction was monitored by following the change in ellipticity at 262 nm. The reaction was maintained at the desired temperature using a thermostatted rectangular cell holder with a remote temperature probe connected to a Neslab RTE-111 water bath.

3.2.5 Determination of K_S

The value of K_S for (R)- and (S)-mandelate was determined by assaying the activity of MR with the alternative substrate (S)-p-nitromandelate in the presence of the "competitive inhibitor", (R,S)-mandelate (see section 3.3). MR activity was assayed using a CD assay similar to that described by Sharp *et al.* (1979), however, the CD signal was monitored at 232 nm over 5 min. Final concentrations of (S)-p-nitromandelate were 1.0, 1.5, 2.0, 2.5, 3.0 and 3.5 mM. Final concentrations of (R,S)-mandelate were 0.0, 0.5, 1.0, and 2.0 mM. Assays were conducted at 25 °C in HEPES buffer (0.1 M, pH 7.5) containing $MgCl_2$ (3.3 mM) using a rectangular quartz cuvette with a 0.1 cm light path. Reactions were initiated by addition of MR (50 µL, 2.0 µg/mL, 0.1% BSA) to a solution (200 µL) containing both (S)-p-nitromandelate (substrate) and (R,S)-mandelate (inhibitor) that had been pre-incubated at 25 °C for 5 min. (Initiation of the reaction with (S)-p-nitromandelate following a 5 min pre-incubation of 2 µg/mL MR with (R,S)-mandelate did not change the observed initial velocity.) Apparent V_{max}/K_m values were determined in triplicate at each concentration of (R,S)-mandelate.

3.2.6 Data Analysis

The values of V_{max} and K_m were determined from plots of the initial velocity (v_i) versus substrate concentration ([S]) by fitting the data to equation 2.1 using nonlinear regression analysis and the program *EnzymeKinetics* v1.5b5 (Trinity Software; Plymouth, NH). Kinetic constants were determined in duplicate for the temperature dependence experiments and in triplicate for all other experiments. The reported errors are the standard deviations. Protein concentrations were determined using the Bio-Rad Protein Assay (Bio-Rad Laboratories; Mississauga, ON) with BSA standards and k_{cat} values were obtained by dividing V_{max} values by the total enzyme concentration using M_r 40 728.

3.3 Results

3.3.1 Viscosity Effects

The rates of external steps such as those occurring during enzyme–substrate association and enzyme–product dissociation are expected to be inversely proportional to the solvent microviscosity while the rates of internal processes (i.e., those occurring within enzyme–substrate complexes) are expected to be independent of solvent microviscosity (Adams & Taylor, 1992; Bazelyansky et al., 1986; Blacklow et al., 1988; Brouwer & Kirsch, 1982; Caldwell et al., 1991; Christensen et al., 1990; Goldberg & Kirsch, 1996; Hale et al., 1993; Hardy & Kirsch, 1984; Kurz et al., 1987; Li et al., 1997; Mattei et al., 1999; Pocker & Janjic, 1987; Simopoulos & Jencks, 1994; Steyaert et al., 1991; Stone & Morrison, 1988; Stratton et al., 2001). In order to determine whether substrate binding or product release is rate–determining for the reaction catalyzed by MR, the viscosity variation method was employed (Brouwer & Kirsch, 1982) to investigate the dependence of k_{cat} and k_{cat}/K_m on viscosity in both the $R{\to}S$ (table 3.1) and $S{\to}R$ (table 3.2) reaction directions. A partial viscosity dependence was observed for relative values of k_{cat} (i.e., $k_{cat}^{o}/k_{cat}^{\eta}$) in the presence of both sucrose (figures 3.1A and 3.2A) and trehalose (figure 3.3A), suggesting that product release is partially rate–determining for MR catalysis in both reaction directions.

Studies using the viscosity variation method are subject to a variety of potential complications which must be considered before the results can be interpreted in terms of diffusion–controlled processes. The high concentrations of polyhydroxylated compounds employed as viscosogenic cosolutes can have a variety of diffusion–unrelated effects including alteration of the free energy of both unbound and bound species, alteration of the pH–profile for the kinetic parameters (see section 3.2.3), perturbations in solvent structure, alteration of substrate and enzyme conformations, and inhibition or activation of the enzymatic reaction. Assurances against the occurrence of effects that do not involve diffusive processes can be obtained by (a) demonstrating that similar kinetic

Table 3.1 Dependence of $k_{cat}^{R \to S}$ and $(k_{cat}/K_m)^{R \to S}$ on viscosity for wild–type and N197A MR.

Viscosogen [% (w/v)]	η/η°	$k_{cat}^{R \to S}$ (s^{-1})	$(k_{cat}/K_m)^{R \to S}$ ($\times 10^5$ M^{-1}s^{-1}) observed	corrected[a]
		Sucrose (wild–type)		
0.0	1.00	654 ± 58	6.41 ± 0.57	6.41 ± 0.57
10.0	1.32	556 ± 32	5.90 ± 1.20	5.63 ± 1.14
20.0	1.88	506 ± 43	5.69 ± 0.60	5.05 ± 0.53
27.5	2.48	446 ± 25	6.21 ± 0.56	5.03 ± 0.45
32.5	3.06	399 ± 26	5.76 ± 0.62	4.42 ± 0.48
35.0	3.42	370 ± 35	6.21 ± 1.91	4.49 ± 1.38
		Sucrose (N197A)		
0.0	1.00	17.9 ± 1.2	0.027 ± 0.005	0.027 ± 0.005
10.0	1.34	18.3 ± 3.1	0.029 ± 0.006	0.028 ± 0.006
20.0	1.88	19.7 ± 3.7	0.031 ± 0.009	0.027 ± 0.008
27.5	2.56	18.2 ± 2.0	0.039 ± 0.008	0.029 ± 0.006
32.5	3.18	20.2 ± 4.4	0.043 ± 0.013	0.028 ± 0.008
35.0	3.69	21.2 ± 5.3	0.043 ± 0.014	0.025 ± 0.008
		Trehalose (wild–type)		
0.0	1.00	779 ± 45	8.38 ± 1.78	
20.0	1.73	663 ± 22	7.45 ± 1.49	
25.0	2.10	614 ± 8	8.94 ± 0.60	
30.0	2.73	506 ± 27	9.85 ± 1.81	
35.0	3.43	435 ± 16	7.72 ± 2.02	

[a]The slope of relative $(k_{cat}/K_m)^{R \to S}$ vs. η/η° for the N197A enzyme (slope = –0.163 ± 0.002; figure 3.1) in the presence of sucrose was used to correct the observed relative $(k_{cat}/K_m)^{R \to S}$ values for the wild–type enzyme using the equation $[(k_{cat}/K_m)^\circ/(k_{cat}/K_m)^\eta]_{corr} = [(k_{cat}/K_m)^\circ/(k_{cat}/K_m)^\eta]_{obs} + 0.16(\eta/\eta^\circ - 1)$, based on references (Blacklow et al., 1988) and (Sampson & Knowles, 1992).

Table 3.2 Dependence of $k_{cat}^{S \to R}$ and $(k_{cat}/K_m)^{S \to R}$ on viscosity for wild–type and N197A MR.

viscosogen [% (w/v)]	η/η°	$k_{cat}^{S \to R}$ (s^{-1})	$(k_{cat}/K_m)^{S \to R}$ ($\times 10^5$ M^{-1}s^{-1}) observed	corrected[a]
		Sucrose (wild–type)		
0.0	1.00	491 ± 14	6.11 ± 0.64	6.11 ± 0.64
10.0	1.32	464 ± 39	6.10 ± 1.20	5.79 ± 1.14
20.0	1.88	389 ± 35	6.63 ± 1.05	5.71 ± 0.90
27.5	2.48	349 ± 42	6.04 ± 1.52	4.85 ± 1.22
32.5	3.06	314 ± 42	5.79 ± 2.15	4.36 ± 1.62
35.0	3.42	291 ± 13	5.74 ± 0.67	4.15 ± 0.48
		Sucrose (N197A)		
0.0	1.00	4.4 ± 0.3	0.025 ± 0.009	0.025 ± 0.009
10.0	1.34	4.5 ± 0.2	0.031 ± 0.013	0.029 ± 0.012
20.0	1.88	4.3 ± 0.2	0.029 ± 0.009	0.025 ± 0.008
27.5	2.56	4.2 ± 0.3	0.039 ± 0.009	0.028 ± 0.006
32.5	3.18	4.1 ± 0.7	0.034 ± 0.026	0.023 ± 0.017
35.0	3.69	4.0 ± 0.4	0.048 ± 0.008	0.026 ± 0.004

[a]The slope of relative $(k_{cat}/K_m)^{S \to R}$ vs. η/η° for the N197A enzyme (slope = –0.174 ± 0.003; figure 3.2) in the presence of sucrose was used to correct the observed relative $(k_{cat}/K_m)^{S \to R}$ values for the wild–type enzyme using the equation $[(k_{cat}/K_m)^\circ/(k_{cat}/K_m)^n]_{corr} = [(k_{cat}/K_m)^\circ/(k_{cat}/K_m)^n]_{obs} + 0.17(\eta/\eta^\circ - 1)$, based on references (Blacklow et al., 1988) and (Sampson & Knowles, 1992).
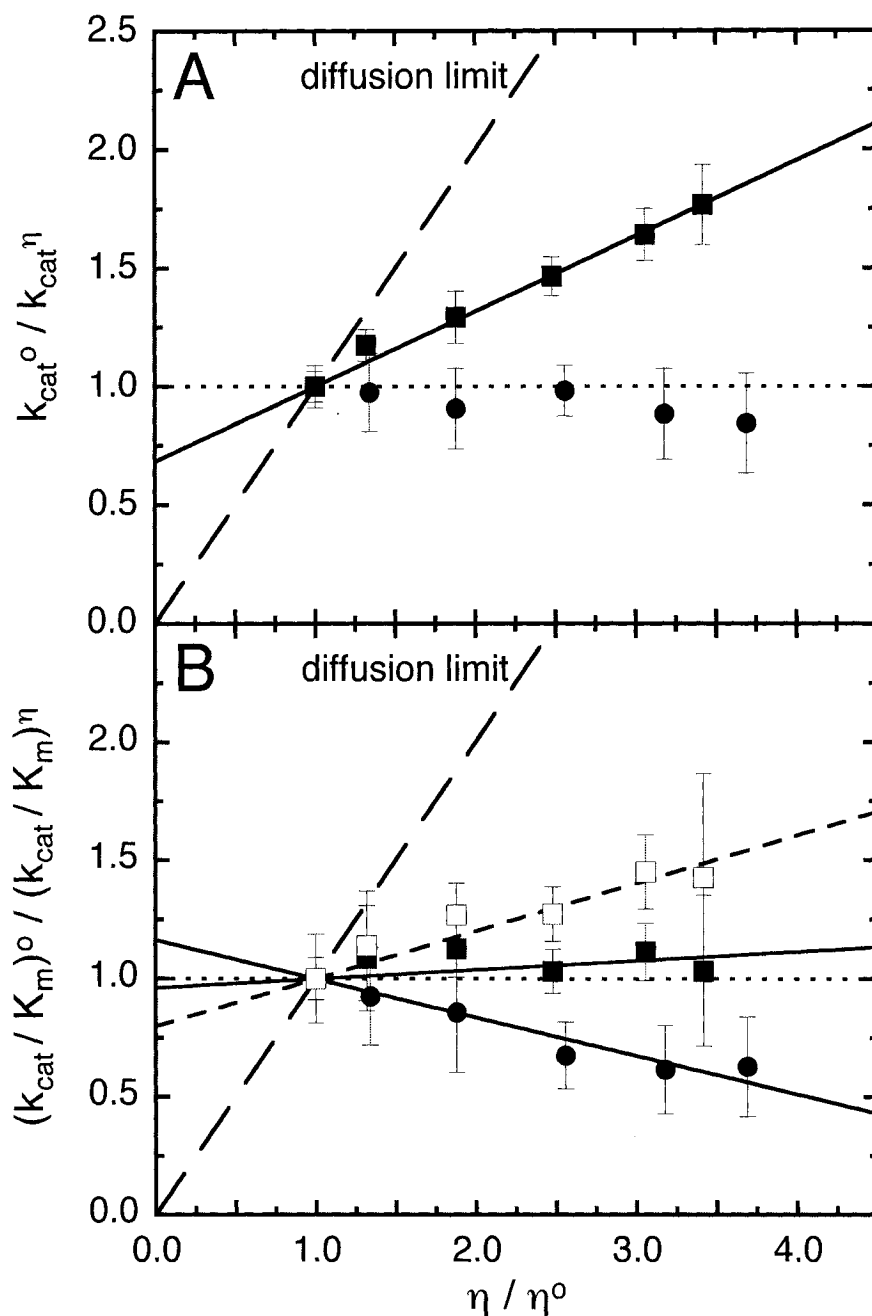
Figure 3.1 Dependence of relative kinetic parameters for the racemization of (R)-mandelate on relative solvent viscosity. The values of relative k_{cat} (**A**) and relative k_{cat}/K_m (**B**) for both wild-type MR (■) and N197A (●) were determined at 25 °C at varying values of η_{rel} using sucrose as the viscosogen. The relative k_{cat} values for wild-type MR were proportional to η_{rel} (slope = 0.288 ± 0.005), while the relative k_{cat} values for the N197A mutant showed no viscosity dependence in the presence of sucrose. The relative k_{cat}/K_m values for the N197A mutant varied inversely with η_{rel} (slope = –0.163 ± 0.002). Relative k_{cat}/K_m values for the wild-type enzyme that have been corrected for diffusion-unrelated effects (see **table 3.1**) are also shown (□). The slope of the corrected line (short dashes) is 0.186 ± 0.004.
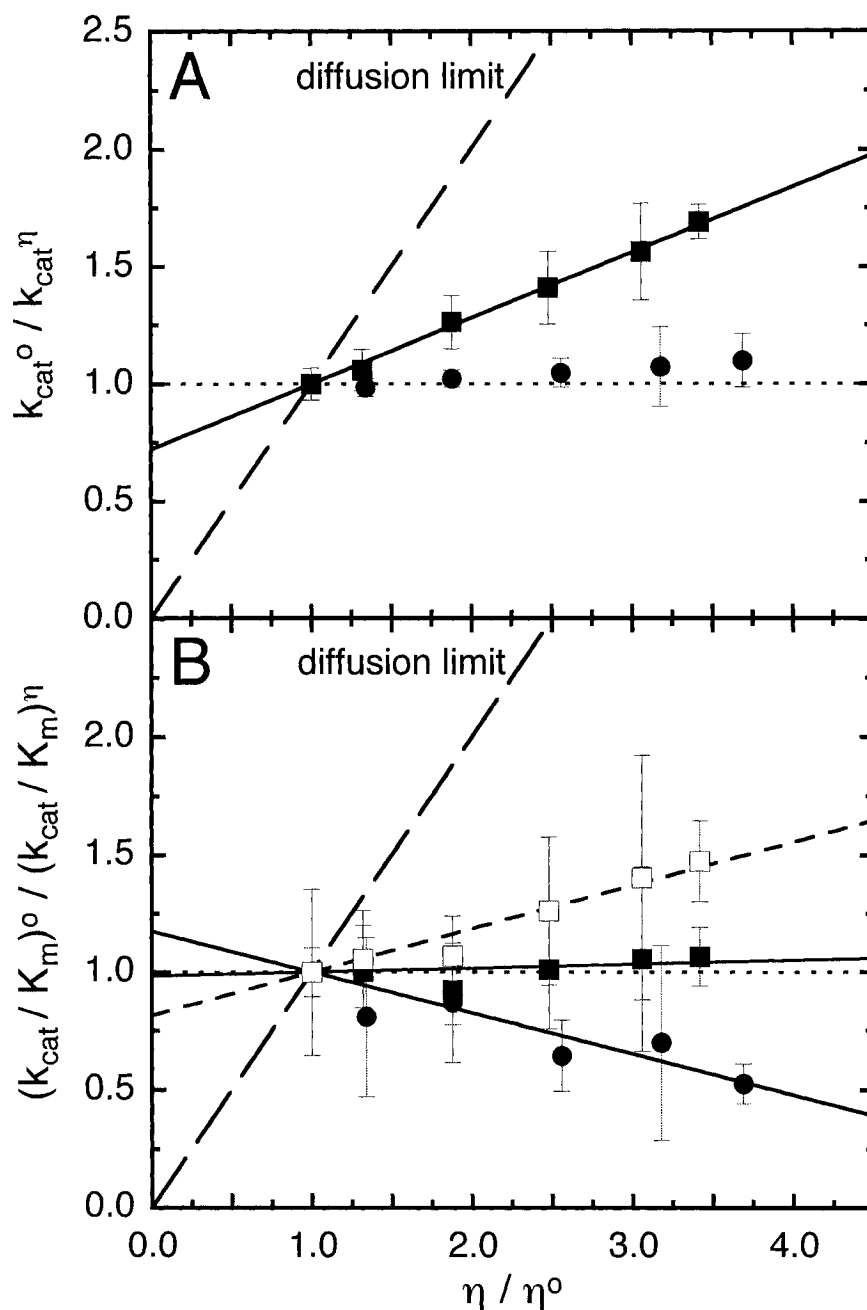
Figure 3.2 Dependence of relative kinetic parameters for the racemization of (S)-mandelate on relative solvent viscosity. The values of relative k_{cat} (**A**) and relative k_{cat}/K_m (**B**) for both wild-type MR (■) and N197A (●) were determined at 25 °C at varying values of η_{rel} using sucrose as the viscosogen. The relative k_{cat} values for wild-type MR were proportional to η_{rel} (slope = 0.259 ± 0.002), while the relative k_{cat} values for the N197A mutant showed no viscosity dependence in the presence of sucrose. The relative k_{cat}/K_m values for the N197A mutant varied inversely with relative viscosity (slope = –0.174 ± 0.003). Relative k_{cat}/K_m values for the wild-type enzyme that have been corrected for diffusion-unrelated effects (see **table 3.1**) are also shown (□). The slope of the corrected line (short dashes) is 0.172 ± 0.002.
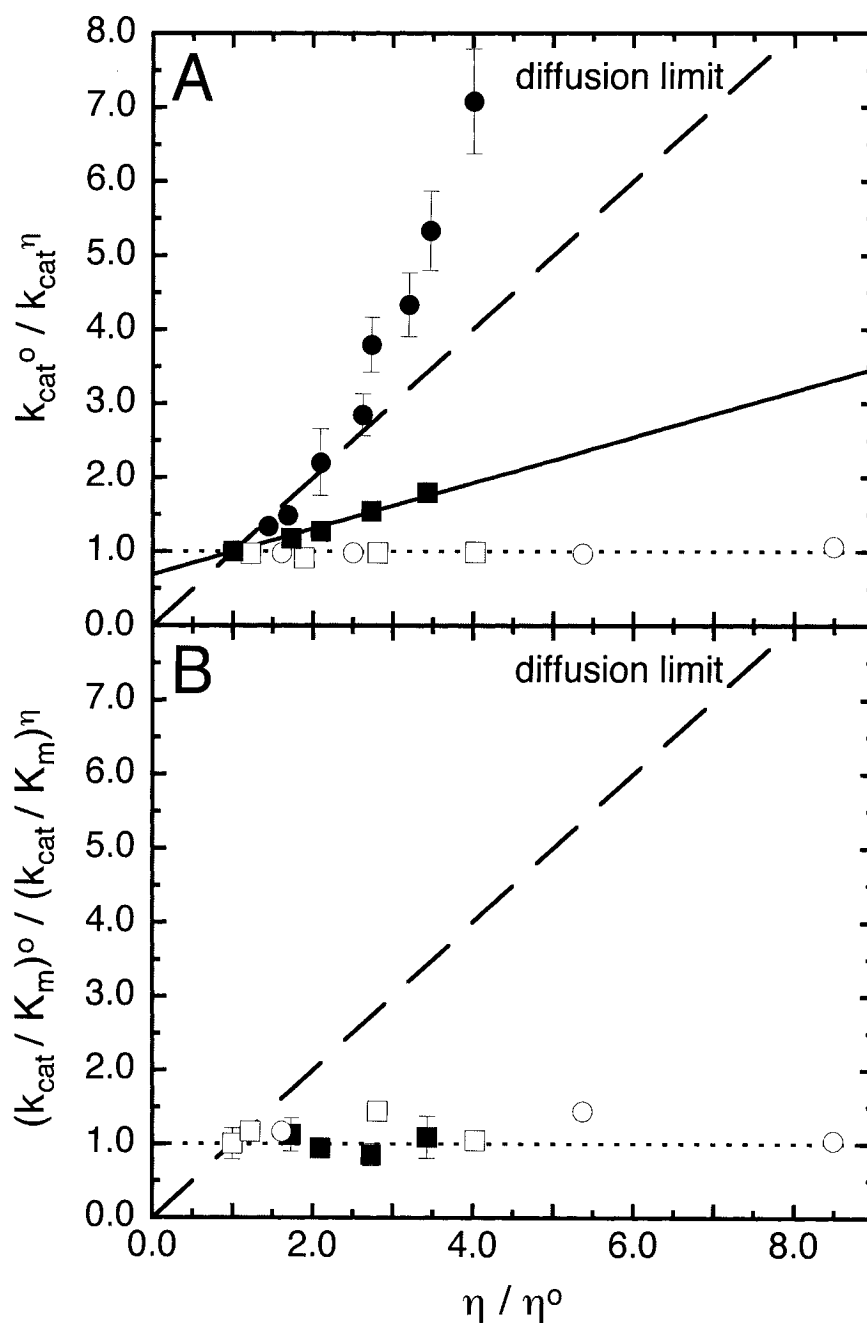
Figure 3.3   Dependence of relative kinetic parameters for MR-catalyzed racemization of (*R*)-mandelate on relative solvent viscosity in the presence of various viscosogens. The values of relative k_{cat} (**A**) and relative k_{cat}/K_m (**B**) for wild-type MR are shown in the presence of the monomeric viscosogens glycerol (●) and trehalose (■), and the polymeric viscosogens ficoll 400 (□) and PEG (○). The slope of the solid line in **A** is 0.309 ± 0.007.

behavior is observed when different monomeric viscosogens (which affect both solvent microviscosity and macroviscosity) are used, (b) demonstrating that polymeric viscosogens (which affect only the solvent macroviscosity) do not alter the kinetic parameters, and (c) characterizing the effect of viscosogens on the activity of a "sluggish" mutant (Blacklow et al., 1988). In the present work, the viscosity dependence observed for the relative k_{cat} values was similar in the presence of both sucrose and trehalose (**figures 3.1–3.3**). The relative k_{cat} value also exhibited a viscosity dependence in the presence of glycerol. However, this dependence was curvilinear, especially at relative viscosities greater than 2.5 (**figure 3.3A**). Glycerol, a relatively small molecule, may be acting as an inhibitor of the enzyme in addition to mediating solvent viscosity effects and, therefore, was not considered to be suitable as a viscosogen in the present study. Such aberrant behavior of glycerol in solvent viscosity studies has been reported for several enzymes, including carbonic anhydrase (Pocker & Janjic, 1987), alkaline phosphatase (Simopoulos & Jencks, 1994), and acetylcholinesterase (Bazelyansky et al., 1986). In the presence of the polymeric viscosogens ficoll and PEG, no viscosity dependence was observed for relative values of k_{cat} and k_{cat}/K_m up to a relative viscosity of 8.4 (**figure 3.3**). In addition, the relative k_{cat} value for the sluggish mutant, N197A (k_{cat}/K_m = 3.1 × 10^3 $M^{-1}s^{-1}$), for which the proton abstraction step is expected to be solely rate-determining (St. Maurice & Bearne, 2000), displays no viscosity dependence (**figures 3.1A and 3.2A**). Finally, the CD spectra of wild–type MR in the absence and presence of 35% sucrose (η_{rel} = 3.42) are indistinguishable (**figure 3.4**). This suggests that sucrose does not significantly alter the secondary structure of the enzyme, although slight changes in enzyme conformation in the presence of the viscosogen cannot be ruled out. These observations are all consistent with the observed viscosity dependence of k_{cat} being a diffusion–related process.

A slight dependence of the relative catalytic efficiency $((k_{cat}/K_m)^o/(k_{cat}/K_m)^\eta)$ on viscosity was observed for wild–type MR in the presence of sucrose (**figures 3.1B and**
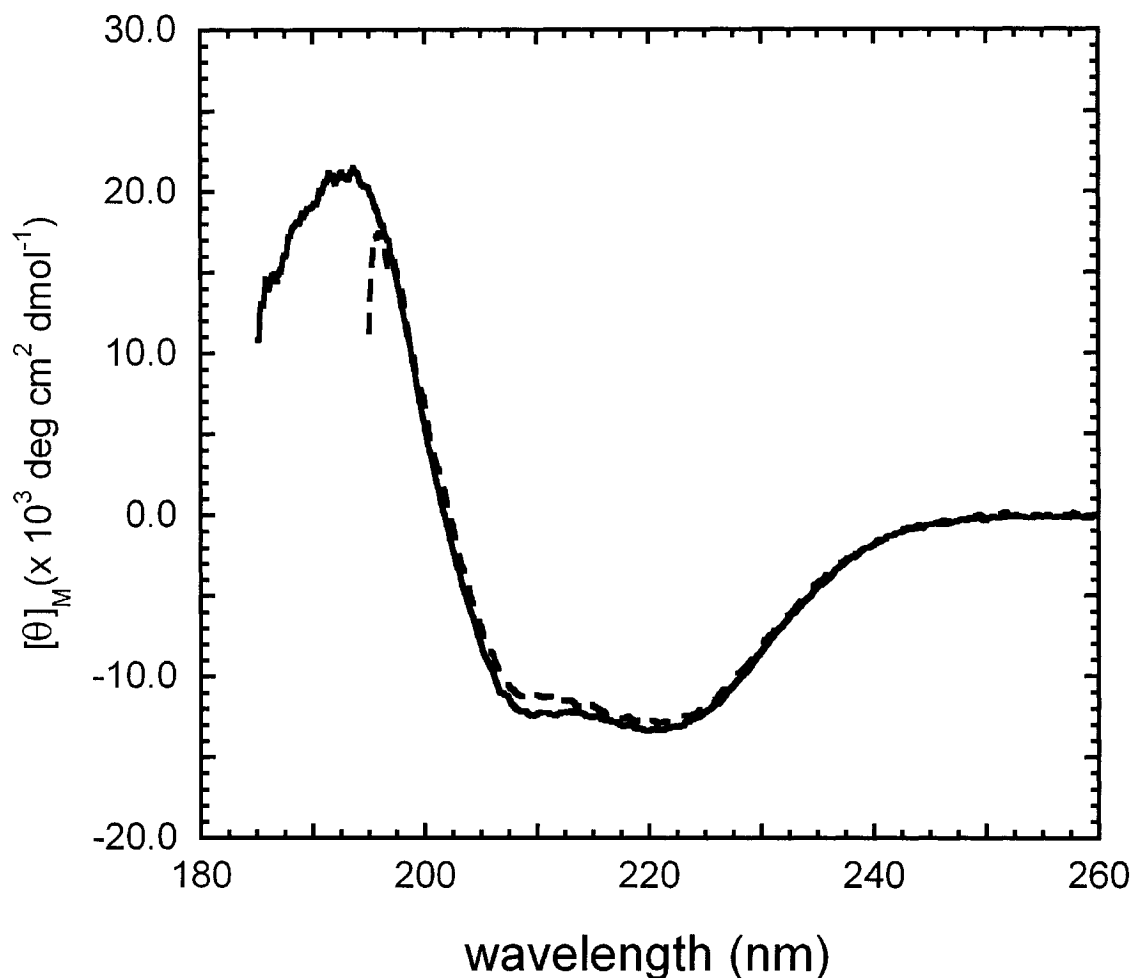
Figure 3.4 CD spectra for wild-type MR (161 μg/ml) in the absence (solid line) **and presence** (dashed line) **of 35% sucrose.** CD spectra were measured at 25 °C, pH 7.3 in Na⁺-phosphate buffer (7 mM) containing MgSO₄ (2.1 mM) and sucrose (0% or 35%). The CD spectrum for MR in the presence of 35% sucrose was obtained by subtracting the CD spectrum of Na⁺-phosphate buffer (7 mM) containing MgSO₄ (2.1 mM) and sucrose (35%) from the CD spectrum of MR (161 μg/ml) in Na⁺-phosphate buffer (7 mM) containing MgSO₄ (2.1 mM) and sucrose (35%). All samples were incubated at 25°C for 10 minutes prior to measuring the CD spectrum. The high absorbance of sucrose at ≤200 nm prevented measurements of CD spectra in the presence of sucrose at wavelengths below 200 nm.

3.2B) and trehalose (**figure 3.3B**). The larger errors associated with the k_{cat}/K_m data, relative to the k_{cat} data, were the result of difficulty in accurately measuring reaction velocities at low substrate concentrations in the presence of viscosogens. For the N197A enzyme, a slight activating effect was observed in the presence of sucrose (increased k_{cat}/K_m values in **tables 3.1** and **3.2**). Such activation is not unprecedented (Bazelyansky *et al.*, 1986; Christensen *et al.*, 1990; Goldberg & Kirsch, 1996), and the observed k_{cat}/K_m values for the wild–type enzyme must be corrected for this minor diffusion–unrelated effect as described in **tables 3.1** and **3.2** (Blacklow *et al.*, 1988; Sampson & Knowles, 1992). The partial viscosity dependence of the corrected relative k_{cat}/K_m values in the $R{\rightarrow}S$ and $S{\rightarrow}R$ directions (**figures 3.1B** and **3.2B**) suggests that substrate binding is also partially rate–determining for MR catalysis in both reaction directions.

The viscosity dependence of an enzyme–catalyzed reaction may be used to estimate the rate constants for various steps along the reaction pathway (Adams & Taylor, 1992; Bazelyansky *et al.*, 1986; Brouwer & Kirsch, 1982; Caldwell *et al.*, 1991; Christensen *et al.*, 1990; Hardy & Kirsch, 1984; Kurz *et al.*, 1987; Mattei *et al.*, 1999; Steyaert *et al.*, 1991; Stone & Morrison, 1988; Stratton *et al.*, 2001). **Scheme 3.1** shows a kinetic mechanism that describes the reaction catalyzed by MR. Utilizing sucrose as the viscosogen, the viscosity dependence of MR–catalyzed racemization in both the $R{\rightarrow}S$ and $S{\rightarrow}R$ directions has been used to estimate each of the rate constants defined in **scheme 3.1**. The viscosity dependence for $1/k_{cat}$ (**figure 3.5A**) and K_m/k_{cat} (**figure 3.5B**) were determined in both reaction directions at 25 °C. Following a method similar to that described previously (Brouwer & Kirsch, 1982; Mattei *et al.*, 1999), the steady–state initial velocity expressions for reactions in the $R{\rightarrow}S$ (i.e., $k_{-3}[(S)\text{-man}] \approx 0$) and $S{\rightarrow}R$ (i.e., $k_1[(R)\text{-man}] \approx 0$) directions were used to derive expressions for k_{cat} and k_{cat}/K_m (equations 3.3–3.6). The rate constants k_1, k_{-1}, k_3, and k_{-3} are inversely proportional to the solvent microviscosity (i.e., $k_i = k_i^{\circ}/\eta_{rel}$, where i = 1, –1, 3, or –3, and $\eta_{rel} = \eta/\eta^{\circ}$;

Scheme 3.1 A kinetic mechanism describing the reaction catalyzed by MR.

$$\text{E} + (R)\text{-man} \underset{k_{-1}}{\overset{k_1}{\rightleftharpoons}} \text{E}\bullet(R)\text{-man} \underset{k_{-2}}{\overset{k_2}{\rightleftharpoons}} \text{E}\bullet(S)\text{-man} \underset{k_{-3}}{\overset{k_3}{\rightleftharpoons}} \text{E} + (S)\text{-man}$$
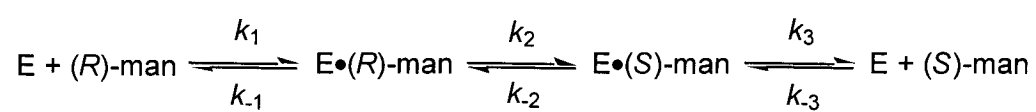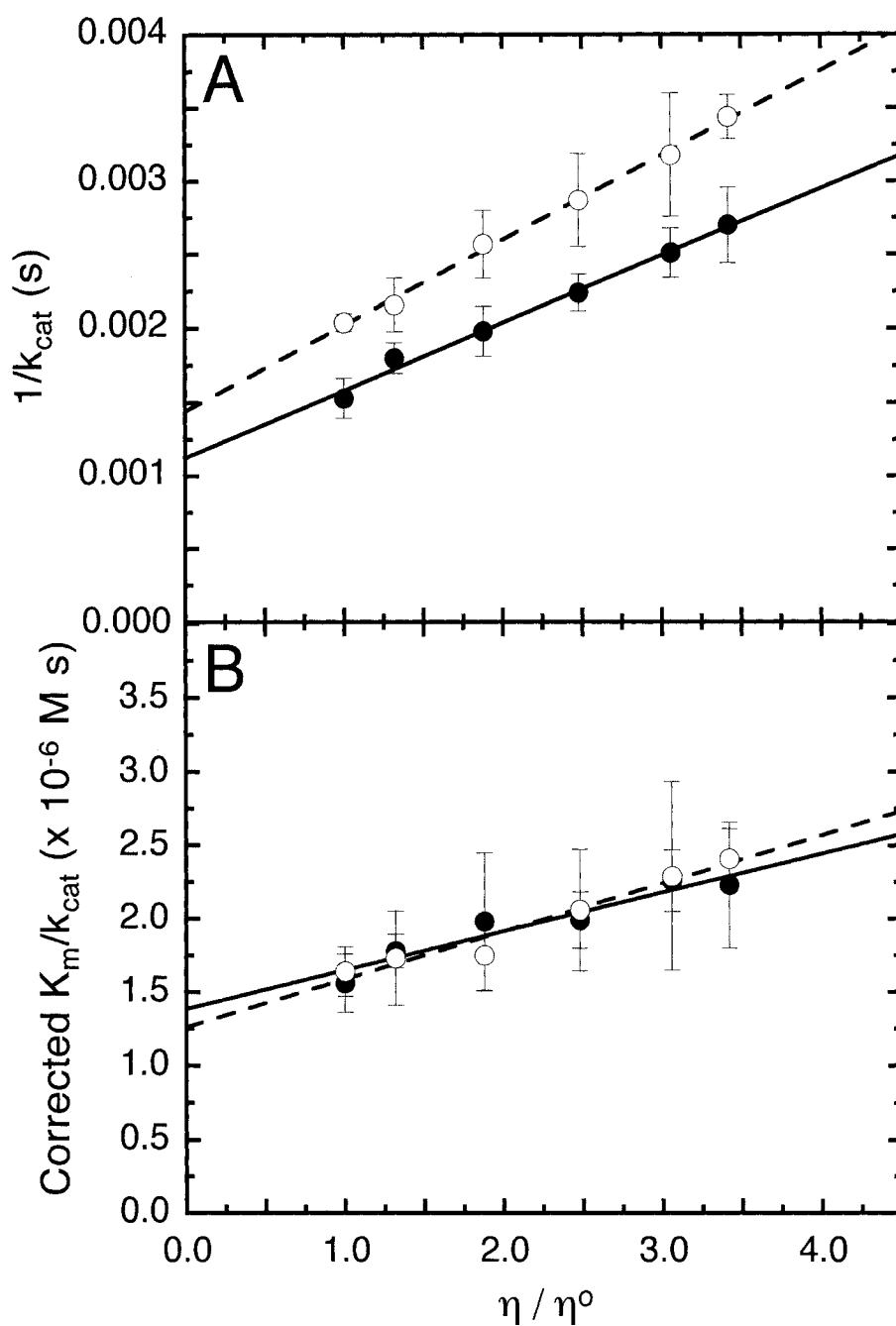
Figure 3.5 Dependence of $1/k_{cat}$ **(A) and corrected** K_m/k_{cat} **(B) on relative solvent viscosity for the racemization of** (R)**-mandelate (●) and** (S)**-mandelate (○) by MR in sucrose-containing buffers at 25 °C.** The corrected values of K_m/k_{cat} were obtained as described in **table 3.1**.

where the superscript $^\circ$ denotes the parameter in the absence of viscosity). Therefore, equations 3.3 – 3.6 may be expressed in terms of η/η° as shown in equations 3.7 – 3.10.

$$k_{cat}^{R\to S} = \frac{k_2 k_3}{k_{-2} + k_2 + k_3} \quad (3.3)$$

$$k_{cat}^{S\to R} = \frac{k_{-1} k_{-2}}{k_{-1} + k_{-2} + k_2} \quad (3.4)$$

$$\frac{k_{cat}^{R\to S}}{K_m^{(R)-man}} = \frac{k_1 k_2 k_3}{k_{-1} k_{-2} + k_{-1} k_3 + k_2 k_3} \quad (3.5)$$

$$\frac{k_{cat}^{S\to R}}{K_m^{(S)-man}} = \frac{k_{-1} k_{-2} k_{-3}}{k_{-1} k_{-2} + k_{-1} k_3 + k_2 k_3} \quad (3.6)$$

$$\frac{1}{k_{cat}^{R\to S}} = \left(\frac{k_{-2} + k_2}{k_2 k_3^\circ}\right)\frac{\eta}{\eta^\circ} + \frac{1}{k_2} \quad (3.7)$$

$$\frac{K_m^{(R)-man}}{k_{cat}^{R\to S}} = \frac{1}{k_1^\circ}\left(\frac{k_{-1}^\circ k_{-2}}{k_2 k_3^\circ} + 1\right)\frac{\eta}{\eta^\circ} + \frac{k_{-1}^\circ}{k_1^\circ k_2} \quad (3.8)$$

$$\frac{1}{k_{cat}^{S\to R}} = \left(\frac{k_{-2} + k_2}{k_{-1}^\circ k_{-2}}\right)\frac{\eta}{\eta^\circ} + \frac{1}{k_{-2}} \quad (3.9)$$

$$\frac{K_m^{(S)-man}}{k_{cat}^{S\to R}} = \frac{1}{k_{-3}^\circ}\left(\frac{k_2 k_3^\circ}{k_{-1}^\circ k_{-2}} + 1\right)\frac{\eta}{\eta^\circ} + \frac{k_3^\circ}{k_{-2} k_{-3}^\circ} \quad (3.10)$$

The plot of $1/k_{cat}$ versus η/η° (**figure 3.5A**) has an intercept equal to $1/k_2$ in the $R\to S$ direction and $1/k_{-2}$ in the $S\to R$ direction. The values for k_2 and k_{-2} can be used to calculate k_3° and k_{-1}° from the slopes of these plots. Both the intercepts and slopes from plots of K_m/k_{cat} versus η/η° in the $R\to S$ and $S\to R$ directions (**figure 3.5B**), combined with the values of the rate constants determined from the $1/k_{cat}$ versus η/η° plots, can be used to estimate k_1° and k_{-3}°, respectively. The values for all the rate constants defined in **scheme 3.1** are given in **table 3.3**.

3.3.2 Determination of K_S Using an Alternative Substrate

All kinetic assays with (S)-p-nitromandelate were conducted at 232 nm where (S)-p-nitromandelate gave a strong CD signal ($[\theta]_{232} = 8910$ deg cm^2 dmol^{-1}) with a

Table 3.3 Rate constants for the reaction catalyzed by MR.

	Rate Constant	Apparent $\Delta G^{\ddagger}$ (kcal mol^{-1}) at 25 °C
k_1	$(3.21 \pm 0.31 \times 10^6 \ M^{-1}s^{-1})^a$	8.6 ± 0.8^c
	$(6.73 \pm 0.80 \times 10^6 \ M^{-1}s^{-1})^b$	8.2 ± 1.0^c
k_{-1}	$3948 \pm 199 \ s^{-1}$	12.5 ± 0.6
k_2	$889 \pm 40 \ s^{-1}$	13.4 ± 0.6
k_{-2}	$693 \pm 20 \ s^{-1}$	13.6 ± 0.4
k_3	$3896 \pm 276 \ s^{-1}$	12.6 ± 0.9
k_{-3}	$(4.46 \pm 0.45 \times 10^6 \ M^{-1}s^{-1})^a$	8.4 ± 0.8^c
	$(6.87 \pm 0.64 \times 10^6 \ M^{-1}s^{-1})^b$	8.1 ± 0.8^c

[a]Values calculated from the y-intercepts of $(K_m/k_{cat})_{corr}$ vs. η_{rel} (Figure 3.5B).
[b]Values calculated from the slopes of $(K_m/k_{cat})_{corr}$ vs. η_{rel} (Figure 3.5B).
[c]Values calculated for a standard state of 1 M.

relatively low absorbance (**figure 3.6**). Nevertheless, the absorbance of (S)-p-nitromandelate at 232 nm did restrict assays to substrate concentrations less than 15 mM. MR appears to have a very low affinity for (S)-p-nitromandelate since saturation kinetics were not observed at substrate concentrations up to 15 mM. Although this precluded measurements of individual K_m and V_{max} values, V_{max}/K_m values for (S)-p-nitromandelate were obtained from the initial rates observed at substrate concentrations less than 3 mM (i.e., where [S] $\ll$ K_m and v_i = V_{max}[S]/K_m). MR catalyzes the racemization of (S)-p-nitromandelate less efficiently (k_{cat}/K_m = 4.08 ± 0.05 × 10^4 $M^{-1}s^{-1}$) than it catalyzes the racemization of (S)-mandelate (k_{cat}/K_m = 7.2 ± 0.5 × 10^5 $M^{-1}s^{-1}$ (St. Maurice & Bearne, 2000)).

The substrate dissociation constants for (R)-mandelate ($K_S^{(R)\text{-}man}$) and (S)-mandelate ($K_S^{(S)\text{-}man}$) were determined kinetically by conducting assays with (S)-p-nitromandelate as the substrate and using (R,S)-mandelate as a "competitive inhibitor" of the reaction. Equation 3.11 gives the velocity expression describing classical competitive inhibition where [S] is the concentration of (S)-p-nitromandelate. The apparent inhibition constant for (R,S)-mandelate (K_i^{app}) was calculated from plots of the observed K_m/V_{max} values against the concentration of (R,S)-mandelate as shown in **figure 3.7**. The kinetic mechanism describing such inhibition is shown in **scheme 3.2** and the corresponding steady–state initial velocity expression (where $d[(R)\text{-man}]/dt$ = $d[(S)\text{-man}]/dt$ = 0) for competitive inhibition may be re-written in terms of the concentrations of (S)-mandelate ([(S)-man]) and (R)-mandelate ([(R)-man]) as shown in equation 3.12.

$$\frac{v_i}{[E]_t} = \frac{k_{cat}[S]}{[S] + K_m\left[1 + \dfrac{[(R,S) - \text{man}]}{K_i^{app}}\right]} \tag{3.11}$$

$$\frac{v_i}{[E]_t} = \frac{k_{cat}[S]}{[S] + K_m\left[1 + \dfrac{[(S) - \text{man}]}{K_S^{(S)-\text{man}}} + \dfrac{[(R) - \text{man}]}{K_S^{(R)-\text{man}}}\right]} \tag{3.12}$$
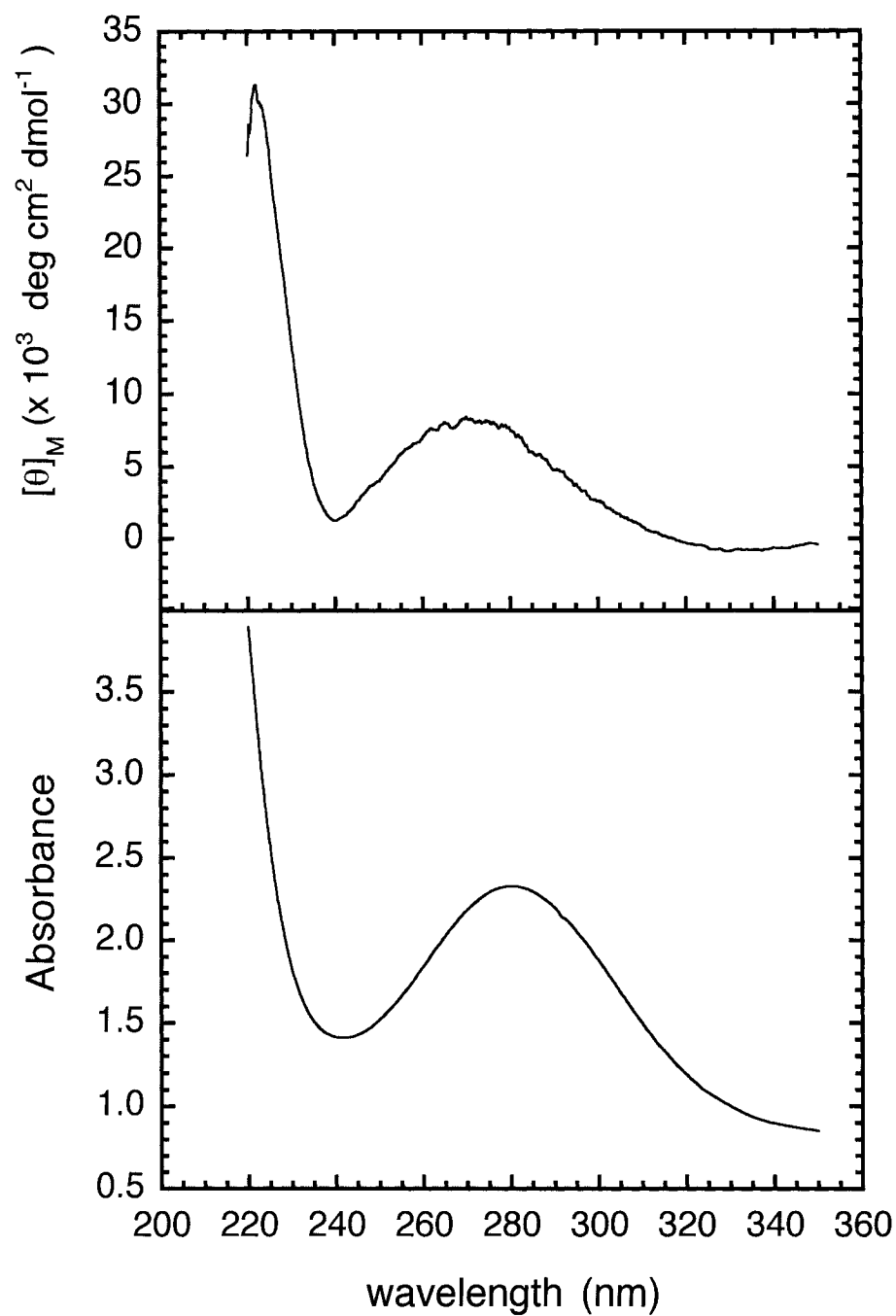
Figure 3.6 Ultraviolet absorbance and circular dichroic molar ellipticity spectra for (S)-p-nitromandelate. The spectra were recorded in a quartz cuvette (0.1 cm pathlength) for 1 mM (S)-p-nitromandelate in Na^+-HEPES buffer (0.1 M, pH 7.5) containing $MgCl_2$ (3.3 mM).
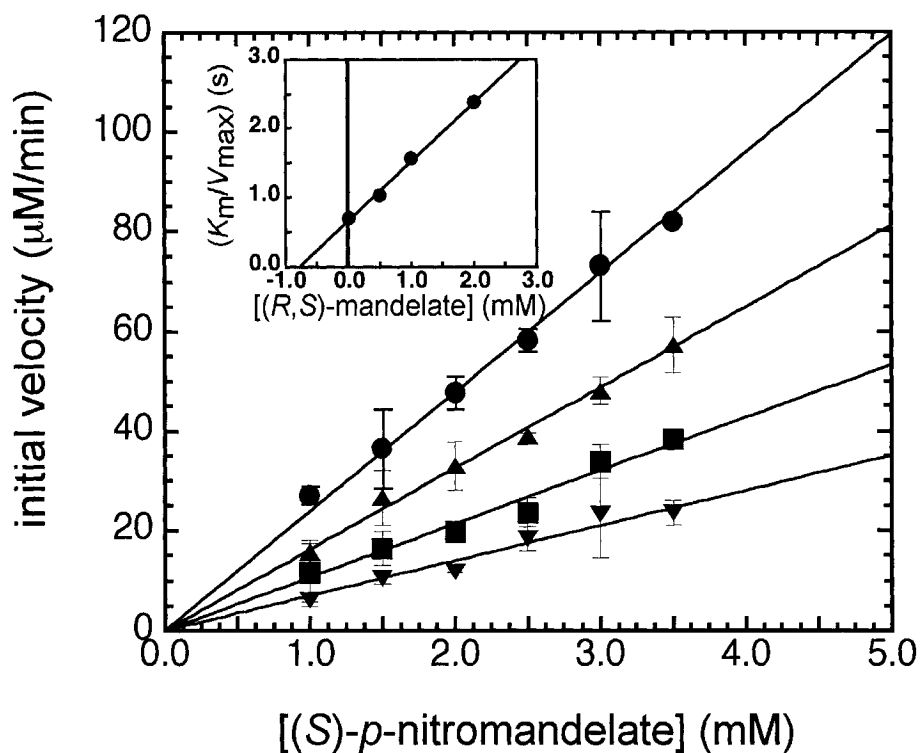
Figure 3.7 Initial velocity curves for the MR-catalyzed racemization of (S)-p-nitromandelate. Assays were conducted at 25 °C in the presence of 0 mM (●), 0.5 mM (▲), 1.0 mM (■) and 2.0 mM (▼) (R,S)-mandelate. Each point is the average of three determinations. **Inset:** Replot of the reciprocal slopes obtained from the initial velocity curves (i.e., K_m/V_{max}) as a function of (R,S)-mandelate concentration. K_i^{app} is equal to 0.78 ± 0.04 mM.

Scheme 3.2 A kinetic mechanism describing the competitive inhibition of MR by (*R*,*S*)-mandelic acid.

$$\text{E}\bullet(R)\text{-man} \underset{k_{-2}}{\overset{k_2}{\rightleftharpoons}} \text{E}\bullet(S)\text{-man}$$

$$K_S^{(R)\text{-man}} \qquad k_1 \diagup\!\!\!\diagdown k_{-1} \qquad k_3 \diagup\!\!\!\diagdown k_{-3} \qquad K_S^{(S)\text{-man}}$$

$$(R)\text{-man} \qquad\qquad (S)\text{-man}$$

$$\text{E} + \text{S} \underset{K_m}{\rightleftharpoons} \text{ES} \overset{k_{cat}}{\longrightarrow} \text{E} + \text{P}$$
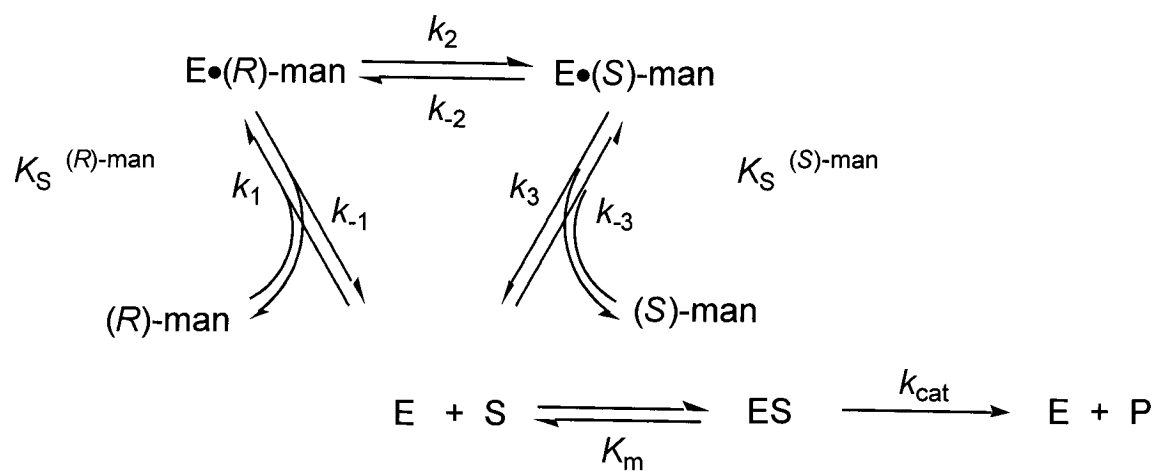
Thus, K_i^{app} is related to the individual dissociation constants for (R)- and (S)-mandelate as shown in equation 3.13.

$$\frac{[(R,S)-\text{man}]}{K_i^{app}} = \frac{[(S)-\text{man}]}{K_s^{(S)-\text{man}}} + \frac{[(R)-\text{man}]}{K_s^{(R)-\text{man}}}$$ (3.13)

Since the overall equilibrium constant for the interconversion of the enantiomers of mandelate is unity (i.e., $(k_1 k_2 k_3)/(k_{-1} k_{-2} k_{-3}) = K_{eq} = 1$), the ratio of the dissociation constants may be expressed as a function of individual rate constants as shown in equation 3.14.

$$\frac{k_{-2}}{k_2} = \frac{k_1 k_3}{k_{-1} k_{-3}} = \frac{K_s^{(S)-\text{man}}}{K_s^{(R)-\text{man}}}$$ (3.14)

Using equilibrium concentrations of (R)- and (S)-mandelate (i.e., $[(R)\text{-man}] = [(S)\text{-man}] = [(R,S)\text{-man}]/2$), substitution of equation 3.14 into equation 3.13 yields equation 3.15 which relates the apparent inhibition constant for the racemic mixture to the true dissociation constants for (R)-mandelate and (S)-mandelate.

$$K_i^{app} = \frac{2 k_{-2} K_s^{(R)-\text{man}}}{(k_{-2} + k_2)} = \frac{2 k_2 K_s^{(S)-\text{man}}}{(k_{-2} + k_2)}$$ (3.15)

The rate constants k_2 and k_{-2} are known from the viscosity experiments and, therefore, $K_S^{(R)-\text{man}}$ and $K_S^{(S)-\text{man}}$ can be calculated.

The value of K_i^{app} is 0.78 ± 0.04 mM (**figure 3.7**). Substitution of this value into equation 3.15 gives dissociation constants of $K_S^{(R)-\text{man}} = 0.89 \pm 0.07$ mM and $K_S^{(S)-\text{man}} = 0.69 \pm 0.06$ mM. These values are very similar to the corresponding K_m values reported for (R)-mandelate (0.81 ± 0.12 mM) and (S)-mandelate (0.62 ± 0.04 mM) (St. Maurice & Bearne, 2000) indicating that, for MR, $K_m \approx K_S$. This conclusion is further supported by calculation of the dissociation constants using the rate constants obtained from the viscosity studies ($K_S^{(R)-\text{man}} = k_{-1}/k_1 = 0.59 \pm 0.08$ mM and $K_S^{(S)-\text{man}} = k_3/k_{-3} = 0.57 \pm 0.07$ mM using k_{-1} and k_3 determined from the slope data in **table 3.3**).

3.3.3 Temperature Effects.

MR–catalyzed racemization of (R)-mandelate was investigated at temperatures ranging from 10 °C to 45 °C. The variation of $K_m^{(R)\text{-man}}$ with temperature is shown in **figure 3.8**. The enthalpy $(\Delta H_{E \cdot (R)})$ and entropy $(T\Delta S_{E \cdot (R)})$ changes accompanying formation of the enzyme–(R)-mandelate complex are -8.9 ± 0.8 kcal/mol and -4.8 ± 0.8 kcal/mol at 25 °C, respectively, corresponding to a free energy change $(\Delta G_{E \cdot (R)})$ of -4.1 ± 1.1 kcal/mol at 25 °C.

To determine the activation parameters for conversion of enzyme–bound (R)-mandelate to enzyme–bound (S)-mandelate, k_2 was determined from viscosity experiments conducted at temperatures ranging from 10 °C to 45 °C. Values of k_2 were obtained from the reciprocals of the y-intercepts on plots of $1/k_{cat}$ versus η_{rel}, and an Erying plot was used to obtain the corresponding activation parameters **(figure 3.9)**. The enthalpy $(\Delta H^{\ddagger}_{E \cdot (R)})$ and entropy $(T\Delta S^{\ddagger}_{E \cdot (R)})$ of activation are 15.4 ± 0.4 kcal/mol and $+2.0 \pm 0.1$ kcal/mol at 25 °C, respectively, corresponding to a free energy of activation $(\Delta G^{\ddagger}_{E \cdot (R)})$ equal to $+13.4 \pm 0.4$ kcal/mol at 25 °C.

The thermodynamic parameters describing the formation of the enzyme–substrate complex in the transition state were obtained from a van't Hoff plot **(figure 3.10)** of K_{tx}, where $K_{tx} = k_{non}/(k_2/K_m)$. The nonenzymatic rate constants (k_{non}) were obtained by extrapolation of values determined by Bearne and Wolfenden (Bearne & Wolfenden, 1997) to temperatures between 10 °C and 45 °C. The enthalpy (ΔH_{tx}) and entropy $(T\Delta S_{tx})$ changes accompanying formation of the enzyme–substrate complex in the transition state are -22.9 ± 0.8 kcal/mol and $+1.8 \pm 0.8$ kcal/mol at 25 °C, corresponding to a free energy of formation for the enzyme–substrate complex in the transition state (ΔG_{tx}) equal to -24.7 ± 1.0 kcal/mol at 25 °C. The thermodynamic parameters describing MR catalysis are summarized in **figure 3.11**.
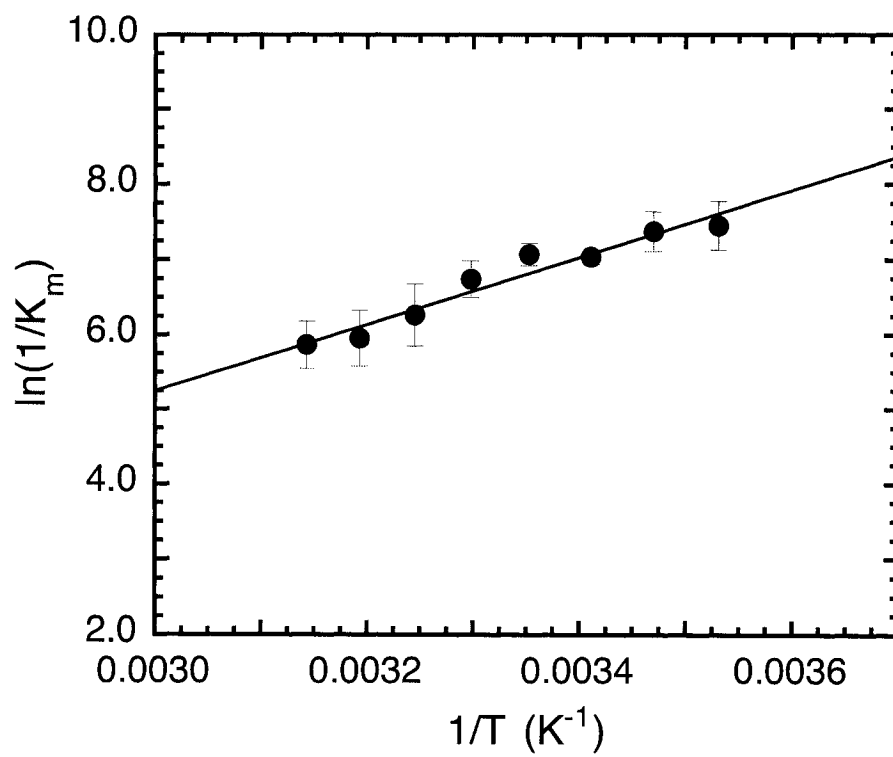
Figure 3.8 Effect of temperature on the reciprocal value of the Michaelis constant ($1/K_m$) for (R)-mandelate. Each point represents the average of at least five determinations.
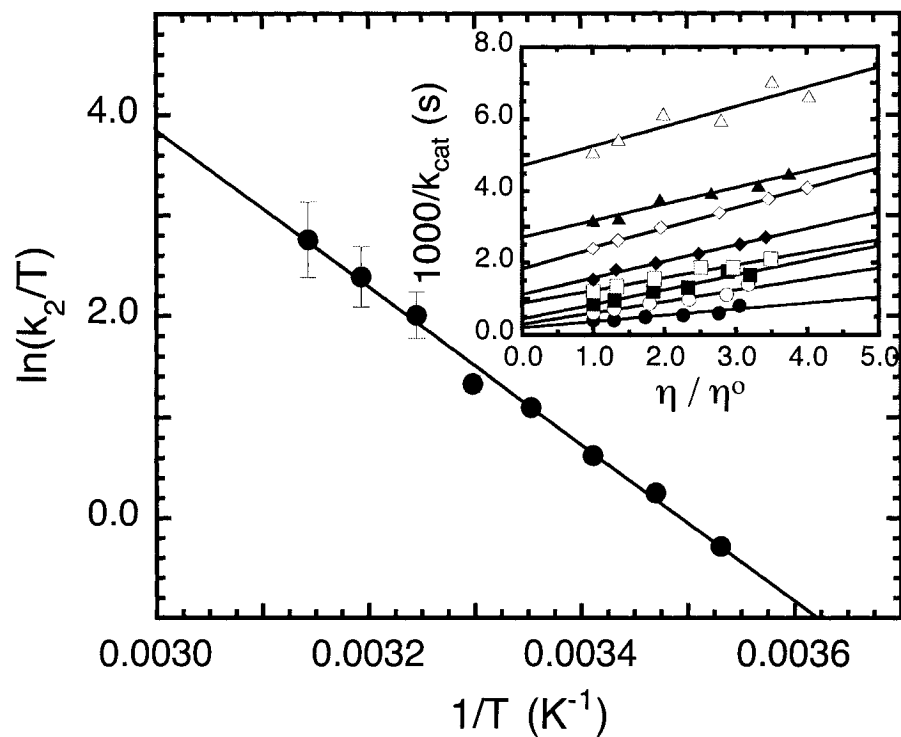
Figure 3.9 Plot of k_2/T for MR acting on (R)-mandelate. Error bars represent the error in determining the value of the y-intercept from plots of $1/k_{cat}$ as a function of relative solvent viscosity. **Inset:** Dependence of $1/k_{cat}$ (average of two determinations) on relative solvent viscosity at 10 °C (Δ), 15 °C (▲), 20 °C (◇), 25 °C (◆), 30 °C (□), 35 °C (■), 40 °C (O), and 45 °C (●) using sucrose as the viscosogen.
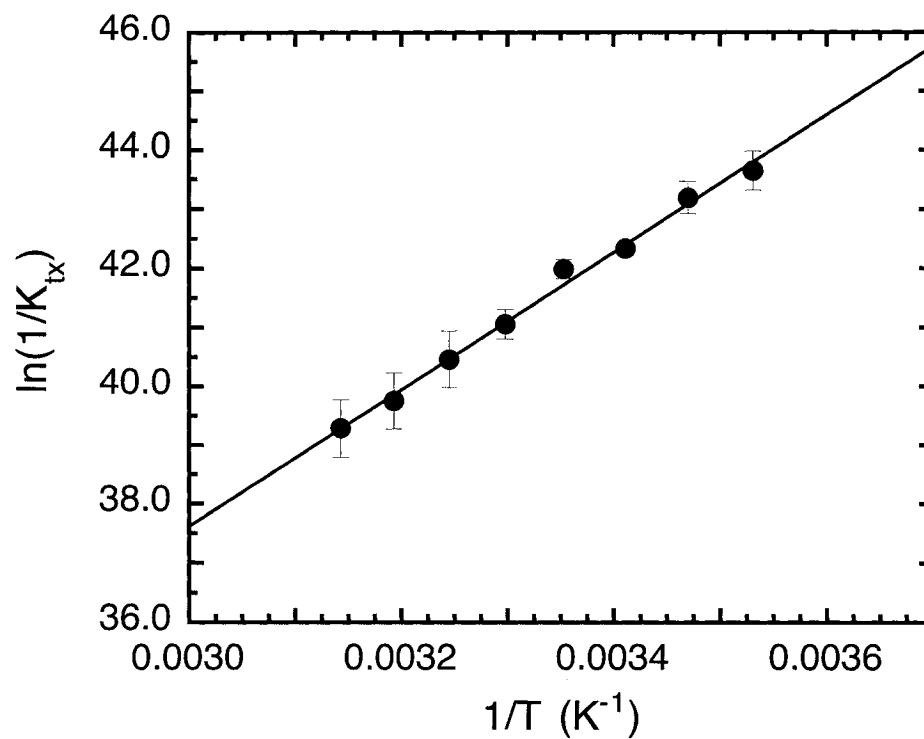
Figure 3.10 Plot of $1/K_{tx}$ for MR acting on (*R*)-mandelate. For each point, K_{tx} was determined from the relationship $K_{tx} = k_{non}/(k_2/K_m)$. Each point represents the average of two determinations.
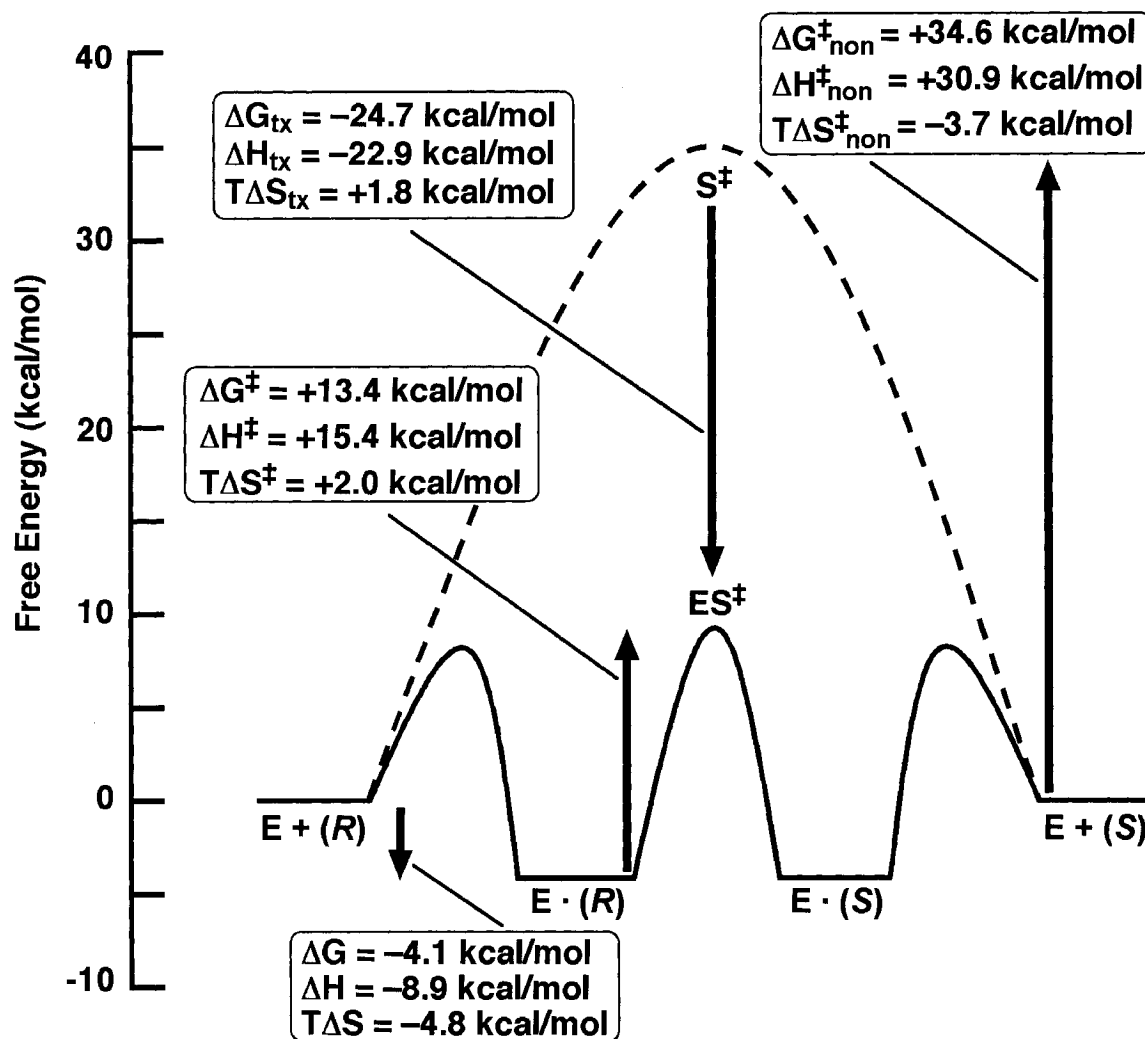
Figure 3.11 Free energy profiles (pH 7.5, 25 °C) for the uncatalyzed (dashed line) **and MR-catalyzed** (solid line) **racemization of (R)-mandelate, (R), and (S)-mandelate, (S)**. Energy barriers are drawn to scale using free energies calculated from the rate constants for both the enzymatic reaction (Table 2) and the nonenzymatic reaction (Bearne & Wolfenden, 1997) using the Eyring equation [k_i = $(k_BT/h)\exp(-\Delta G_i^\ddagger/RT)$]. ES‡ is the enzyme-substrate complex in the transition state and S‡ is the altered substrate in the transition state for the corresponding nonenzymatic reaction. For simplicity, the "enolic intermediate" (Gerlt & Gassman, 1993a) is not shown on the profile. (Values are calculated for a standard state of 1 M.)

3.4 Discussion

The enthalpy and entropy changes that accompany progress along the reaction coordinate of both an enzyme–catalyzed reaction (not involving a covalent enzyme–substrate adduct) and the corresponding nonenzymatic reaction have been described for only a few enzymes including fumarase, ribonuclease A, and carbonic anhydrase (Bearne & Wolfenden, 1995), and more recently for cytidine deaminase (Snider *et al.*, 2000). For each of these enzymes, enthalpy is the major contributor to the transition state stabilization free energy, providing additional evidence that enzymes stabilize reactive intermediates and transition states through numerous synergistic protein–ligand interactions (Wolfenden *et al.*, 1999). It is these interactions that permit proficient enzymes to discriminate between the substrate in the ground state and the altered substrate in the transition state, binding the latter with much greater affinity (Lienhard, 1973; Polanyi, 1921; Radzicka & Wolfenden, 1995; Wolfenden, 1972, 1974, 1976). To better understand the thermodynamics that contribute to enzyme proficiency, the changes in enthalpy and entropy occurring during the racemization reaction catalyzed by MR were investigated. In order to assess the enthalpy and entropy changes associated with formation of the enzyme–transition state complex, as defined by the virtual dissociation constant K_{tx} (equation 3.1), it was necessary to confirm that, for MR, $K_m = K_S$ and that k_{cat}/K_m and k_{cat} were not limited by substrate binding or product release, respectively.

3.4.1 Viscosity Effects

To accurately estimate the affinity of the enzyme for the altered substrate in the transition state (K_{tx}) using equation 3.1, either the rate constant describing the chemical step must be determined directly, or it must be shown that neither substrate encounter nor product dissociation is rate–determining. The viscosity dependence of k_{cat}/K_m and k_{cat} were used to assess the degree to which substrate association and/or product dissociation were rate–determining for the reaction catalyzed by MR. The observation that the value

of k_{cat} in both the $R{\rightarrow}S$ and $S{\rightarrow}R$ directions depends on the solvent viscosity is qualitative evidence that the rate of product release (k_3 or k_{-1} in **scheme 3.1**) is not significantly faster than the rate of chemical interconversion of bound enantiomers (k_2, k_{-2}). In addition, a viscosity dependence for k_{cat}/K_m was observed in both the $R{\rightarrow}S$ and $S{\rightarrow}R$ directions suggesting that substrate binding is also partially rate–determining for MR catalysis. Interestingly, the values of k_1 and k_{-3} are about 1–2 orders of magnitude less than typical values of diffusive association rate constants for enzymatic reactions (Alberty & Hammes, 1958). Such low values for association rate constants may arise because the conformation of the unliganded enzyme required for substrate binding exists as a rare form (Blacklow et al., 1988), extensive desolvation of both the substrate and the active site is required (Bartlett & Marlowe, 1987; Blacklow et al., 1988), nonproductive substrate binding occurs (Simopoulos & Jencks, 1994), or a rate–determining conformational change occurs after substrate binding but prior to the chemical step (Hoggett & Kellett, 1976; Kurz et al., 1987; Wang et al., 1999a). For example, substrate binding and concomitant chelation of the active site Mg^{2+} may be accompanied by slow displacement of the water molecules coordinated to the metal ion (and possibly a concomitant conformational change) which may limit the apparent rate of association. X-Ray crystal structures of MR have revealed the presence of a flexible loop (residues 19–30) which is closed over the active site when substrate is bound (Neidhart et al., 1991). Viscosity effects may arise because the opening and closing motions of this flexible loop contribute to the physical barrier which limits external steps. Rapid opening and closing motions have been reported for the catalytically essential mobile loops found in triosephosphate isomerase (Derreumaux & Schlick, 1998; Williams & McDermott, 1995) and Yersinia protein tyrosine phosphatase (Juszczak et al., 1997), and the rates of these motions are compatible with on rates approaching the diffusion limit. For triosephosphate isomerase, the loop–open form of the unliganded enzyme is favored over the loop–closed form by 1.8 kcal/mol (Derreumaux & Schlick, 1998; Williams &

McDermott, 1995). If MR behaves like these enzymes, then the loop–open form would not constitute a rare form of the enzyme and it is unlikely that loop motions would limit the apparent rate of substrate association. However, release of product from MR may well be limited by the rate of loop opening. The loop–closed form of triosephosphate isomerase is favored by 1.5–2.8 kcal/mol when ligand is bound (Derreumaux & Schlick, 1998; Williams & McDermott, 1995) and loop opening has been suggested to be responsible for the external kinetic step that limits k_{cat} for other enzymes including staphylococcal nuclease (Hale *et al.*, 1993), dihydrofolate reductase (Falzone *et al.*, 1994), and orotate phosphoribosyltransferase (Wang *et al.*, 1999a; Wang *et al.*, 1999b).

The partial viscosity dependence of MR catalysis at 25 °C was used to directly estimate the rate constants (**table 3.3**) for the kinetic mechanism shown in **scheme 3.1**. The free energy barrier for racemization of bound substrate, in both reaction directions, is approximately 1 kcal/mol greater than the free energy barriers for dissociation of bound ligands, indicating that, for MR, enzyme–substrate or enzyme–product dissociation is not significantly favored over proton abstraction. For example, under initial velocity conditions in the $R{\rightarrow}S$ direction, approximately 85% of the enzyme–product complex goes on to form free product. This observation is in agreement with the prediction of Gerlt and Gassman (1993a) that, for enzyme–catalyzed concerted general acid–general base reactions, the rate of enolization of the substrate carbon acid is expected to be similar to the rates of substrate binding and/or product release. Because the sum of the rate constants for the chemical steps (i.e., $k_{-2} + k_2$) is similar in magnitude to the rate constants for product dissociation (k_3 or k_{-1}), the observed value of k_{cat} underestimates k_2 by approximately 30% in either direction. The efficiency of MR catalysis, therefore, is limited in both directions as much by the diffusion–controlled external steps as it is by the rate of chemical conversion of the bound substrate to bound product. Given these physical constraints, MR may be regarded as a *nearly* perfect enzyme. Indeed, there is little evolutionary pressure for an enzyme to evolve such that it can catalyze a chemical

step faster than the rates for the physical exchange of substrate or product with solvent (Albery & Knowles, 1977; Burbaum *et al.*, 1989). Other enzymes such as carbonic anhydrase (Hasinoff, 1984) and β-lactamase (Christensen *et al.*, 1990), which are also only *partially* limited by the rates of diffusion, are considered to have reached the limit of their evolution, such that no further improvements in the rate of their chemical steps can increase their overall enzyme efficiency.

Because proton abstraction is not solely rate–determining, the observed deuterium kinetic isotope effects, reported previously (Mitra *et al.*, 1995; Whitman *et al.*, 1985), likely underestimate the intrinsic deuterium isotope effect (Jencks, 1987). The values of the rate constants determined in the present study can be used to estimate the intrinsic deuterium isotope effect for the forward and reverse enzyme–catalyzed reactions using equations 3.16 and 3.17, derived following the method described by Northrop (Northrop, 1975) and assuming that the forward and reverse intrinsic kinetic isotope effects are equal (i.e., $k_{2H}/k_{2D} = k_{-2H}/k_{-2D}$).

$$\frac{V_H^{R \to S}}{V_D^{R \to S}} = \frac{\dfrac{k_{2H}}{k_{2D}} + \left(\dfrac{k_{-2} + k_2}{k_3}\right)^H}{\left(\dfrac{k_{-2} + k_2}{k_3}\right)^H + 1} \tag{3.16}$$

$$\frac{V_H^{S \to R}}{V_D^{S \to R}} = \frac{\dfrac{k_{-2H}}{k_{-2D}} + \left(\dfrac{k_{-2} + k_2}{k_{-1}}\right)^H}{\left(\dfrac{k_{-2} + k_2}{k_{-1}}\right)^H + 1} \tag{3.17}$$

The values of V_H/V_D are equal to 3.20 ± 0.11 and 3.56 ± 0.12 for catalysis in the $R \to S$ and $S \to R$ directions, respectively (Whitman *et al.*, 1985). Substitution of these values and the values for the rate constants from **table 3.3** into equations 3.16 and 3.17 gives $k_{2H}/k_{2D} = 4.1 \pm 0.5$ and $k_{-2H}/k_{-2D} = 4.6 \pm 0.5$ for catalysis in the $R \to S$ and $S \to R$

directions. Interestingly, these values are less than those expected for "normal" deuterium isotope effects (k_H/k_D = 6–10; (Jencks, 1987)), but are consistent with the occurrence of late transition states for enzyme–catalyzed proton abstraction in both the forward and reverse reactions (Gerlt & Gassman, 1993a; Jencks, 1987).

3.4.2 Substrate Binding

The dissociation constants for (R)- and (S)-mandelate were determined using a kinetic approach in which (R,S)-mandelate was used to competitively inhibit the racemization of the alternative substrate, (S)-p-nitromandelate. The inhibition constant for (R,S)-mandelate was subsequently used to calculate the true substrate dissociation constants. The 10-fold reduction in k_{cat}/K_m for (S)-p-nitromandelate, relative to that for (S)-mandelate, was not initially expected since the electron–withdrawing bromo and chloro para–substituted mandelic acids have values of k_{cat}/K_m that are greater than that observed for mandelate (Hegeman et al., 1970). However, the absence of saturation kinetics at concentrations of (S)-p-nitromandelate up to 15 mM indicates that binding of (S)-p-nitromandelate is unfavorable, accounting for the decreased k_{cat}/K_m value.

For MR, the Michaelis constant (K_m) is equal to the dissociation constant (K_S). This result agrees with inactivation experiments with (R,S)-phenylglycidate, where (R)- and (S)-mandelate protect MR with dissociation constants comparable to their K_m values (Fee et al., 1974a). Titration of a Mn^{2+}–MR binary complex with (R,S)-mandelic acid has also been used to demonstrate that the dissociation constant for (R)-mandelate is nearly equivalent to the experimentally derived K_m value (Maggio et al., 1975). In addition, the values for the rate constants obtained using the viscosity variation method also support this conclusion. Two sets of conditions will satisfy equation 3.18 such that $K_m^{(R)\text{-man}} \approx k_-$ $_1/k_1 = K_S^{(R)\text{-man}}$. First, the chemical step may be completely rate–determining in the forward and reverse directions (i.e., $k_{-1} >> k_2,k_{-2}$ and $k_3 >> k_2,k_{-2}$). However, this scenario is not compatible with the partial viscosity dependence exhibited by MR which

indicates that the rates of substrate and product dissociation are similar to the rate of chemical interconversion of bound substrate and product. Second, if the off rates are equal for both substrates (i.e., $k_{-1} \approx k_3$), then $K_m \approx K_S$. The rate constants shown in **table 3.1** confirm that this is the case for MR.

$$K_m^{(R)-\text{man}} = \frac{k_{-1}k_{-2} + k_{-1}k_3 + k_2k_3}{k_1(k_{-2} + k_2 + k_3)} \tag{3.18}$$

For the determination of K_i^{app}, both (R)- and (S)-mandelate are present at equilibrium concentrations. It is possible that MR behaves like proline racemase (also a two–base racemase) for which the interconversion of two free forms of the enzyme becomes rate–determining as concentrations of substrate and product approach "oversaturation" (i.e., [(R)-proline] and [(S)-proline] $\geq \sim 34K_m$) (Fisher *et al.*, 1986). **Scheme 3.2** would not be valid under such conditions. However, our assay conditions are such that the concentration of (R,S)-mandelate does not exceed 2 mM (i.e., $\sim 2.5K_m$). This is well below the concentrations of substrate and product required to yield the "oversaturation" kinetics observed for proline racemase.

3.4.3 Changes in Enthalpy and Entropy During Catalysis

The temperature dependence of K_m and k_2 has been investigated to obtain an estimate of the enthalpic and entropic contributions to the free energy of substrate binding in the ground state, and to the activation free energy for the chemical step (conversion of E·(R)-man to E·(S)-man) in the $R \rightarrow S$ direction (data are summarized in **table 3.3** and **figure 3.11**). Substrate binding ($1/K_m$) is accompanied by an enthalpy release (–8.9 kcal/mol), consistent with the formation of noncovalent bonds between the enzyme and the substrate in the enzyme–substrate complex. In addition, substrate binding is accompanied by a loss of entropy (–4.8 kcal/mol at 25 °C), consistent with the

organization of two molecules into a single complex. For the chemical step, a substantial enthalpy of activation is associated with catalysis (+15.4 kcal/mol) which is similar to the enthalpy of activation recently reported for cytidine deaminase (Snider *et al.*, 2000). Although this enthalpy change is large relative to values of 9 – 13 kcal/mol reported for other enzymes (Wolfenden *et al.*, 1999), it does, nevertheless, represent an impressive 15 kcal/mol decrease in activation enthalpy relative to the nonenzymatic reaction ($\Delta H^{\ddagger}$ = +30.9 kcal/mol (Bearne & Wolfenden, 1997)). This $\Delta \Delta H^{\ddagger}$ is well within the range exhibited by other enzymes ($\Delta \Delta H^{\ddagger}$ = 7 – 33 kcal/mol) (Snider *et al.*, 2000; Wolfenden *et al.*, 1999). Interestingly, unlike cytidine deaminase (Snider *et al.*, 2000), the release of enthalpy accompanying substrate binding does not match the enthalpy of activation associated with the subsequent chemical step. The free energy of activation for the enzymatic reaction is accompanied by a favorable gain in entropy (+2.0 kcal/mol) while a loss of entropy is associated with the nonenzymatic reaction ($T\Delta S^{\ddagger}$ = –3.7 at 25 °C). The positive difference in activation entropies (i.e., $T\Delta \Delta S^{\ddagger}$ = +5.7 kcal/mol) between the enzymatic and nonenzymatic reactions is in qualitative agreement with the prediction of Gerlt and Gassman (Gerlt & Gassman, 1993a) that the intrinsic entropy of activation for a concerted enzymatic reaction is expected to be less negative than the corresponding base–catalyzed nonenzymatic reaction, thereby providing a mechanism for lowering the free energy of activation on the enzyme. Such a positive $\Delta S^{\ddagger}$ for the enzyme–catalyzed reaction could arise from either an enzyme conformational change, as implicated by the viscosity variation results, and/or changes in solvation during the reaction (Laidler & Peterman, 1979).

3.4.4 Thermodynamics of Transition State Affinity

After a substrate is bound by an enzyme, the affinity of the enzyme for the substrate increases by a factor proportional to the rate enhancement produced by that enzyme (Radzicka & Wolfenden, 1995; Wolfenden, 1972, 1974). The method of

viscosity variation has been used to determine the rate constant (k_2) corresponding to the chemical conversion of bound (R)-mandelate into (S)-mandelate, thereby permitting an accurate estimate of the value of the true rate enhancement (k_2/k_{non}) and calculation of the virtual dissociation constant for the enzyme–substrate complex in the transition state (K_{tx}). Values of K_{tx} were estimated over a range of temperatures by dividing the rate constant for the reaction in the absence of enzyme (k_{non}, obtained by extrapolation of the data of Bearne and Wolfenden (Bearne & Wolfenden, 1997)) by the apparent second order rate constant k_2/K_m for the enzyme–catalyzed reaction at the same temperature. It is important to note that calculation of K_{tx} using k_{cat}/K_m rather than k_2/K_m would result in an underestimation of the affinity of the enzyme for the altered substrate in the transition state by approximately 30%. The variation of $1/K_{tx}$ with temperature (**figure 3.10**) indicates that enthalpy is the major contributor to transition state stabilization, providing –22.9 kcal/mol of energy to the apparent binding free energy of the altered substrate in the transition state. This substantial release of energy is compatible with the development of enhanced hydrogen–bonding, electrostatic interactions, and nonpolar interactions in the enzyme–transition state complex (Wolfenden et al., 1999). As discussed in Chapter 1, the importance of such interactions in MR catalysis has been suggested by X-ray crystal structures of bound ground state ligands (Neidhart et al., 1991) and site–directed mutagenesis experiments (Bearne & Wolfenden, 1997; Kallarakal et al., 1995; Landro et al., 1994; Landro et al., 1991; Mitra et al., 1995; St. Maurice & Bearne, 2000).

The entropy change associated with *binding* of the altered substrate in the transition state is estimated to be $T\Delta S_{tx} = +1.8$ kcal/mol at 25 °C. Positive entropies for transition state binding have been reported for fumarase (Bearne & Wolfenden, 1995) and cytidine deaminase (Snider et al., 2000). Whether the positive entropic component of transition state stabilization by MR arises from the release of an ordered water molecule from the active site as is believed to be the case for cytidine deaminase (Snider et al., 2000; Snider & Wolfenden, 2001) or from more general changes in solvation and enzyme

conformation is not presently clear. There is no evidence from the available crystal structures of MR for the presence of an ordered water molecule in the enzyme–substrate complex. However, dynamics of the enzyme and substrate (see Chapter 5) could potentially account for an increase in entropy in the enzyme–transition state complex.

Thus, MR stabilizes the transition state for proton abstraction (ΔG_{tx}) by reducing the enthalpy of activation (by ΔH_{tx}) and increasing the entropy of activation (by ΔS_{tx}) relative to the nonenzymatic reaction. Molecular interactions between MR and its altered substrate in the transition state appear to be maximized to the extent that diffusion–dependent processes are partially rate–determining, suggesting that MR has evolved close to the limit of its catalytic proficiency. The high proficiency of MR is achieved principally through 23 kcal/mol of enthalpic reduction, suggesting that enzyme residues play a critical role in transition state stabilization by providing specific, non–covalent bonding interactions with the altered substrate in the transition state. To further investigate the molecular origins of these interactions, a high affinity, intermediate analogue inhibitor must be identified that can act as a stable probe for the enzyme–transition state complex.

CHAPTER 4

INTERMEDIATE ANALOGUE INHIBITORS OF MR

4.1 Introduction

Stable analogues of transition states and intermediates serve as useful tools for investigating the enzyme–transition state interactions at the active site of an enzyme. Proficient enzymes, such as MR, are often strongly inhibited by analogues either of the altered substrate in the transition state or of unstable intermediates that resemble the transition state (Mader & Bartlett, 1997; Radzicka & Wolfenden, 1995; Wolfenden, 1972, 1974, 1976). MR is able to catalyze carbon–hydrogen bond cleavage, in part, by stabilizing the intermediate formed in the reaction. Nitronate, hydroxamate, and phosphonate analogues of *aci*-carboxylate intermediates are potent inhibitors of a variety of enzymes catalyzing the formation of a carbanion α to a carbonyl or carboxyl group. For example, nitro analogues of the substrates acted on by aspartase, fumarases (Flint, 1994; Porter & Bright, 1980), aconitase (Schloss *et al.*, 1980), isocitrate lyase (Schloss & Cleland, 1982), enolase (Anderson *et al.*, 1984), L-(+)-lactate dehydrogenase (Genet & Lederer, 1990), adenylosuccinate synthetase, and adenylosuccinate lyase (Porter *et al.*, 1983; Raushel, 1984) all inhibit these enzymes and are bound by the enzyme with an affinity much greater than that displayed for the corresponding substrate. Both hydroxamate analogues (Wedekind *et al.*, 1994) and phosphonate analogues (Bearne & Kluger, 1992) have been used to inhibit enolase, although the latter class of inhibitors only exhibited binding affinities similar to that of the substrate.

The present chapter describes the competitive inhibition of MR by carboxylate-, hydroxamate-, and phosphonate-containing analogues of the *aci*-carboxylate intermediate. Gerlt and Gassman (1993a) have used the term "enolic intermediate" to describe this species rather than terms such as "carbanion", "enolate" (*aci*-carboxylate), or "enol"

(protonated *aci*-carboxylate) to avoid specifying the extent to which the proton is transferred from the active site general acid catalyst (Glu 317) to the oxygen atom of the intermediate. In agreement with Gerlt and Gassman, the intermediate is not implied to be an enolate but, rather, the term *aci*-carboxylate is used to describe the structure of the intermediate in the enzyme–catalyzed reaction in order to facilitate comparison with the various analogues examined in the present chapter. α-Hydroxybenzylphosphonate (α-HBP) and benzohydroxamate (BHA) are identified as competitive inhibitors of MR, binding to the enzyme more tightly than the substrate by two orders of magnitude. The α-HBP and BHA monoanions are preferentially bound by MR. In addition, the α-hydroxyl function is identified as an important binding determinant for recognition of ligands as reactive intermediate analogues. To learn more about how variation of substituents on the α-carbon affect inhibitor binding, the binding affinity of a series of α-fluorinated phosphonate derivatives for MR is evaluated. Unlike the α-OH function that can function both as an H-bond donor and acceptor, the α-fluoro group can act only as an H-bond acceptor. The low affinity of the fluorinated phosphonate inhibitors relative to α-HBP may be attributed, in part, to the loss of an H-bond donor and loss of magnesium chelation at the α-hydroxyl position of the intermediate analogues.

4.2 Materials and Methods

4.2.1 General

Racemic, (R)-, and (S)-mandelic acid, benzohydroxamic acid (BHA), benzoylformic acid, phenylacetic acid, (1S,2S)-(–)-ephedrine, and (S)-(–)-α-methylbenzylamine were purchased from Sigma–Aldrich Canada Ltd. (Oakville, ON). AG 50W-X8 was purchased from BioRad Laboratories (Mississauga, ON). Benzylphosphonate was purchased from Lancaster Synthesis (Windham, NH, USA). Acetonitrile (HPLC–grade) was purchased from Fisher Scientific (Nepean, ON). All other reagents were purchased from Sigma–Aldrich. Difluorobenzylphosphonic acid (α-F$_2$BP) and (R,S), (R)- and (S)-α-fluorobenzylphosphonic acid (α-FBP) were prepared by Dr. Scott Taylor (University of Waterloo) as described previously (Kotoris et al., 2000; Taylor et al., 1996). The absolute configurations of (R)- and (S)-α-FBP were determined crystallographically (Kotoris et al., 2000). Melting points (uncorrected) were determined using a Gallenkamp melting point apparatus, and optical rotations at 589 nm were measured using a Rudolph Instruments Digipol 781 Automatic Polarimeter. NMR spectra were obtained using a Bruker AC 250F spectrometer. Chemical shifts (δ) for proton (^{1}H) and phosphorus (^{31}P) spectra are reported in ppm relative to 3-(trimethylsilyl)propanesulfonic acid and external H$_3$PO$_4$ (85% w/v in D$_2$O), respectively. Circular dichroism assays were conducted using a JASCO J-810 spectropolarimeter. Elemental analyses were conducted by Canadian Microanalytical Service Ltd. (Delta, BC). The wild–type enzyme was purified by metal ion affinity chromatography as described previously (section 2.2.2). Once eluted from the Ni^{2+} affinity column, the enzyme was dialyzed into HEPES buffer (0.1 M, pH 7.5) containing MgCl$_2$ (3.3 mM).

4.2.2 α-Hydroxybenzylphosphonate (α-HBP)

α-Hydroxybenzylphosphonate (α-HBP) was synthesized in the Bearne laboratory by Anathea Flaman. Dimethyl (α-hydroxybenzyl) 1-C-phosphonate (prepared by reaction

of dimethyl phosphite with benzaldehyde as described by Abramov (1950)) was demethylated by treatment with trimethylsilylbromide using a procedure similar to that described by Freeman *et al.* (1991). Dimethyl (α-hydroxybenzyl) 1-C-phosphonate (0.5 g, 2.31 mmol) was dissolved in dry acetonitrile (5 mL). Trimethylsilylbromide (1.5 mL, 11 mmol, 4.8 equiv.) was added dropwise to the solution. The solution was refluxed for 30 min under an atmosphere of argon. Solvent was removed by rotary evaporation yielding a viscous yellow liquid. Dioxane (1.7 mL), water (1.7 mL), and cyclohexylamine (0.8 mL) were added and the solution was stirred for 40 min. After removal of the solvent by rotary evaporation, a white powder remained. This was dissolved in water (8.2 mL) and the solution was filtered. Acetone (74 mL) was added and a white precipitate, the cyclohexylamine salt, formed. The solution was stored at 4 °C for one hour and the precipitate was collected by suction filtration. The cyclohexylamine salt was then converted to the sodium salt by passing it through an AG 50W-X8 (Na^+-form) column. The eluent was collected and the volume was reduced by rotary evaporation. Lyophilization yielded 0.267 g (55%) of a white powder: mp >300 °C; ^1H NMR δ (250.13 MHz; D_2O, ppm) 4.78 (1H, d, J_{P-H} 12.21, P-CH), 7.39 (5H, m); ^{31}P NMR δ (101.26 MHz; D_2O) 16.65 (s, ^1H decoupled; d, J_{P-H} 11.44, ^1H coupled). Anal. Calcd for $C_7H_7O_4PNa_2$: C, 36.22; H, 3.05; P, 13.34. Found: C, 36.36; H, 3.53; P, 13.34.

4.2.3 Partial Resolution of (*R*)- and (*S*)-α-HBP

(*R*)- and (*S*)-α-HBP were partially resolved from a racemic mixture of the acid using a procedure similar to that described by Hoffmann (1985). Racemic α-HBP (1.50 g, 8 mmol) and (1*R*,2*S*)-(–)-ephedrine hemihydrate (1.39 g, 8 mmol) were dissolved in boiling ethanol (20 mL). The solution was cooled for 24 h at 4 °C. The precipitate (1.14 g) was collected using suction filtration and 0.50 g of this precipitate was recrystallized from 95% ethanol. The salt was collected using suction filtration, dissolved in water,

applied to an AG 50W-X8 (Na$^+$-form) column (2 × 40 cm), and eluted with water. Fractions containing the phosphonate were pooled and lyophilized to yield 0.13 g (39% yield) of the α-HBP sodium salt $[\alpha]_D^{22}$ =+26.57° (c=2, H$_2$O). The specific rotation of this sample indicates that the (R)-α-HBP was prepared with an enantiomeric excess equal to 76% (88% (R)-(+)-α-HBP and 12% (S)-(–)-α-HBP) based on the specific rotation of $[\alpha]_D^{20}$ =+35° (c=1, H$_2$O) reported for enantiomerically pure (R)-(+)-α-HBP (Hoffmann, 1985, 1988; Smaardijk et al., 1985).

The filtrate from the preceding step was collected, applied to an AG 50W-X8 (H$^+$-form) column (2 × 40 cm), and eluted with water. Fractions containing the phosphonate were then pooled and lyophilized. The resulting phosphonic acid (0.39 g) was mixed with (S)-(–)-α-methylbenzylamine (0.25 g) and dissolved in boiling 90% ethanol (17 mL). The solution was cooled at 4 °C for 48 h over which time an additional 10 mL of cold acetone was added. The resulting crystals were collected using suction filtration, dissolved in water, applied to an AG 50W-X8 (Na$^+$-form) column (2 × 40 cm), and eluted with water. Fractions containing the phosphonate were pooled and lyophilized to yield 35 mg (11% yield) of the α-HBP sodium salt $[\alpha]_D^{22}$ = –28.66° (c=2, H$_2$O). The specific rotation of this sample indicates that the (S)-α-HBP was prepared with an enantiomeric excess equal to 82% (91% (S)-(–)-α-HBP and 9% (R)-(+)-α-HBP).

4.2.4 Methyl α-Hydroxybenzylphosphonate

Methyl α-hydroxybenzylphosphonate was synthesized in the Bearne laboratory by Anathea Flaman. Sodium iodide (6.9 g, 46 mmol) and dimethyl (α-hydroxybenzyl) 1-C-phosphonate (4.97 g, 23 mmol) were dissolved in dry acetone (150 mL). The solution was refluxed for one hour and then cooled on ice producing a white precipitate. This precipitate was collected by suction filtration and dried under vacuum to yield a fine white powder (2.00 g, 39%). mp >300 °C; ^{1}H NMR δ (250.13 MHz; D$_2$O, ppm) 3.59 (3H, d, J_{P-H} 10.01, P-OCH$_3$), 4.91 (1H, d, J_{P-H} 12.21, P-CH), 7.41 (5H, m); ^{31}P NMR δ

(101.26 MHz; D$_2$O) 19.89 (s, ^{1}H decoupled), 19.89 (m, ^{1}H coupled).   Anal. Calcd for C$_8$H$_{10}$O$_4$PNa: C, 42.87; H, 4.51; P, 13.82.   Found: C, 41.41; H, 4.41; P, 12.59.

4.2.5 Benzoylphosphonate

Dimethyl benzoylphosphonate was prepared by reaction of trimethyl phosphite with benzoyl chloride as described by Kluger and Chin (1978).   Dimethyl benzoylphosphonate was then demethylated by treatment with trimethylsilylbromide using the procedure of Sekine *et al.* (1982) similar to that described for α-HBP. Bis(trimethylsilyl) benzoylphosphonate (3.37 g, 9.3 mmol) was treated with cyclohexylamine (2.3 mL, 20.4 mmol) to give the cyclohexylammonium salt (3.38 g, 95%) as described for the synthesis of α-HBP.   The cyclohexylammonium salt was recrystallized from 95% ethanol and converted to the sodium salt by passing it through an AG 50W-X8 (Na$^+$-form) column.   Fractions containing the phosphonate were collected, pooled and the volume was reduced by rotary evaporation.   Lyophilization yielded a pale yellow powder: mp >300 °C; ^{1}H NMR δ (250.13 MHz; D$_2$O, ppm) 7.45 (phenyl H, m); ^{31}P NMR δ (101.26 MHz; D$_2$O) 0.37 (s, ^{1}H decoupled).   Anal. Calcd for C$_7$H$_5$O$_4$PNa$_2$: C, 36.54; H, 2.19; P, 13.46.   Found: C, 36.03; H, 2.29; P, 13.29.

4.2.6 Determination of pK_{a2} for α-HBP and benzoylphosphonate

The pK_a values for ionization of the α-HBP monoanion and the benzoylphosphonate monoanion were determined by potentiometric titration of standardized NaOH (2.5 mM) and either α-HBP (2.5 mM) or benzoylphosphonate (2.5 mM) with standardized HCl (25 mM) (ionic strength maintained at 1.0 M using KCl; 24 °C).   The titration data were adjusted by subtracting a blank titration of NaOH (2.5 mM) with HCl (25 mM) (ionic strength maintained at 1.0 M using KCl; 24 °C).   The blank curve was fit to equation 4.1 (Kolthoff & Stenger, 1942), where V$_A$ is the volume of HCl, C$_A$ is the concentration of HCl, C$_B$ is the initial concentration of NaOH, V$_B$ is the initial

volume of NaOH and α_{A^-} and α_{BH} are the fractional dissociation constants for the conjugate base and the conjugate acid, respectively. The fractional dissociation constants, α_{A^-} and α_{BH}, account for the presence of contaminating buffer components in the blank titration.

$$pH = -\log\left[\frac{\left(\frac{\alpha_{A^-}C_A V_A - \alpha_{BH}C_B V_B}{V_B + V_A}\right) + \sqrt{\left(\frac{\alpha_{A^-}C_A V_A - \alpha_{BH}C_B V_B}{V_B + V_A}\right)^2 + 4\times10^{-14}}}{2}\right]$$ (4.1)

The corrected titration curve for α-HBP was fit to equation 4.2, a modified form of the Henderson–Hasselbalch equation, where $V_{A^-_i}$ is the volume of HCl required to reach the equivalence point for the α-HBP dianion, V_{BH} is the volume of HCl required to reach the equivalence point for the α-HBP monoanion and V_{HCl} is the volume of HCl titrant added.

$$pH = pK_a + \log\left(\frac{V_{A^-_i} - V_{HCl}}{V_{HCl} - V_{BH}}\right)$$ (4.2)

The reported pK_a is the average of three determinations and the error is reported as the standard deviation. A separate blank titration was performed for each individual titration.

4.2.7 MR Assays

MR activity was assayed using either the HPLC–based assay described previously (Bearne *et al.*, 1999; Chapter 1) or the CD assay described by Sharp *et al.* (1979). The HPLC assay was used to determine the inhibition constants for all of the intermediate analogues initially screened. Inhibition assays containing either α-HBP (9.5, 19.0, and 28.5 μM), methyl α-HBP (1.43 2.85, and 5.70 mM), benzoylphosphonate (0.48, 0.95 and 1.90 mM), benzylphosphonate (2.38, 4.75 and 9.50 mM), BHA (4.75, 9.5, and 19.0 μM), phenylacetate (0.48, 0.95 and 1.90 mM), or benzoylformate (0.48, 0.95 and 1.90 mM) at the three concentrations indicated, were conducted at 25 °C in Tris-HCl buffer (0.1 M,

pH 7.5) containing $MgCl_2$ (3.3 mM) and wild–type MR (15 ng/mL). Substrate ((R)-mandelate) concentrations were 0.095, 0.238, 0.475, 0.950, 2.38, and 4.75 mM. Removal of the N-terminal $(His)_6$–tag did not alter the observed K_i for α-HBP.

Inhibition of wild–type MR activity by partially resolved (R)- and (S)-α-HBP was assayed in both the $R{\to}S$ and $S{\to}R$ directions using the CD assay. Assays were conducted at 25 °C in Na^+-HEPES buffer (0.1 M, pH 7.5) containing $MgCl_2$ (3.3 mM). The substrate concentrations ((R)- or (S)-mandelate) were 0.238, 0.475, 0.95, 2.38, and 4.75 mM and the reactions were initiated by the addition of enzyme (final assay concentration=100 ng/mL). The pH–dependence of the kinetic parameters K_m and k_{cat}, and the inhibition constant (K_i) for both α-HBP and BHA were also determined using the CD assay. The enzyme was assayed using (R)-mandelate as a substrate in buffers containing $MgCl_2$ (3.3 mM). The buffers used were MES (0.1 M, pH 6.3 and 6.7); HEPES (0.1 M, pH 6.7, 7.1, 7.5, and 7.9); and TAPS (0.1 M, pH 7.9, 8.3, 8.7, and 9.1). Initial velocities were determined using 100 ng/mL MR with substrate concentrations of 0.238, 0.475, 0.950, 2.38, and 4.75 mM at each of three separate concentrations of inhibitor typically ranging between 0.95 and 475 μM for α-HBP and 0.95 and 95 μM for BHA depending on the pH of the assay.

Inhibition assays with the α-fluorobenzylphosphonates were conducted using the CD assay. The inhibitors α,α-F_2BP (0.89 – 6.67 mM), (R,S)-α-FBP (0.22 – 1.78 mM), (R)-α-FBP (0.17 – 0.713 mM), and (S)-α-FBP (0.11 – 0.67 mM) were assayed at the concentrations indicated. Inhibition assays at pH 7.5 were conducted at 25 °C in Na^+-HEPES buffer (0.1 M, pH 7.5) containing $MgCl_2$ (3.3 mM) and the substrate concentration ((R)-mandelate) ranged between 0.22 and 9.50 mM. Inhibition assays at pH 6.3 were conducted at 25 °C in Na^+-MES buffer (0.1 M, pH 6.3) containing $MgCl_2$ (3.3 mM) and the substrate concentration ((R)-mandelate) ranged between 0.5 and 9.50 mM. The reactions were initiated by the addition of wild–type MR (the final assay concentration was 150 ng/mL at pH 7.5 and 300 ng/mL at pH 6.3). Competitive

inhibition constants (K_i) were determined in triplicate from plots of the apparent K_m/V_{max} values versus inhibitor concentration. To determine whether or not α-FBP could act as a substrate for MR, (R)-α-fluorobenzylphosphonate (9.6 mM) was incubated in the dark with wild–type MR (final assay concentration=30 μg/mL) for 24 h at 25 °C. The CD signal at 269.8 nm ($[\theta]^R_{269.8} = -14690$ deg mol^{-1} cm^2) was measured after 0, 2, 4, 19 and 24 h of incubation.

4.2.8 Data Analysis

The values of V_{max} and K_m were determined from plots of the initial velocity (v_i) versus substrate concentration ([S]) by fitting the data to equation 2.1 using nonlinear regression analysis and the program *EnzymeKinetics* v1.5b5 (Trinity Software; Plymouth, NH). Kinetic constants were determined in triplicate and average values are reported. The reported errors are the standard deviations. Protein concentrations were determined using the Bio-Rad Protein Assay (Bio-Rad Laboratories; Mississauga, ON) with BSA standards and k_{cat} values were obtained by dividing V_{max} values by the total enzyme concentration using M_r 40 728.

4.2.9 Deuterium Exchange

Wild–type MR (440 ng/mL) was incubated (10.00 mL reaction volume) either with (R)-[α-^{1}H]mandelate (10 mM) or (R,S)-[α-^{1}H]hydroxybenzylphosphonate (10 mM) for 12 h at 25 °C in deuterated Tris-DCl buffer (0.1 M, pD 7.5) containing MgCl$_2$ (3.3 mM). At various times, aliquots (1.00 mL) were removed and the reaction was terminated by boiling for 3 min. The samples were adjusted to pH 5 using HCl (1 M) and passed through an AG 50W-X8 (Na$^+$-form) column (1.5 × 15 cm) to remove the buffer components. Fractions containing either mandelate or phosphonate were pooled, lyophilized and reconstituted in D$_2$O (600 μL). Concentrated DCl (5 μL) was added to each sample to adjust the pD to ~1, and proton NMR was used to measure the peak area

corresponding to the α-proton relative to the peak area corresponding to the phenyl protons (multiplet between 7.35 – 7.52 ppm). Relative peak areas were then used to calculate the percentage of deuterium incorporated at the α position at various time points. Acidification of the sample was necessary to shift the signal corresponding to the α-proton of either mandelate (singlet at 5.01 ppm) or the phosphonate (doublet at 5.06 ppm) downfield from the HOD signal (4.82 ppm) thereby permitting accurate integration of the peak corresponding to the α-proton.

4.2.10 Determination of Stability Constants for Mg^{2+} Chelation
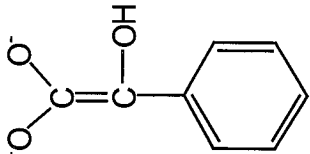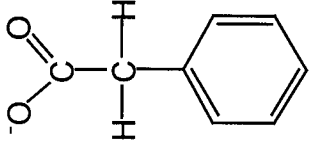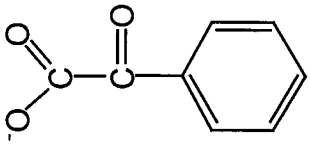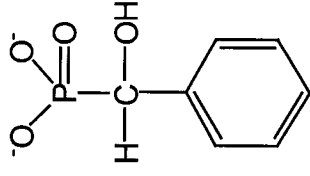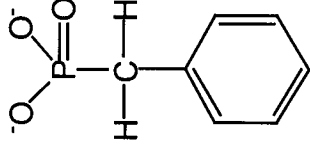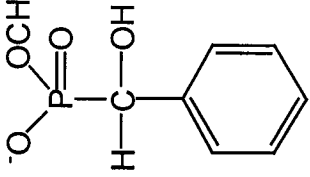
The stability constants for Mg^{2+} chelation by α-HBP, BHA and mandelate were determined spectrophotometrically by competition with 8-hydroxyquinoline according to the method described by Manchester (1980). The exact concentration of $MgCl_2$ in the competition assay was determined by back–titration of the $MgCl_2$ solution containing excess $AgNO_3$ with KSCN (19.9 mM) using $Fe(NO_3)_3$ as an end–point indicator. Assays were performed in Na^+-HEPES buffer (0.1 M, pH 8.0) containing 8-hydroxyquinoline (0.5 mM) and tetramethylammonium chloride (0.1 M). The absorbance at 358 nm was measured in the presence of both $MgCl_2$ (0.0 – 5.0 mM) and the ligand (10.0 – 20.0 mM). The Mg^{2+} binding constant, K_d, was calculated using a value of 350 M^{-1} for K' (Manchester, 1980), where K' is the formation constant for the Mg^{2+} complex with 8-hydroxyquinoline. The K_d for each ligand is reported as the average of fifteen determinations. The reported errors are the standard deviations.

4.3 Results

To better understand the protein–ligand interactions that contribute to the stabilization of the altered substrate in the transition state at the active site of MR, intermediate analogue inhibitors were designed based on the structural and electronic characteristics of the *aci*-carboxylate intermediate. **Table 4.1** shows the structures and inhibition constants for a number of such analogues. Each of these compounds was a competitive inhibitor of MR with respect to (*R*)-mandelate at pH 7.5. Of the seven analogues shown in **table 4.1**, several were bound by the enzyme with an affinity that was similar to that observed for the substrate, while two of the inhibitors were bound with an affinity that was two orders of magnitude greater than that exhibited for the substrate. Of the four phosphonate compounds examined as potential inhibitors of MR, only α-hydroxybenzylphosphonate (α-HBP) was a potent inhibitor of the enzyme (**figure 4.1**). Benzohydroxamate (BHA) was also a potent inhibitor of MR, binding two orders of magnitude more tightly than the substrate (**figure 4.2**). The formation constants for the Mg^{2+} complexes with mandelate, α-HBP and BHA were 192 ± 17 M^{-1}, 183 ± 23 M^{-1}, and 118 ± 29 M^{-1} respectively. The inhibition of MR by the individual enantiomers of α-HBP was investigated with respect to both (*R*)- and (*S*)-mandelate (**table 4.2**). MR bound (*S*)-α-HBP with an affinity that was $30 - 40$-fold greater than that observed for (*R*)-α-HBP.

The pH-dependence of the inhibition of MR by α-HBP was investigated to determine which ionization state of the phosphonate function is preferentially bound by the enzyme. **Figure 4.3** shows that the observed pK_m value for (*R*)-mandelate remained unchanged over pH values ranging between 6.3 and 8.3, and then decreased above pH 8.5 approaching a limiting slope of –1 with respect to pH. On the other hand, as the pH was increased from 6.3 to 9.1, the observed pK_i value for α-HBP decreased to a limiting slope of –2 with respect to pH. The pK_m data was fit to equation 4.3, where K_m is the apparent Michaelis constant, $\widetilde{K}_m$ is the pH–independent Michaelis constant, and K_a^e represents the

Table 4.1 Competitive inhibition of MR by carboxylate, phosphonate, and hydroxamate analogues[a]

	Substrate Analogues		Intermediate Analogue
***aci*-carboxylate intermediate**	phenylacetate $2.0\ (\pm 1.1) \times 10^{-4}$ M	benzoylformate $6.5\ (\pm 0.2) \times 10^{-4}$ M	benzohydroxamic acid $9.3\ (\pm 2.5) \times 10^{-6}$ M
Intermediate Analogues Containing the Phosphonate Function			
(R,S)-α-HBP $8.7\ (\pm 1.7) \times 10^{-6}$ M	benzylphosphonate[b] $3.5\ (\pm 1.3) \times 10^{-3}$ M	benzoylphosphonate $3.0\ (\pm 0.6) \times 10^{-4}$ M	(R,S)-methyl α-HBP $5.1\ (\pm 1.1) \times 10^{-3}$ M

[a] K_i values were determined using the HPLC assay and are shown under each compound. [b] Benzylphosphonate was incompatible with the HPLC column at high concentrations and only a single K_i determination was performed. The reported error is the error in the regression line for the replot of K_m/V_{max} vs. benzylphosphonate concentration. Re-determination of the inhibition constant using the CD assay gave a similar K_i value equal to 3.6 ($\pm$0.7) x 10^{-3} M (average of three determinations).
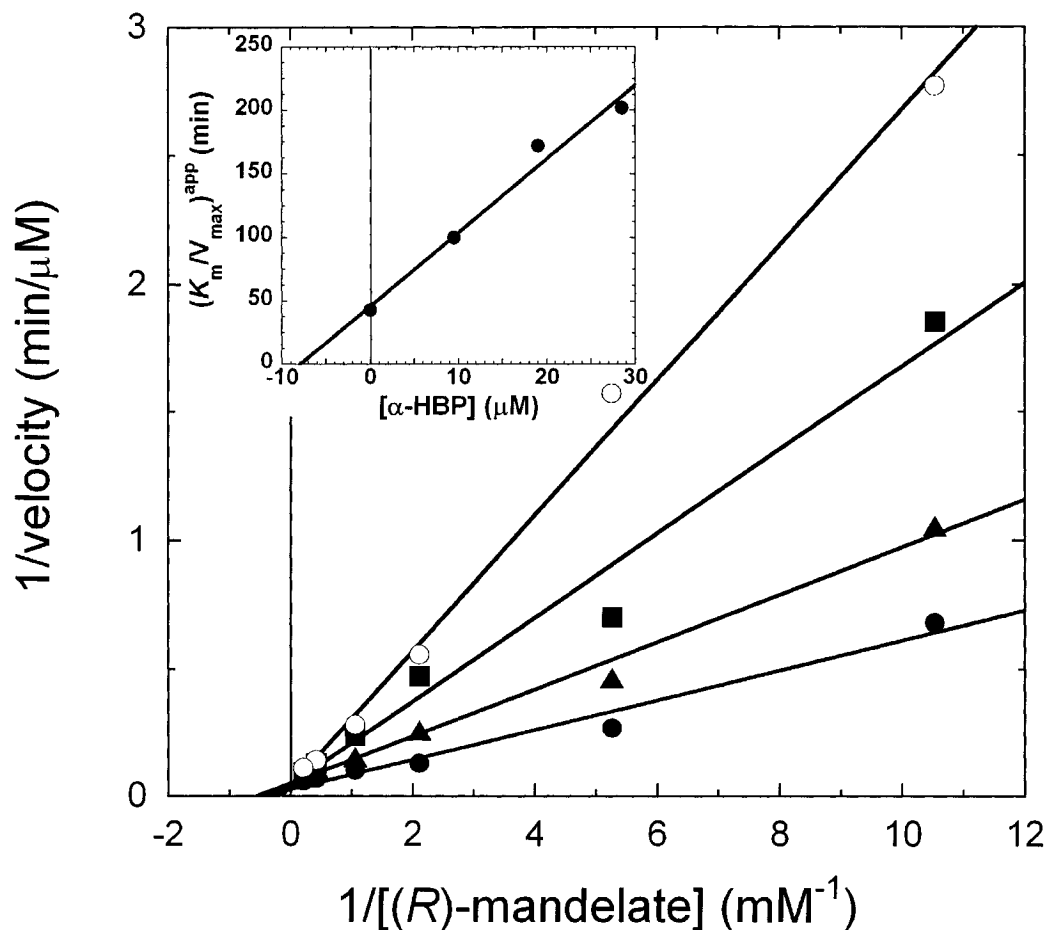
Figure 4.1 Representative Lineweaver-Burk plot for the competitive inhibition of MR activity by (R,S)-α-HBP. Initial concentrations of (R)-mandelate ranged between values of 0.095 mM and 4.75 mM. (R,S)-α-HBP concentrations were 0 μM (●), 9.5 μM (▲), 19 μM (■), and 28.5 μM (○). Assay conditions were as described in section 4.2.7. **Inset.** Replot of $((K_m/V_{max})^{app})$ as a function of (R,S)-α-HBP concentration. From this plot, the K_i value for (R,S)-α-HBP is equal to 8.2 ± 0.5 μM.
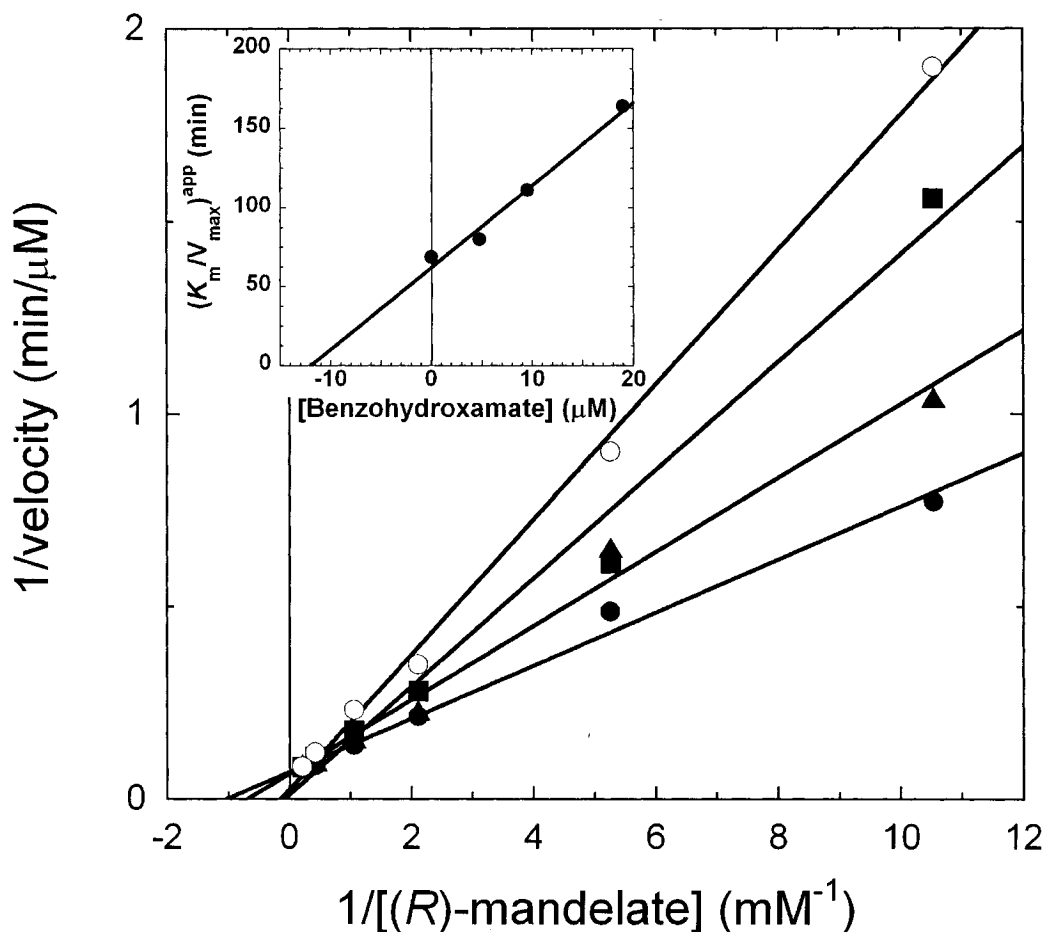
Figure 4.2 Representative Lineweaver-Burk plot for the competitive inhibition of MR activity by BHA. Initial concentrations of (R)-mandelate ranged between values of 0.095 mM and 4.75 mM. BHA concentrations were 0 μM ($\bullet$), 4.75 μM ($\blacktriangle$), 9.5 μM ($\blacksquare$), and 19 μM ($\bigcirc$). Assay conditions were as described in section 4.2.7. **Inset.** Replot of $((K_m/V_{max})^{app})$ as a function of BHA concentration. From this plot, the K_i value for BHA is equal to 11.9 ± 1.4 μM.

Table 4.2 Inhibition of MR by mixtures of the enantiomers of α-HBP[a]

Mixture of α-HBP Enantiomers	enantiomeric excess	$(R) \rightarrow (S)$	$(S) \rightarrow (R)$
		K_i (μM)	K_i (μM)
(R,S)	0	4.7 ± 0.7	3.9 ± 0.9
(S)	82%	1.1 ± 0.3	1.6 ± 0.2
(R)	76%	34 ± 9	35 ± 2

[a] K_i values were determined using the CD assay.
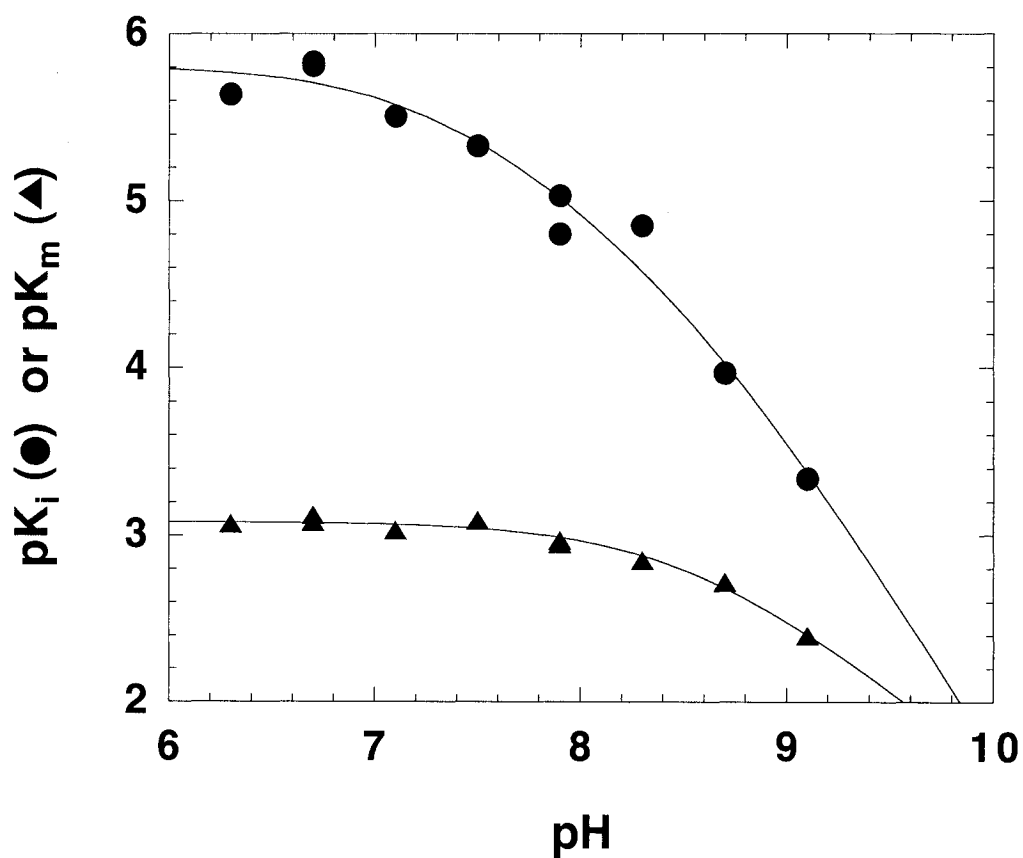
Figure 4.3 pH-Dependence of pK_i (●) and pK_m (▲) for the competitive inhibition of MR by α-HBP with respect to (R)-mandelate. Assay conditions were as described in section 4.2.7. The pK_m data were fit to equation 4.3, yielding a pK_a^e value of 8.52 ± 0.04. The pK_i data were fit to equation 4.4 (using the pK_a^e value of 8.52 ± 0.04), resulting in a pK_a^i for α-HBP of 7.3 ± 0.3.

ionization constant for the free enzyme. This equation was derived using a kinetic mechanism where the substrate is bound exclusively by the protonated form of the free enzyme (**scheme 4.1A & B**) and is based on the assumption that a single ionization on the free enzyme occurs over the pH range studied.

$$pK_m = p\tilde{K}_m - \log(10^{-pH} + 10^{-pK_a^e}) - pH \tag{4.3}$$

From a fit of the pK_m data to equation 4.3, the value of pK_a^e was determined to be 8.52 ± 0.04. The downward curvature in the pK_m vs. pH plot is consistent with a single ionization occurring on the free enzyme (Tipton & Dixon, 1979).

The curve shown in **figure 4.3** was generated by fitting the pK_i data to equation 4.4, where K_i is the apparent inhibition constant, $\tilde{K}_i$ is the pH–independent inhibition constant, K_a^i represents the ionization constant for the free inhibitor, and K_a^e represents the ionization constant for the free enzyme. This equation describes a single ionization in both the free enzyme and the free inhibitor, where the inhibitor is bound exclusively when it is in the *protonated* form (**scheme 4.1A**).

$$pK_i = p\tilde{K}_i - \log(10^{-pH} + 10^{-pK_a^i}) - \log(10^{-pH} + 10^{-pK_a^e}) - 2pH \tag{4.4}$$

From a fit of the pK_i data to equation 4.4, the value of pK_a^i for α-HBP was determined to be 7.3 ± 0.3 using the pK_a^e value of 8.52 ± 0.04 obtained from the fit of the corresponding pK_m data. The limiting slope of -2 on the descending arm is consistent with two ionizations contributing to the observed loss of inhibition at higher pH values (**scheme 4.1A**) (Fersht, 1985; Tipton & Dixon, 1979). The observed value of pK_a^i agrees well with the value of 6.89 ± 0.01 determined potentiometrically for the pK_a of the α-HBP monoanion (**figure 4.4**). Thus, optimal inhibition by α-HBP is observed when the

Scheme 4.1 Kinetic schemes for the inhibition of MR by the α-HBP monoanion (A) and the deprotonated form of BHA (B).

A.

$$EHI^-$$

$$\Big\updownarrow K_i$$

$$\alpha\text{-HBPH}^- \xrightleftharpoons{K_a^i} \alpha\text{-HBP}^{2-} + H^+$$

$$+$$

$$EH + S \xrightleftharpoons{K_S} EHS \xrightarrow{k_{cat}} EH + P$$

$$\Big\updownarrow K_a^e$$

$$H^+$$

$$+$$

$$E^-$$

B.

$$EHI^-$$

$$\Big\updownarrow K_i$$

$$RHA^- + H^+ \xrightleftharpoons{K_a^i} BHAH$$

$$+$$

$$EH + S \xrightleftharpoons{K_S} EHS \xrightarrow{k_{cat}} EH + P$$

$$\Big\updownarrow K_a^e$$

$$H^+$$

$$+$$

$$E^-$$
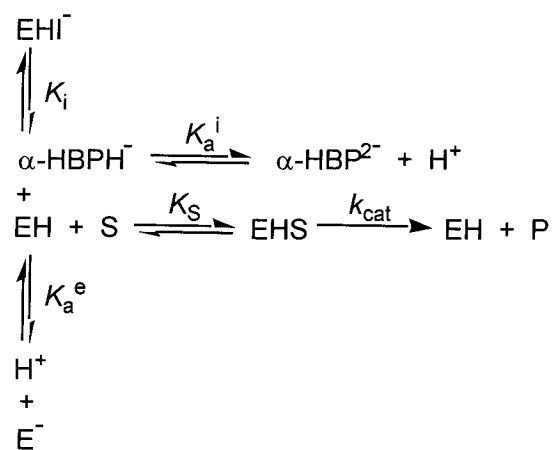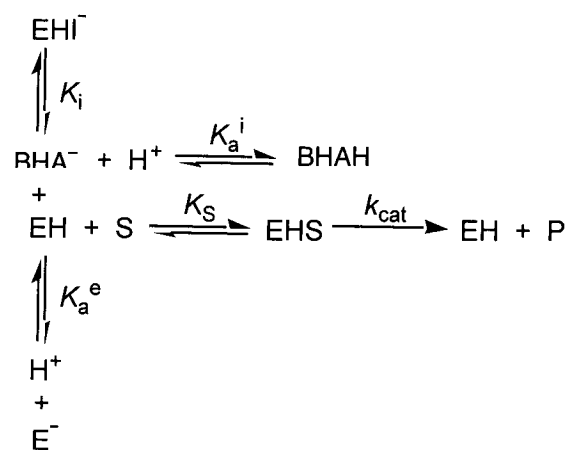
Kinetic mechanisms describing the observed pH-dependence of inhibition by α-HBP (**A**) and benzohydroxamate (**B**).
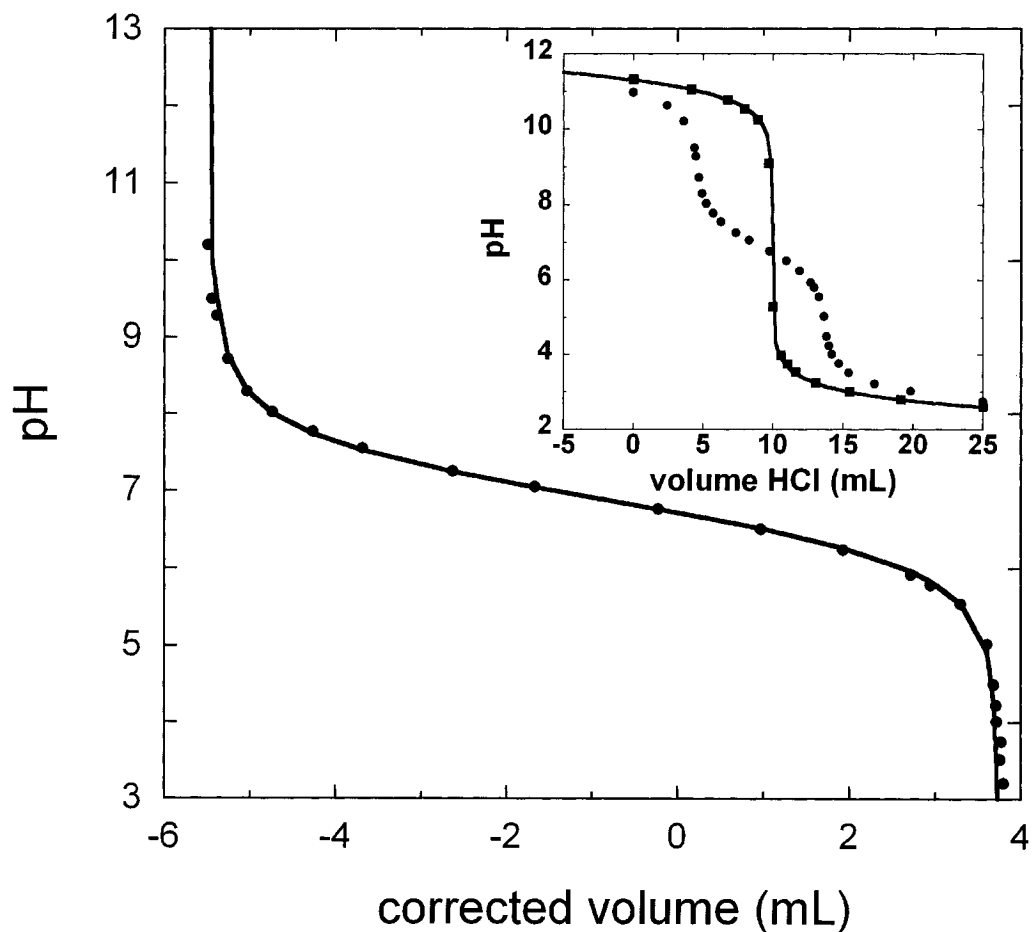
Figure 4.4 Representative corrected titration curve for the titration of α-HBP (2.5 mM) with HCl (25 mM). The titration was performed as described in section 4.2.6. The corrected titration data were fit to equation 4.2 giving a pK_{a2} for α-HBP of 6.89. **Inset.** Blank titration of NaOH (2.5 mM) with HCl (25 mM) (■) and titration of NaOH (2.5 mM) and α-HBP (2.5 mM) with HCl (25 mM) (●). The blank titration data were fit to equation 4.1.

free enzyme is protonated and the phosphonate function of α-HBP exists as the monoanion.

The pK_a of benzoylphosphonate was determined potentiometrically to be 5.46 ± 0.02 (**figure 4.5**). The decoupled ^{31}P NMR spectra for benzoylphosphonate (100 mM in D$_2$O, pD 7.5) revealed only a single peak at 2.39 ppm, indicating that there is little or no hydrated species in solution at the assay pH.

The pH dependence of the inhibition by BHA was investigated to determine which ionization state of BHA was preferentially bound by the enzyme (**figure 4.6**). As the pH was increased from 6.7 to 9.1, the observed pK_i value followed a roughly bell–shaped curve with respect to pH and with limiting slopes of +1 and –1 at low and high pH, respectively. Again, the pK_m value for (*R*)-mandelate remained unchanged over pH values between 6.7 and 8.3, and then decreased above pH 8.3 approaching a limiting slope of –1 with respect to pH. The curve shown in **figure 4.5** is from a fit of the pK_i data to equation 4.5. This equation describes a single ionization of both the free enzyme and the free inhibitor, where the inhibitor is bound exclusively as the *unprotonated* form (**scheme 4.1B**).

$$pK_i = p\tilde{K}_i - pK_a - \log(10^{-pH} + 10^{-pK_a^i}) - \log(10^{-pH} + 10^{-pK_a^e}) - pH \qquad 4.5$$

Using these data, the pK_a^i and pK_a^e values for the ionization of BHA and a group on the free enzyme were determined to be 8.7 ± 0.3 and 8.5 ± 0.1, respectively (**figure 4.6** and **scheme 4.1B**). The pK_a^i value of 8.7 ± 0.3 is in excellent agreement with the pK_a value of 8.8 for benzohydroxamic acid (Exner *et al.*, 1993; Farkas *et al.*, 2000). Thus MR preferentially binds the deprotonated form of benzohydroxamic acid.

Deuterium exchange experiments were conducted to determine whether α-HBP could act as a substrate for MR (**figure 4.7**). Proton NMR was used to follow the
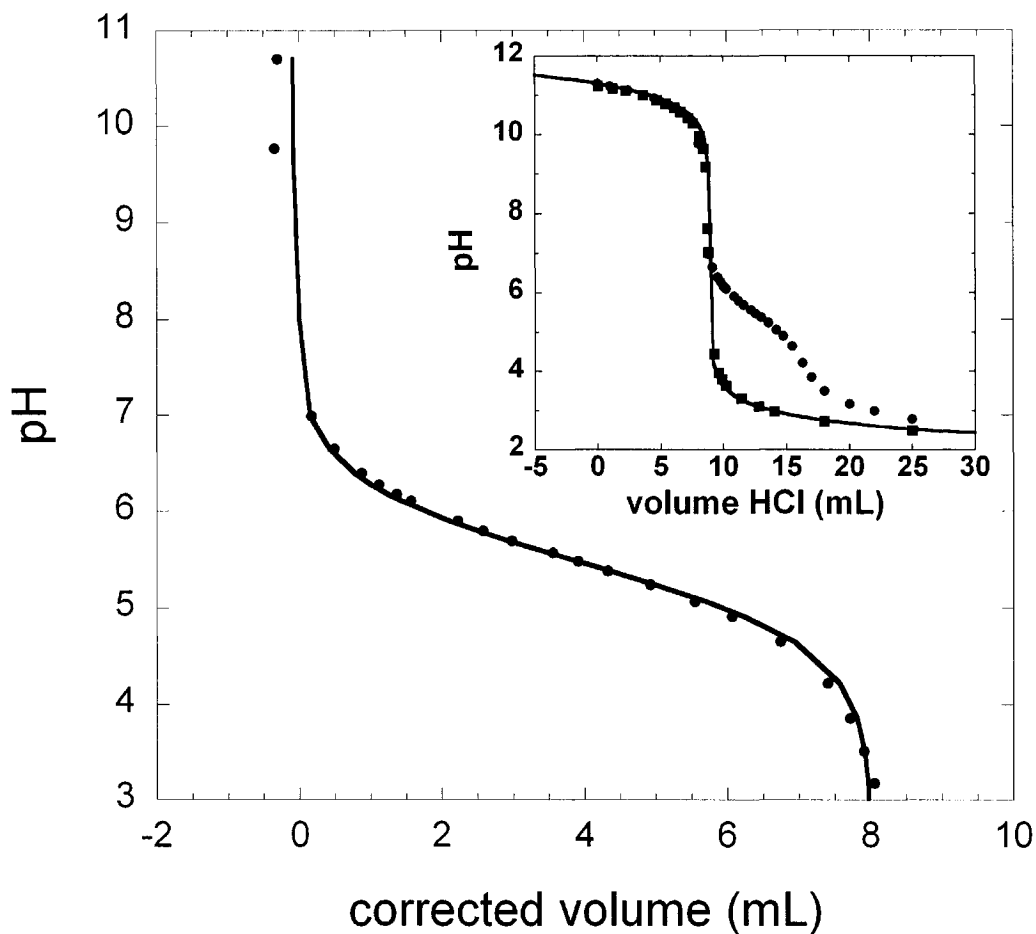
Figure 4.5 Representative corrected titration curve for the titration of benzoylphosphonate (2.5 mM) with HCl (25 mM). The titration was performed as described in section 4.2.6. The corrected titration data were fit to equation 4.2 giving a pK_{a2} for benzoylphosphonate of 5.47. **Inset.** Blank titration of NaOH (2.5 mM) with HCl (25 mM) (■) and titration of NaOH (2.5 mM) and benzoylphosphonate (2.5 mM) with HCl (25 mM) (●). The blank titration data were fit to equation 4.1.
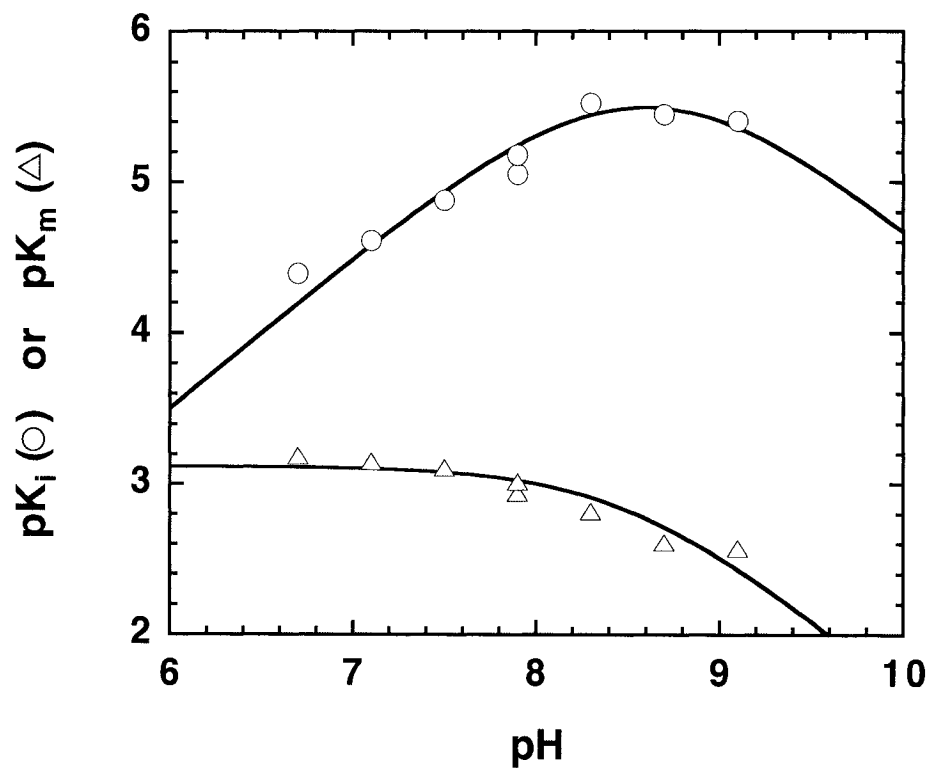
Figure 4.6 pH-Dependence of pK_i (O) and pK_m ($\triangle$) for the competitive inhibition of MR by BHA with respect to (R)-mandelate. Assay conditions were as described in section 4.2.6. From a fit of the data to equation 4.5, the value of pK_a^i for BHA was determined to be 8.7 ± 0.3 using a pK_a^e value of 8.51 ± 0.13 (obtained from a fit of the corresponding pK_m data).
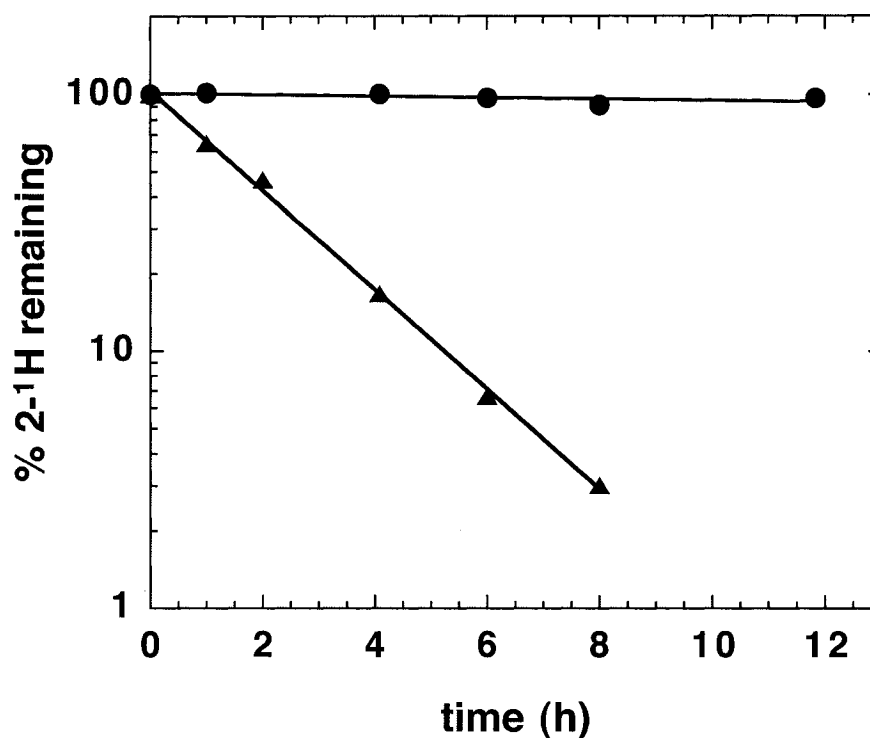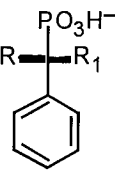
Figure 4.7 Time dependence for the exchange of the α-proton of (R)-mandelate (▲) and (R,S)-α-HBP (●) with solvent (D₂O) catalyzed by MR. The proton NMR signals were integrated after incubation of 10 mM (R)-[α-¹H]mandelate or 10 mM (R,S)-[α-¹H]hydroxybenzylphosphonate with 440 ng/mL MR for the indicated reaction times. Reaction conditions were as described in section 4.2.9. The peak area corresponding to the signal of the α-proton of either (R)-[α-¹H]mandelate or (R,S)-[α-¹H]hydroxybenzylphosphonate was measured relative to the peak area of the signal corresponding to the protons of the phenyl ring at the indicated times.

exchange of deuterium from solvent (D_2O) into the α-position of both (*R*)-mandelate and (*R*,*S*)-[α-^{1}H]HBP. While the α-proton of (*R*)-mandelate was completely exchanged in a first–order process, the α-proton of (*R*,*S*)-[α-^{1}H]HBP was not exchanged with solvent over 24 h, indicating that it was not a substrate for MR.

The inhibition of MR by α-fluorobenzylphosphonates was investigated to explore the effect of an isosteric substitution at the α-hydroxy position on inhibitor binding. The inhibition constants at 25 °C, pH 7.5 and pH 6.3 for (*R*,*S*)-, *(R)*-, and (*S*)-α-fluorobenzylphosphonate (α-FBP) and α,α-difluorobenzylphosphonate (α,α-F_2BP) are presented in **table 4.3**. (*R*)-α-FBP (9.6 mM) incubated with wild–type MR (30 μg/mL) showed no detectable change in the CD signal over 24 h, indicating that it was not a substrate for MR.

Table 4.3 Inhibition of MR by α-hydroxy and α-fluorobenzylphosphonates

Ligand	R	R_1	pK_{a2}	K_i (mM) pH 7.5	K_i (mM) pH 6.3
	PO_3H^- R——R_1 general structure of benzylphosphonate inhibitors				
(R,S)-α-HBP	H/OH	H/OH	6.89^a	0.0047 (±0.0007)	0.0023
α,α-F_2BP	F	F	5.71^b	12 (± 4)	1.0 (± 0.2)
(R,S)-α-FBP	H/F	H/F	6.60^b, 6.5^c	0.81 (± 0.34)	–
(R)-α-FBP	H	F	6.60^b, 6.5^c	1.1 (± 0.5)	–
(S)-α-FBP	F	H	6.60^b, 6.5^c	0.53 (± 0.17)	0.087 (± 0.012)

[a] pK_{a2} value from **figure 4.4**
[b] pK_{a2} value from (Smyth *et al.*, 1992)
[c] pK_{a2} value from (Blackburn & Kent, 1986)

4.4 Discussion

MR is a remarkably proficient enzyme, reducing the activation barrier for proton abstraction by 26 kcal/mol and producing a rate enhancement exceeding 15 orders of magnitude (Bearne & Wolfenden, 1997). Such proficient enzymes are expected to be extremely sensitive to inhibition by analogues of either transition states or high energy intermediates formed during catalysis (Mader & Bartlett, 1997; Wolfenden, 1972, 1974, 1976; Wolfenden & Frick, 1987). MR catalyzes the interconversion of the two enantiomers of mandelic acid in a stepwise manner, with the abstraction of the α-proton from either enantiomer leading to the formation of an enolic/ate intermediate (Hegeman *et al.*, 1970; Kenyon & Hegeman, 1970). Gerlt and Gassman have proposed that concerted general acid–general base catalysis promotes enolization of the mandelate anion (Gerlt & Gassman, 1992, 1993a, b; Gerlt *et al.*, 1991). Guthrie and Kluger (Guthrie & Kluger, 1993), on the other hand, have argued that the principal source of catalysis is electrostatic stabilization. Although the precise structure of the transition state for the enolization reaction catalyzed by MR is not known, it is reasonable to propose that it resembles either the putative *aci*-carboxylate intermediate or one of its conjugate acids. Indeed, studies conducted on the nonenzymatic exchange of deuterium into the α-position of mandelate, a reaction which is mechanistically similar to the enzyme–catalyzed reaction, support this proposal. The free energy of the transition state for the nonenzymatic exchange reaction has been estimated to be approximately 35 kcal/mol higher than the mandelate anion (Bearne & Wolfenden, 1997), while the neutral enol, enolate anion, and enolate dianion (*aci*-carboxylate) of mandelate lie 26.5, 25.3, and ~29 kcal/mol respectively above mandelate at pH 7.5, 25 °C (Bearne & Wolfenden, 1997; Chiang *et al.*, 1997; Chiang *et al.*, 1990; Kresge, 1991). Therefore, the structure of the transition state of the nonenzymatic exchange reaction is expected to resemble either the *aci*-carboxylate or one of its conjugate acids since these species have similar energies (Bearne & Wolfenden, 1997; Hammond, 1955).

Several reactive intermediate analogue inhibitors were designed based on the structural and electronic characteristics of the *aci*-carboxylate intermediate (**scheme 4.2**). Since the substrate, the *aci*-carboxylate intermediate, and the product have very similar structures, there are only a limited number of structural changes which can be made that will mimic the electronic features of the intermediate while remaining approximately isosteric with the intermediate. Of the seven analogues shown in **table 4.1**, several bind with an affinity that is similar to that observed for the substrate, while α-HBP and BHA bind two orders of magnitude more tightly. Both α-HBP and BHA bind Mg^{2+} with affinities equal to that of the substrate and, therefore, the high affinity of these inhibitors can not be attributed to an increase in Mg^{2+} binding affinity. The Mg^{2+} binding constants reported here are comparable to values reported in the literature for BHA with Mg^{2+} (118 M^{-1} compared with 470 M^{-1} (Farkas *et al.*, 2000) and mandelate with Ni^{2+} (45 M^{-1} (Che & Kustin, 1981) compared with 192 M^{-1} for mandelate with Mg^{2+}).

4.4.1 Inhibition by Carboxylate-Containing Analogues

Both phenylacetate and benzoylformate are bound to MR with an affinity similar to that observed for binding of the substrate ($K_m = K_S = 0.79$ mM and 0.74 mM for (*R*)-, and (*S*)-mandelate, respectively; see sections 2.3 and 3.3.2). Phenylacetate, in which the α-hydroxyl group of mandelate is replaced by a hydrogen atom, is bound by the enzyme slightly better than the substrate. Benzoylformate has an sp^2 center at the α-carbon and, therefore, might be expected to mimic the *aci*-carboxylate intermediate. However, the enzyme's affinity for benzoylformate is almost identical to its affinity for the substrate (neither hydration nor enolization of benzoylformate is expected to be significant at pH 7.5 based on the low equilibria for hydration ($K_{hyd}=0.057$) and enolization ($K_{enol}=2.6 \times 10^{-5}$) of the pyruvate anion at 25 °C (Esposito *et al.*, 1999)). Thus, the presence or absence of a hydroxyl function on the α-carbon does not seem to significantly affect binding of the carboxylate–containing analogues.

Scheme 4.2 General chemical structures of nitro, hydroxamate and phosphonate analogues of *aci*-carboxylate intermediates.

carbanion   *aci*-carboxylate   nitro analogue ($R_3 = O^-$)   phosphonate analogue

$(R_1 = Ph, R_2 = OH)$

hydroxamate analogue
$(R_2 = OH, R_3$ absent)
$(R_1 = Ph)$

$(R_2 = H$ or OH$)$
$(R_1 = Ph)$
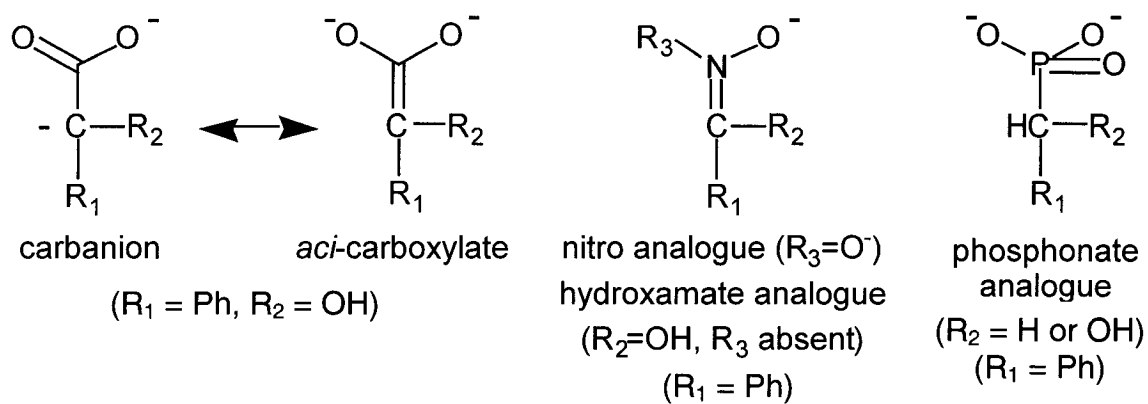
MR does not catalyze the exchange of the α-protons of phenylacetate with deuterated solvent despite having a similar affinity for both phenylacetate and mandelate, indicating that the α-hydroxyl function is required for catalysis (Landro *et al.*, 1994). Indeed, crystal structures of wild–type MR complexed with α-phenylglycidate, or (*S*)-atrolactate (Landro *et al.*, 1994), and mutant forms of MR complexed with (*S*)-mandelate (Kallarakal *et al.*, 1995) or (*S*)-atrolactate (Mitra *et al.*, 1995; Schafer *et al.*, 1996), all show the α-hydroxyl function coordinated to a magnesium ion known to be essential for catalysis (Fee *et al.*, 1974a, b). Because coordination of the magnesium ion by the α-hydroxyl function appears to be important for stabilization of the altered substrate in the transition state (i.e., catalysis) and not substrate binding, one might expect the binding affinity of a transition state or reactive intermediate analogue to be extremely sensitive to the presence of a hydroxyl function at the α-position.

4.4.2 Inhibition by Phosphonate–Containing Analogues

The dianionic phosphonate function is expected to resemble the *aci*-carboxylate group of the putative intermediate (**scheme 4.2**). Of the four phosphonate compounds examined as potential inhibitors of MR, only α-HBP was a potent inhibitor of the enzyme at pH 7.5. Unlike the carboxylate–containing analogues, inhibition of MR by the phosphonate analogues was enhanced by the presence of a hydroxyl group on the α-carbon. Benzylphosphonate, in which the α-hydroxy group of α-HBP is replaced by a hydrogen atom, is bound by the enzyme approximately 400 times less tightly than α-HBP. The presence of a carbonyl group at the α-carbon position also reduces the binding affinity, as evidenced by the 100-fold increase in the K_i value for benzoylphosphonate relative to α-HBP. It is unlikely that this weak binding, relative to the α-hydroxylated phosphonate, arises due to a difference between each compound's ability to chelate the active site magnesium ion. Comparison of the stability constants for the chelation of divalent metal ions (Zn^{2+} and Cu^{2+}) by α-ketobutyric acid compared to 2-

hydroxybutanoic acid, and by acetoacetate compared to 3-hydroxybutyric acid (Kubala & Martell, 1982) indicates that, while α-hydroxy acids tend to form slightly stronger chelates than the corresponding keto acids by factors ranging between 1.1 and 3.2, this added strength of association with the metal ion is not enough to account for the observed 100-fold decrease in binding affinity. The increased value of K_i for benzoylphosphonate relative to α-HBP may result from differences in the ionization state of the two inhibitors at pH 7.5. The pH-dependence of inhibition by α-HBP indicates that α-HBP is bound preferentially in the monoanionic ionization state (discussed below). If benzoylphosphonate is also bound as the monoanion, then differences in pK_{a2} values between the two inhibitors will influence their relative apparent K_i values observed at pH 7.5. The pK_{a2} value for benzoylphosphonate was determined potentiometrically to be 5.46 (**figure 4.5**). This value is similar to the pK_{a2} of ~5.6 determined for acetylphosphonate (O'Brien *et al.*, 1980). Using the pK_{a2} values to adjust for the concentration of the monoanion species present at pH 7.5, the K_i values for α-HBP and benzoylphosphonate *monoanion* may be corrected to 0.22 μM and 2.7 μM, respectively (see section 4.4.4). A single peak in the ^{31}P NMR spectra of benzoylphosphonate at pD 7.5 indicates the presence of only one species at the assay pH. Hydration of benzoylphosphonate, therefore, is not significant at pH 7.5. This is consistent with the low proportion (8%) of the methyl acetylphosphonate monoanion that exists as the hydrate at neutral pH (O'Brien *et al.*, 1980). Thus, benzoylphosphonate is considered to be entirely in the keto form at pH 7.5. The 10-fold difference in binding affinity between benzoylphosphonate and α-HBP indicates that MR is sensitive to the presence of the hydroxyl function at the α-position of the phosphonate analogues suggesting that a hydrogen–bond *donor* at the α-position may be responsible for providing the high binding affinity of α-HBP (discussed further in section 4.4.5). Based on this sensitivity to the catalytically essential α-hydroxyl function, α-HBP may be regarded as a mimic of the *aci*-carboxylate intermediate, or of the transition states for the intermediate's formation

starting from either substrate enantiomer (Hammond, 1955).

The pH–dependence of the inhibition of MR by α-HBP indicated that optimal inhibition is observed when the free enzyme is protonated and the phosphonate function of α-HBP is monoanionic (**figure 4.3**). It is not clear why the enzyme preferentially binds the monoanionic species. The most likely explanation is that residues in the active site are arranged to optimally bind the planar carboxylate or *aci*-carboxylate function and not a phosphonate function in which the negatively charged oxygen atoms are arranged tetrahedrally about the phosphorus atom. The two oxygens sharing the formal negative charge on the phosphonate monoanion, however, could mimic the planar carboxylate or *aci*-carboxylate function while the remaining phosphonate oxygen is protonated. Since it is possible that the intermediate might have enolic character, one might expect the monoanionic phosphonate function to mimic the protonated *aci*-carboxylate. However, this places the partially delocalized negative charge of the monoanion above the plane defined by the HO-P-O⁻ bonds, a configuration which resembles that expected for the phosphonate dianion (**scheme 4.3**) and appears to be unfavorable. In addition, if the developing negative charge on the carbonyl oxygen is one of the features that permits the active site to stabilize the intermediate through proton transfer from the general acidic catalyst (Gerlt, 1994; Mitra *et al.*, 1995), then one would expect proton transfer to the anionic oxygen of a phosphonate to be a significant factor in analogue binding.

Deuterium exchange experiments were conducted to determine whether α-HBP could act as a substrate for MR (**figure 4.6**). While mandelate completely exchanged its α-proton in a first order process, α-HBP did not exchange its α-proton with solvent over 24 h, indicating that it was not a substrate in the reaction catalyzed by MR. It is unlikely that differences in the electron withdrawing abilities of the phosphonate and carboxylate functions account for this observed lack of reactivity. The monoanionic phosphonate function is only slightly more electron withdrawing (σ_{para}= 0.17) than the carboxylate function (σ_{para}= 0.00 (Hansch & Leo, 1979)), while the dianionic phosphonate function is

Scheme 4.3 Possible binding orientations of active site ligands of MR

(R)-mandelate

aci-carboxylate
intermediate

α-HBP
monoanion

α-HBP
dianion

α-HBP
monoanion
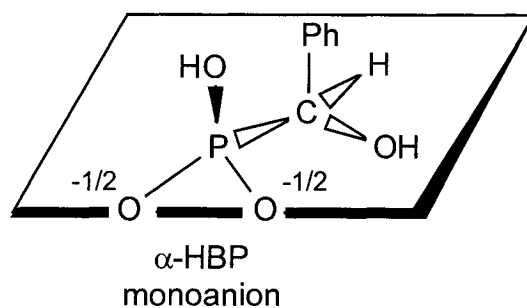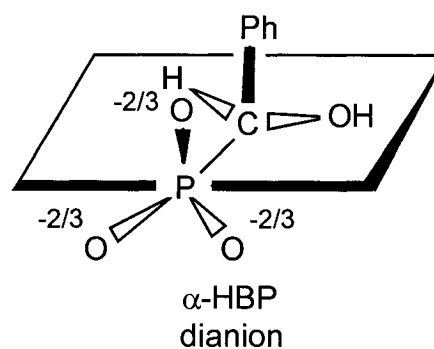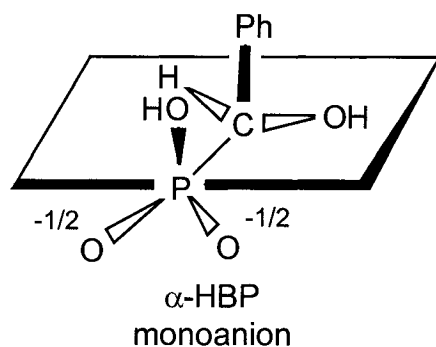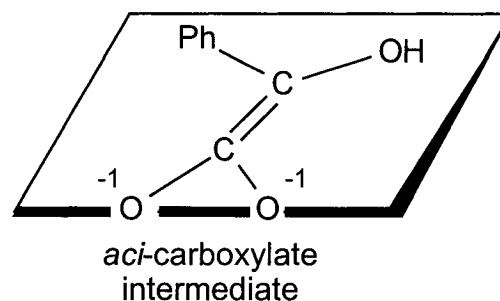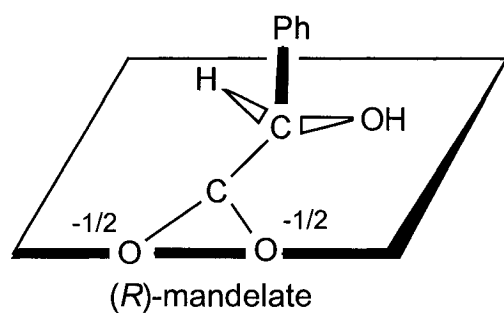
α-HBP is shown binding in a "skewed" orientation when the phosphonate oxygens bearing the negative charge are located in the same plane as the oxygens of the aci-carboxylate intermediate. (Solid and open wedges are used for groups which lie above and below the indicated planes.)

only slightly electron donating (σ_{para}= –0.16) (Martin & Griffin, 1965). A more likely explanation is that the α-hydrogen atom is not correctly positioned for abstraction. The added steric bulk of the phosphonate function could alter the position and orientation of α-HBP in the active site relative to that normally occupied by mandelate. The importance of steric bulk is illustrated by the observation that MR binds methyl α-HBP with much less affinity than it binds α-HBP. In addition to steric differences, the monoanionic phosphonate does not possess a rotationally symmetrical charge distribution like the carboxylate (**scheme 4.3**). The consequence of this difference in angular charge distribution is that α-HBP may bind in a "skewed" orientation and therefore behave as an inhibitor and not a substrate of the enzyme (Bearne & Kluger, 1992; Kluger *et al.*, 1978). In the carboxylate group of both mandelate and the *aci*-carboxylate, the negative charge is rotationally symmetrical about the line which bisects the angle made by the carboxyl carbon and the two anionic oxygens. This line also makes an angle of 180° relative to the bond between the carboxyl carbon and the α-carbon. The negative charge of the α-HBP dianion is also rotationally symmetrical with respect to such a line. However, this is not the case for the α-HBP monoanion. Orientation of monoanionic phosphonate function so that its negative charge aligns with that of the substrate or *aci*-carboxylate intermediate results in "skewed binding" of this analogue as illustrated in **scheme 4.3**. This may account for the observation that the α-HBP monoanion is an inhibitor of MR and not a substrate. In the absence of structural data, it is not clear why the phosphonate dianion is not preferentially bound at the active site of MR. One explanation is that the enzyme cannot tolerate a negatively charged substituent above or below the plane defined by the carboxylate function as shown in **scheme 4.3**.

4.4.3 Enantioselective Binding of α-HBP

The inhibition of MR by the individual enantiomers of α-HBP was investigated with respect to both (*R*)- and (*S*)-mandelate (**table 4.2**). MR bound (*S*)-α-HBP with an affinity that was 30 – 40-fold greater than that observed for (*R*)-α-HBP. This result provides the first example of an intermediate analogue which unmasks a "functional asymmetry" within the active site of MR. While such a strong binding preference for one enantiomer over the other might be unexpected for a "pseudosymmetric" enzyme such as MR, enantioselective binding preferences have been noted for the competitive inhibitors (*R*)- and (*S*)-atrolactate, the irreversible inhibitor (*R*)-phenylglycidate (Landro *et al.*, 1994) and the competitive inhibitors (*R*)- and (*S*)-hexahydromandelate (described in Chapter 5). It is of interest to note that (*S*)-hexahydromandelate, (*S*)-atrolactate and (*R*)-α-phenylglycidate all have the same relative configuration of atoms about the α-carbon as (*S*)-mandelate and are all bound more tightly than their enantiomers. However, the configuration of atoms about the α-carbon of (*S*)-α-HBP resembles (*R*)-mandelate and, therefore, would be expected to bind with *lower* affinity than the corresponding (*R*)-enantiomer. The most likely explanation for the observed binding preference for (*S*)-α-HBP relative to (*R*)-α-HBP is that "skewed" binding induced by the phosphonate function and the resulting altered position of the α-hydroxyl function produces different interactions between active site residues and the two enantiomeric ligands.

4.4.4 Inhibition by BHA

Like α-HBP, BHA is also a potent inhibitor of MR, binding two orders of magnitude more tightly than the substrate. This result is interesting in light of the recent

report that D-glucarate dehydratase, a member of the MR subgroup of the enolase superfamily of enzymes, binds xylarohydroxamate with an affinity (K_i = 0.8 mM; K_m for D-glucarate = 0.16 mM) which is much lower than would be expected if the hydroxamate was a mimic of the enolic intermediate (Gulick *et al.*, 2000). BHA has also recently been reported to be a competitive inhibitor of long–chain hydroxy acid oxidase, but it binds the enzyme with an affinity nearly 100-fold lower than that of the mandelate substrate and is, therefore, not considered to be an intermediate analogue for this enzyme (Amar *et al.*, 2002).

The pH–dependence of BHA inhibition of MR was consistent with the deprotonated form of BHA being preferentially bound by the enzyme. Using the pK_a value of 8.8 for BHA (Exner *et al.*, 1993; Farkas *et al.*, 2000) to account for the concentration of the deprotonated species at pH 7.5, the K_i value for the BHA anion may be adjusted to 0.44 μM, a value very similar to that of the α-HBP monoanion. Since BHA possesses two sites of deprotonation (i.e., nitrogen and oxygen), several structures may exist in solution (**scheme 4.4**) and the actual structure of the conjugate base of BHA has been the subject of a long–standing debate (Bagno *et al.*, 1994; Exner *et al.*, 1993; Ventura *et al.*, 1993). In water, BHA exists primarily in the keto form. The conjugate bases arising from *O*-deprotonation and *N*-deprotonation of the keto form have both been observed depending on the dielectric of the solvent. The *O*-deprotonated form of the enol has never been observed (Exner *et al.*, 1993). In water, experimental evidence suggests that BHA undergoes *O*-deprotonation (Exner *et al.*, 1993) yielding a species which resembles benzoylformate more than the putative *aci*-carboxylate intermediate. If MR recognizes the α-hydroxyl function as an important binding determinant of the reactive intermediate, as suggested by the carboxylate and phosphonate analogue studies, one would not expect

Scheme 4.4 Structures of BHA in solution.

"keto"

$\pm H^+$

K_a

"enol"

K_E

K_E'

$\pm H^+$

K_a^E

(For clarity, only the *cis*-form of the enol tautomer has been illustrated.)
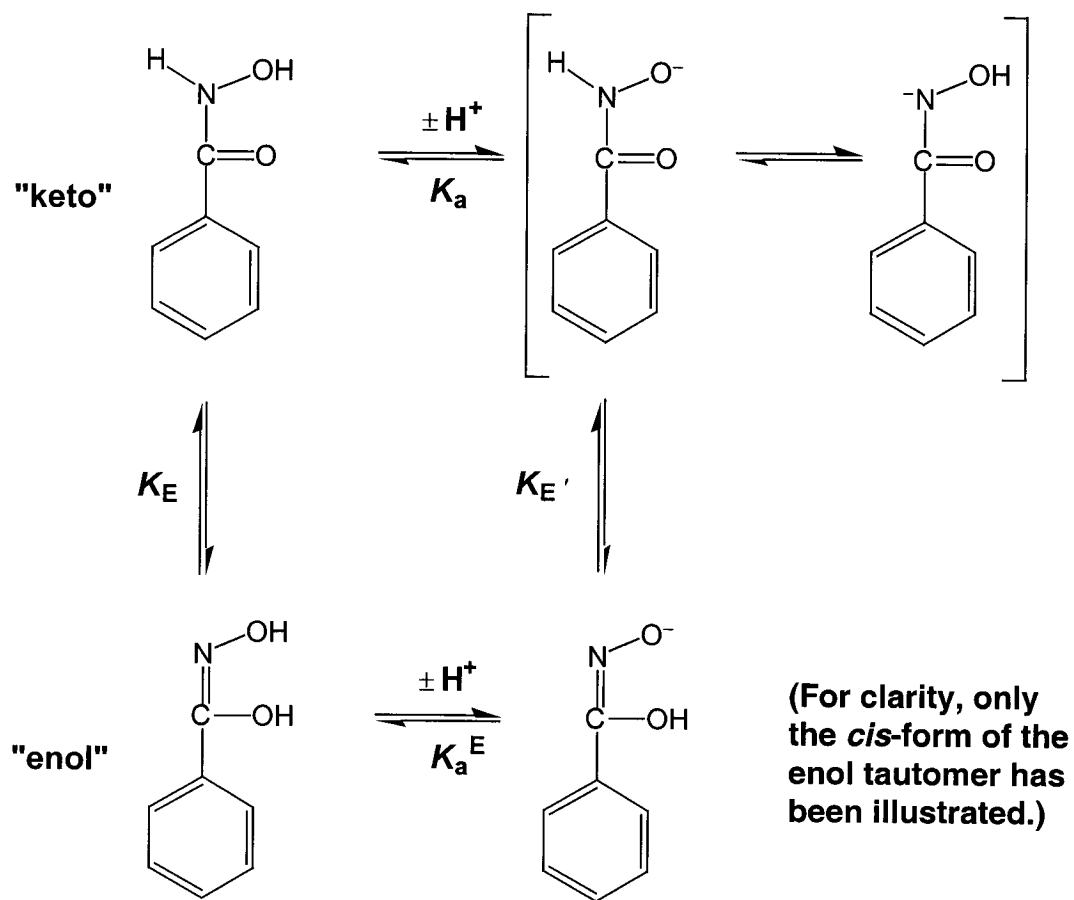
the enzyme to bind the keto form of BHA with the high affinity that is observed. On the other hand, the O-deprotonated form of the BHA enol (*cis* or *trans*) more closely resembles the putative *aci*-carboxylate intermediate. MR may stabilize this rare form of the inhibitor, promoting O-deprotonation of the enol to yield the monoanionic species within the active site.

4.4.5 Inhibition by α-Fluorobenzylphosphonates

To further test the hydrogen bond (H-bond) donating requirement at the α-hydroxy position of the substrate, a series of α-fluorobenzylphosphonates were assayed for their ability to act as inhibitors of MR. Fluorine is often used as an isosteric replacement for hydroxyl groups (Welsh, 1987) but the fluorine substituent can act only as an H-bond acceptor, restricting the hydrogen bonding capability of the ligand. Replacement of the α-OH by α-F can alter the properties of a phosphonate ligand in a number of additional ways. First, the substitution of the highly electronegative fluorine atom on the α-methylene of phosphonates lowers the pK_a of the phosphonate (Blackburn & Kent, 1986; Smyth *et al.*, 1992). In addition, the presence of the fluorine polarizes the C_α-H bond so that it may act as an H-bond donor (Abraham *et al.*, 1990) and it reduces coordination of the active site Mg^{2+} by the ligand.

The fluorinated analogues of the intermediate analogue inhibitor α-HBP ((R,S)-, (R)-, and (S)-α-FBP, and α,α-F$_2$BP) were all competitive inhibitors of MR. The values of the inhibition constants are given in **table 4.3**. MR binds the various α-FBPs with approximately 67–1400 times *less* affinity than it exhibits for (R,S)-α-HBP. Again, MR displayed a slightly higher affinity for the S enantiomer over the corresponding R enantiomer, consistent with the previous observations with (S)- and (R)-α-HBP (section 4.4.3). As with α-HBP, α-FBP is not a substrate for the enzyme. Examination of the pK_a values for the phosphonates in **table 4.3** suggests that the apparent lower binding affinity results, in part, from differences in the pK_a of the phosphonate function such that less of

the FBPs exist in solution as the monoanions. For example, the percentages of (S)-α-HBP, (S)-α-FBP, and α,α-F_2BP present as the monoanionic species at the assay pH of 7.5 are approximately 20%, 10%, and 1.6%, respectively. Indeed, the enzyme's affinity for both (S)-α-FBP and α,α-F_2BP improves 6- and 12-fold, respectively, when the assay pH is reduced from 7.5 to 6.3 (**table 4.3**) while the same change in the assay pH does not significantly alter the K_m for (R)-mandelate (**figures 4.3** and **4.6**). The K_i values listed in **tables 4.1** and **4.3** may be adjusted based on their pK_{a2} values to reflect the concentration of phosphonate monoanion present at pH 7.5. **Table 4.4** lists the adjusted K_i values and the corresponding free energy changes associated with binding of the phosphonate monoanion inhibitors reported in **tables 4.1** and **4.3**.

The change in free energy associated with replacing the α-OH with α-F represents both the loss of Mg^{2+} chelation and the loss of an H-bond donor. In addition, the α-F group could introduce a new and favourable H-bond interaction between the α-C-H of the ligand and one of the general base catalysts. The free energy change for binding of benzylphosphonate represents the loss of Mg^{2+} chelation and all H-bonding interactions. The keto form of benzoylphosphonate can chelate Mg^{2+} and can act as a weak H-bond acceptor, but the change in hybridization state of the α-carbon makes it likely that it binds in an altered configuration relative to α-HBP. Thus, it is not possible to unambiguously assign a free energy to the H-bond donor interaction of the ligand from a comparative analysis of the inhibitors in **table 4.4**. Nevertheless, the data presented in this chapter clearly indicates an important role for Mg^{2+} chelation and H-bond interactions at the α-OH position of the ligand in intermediate analogue binding, suggesting that both H-bond interactions and Mg^{2+} chelation become more important factors as the enzyme–catalyzed reaction approaches the transition state. Site–directed mutagenesis of Asn 197, a H-bond partner with the α-OH of the ligand, further reveals an important role for an H-bond interaction at the α-OH position in transition state stabilization (Chapter 6).

Table 4.4   Adjusted phosphonate K_i values reflecting the concentration of monoanion present at pH 7.5

Ligand	pK_{a2}	K_i (μM)	ΔG (kcal/mol)
benzylphosphonate	7.72[a], 7.6[b]	2200	–3.6
benzoylphosphonate	5.46[c]	2.7	–7.6
(S)-α-HBP	6.89[d]	0.22	–9.1
α,α-F$_2$BP	5.71[a]	190	–5.1
(S)-α-FBP	6.60[a], 6.5[b]	66	–5.7

[a] pK_{a2} value from (Smyth *et al.*, 1992)
[b] pK_{a2} value from (Blackburn & Kent, 1986)
[c] pK_{a2} value from **figure 4.5**
[d] pK_{a2} value from **figure 4.4**

Both α-HBP and BHA were designed to mimic features of the *aci*-carboxylate intermediate and represent the most potent reversible inhibitors yet to be reported for MR. The high affinity of these inhibitors results from their potential for H-bonding and Mg^{2+} chelation at the oxygen of the α-carbon, both of which are an absolute requirement for catalysis. These intermediate analogue inhibitors will serve as stable probes of the enzyme-intermediate complex of MR and will allow for the identification of important stabilizing interactions between MR and the altered substrate in the transition state.

CHAPTER 5

THE ROLE OF THE HYDROPHOBIC CAVITY IN GROUND STATE AND TRANSITION STATE STABILIZATION

5.1 Introduction

Crystal structures of MR complexed with substrate and substrate analogues (Kallarakal *et al.*, 1995; Landro *et al.*, 1994; Mitra *et al.*, 1995; Schafer *et al.*, 1996) reveal the aromatic ring of all ground state ligands located within a large, hydrophobic cavity at the mouth of the enzyme active site, remote from the site of proton abstraction (**figure 5.1**). The cavity is composed of hydrophobic amino acid residues from both the *N*-terminal and central β-barrel domains of the enzyme, and also includes Leu 93 from an adjacent two-fold related subunit (Neidhart *et al.*, 1991). A major component of the hydrophobic cavity is a large, mobile and amphipathic β-meander flap that extends over the active site substrate binding pocket (Neidhart *et al.*, 1991). The hydrophobic cavity of MR appears to accommodate a variety of substrates, including several *para* substituted mandelates (Felfer *et al.*, 2001; Kenyon & Hegeman, 1970; St. Maurice & Bearne, 2002), *p*-(bromomethyl)mandelate (Lin *et al.*, 1988), propargyglycolate (Landro *et al.*, 1992), vinylglycolate (Li *et al.*, 1995), *o*-chloromandelate and furyl, thienyl and naphthyl substituted glycolates (Felfer *et al.*, 2001). The spectrum of hetero- and aryl-substituted derivatives of mandelate that are accepted as substrates by MR reveals a relatively low degree of steric hinderance for substrate binding within the active site, hydrophobic cavity. Despite this broad substrate specificity, β,γ-unsaturation is required for catalysis (Li *et al.*, 1995). For example, vinylglycolate is a substrate for mandelate racemase while ethylglycolate is not (Li *et al.*, 1995). Hence, stabilization of the intermediate and/or the transition state by delocalization of negative charge into a β,γ-unsaturated system is required for catalysis (Felfer *et al.*, 2001; Kenyon & Hegeman, 1970; Li *et al.*, 1995). While the structure of the MR hydrophobic cavity has been well characterized and the

140

Figure 5.1 X-Ray crystal structure of the active site hydrophobic cavity of wild-type MR with bound (*S*)-atrolactate [pdb key = 1MDR (Landro *et al.*, 1994)]. The general acid/base catalysts His 297 and Lys 166 are shown along with the catalytically essential Mg^{2+} ion. The van der Waals radii for residues making up the hydrophobic pocket are displayed. Side chain residues contributed by the flexible hinged loop are shaded in yellow.

requirement for β,γ-unsaturation in MR catalysis is clear, the contribution to catalysis from enzyme–substrate and enzyme–transition state interactions in the hydrophobic cavity has not been clearly established.

The high proficiency of MR is achieved principally through the contribution of nearly 23 kcal/mol of enthalpic energy to the apparent binding free energy of the altered substrate in the transition state (St. Maurice & Bearne, 2002). This substantial release of energy is compatible with the development of enhanced hydrogen bonding, electrostatic interactions and nonpolar interactions in the enzyme–transition state complex (Wolfenden *et al.*, 1999). Several polar residues in the MR active site could serve to provide enhanced stabilization energy to the altered substrate in the transition state (Chapter 6). However, nonpolar interactions originating in the hydrophobic cavity may also contribute a degree of stabilization to the enzyme–transition state complex.

This chapter examines the role of the active site, hydrophobic cavity of MR in ground state and transition state stabilization. A series of modified substrate and intermediate analogue inhibitors are used to probe the interactions that exist between bound ligands and the hydrophobic cavity. The enzyme–catalyzed racemization of the alternative substrate, 2-naphthylglycolate, is reported, demonstrating a reduction in the rate of catalysis that correlates with a reduction in binding affinity for the 2-naphthyl intermediate analogue inhibitor. The plasticity of the active site, hydrophobic pocket is demonstrated using substrate and substrate/product analogues with increased steric bulk. Competitive inhibition of MR by benzilate, a substrate/product analogue, combined with molecular modeling of benzilate within the active site demonstrates a potential for the aromatic ring of both substrate and product to simultaneously occupy separate regions of the hydrophobic cavity. On the basis of this result, a dynamic model for MR catalysis is proposed, involving significant movement of the substrate's aromatic ring through the hydrophobic pocket as catalysis proceeds. Movement of the phenyl group provides a

mechanism for selective stabilization of the transition state relative to the ground state through increased interactions between the enzyme and the planar intermediate.

5.2 Materials and Methods

5.2.1 General

Racemic, (R)- and (S)-mandelic acid, (R)- and (S)-hexahydromandelic acid, (R)- and (S)-lactic acid, (S)-(–)-2-hydroxy-3,3,-dimethylbutyric acid (t-butylglycolic acid), glycolic acid, benzilic acid, acetohydroxamic acid, benzohydroxamic acid, benzyl alcohol, and (R)- and (S)-α-1-phenylethylamine were purchased from Sigma–Aldrich Canada Ltd. (Oakville, ON). (S)-Cyclohexylphenylglycolic acid was a gift from Sepracor Canada Ltd. (Windsor, NS). All other reagents were purchased from Sigma–Aldrich. Recombinant MR from *Pseudomonas putida* was overexpressed in and purified from *Escherichia coli* strain BL21(DE3) cells transformed with a pET15b plasmid (Novagen, Madison, WI, USA) containing the MR gene. This construct encodes the MR gene product with an N-terminal polyhistidine tag (MGSS(H)$_6$SSGLVPRGSHM$_1$...MR). The enzyme was purified by metal ion affinity chromatography as described previously (section 2.2.2). Once eluted from the Ni^{2+} affinity columns, wild–type MR was dialyzed into HEPES buffer (0.1 M, pH 7.5) containing MgCl$_2$ (3.3 mM) and NaCl (0.2 M). Melting points (uncorrected) were determined using a Gallenkamp melting point apparatus, and optical rotations at 589 nm were measured using a Rudolph Instruments Digipol 781 Automatic Polarimeter. NMR spectra were obtained using a Bruker AC 250F spectrometer. Chemical shifts are reported relative to the deuterium lock signal calibrated for the indicated deuterated solvent. Circular dichroism assays were conducted using a JASCO J-810 spectropolarimeter. Elemental analyses were conducted by Canadian Microanalytical Service Ltd. (Delta, BC).

5.2.2 (R,S)-1-Naphthylglycolic Acid

(R,S)-1-Naphthylglycolic acid was prepared by Dr. S. L. Bearne using a procedure based on the synthesis of mandelate from benzaldehyde described by Maggio *et al.* (1975). 1-Naphthaldehyde (15.62 g, 0.1 mol) was added to a solution of sodium

bisulfite (11 g, 0.1 mol) in water (30 mL) and the mixture was swirled vigorously for 20 min. Potassium cyanide (14 g, 0.2 mol) dissolved in water (30 mL) was then added and the mixture was swirled vigorously for an additional 20 min. A yellow–orange oil separated and the resulting solution was extracted with ether. The ether extract was washed with water and twice with saturated sodium chloride. The ether extract was dried over magnesium sulfate and was removed by rotary evaporation leaving an orange oil. The oil (4 g) was added dropwise to hot hydrochloric acid (5.3 M). After refluxing for 3 h, the solution was cooled to room temperature and any unreacted brown oil was removed using a disposable pipette. The solution was then extracted twice with ether and the combined ether extracts were dried over magnesium sulfate. Removal of the ether by rotary evaporation gave a crude product that was recrystallized from benzene to yield silver crystals of racemic 1-naphthylglycolic acid (1.12 g, 25% yield): mp 89-92 °C (lit. 87-88 °C (Compere Jr., 1968)); ^{1}H NMR δ (250.13 MHz; CDCl$_3$, ppm): 5.81 (1 H, s), 7.28-8.31 (7 H, m); Anal. Calcd for C$_{12}$H$_{10}$O$_3$: C, 71.28; H, 4.98. Found: C, 71.16; H, 5.02.

5.2.3 (R,S)-2-Naphthylglycolic acid

Racemic 2-naphthylglycolic acid was prepared according to the procedure described by Compere Jr. (1968). 1,4-Dioxane (100 mL), 2-naphthaldehyde (15.6 g, 0.1 mol), and bromoform (25.24 g, 0.1 mol) were added to a slurry of lithium chloride (8.48 g, 0.2 mol), potassium hydroxide (23.6 g, 0.4 mol), and ice (100 g). After stirring for 24 h at 4 °C, the pH was adjusted to 12 by addition of 6 M potassium hydroxide (8 mL) and the solution was stirred for an additional 24 h at 37 °C. The solution was then diluted with water (100 mL), acidified with concentrated hydrochloric acid (20 mL), and extracted twice with ether (50 mL). The combined ether extracts were washed with saturated sodium chloride and dried over magnesium sulfate. An orange solid remained after the ether was removed using rotary evaporation. Recrystallization from

chloroform:hexanes:ethanol (8:2:1) afforded white needles of racemic 2-naphthylglycolic acid (9.6 g, 48% yield): mp 148-150 °C (lit. 155-156 °C (Compere Jr., 1968), 163.5-167 °C (Kinbara *et al.*, 2000)); ^{1}H NMR δ (250.13 MHz; CD$_3$OD, ppm): 5.31 (1 H, s), 7.45-7.86 (7 H, m); Anal. Calcd for C$_{12}$H$_{10}$O$_3$: C, 71.28; H, 4.98. Found: C, 70.54; H, 4.98.

5.2.4 Resolution of (*R*)- and (*S*)-2-Naphthylglycolic acid

Both (*R*)- and (*S*)-2-naphthylglycolic acid were resolved using the procedure of Kinbara *et al.* (2000). (*R*)-1-Phenylethylamine (3.44 mL, 26.8 mmol) was added to a solution of (*R,S*)-2-naphthylglycolic acid (5.4 g, 26.8 mmol) in ethanol (150 mL). The solution was refluxed for 30 min and then slowly cooled to room temperature. Crystals (5.90 g) that appeared after two days were subsequently recrystallized twice from aqueous ethanol (90%). The resulting salt was dissolved in water (100 mL). Upon acidification of this solution with HCl (3 M, 50 mL), a white precipitate formed. The solid and aqueous phase were extracted four times with ether (100 mL) and the combined ether extracts were dried over magnesium sulfate. Removal of the ether by rotary evaporation gave a white powder. Recrystallization of this crude product from chloroform:ethanol (10:1) afforded pure (*R*)-2-naphthylglycolic acid (0.32 g, 6% yield), $[\alpha]_D^{20} = -144.9$ (*c* = 1.7, EtOH) (lit. $[\alpha]_D^{20} = -145.6$ (*c* = 0.98, EtOH) (Kinbara *et al.*, 2000), $[\alpha]_D^{21} = -142.2$ (*c* = 0.98, EtOH) (Howe *et al.*, 1973)).

(*S*)-2-Naphthylglycolic acid was resolved by addition of (*S*)-1-phenylethylamine (3.70 mL, 28.8 mmol) to a solution of (*R,S*)-2-naphthylglycolic acid (5.8 g, 28.8 mmol) in ethanol (100 mL). The solution was refluxed for 30 min and then slowly cooled to room temperature. Crystals (4.37 g) that appeared after 24 h were subsequently recrystallized twice from aqueous ethanol (90%). Crude (*S*)-2-naphthylglycolic acid was liberated from the salt as described for (*R*)-2-naphthylglycolic acid and recrystallized from chloroform:ethanol (15:1) to afford pure (*S*)-2-naphthylglycolic acid (94.1 mg, 2% yield),

$[\alpha]_D^{20} = +146.8$ ($c = 0.8$, EtOH) (lit. $[\alpha]_D^{20} = +144.7$ ($c = 0.98$, EtOH) (Kinbara *et al.*,

2000), $[\alpha]_D^{21} = +142.5$ ($c = 0.98$, EtOH) (Howe *et al.*, 1973)).

5.2.5 2-Naphthohydroxamic Acid

2-Naphthohydroxamic acid was prepared according to the procedure described by

Summers *et al.* (1987). 2-Naphthoic acid (2.5 g, 14.5 mmol) was dissolved in

dichloromethane (100 mL) containing DMF (1.06 g, 14.5 mmol). The solution was

cooled to 0 °C and oxalyl chloride (4.4 g, 32.6 mmol) was added dropwise. After stirring

for 45 min, this solution was added to a solution of hydroxylamine hydrochloride (3.75 g,

58 mmol) and triethylamine (8.8 g, 87 mmol) in THF:water (5:1, 60 mL) while the

temperature was maintained at 0 °C. The solution was stirred for an additional 30 min at

25 °C, poured into aqueous HCl (2 M, 100 mL), and the resulting acidic solution was

then extracted with dichloromethane (200 mL). A precipitate quickly formed in the

dichloromethane which was collected by suction filtration and recrystallized from ethanol

(100%) to afford colourless needles of pure 2-naphthohydroxamic acid (400 mg, 15%

yield): mp 162-164 °C (lit. 169-170 °C (Summers *et al.*, 1987)); ^{1}H NMR δ (250.13

MHz; CD$_3$OD, ppm): 7.5-8.25 (m); Anal. Calcd for C$_{11}$H$_9$NO$_2$: C, 70.58; H, 4.85; N,

7.48. Found: C, 70.51; H, 5.11; N, 7.49.

5.2.6 Cyclohexanecarbohydroxamic Acid

Methyl cyclohexanecarboxylate was reacted with (*O*-benzylhydroxylamine)methyl

aluminum chloride on a 10 mmol scale to generate the *O*-benzylcyclohexylhydroxamic

acid according to the general procedure described by Pirrung and Chau (1995). The crude

O-benzylcyclohexyl hydroxamic acid was a yellow oil which, after purification by silica

chromatography using hexanes:ethyl acetate (3:1) as the mobile phase, was a white

crystalline product. The *O*-benzyl hydroxamic acid (117 mg, 0.5 mmol) was

subsequently dissolved in methanol (20 mL) and hydrogenated over palladium for 14 h

according to the procedure described by Pirrung and Chau (1995). The resulting white

powder was recrystallized from hexanes:ethyl acetate (3:1) to give

cyclohexanecarbohydroxamic acid as white needles (40.7 mg, 3% yield): mp 119-120 °C

(lit. 125-129 °C (Pirrung & Chau, 1995), 137-139 °C (Nagarajan *et al.*, 1991)); ^{1}H NMR

δ (250.13 MHz; D$_2$O, ppm): 1.14-2.19 (m); Anal. Calcd for C$_7$H$_{13}$NO$_2$: C, 58.71; H,

9.15; N, 9.78. Found: C, 59.51; H, 9.24; N, 9.91.

5.2.7 Propianohydroxamic Acid

Propianohydroxamic acid was synthesized according to the general methods

described by Larsen *et al.* (1982) and Fishbein *et al.* (1969). Sodium hydroxide (4.3 g,

0.11 mol) and ethyl propionate (10.21 g, 0.10 mol) were added to a solution of

hydroxylamine hydrochloride (6.95 g, 0.10 mol) in methanol (100 mL). The mixture was

stirred at room temperature for 36 h at which point formation of the hydroxamic acid was

complete as indicated by the distinctive purple color of a spot of the reaction mixture on a

silica plate treated with ferrous chloride. The solution was adjusted to pH 6 by addition

of methanolic HCl, filtered, and evaporated to yield a yellow oil. Methanol (100 mL) was

added and, again, the solution was evaporated to a yield yellow oil and some crystals.

The crude mixture was extracted with boiling ethyl acetate (100 mL) and hot filtered.

The volume of the filtrate was reduced by boiling to ~10 mL and acetone (2 mL) was

added. Crystallization overnight at room temperature afforded pure propianohydroxamic

acid as colourless needles (1.54 g, 17 % yield): mp 90-95 °C (lit. 92-96 °C (Fishbein *et

al.*, 1969), 91-92 °C (Sosnovsky & Krogh, 1980)) ^{1}H NMR □ (250.13 MHz; D$_2$O, ppm):

1.06-1.12 (3 H, t), 2.11-2.54 (2 H, q). Anal. Calcd for C$_3$H$_7$NO$_2$: C, 40.44; H, 7.92; N,

15.72. Found: C, 40.62; H, 7.57; N, 15.58.

5.2.8 Trimethylacetohydroxamic Acid

Trimethylacetohydroxamic acid was synthesized according to the general method

described by Larsen *et al.* (1982). Sodium hydroxide (4.3 g, 0.11 mol) and methyl

trimethylacetate (13.3 mL, 0.10 mol) were added to a solution of hydroxylamine hyrochloride (6.95 g, 0.10 mol) in methanol (100 mL). The mixture was stirred at room temperature for three days at which point formation of the hydroxamic acid was complete as indicated by the distinctive purple color of a spot of the reaction mixture on a silica plate treated with ferrous chloride. The solution was adjusted to pH 7 by addition of methanolic HCl, filtered, and evaporated to dryness. The crude mixture was extracted three times with ethyl acetate (25 mL) and the combined extracts were evaporated to dryness. Recrystallization from toluene:light petroleum ether (1:1, 100 mL, with a few drops of ethanol) afforded pure trimethylacetohydroxamic acid as colourless needles (0.90 g, 9 % yield): mp 153-155 °C (lit. 154-159 °C (Johnson et al., 1985), 160-161 °C (Berndt & Shechter, 1964)) ^{1}H NMR δ (D$_2$O, ppm): 1.18 (s); Anal. Calcd for C$_5$H$_{11}$NO$_2$: C, 51.26; H, 9.46; N, 11.96. Found: C, 50.90; H, 9.35; N, 11.87.

5.2.9 MR Assays

MR activity was assayed using the CD assay described by Sharp et al. (1979). All inhibition assays were conducted at 25 °C in Na$^+$-HEPES buffer (0.1 M, pH 7.5) containing MgCl$_2$ (3.3 mM) and BSA (0.1%). For all inhibition assays, the conversion of (R)-mandelate to (S)-mandelate was followed, and the concentrations of (R)-mandelate ranged from 0.2375 to 9.50 mM. Reactions with the (R)-mandelate substrate were initiated by addition of enzyme to give a final concentration ranging from 150 to 250 ng/mL. Except where mentioned otherwise, initial velocities were determined by following the change in ellipticity at 262 nm in a quartz cuvette with a 1 cm light path. For inhibition assays with benzilate and benzyl alcohol, the high concentrations of these inhibitors necessitated that the assays be conducted at 268 nm ($[\theta]^R_{268}$ = +2980 deg mol^{-1} cm^2) to overcome the high absorbance at 262 nm. Inhibition assays with 1-

naphthylglycolate and 2-naphthylglycolate were performed at 262 nm using a quartz cuvette with a 0.5 cm light path. The commercial preparation of (S)-$(-)$-t-butylglycolic acid was very hydroscopic. To accurately determine the concentration of (S)-$(-)$-t-butylglycolic acid in the inhibition assays, NMR was used to quantitate the α-hydrogen peak of (S)-$(-)$-t-butylglycolic acid relative to a benzoic acid standard. For inhibition assays with 2-naphthohydroxamic acid, 20% DMSO was added to the 0.1 M Na^+-HEPES buffer to increase the solubility of the inhibitor. The addition of 20% DMSO to the assay buffer altered the molar ellipticity of (R)-mandelate at 262 nm ($[\theta]^R_{262} = +2908$ deg mol^{-1} cm^2) but had no effect on the K_m for (R)-mandelate (0.8 $\pm$ 0.1 mM in 0% DMSO (St. Maurice & Bearne, 2000); 1.0 $\pm$ 0.3 mM in 20% DMSO) or on the K_i for benzohydroxamate (11.7 μM in 0% DMSO (St. Maurice & Bearne, 2000); 11.8 μM in 20% DMSO). For assays with the substrates (R)- and (S)-2-naphthylglycolate, the reactions were followed at 266 nm ($[\theta]^R_{266} = -35\ 000$ deg mol^{-1} cm^2) in a quartz cuvette with a 0.1 cm light path. Reactions were initiated by addition of enzyme to give a final concentration between 0.5 to 2.0 μg/mL.

5.2.10 Data Analysis

The values of V_{max} and K_m were determined as described in Chapter 2. Competitive inhibition constants (K_i) were determined from linear replots of the observed values of K_m/V_{max} versus inhibitor concentration. All kinetic parameters were determined in triplicate and average values are reported. The reported errors are standard deviations. Protein concentrations were determined using the Bio-Rad protein assay (Bio-Rad

Laboratories, Mississauga, ON) with BSA standards, and k_{cat} values were obtained by dividing V_{max} values by the total enzyme concentration using M_r 40 728.

5.2.11 Computer Modeling

Molecular modeling of active site–bound benzilate was performed by conformation searches, prepared and conducted using DISCOVER 3.0 (Accelrys, San Diego, CA) with the CFF91 forcefield. Benzilate was modeled into the active site of MR by modifying the crystal structure of (S)-atrolactate in the MR active site [PDB key: 1MDR; (Landro et al., 1994)]. The ligand geometry was pre-optimized using 1000 iterations of steepest descent energy minimization. The potential energy of the system (protein + ligand) was minimized using 2000 iterations of steepest descent. The molecular dynamics calculations were subsequently conducted using the leapfrog algorithm at 300 K with 1 fs steps for 100 ps on a subset of residues located within 15 Å of the β-carbon atom. The averaged structures were calculated from the coordinates of 20+ trajectory snapshots (20 ps or more) of convergent conformational solutions.
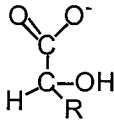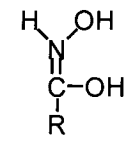
Geometry optimizations and van der Waals surface areas were calculated in the gas phase for glycolate, (S)-lactate, (S)-α–hydroxybutyrate, (S)-t-butylglycolate, (S)-mandelate, (S)-hexahydromandelate, (S)-1- and (S)-2-naphthylglycolcate and the trans– conjugate bases of benzohydroxamic acid, acetohydroxamic acid, propianohydroxamic acid, trimethylacetohydroxamic acid, cyclohexanecarbohydroxamic acid and 2-naphthohydroxamic acid by performing self–consistent field calculations at the 6-31G* level using MacSpartan Plus (Wavefunction, Inc., Irvine, CA).

5.3 Results

The role of the active site hydrophobic cavity of MR in ground state and transition state stabilization was investigated using both substrate and intermediate analogues truncated or modified at the β-carbon atom. The inhibition constants for benzyl alcohol, benzene and a series of glycolate derivatives (substrate analogues) and hydroxamic acid derivatives (intermediate analogues) are given in **table 5.1**. Comparison of the binding constants for (R)- and (S)-mandelate with that of glycolate reveals that the phenyl group contributes approximately 2 kcal/mol of free energy to ground state binding. Benzene, however, does not inhibit MR and benzyl alcohol is a weak competitive inhibitor. In addition, both the t-butyl and cyclohexyl substituted glycolates capture a binding energy equivalent to that of the substrate while the methyl substituted glycolates, (R)- and (S)-lactate, show no improved binding affinity over that of glycolate. Interestingly, MR displays a 10-fold binding preference for the S enantiomer of hexahydromandelate over the R enantiomer. This enantioselectivity was not observed for the other substrate analogues of **table 5.1** but has been observed for the enantiomers of α-HBP (St. Maurice & Bearne, 2000; Chapter 4), atrolactate and the irreversible inactivator phenylglycidate (Landro et al., 1994). (S)-Hexahydromandelate (20 mM) showed no detectable change in CD signal after a 48 h incubation with 20 μg/mL MR and, therefore, was considered not to be a substrate for MR.

Comparison of the inhibition constant for the intermediate analogue benzohydroxamic acid (BHA) with that of acetohydroxamic acid reveals a contribution from the phenyl substituent of 4.6 kcal/mol to the overall binding free energy of the intermediate. This is more than twice the energy contributed by the phenyl substituent to substrate binding and suggests that interactions between the enzyme and the aromatic ring of the ligand are a source for tighter binding of the enzyme–intermediate complex. Neither the ethyl, t-butyl nor the cyclohexyl substituted hydroxamic acids capture greater

Table 5.1 Inhibition Constants at 25 °C for MR with a Series of Substrate and Intermediate Analogues and their Pieces.

R	glycolate derivatives		hydroxamic acid derivatives
H (glycolate)	$K_i = 30.2 \pm 5.7$ mM		—
	(R) K_i, mM ($\Delta\Delta G$, kcal/mol)	**(S)** K_i, mM ($\Delta\Delta G$, kcal/mol)	K_i, mM ($\Delta\Delta G$, kcal/mol)
methyl (lactate)	32.0 ± 1.4 $(0.03 \pm 0.01)^a$	26.1 ± 3.1 $(-0.09 \pm 0.02)^a$	26.5 ± 2.6 —
ethyl (α-hydroxy-butyrate)	3.6 ± 0.4^b (-1.3 ± 0.3)		11.9 ± 3.6 $(-0.5 \pm 0.2)^c$
t-butyl (t-butyl-glycolate)	—	1.39 ± 0.27 $(-1.8 \pm 0.5)^a$	0.81 ± 0.17 $(-2.1 \pm 0.5)^c$
cyclohexyl (hexahydro-mandelate)	0.70 ± 0.24 $(-2.2 \pm 0.9)^a$	0.071 ± 0.029 $(-3.6 \pm 1.6)^a$	0.25 ± 0.03 $(-2.8 \pm 0.4)^c$
phenyl (mandelate)	0.84 ± 0.04 $(-2.1 \pm 0.4)^a$	0.73 ± 0.05 $(-2.2 \pm 0.4)^a$	0.0117 ± 0.0012 $(-4.6 \pm 0.6)^c$

Substrate Analogue Pieces Lacking the Carboxyl Function			
benzyl alcohol	$K_i = 15.4 \pm 1.9$ mM	benzene	$K_i \geq 230$ mM^d $K_i \geq 950$ mM^e

[a] binding free energy at 25 °C due to the glycolate R group [$\Delta\Delta G = -RT\ln(K_i^H/K_i^R)$]

[b] Reported for (R,S)-α-hydroxybutyrate in the $R \rightarrow S$ direction (Li et al., 1995)

[c] binding free energy at 25 °C due to the hydroxamic acid R group [$\Delta\Delta G = -RT\ln(K_i^{CH_3}/K_i^R)$]

[d] K_i value estimated assuming competitive inhibition and a limit of ≥5% detectable loss of activity in the presence of the inhibitor

[e] K_i value estimated assuming noncompetitive inhibition and a limit of ≥5% detectable loss of activity in the presence of the inhibitor

than 3 kcal/mol in binding free energy relative to acetohydroxamic acid, indicating that there exists a marked preference for the phenyl substituent in the binding of hydroxamic acid ligands to MR.

The values of k_{cat} and K_m for the enzyme–catalyzed racemization of the alternative substrates, (R)- and (S)-2-naphthylglycolate, are given in **table 5.2**. Comparison of these kinetic parameters with those determined previously for (R)- and (S)-mandelate (St. Maurice & Bearne, 2000) reveals that the values of k_{cat} and K_m are reduced 16-fold and 2-fold, respectively, for (R)-2-naphthylglycolate relative to (R)-mandelate. When (S)-2-naphthylglycolate is the substrate, the value of k_{cat} is reduced 18-fold relative to (S)-mandelate, while the value of K_m remains essentially unchanged relative to (S)-mandelate. Overall, the efficiency (k_{cat}/K_m) for MR–catalyzed racemization of either (R)- or (S)-2-napthylglycolate is reduced approximately 10-fold relative to (R)- and (S)-mandelate. Comparison of the inhibition constant for 2-naphthohydroxamic acid, an intermediate analogue inhibitor for the racemization of 2-naphthylglycolic acid, to that observed for BHA indicates that the presence of the 2-naphthyl group reduces the binding affinity of the intermediate analogue approximately 5-fold.

The plasticity of the active site, hydrophobic pocket was investigated using the "bulky" substrate and substrate/product analogues shown in **table 5.3**. Both 1-naphthylglycolate and 2-naphthylglycolate were found to be competitive inhibitors of MR with respect to (R)-mandelate. Both of these inhibitors were bound by the enzyme with approximately the same affinity as (R)- or (S)-mandelate, indicating that replacement of the phenyl group of mandelate with a naphthyl group is well tolerated by the hydrophobic pocket. Interestingly, benzilate, a diphenyl □-hydroxy analogue of mandelate, is a competitive inhibitor of MR and is bound by the enzyme with an affinity equal to that of the substrate **(figure 5.2)**. To rationalize how benzilate might be bound by MR, the inhibitor was modeled in the active site and conformational analyses were conducted using energy minimization calculations over 100 ps. The resulting averaged

Table 5.2 Kinetic constants and hydroxamic acid inhibition constants for the MR–catalyzed racemization of mandelate (St. Maurice & Bearne, 2000) and 2-naphthylglycolate.
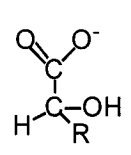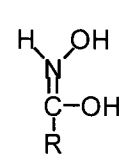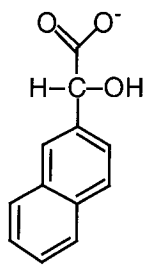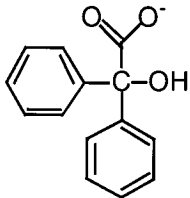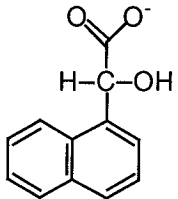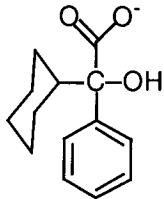
	R = phenyl	R = 2-naphthyl
$K_m^{(R)}$ (mM)	0.81 ± 0.12	0.46 ± 0.06
$k_{cat}^{(R) \to (S)}$ (s^{-1})	514 ± 48	33 ± 1
$\left(\dfrac{k_{cat}}{K_m}\right)^{(R) \to (S)}$ (M^{-1}s^{-1})	$(6.4 \pm 1.1) \times 10^5$	$(7.2 \pm 1.0) \times 10^4$
$K_m^{(S)}$ (mM)	0.62 ± 0.04	0.41 ± 0.03
$k_{cat}^{(S) \to (R)}$ (s^{-1})	447 ± 12	25 ± 1
$\left(\dfrac{k_{cat}}{K_m}\right)^{(S) \to (R)}$ (M^{-1}s^{-1})	$(7.2 \pm 0.5) \times 10^5$	$(6.1 \pm 0.5) \times 10^4$

	R = phenyl	R = 2-naphthyl
K_i (μM)	12 ± 1	57 ± 18

Table 5.3 **Inhibition constants for MR with substrate and substrate/ product analogue inhibitors.**

Substrate Analogue	K_i (mM)	Substrate/ Product Analogue	K_i (mM)
(*R*,*S*)-2-naphthylglycolate	0.52 ± 0.03	benzilate	0.67 ± 0.12
(*R*,*S*)-1-naphthylglycolate	1.9 ± 0.1	(*S*)-cyclohexyl-phenylglycolate	0.50 ± 0.03
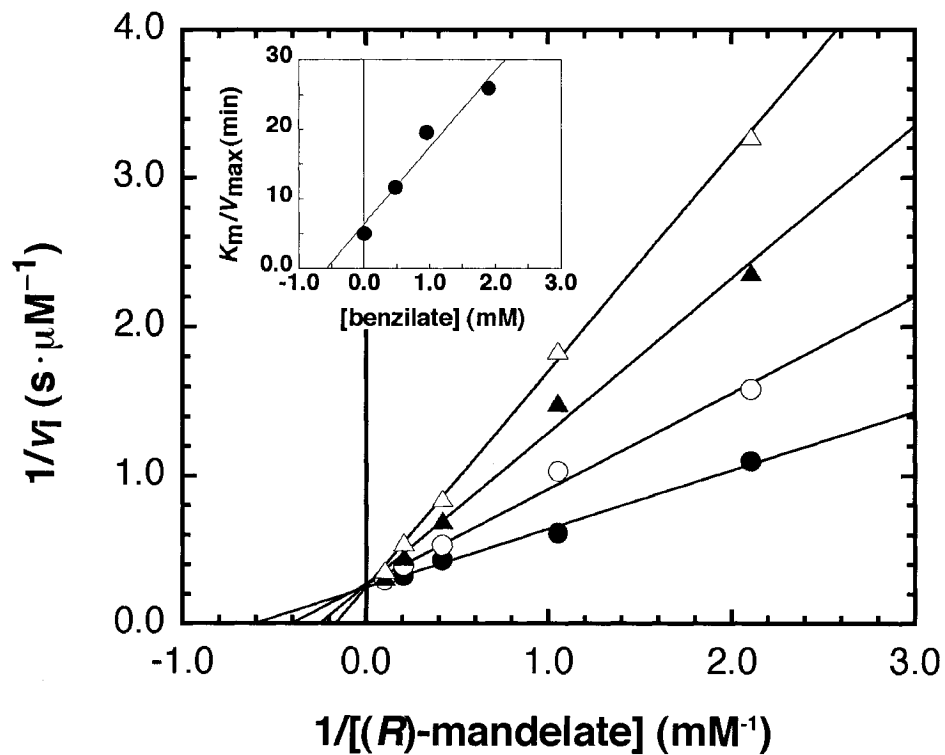
Figure 5.2 **A representative double reciprocal plot for the competitive inhibition of MR by benzilate.** Concentrations of benzilate were 0 mM (●), 0.48 mM (○), 0.95 mM (▲), and 1.90 mM (△). (Inset) Replot of $(K_m/V_{max})^{app}$ as a function of benzilate concentration.

structures from five separate minimizations are shown in **figure 5.3.** There appears to be sufficient spatial flexibility within the hydrophobic cavity to completely accommodate both aromatic rings of benzilate. Finally, the competitive inhibition of MR by (S)-cyclohexylphenylglycolate further illustrates the ability of the hydrophobic pocket to accommodate bulky ground state ligands.

Figure 5.3 Computer modeling of benzilate in the active site of MR. Five averaged backbone structures and their respective benzilate molecules are displayed. Each of the five structures is an independent simulation defined by averaging 20 ps of convergent solution.

5.4 Discussion

Enzymes use many interactive forces, including hydrogen bonding, electrostatic interactions, van der Waals interactions, and entropically driven hydrophobic interactions to bind substrates and stabilize transition states and intermediates during catalysis (Fersht, 1985; Mader & Bartlett, 1997). For MR, such interactions include hydrogen bonding with Glu 317 (Landro et al., 1994; Mitra et al., 1995) and Asn 197 (St. Maurice & Bearne, 2000), and electrostatic interactions with Lys 164 (Neidhart et al., 1991; Schafer et al., 1996) and Mg^{2+} (Fee et al., 1974b; Guthrie & Kluger, 1993; Landro et al., 1994). The importance of these polar interactions is underscored by the major enthalpic contribution that they make to transition state stabilization (St. Maurice & Bearne, 2002). However, the contribution from hydrophobic interactions to catalysis are less well understood, most likely because no distinct point of interaction can be readily identified. The hydrophobic cavity of MR probably contributes a combination of diffuse van der Waals interactions that serve to bind the aromatic ring of the substrate. It is not clear, however, what the role of such interactions might be in transition state stabilization. Using a series of modified substrate and intermediate analogues, the binding free energies arising from interactions within the hydrophobic cavity have been quantified and they demonstrate that these interactions differentially stabilize the transition state (or intermediate) relative to the ground state.

5.4.1 Substrate Analogue Binding Interactions within the Hydrophobic Cavity

The absence of detectable inhibition of MR by benzene and only weak competitive inhibition by benzyl alcohol implies that electrostatic and hydrogen bonding interactions with the substrate carboxylate and α-hydroxyl groups are essential for ligand

binding. However, MR also exhibits only a weak affinity for glycolate and lactate, implying that interactions within the hydrophobic cavity also contribute significantly to the overall substrate binding affinity. Inhibition of MR by phenylacetate (Hegeman et al., 1970; St. Maurice & Bearne, 2000) reveals no net loss in binding affinity upon removal of the α-hydroxyl group of the substrate. Individually, therefore, it appears that no single interaction dominates the overall ground state binding energy and, rather, a variety of interactions between the substrate carboxylate group, α-hydroxyl group, and phenyl group act synergistically to bind the substrate in the ground state.

While the importance of the carboxylate and hydroxyl groups in substrate binding has been recognized previously (Li et al., 1995), the role of the aromatic ring in binding has not been explored in detail. The free energy of binding of the substrate in the hydrophobic cavity could originate from several possible sources, including contributions from entropically driven hydrophobic interactions, specific electrostatic interactions, and van der Waals interactions. It is unlikely that specific electrostatic interactions such as aromatic–aromatic (Burley & Petsko, 1988) or cation–π interactions (Dougherty, 1996) contribute significantly to ground state binding in the hydrophobic cavity since substrate analogues with bulky alkyl groups in place of the aromatic ring (e.g., hexahydromandelate and t-butylglycolate) exhibit binding affinities similar to mandelate. If the active site of MR "solvates" the substrate in a manner similar to a nonpolar solvent, then the free energy changes associated with the binding of substrate and ground state analogues should be proportional to their corresponding free energy changes for partitioning between water and nonpolar solvents such as cyclohexane or octanol. For example, the binding free energies of alkyl glycosides to β-glucosidases increase with

increasing chain length and correlate with the standard free energies of partitioning between octanol and water, implying that a portion of the active site is similar to octanol in its hydrophobicity (Gopalan *et al.*, 1989).

The logarithm of the octanol/water partition coefficient for a *molecule* (log *P*) is a measure of its relative hydrophobicity (Leo *et al.*, 1971). The relative hydrophobicity of a *substituent* is defined as its π value (Leo *et al.*, 1971). The π value is determined by the difference in log *P* values between a derivative compound containing a particular substituent and a parent compound lacking that substituent (eg., $\pi_{CH_3} = \log P_{C_6H_5CH_3} - \log P_{C_6H_6} = 2.69 - 2.13 = 0.56$). A positive value for π means that the substituent favours the octanol phase relative to hydrogen (i.e., it is more hydrophobic) while a negative value means that it disfavours the octanol phase relative to hydrogen (i.e., it is more hydrophilic). Thus, the π value provides a convenient means of comparing the relative hydrophobicities of various substituents.

A plot of the log of the binding constants (K_s for mandelate and K_i for the substrate analogues) against the π values (Hansch & Leo, 1979) is linear, shows good correlation ($r^2 = 0.94$), and has a slope of -0.8 (**figure 5.4A, solid line**). This suggests that the hydrophobic cavity of MR effectively "solvates" the phenyl group of the substrate in an environment that is only slightly less hydrophobic than octanol. A similar plot against the hydrophobicity constant, π, for a series of substituted formanilide inhibitors lead to the suggestion of a hydrophobic binding preference in the active site of chymotrypsin (Fastrez & Fersht, 1973). Neither 1- nor 2-naphthylglycolate was included in the above analysis. The nearly 10-fold reduction in binding affinity for 1-naphthylglycolate relative to 2-naphthylglycolate (**table 5.3**) indicates that the bulkier naphthyl derivatives are
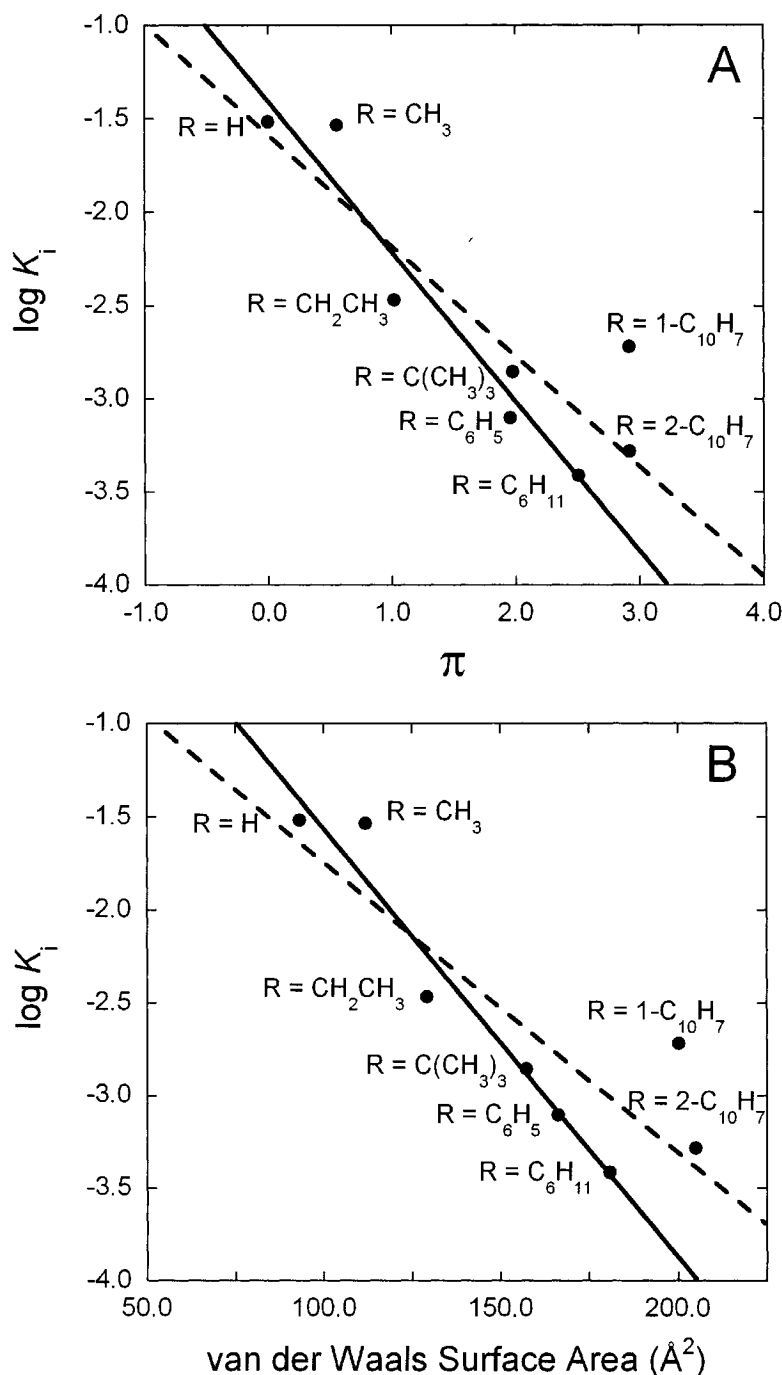
Figure 5.4 Correlation between log K_i values for the modified glycolate inhibitors (average of the K_i values for the R and S enantiomers) and (A) the hydrophobicity constant (π) (Hansch & Leo, 1979) corresponding to the groups at the β-carbon position of the inhibitor and (B) the calculated van der Waals surface areas of the inhibitor molecules (table 5.4). The inhibition constant reported for racemic 2-hydroxybutanoic acid is 3.6 ± 0.4 mM with respect to (R)-mandelate (Li *et al.*, 1995). The dashed line is the linear regression for all of the data points (A: slope = –0.59, r^2=0.78; B: slope = –0.016, r^2=0.76) and the solid line represents the linear regression excluding the naphthyl derivatives (A: slope = –0.80, r^2=0.94; B: slope = –0.023, r^2=0.95).

subject to additional binding constraints within the hydrophobic cavity. The added steric bulk of these inhibitors results in slightly unfavourable binding interactions which complicate interpretation of the data and result in a deviation from the linear correlation with both π and the van der Waals radii (*vide infra*) (**figure 5.4, dashed lines**).

The entropically favourable expulsion of ordered water molecule(s) from an enzyme active site contributes to the strength of the hydrophobic interaction between an enzyme and a bound ligand (Fersht, 1985). Overall, substrate binding by MR is disfavoured entropically (St. Maurice & Bearne, 2002) but a comparison of the crystal structure of MR in the presence (pdb key: 1MDR (Landro *et al.*, 1994)) and absence (pdb key: 2 MNR (Neidhart *et al.*, 1991)) of the substrate analogue (S)-atrolactate reveals the expulsion of two ordered water molecules (HOH 434 and HOH 617 in the 2MNR crystal structure) from the hydrophobic cavity upon formation of the enzyme–substrate complex. The expulsion of ordered water from an enzyme active site has been proposed to provide favourable and significant entropic contributions to the binding of both ground state and transition state species (Snider *et al.*, 2000; Snider & Wolfenden, 2001 and references therein).

One of the principal forces that contribute to the binding of nonpolar substrates in enzyme active sites are van der Waals interactions. For example, van der Waals contacts contribute approximately -120 cal mol^{-1} Å^{-2} to the hydrophobic interaction energies of small ligands binding to the FK506 binding protein (Burkhard *et al.*, 2000). The binding affinity of horseradish peroxidase c for its substrate benzohydroxamate is $>10^4$-fold greater than its affinity for the substrate analogue acetohydroxamate, despite the potential for both compounds to form identical hydrogen bonding interactions within the active site (Schonbaum, 1973). This high binding affinity for benzohydroxamate relative to

acetohydroxamate results from a high number of van der Waals interactions involved in binding the aromatic ring of BHA in horseradish peroxidase c (Henriksen et al., 1998). If van der Waals interactions contribute significantly to the binding of a particular ligand then the free energy changes associated with the binding of various ligands should correlate with their van der Waals surface areas (Bojarski & Mokrosz, 1999; Ibba et al., 1994; Shibaev et al., 1975). **Figure 5.4B** shows a plot of the log K_i values for a series of substrate analogues of MR against their corresponding van der Waals surface areas. The calculated van der Waals surface areas are presented in **table 5.4**. The observed linear relationship (slope = –0.02) shows a strong correlation ($r^2 = 0.95$). It is difficult, however, to establish whether this correlation is the result of increased van der Waals contacts with the ligand in the enzyme active site relative to the solvent or whether it is due to the desolvation of the hydrophobic ligand (i.e., a hydrophobic effect). The desolvation of a hydrophobic ligand is proportional to its hydrophobic surface area. Thus, the correlation with surface area observed in **figure 5.4B** may simply be a manifestation of the hydrophobic effect already described. For example, measurements on the magnitude of the hydrophobic effect range from 25 to 80 cal $mol^{-1}Å^{-2}$ (Chothia & Janin, 1975; Shortle et al., 1990). The slope of the line in **figure 5.4B** (–0.023 $Å^{-2}$) can be converted to a free energy dependence of –31 cal mol^{-1} $Å^{-2}$ at 25 °C (i.e., slope = log $K_i/$ $Å^2$; $\therefore$ 2.303RT(slope) = $\Delta G/$ $Å^2$). This value is in the range generally accepted for desolvated hydrophobic surfaces (Mader & Bartlett, 1997).

Given the role of nonpolar interactions in substrate binding by MR, it is interesting to note the recent X-ray crystal structure of O-succinylbenzoate synthase (OSBS), a member of the enolase superfamily to which MR belongs, complexed with the product O-succinylbenzoate (OSB) (Thompson et al., 2000). The enzyme–product complex reveals

Table 5.4 Calculated van der Waals surface areas and partition coefficients for modified glycolates and *trans*-hydroxamates.

R	Calculated van der Waals Surface Area ($\mathring{A}^2$)		π[a]
	glycolate	*trans*-hydroxamate	
H	93.2	–	0.00
CH_3	111.8	99.0	0.56
CH_2CH_3	129.3	117.2	1.02
$C(CH_3)_3$	157.2	146.1	1.98
C_6H_5	166.3	152.7	1.96
C_6H_{11}	180.9	170.8	2.51
$1\text{-}C_{10}H_7$	200.4	–	2.92[b]
$2\text{-}C_{10}H_7$	205.1	197.4	2.92[b]

[a] From (Hansch & Leo, 1979) except where indicated otherwise.

[b] Calculated from log $P_{C_{10}H_8}$ (Leo *et al.*, 1971)– logP_{H_2} (Leo *et al.*, 1975)

that very few hydrogen bonding or electrostatic interactions are involved in the binding of OSB to the active site and that nonpolar interactions play a significant role in binding the enzyme–product complex. It was proposed that the lack of binding constraints associated with these nonpolar interactions may allow for the rapid evolution of the enzyme's substrate specificity. Indeed, for MR, flexibility in the hydrophobic pocket resulting from a preponderance of nonpolar interactions may be advantageous in allowing the enzyme to bind and racemize many substituted derivatives of mandelate that are naturally available in the local environment of *Pseudomonas putida*. For example, the enzymes responsible for metabolizing (*R,S*)-mandelic acid in *P. putida* also metabolize (*R,S*)-*p*-hydroxymandelic acid (Hegeman *et al.*, 1970).

The 10-fold increase in binding affinity for the *S* enantiomer of hexahydromandelate relative to the *R* enantiomer is surprising for an enzyme that is typically "pseudosymmetric" (Kenyon *et al.*, 1995) but it is not unprecedented. MR has exhibited a significant degree of enantioselectivity with a number of ligands. The two enantiomers of the intermediate analogues α-HBP and α-FBP show a marked difference in binding affinity (St. Maurice & Bearne, 2000) and enantioselective binding has been noted for (*R*)- and (*S*)-atrolactate as well as for the irreversible inhibitor (*R*)-phenylglycidate (Landro *et al.*, 1994). Enantioselective binding of these ligands reveals a degree of structural asymmetry within the active site of MR.

5.4.2 Intermediate Analogue Binding Interactions within the Hydrophobic Cavity

The aromatic ring of the substrate contributes to catalysis by acting as an electron sink to stabilize the α-carbanionic intermediate. The observation that (*S*)-hexahydromandelate is not a substrate for MR combined with the observation by Li *et al.*

(1995) that vinylglycolate is a substrate for MR while ethylglycolate is not, supports the notion that β,γ-unsaturation is required for catalysis. Is the contribution to catalysis from the phenyl group limited to its stabilizing role in charge delocalization or are there other interactions within the hydrophobic cavity that might contribute to stabilization of the intermediate and transition states formed during catalysis?

The intermediate analogue inhibitor, BHA, is a potent competitive inhibitor of MR, binding with an affinity approximately two orders of magnitude greater than that observed for the substrate (St. Maurice & Bearne, 2000). The modeled electrostatic surface potential for BHA reveals several geometric and electronic features in common with the putative aci-carboxylate intermediate in the MR–catalyzed reaction, including an sp^2-hybridized α-carbon and a potential for donation of a hydrogen bond from the α-hydroxy position of the conjugate base of trans-BHA (St. Maurice & Bearne, 2000). While BHA captures only a small fraction of the binding affinity expected of an ideal transition state analogue, its high potency relative to substrate analogue inhibitors of MR supports the notion that it is a reasonable mimic of the intermediate (the degree to which BHA mimics the transition state is discussed in detail in Chapter 6). BHA, rather than α-HBP, was used as the intermediate analogue because (1) BHA has an sp^2-hybridized α-carbon whereas α-HBP does not and (2) competitive inhibition of MR by α-HBP is further complicated by enantioselectivity (St. Maurice & Bearne, 2000).

Replacement of the phenyl ring of benzohydroxamate by bulky alkyl groups such as ethyl, t-butyl and cyclohexyl groups reduces the affinity of the intermediate analogues 20- to 70-fold, respectively, (**table 5.1**) so that the corresponding hydroxamates are bound by MR with an affinity that is comparable to that observed for the substrate. Thus, it appears

that MR exhibits a binding preference for a phenyl group at the β-carbon position of the hydroxamate intermediate analogues, but not of substrate analogues.

Examination of the dependence of the free energies for binding of intermediate analogues on π values and van der Waals surface areas (**figure 5.5**) reveals very good correlation for hydroxamate derivatives of alkanoic and naphthoic acids. However, it is clear that benzohydroxamate does not lie on the linear regression line. In fact, the free energy associated with the binding of benzohydroxamate exceeds by approximately two orders of magnitude that which would be predicted based solely on the correlation of log K_i values with either π or van der Waals surface areas. This observation suggests that further interactions are involved in binding the phenyl group of the intermediate in addition to the entropically driven hydrophobic interactions and van der Waals surface contacts inherent within the hydrophobic cavity.

Why is the binding of the aromatic ring favoured in the planar intermediate and not in the ground state? The stability constants for the metal ion complexes of Cu^{2+}, Ni^{2+}, Zn^{2+}, Ca^{2+} and Mg^{2+} with acetohydroxamic acid, cyclohexanecarbohydroxamic acid and BHA are very similar (Farkas *et al.*, 2000) and cannot account for the 3 orders of magnitude difference in binding affinity observed between these inhibitors. The acid dissociation constants for acetohydroxamic acid, cyclohexanecarbohydroxamic acid and BHA are also very similar (Farkas *et al.*, 2000), precluding any effects on the inhibition constants due to differences in ionization states (i.e., see Chapter 4). Given the relatively low affinity of cyclohexanecarbohydroxamic acid relative to BHA, it is unlikely that further expulsion of ordered water from the active site is responsible for the increased binding affinity of BHA and there is no evidence from the crystal structure of MR with
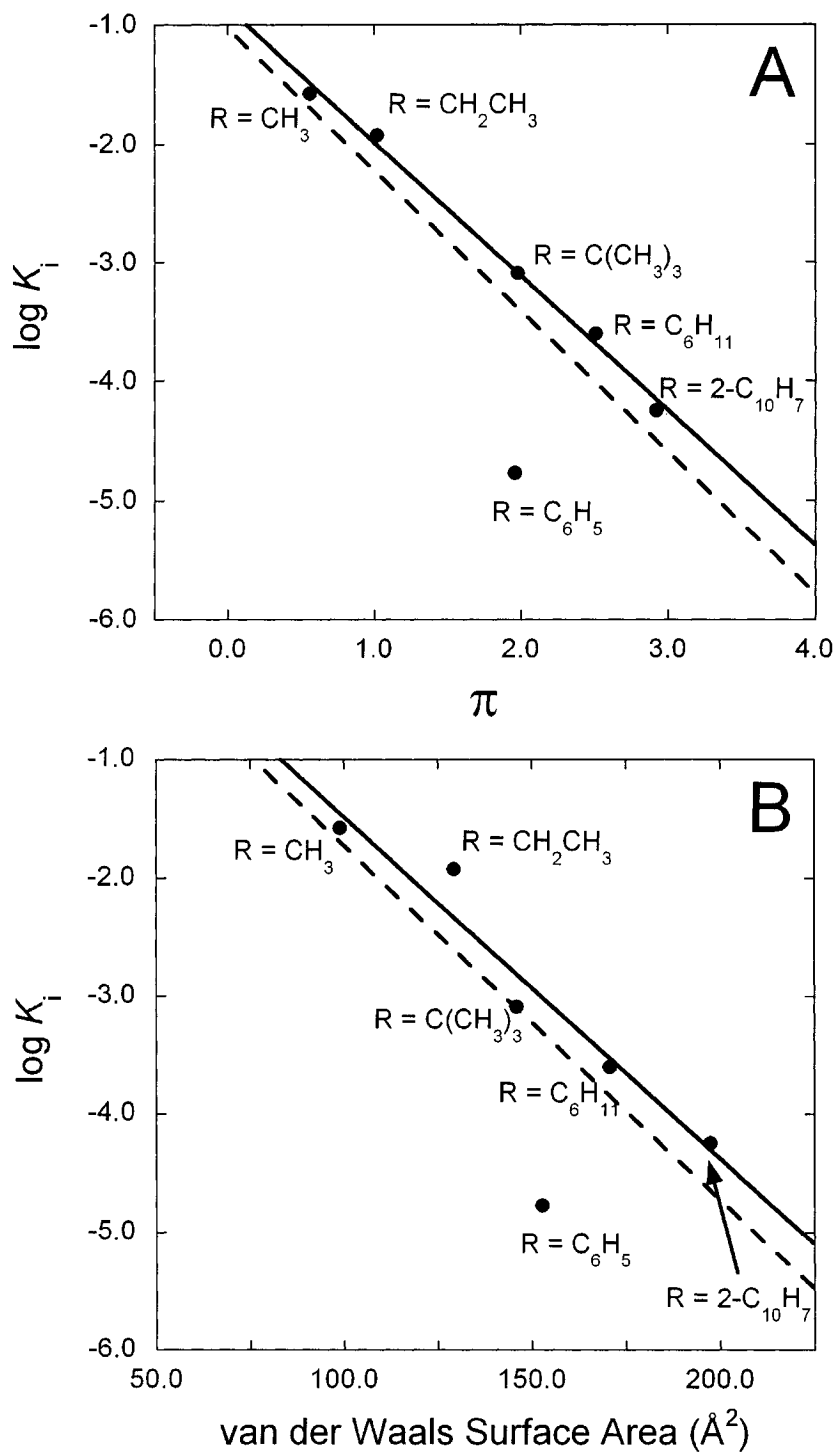
Figure 5.5 **Correlation between hydroxamic acid log K_i values and (A) the hydrophobicity constant (π) (Hansch & Leo, 1979) for the modified groups of the hydroxamic acid inhibitors and (B) the calculated van der Waals surface areas of the hydroxamic acid inhibitor molecules (table 5.4).** The dashed line is the linear regression for all of the data points (A: slope = -1.2, $r^2=0.66$; B: slope = -0.030, $r^2=0.66$) and the solid line represents the linear regression excluding benzohydroxamic acid (A: slope = -0.80, $r^2=0.99$; B: slope = -0.029, $r^2=0.93$).

bound (*S*)-atrolactate of any additional ordered water molecules remaining in the hydrophobic cavity following substrate binding (Landro *et al.*, 1994).

Preferential stabilization of the aromatic ring in the planar intermediate could result from additional van der Waals contacts or specific electrostatic interactions between the ligand's aromatic ring and various enzyme residues and/or backbone amides in the enzyme conformation corresponding to the enzyme–intermediate complex. For example, the specific stabilization of a Phe side chain over Leu in the hydrophobic pocket of neurophysin results from a 3.4 kcal/mol difference in packing energies through van der Waals interactions and an additional 4 kcal/mol difference in binding energies originating from weak polar interactions with backbone nitrogens and side chain sulfurs (Breslow *et al.*, 1999). In order for similar advantageous and specific interactions to occur between the aromatic ring of the planar intermediate and the active site of MR, there must be a relatively high degree of complementarity between the active site and the aromatic ring. This enhanced complementarity could result from the clamping down of the flexible, hinged loop (Neidhart *et al.*, 1991) over the active site during catalysis, providing enhanced van der Waals interactions and weak polar interactions (Burley & Petsko, 1988). However, excluding the BHA data point, the slope of the plot of log K_i against the van der Waals surface area for the hydroxamate analogues (slope = –0.029 Å^{-2}; 39 cal mol^{-1} Å^{-2}; **figure 5.5B**) is essentially unchanged relative to the slope obtained from the same plot with the ground state analogues (slope = –0.023 Å^{-2}; 31 cal mol^{-1} Å^{-2}; **figure 5.4B**). The slope from the plots of log K_i against π are also unchanged. Thus, there is not a significant increase in the strength of the hydrophobic interaction with the intermediate analogues relative to the ground state analogues. It would appear, therefore, that the high affinity of BHA relative to other hydroxamates is due to a *specific* stabilizing interaction

resulting from structural or electronic features of the aromatic ring. This unique stabilization energy may originate from electrostatic interactions (e.g., aromatic–aromatic (Burley & Petsko, 1988) or cation–π interactions (Dougherty, 1996)) with active site residues poised to interact with the intermediate and transition states but not with the substrate in the ground state. For example, His 23 on the flexible loop is oriented away from the active site in the crystal structure of MR with bound (S)-atrolactate (Landro et al., 1994). This residue is well positioned to "switch" its orientation and interact with the aromatic ring of the intermediate.

The extrapolation of these results to the enzyme–intermediate complex relies heavily on the assumption that enzyme–bound BHA is a reasonable mimic of the enzyme–intermediate complex (see Chapter 6). Kinetic analysis of a mutant which places a charged/polar side chain into the hydrophobic cavity (V29D mutant; Chapter 6) lends support to the notion that differential binding is realized, in part, through nonpolar interactions with the ligand in the hydrophobic cavity.

Nonpolar interactions have been shown to play a significant role in transition state stabilization by other enzymes. An investigation of a hydrophobic cavity in γ-glutamylcysteine synthetase revealed an equal contribution to transition state stabilization from a nonpolar substrate Cys residue and a substrate carboxyl group (Hiratake et al., 2002) and a 5,6-carbon–carbon double bond in the substrate for the enzyme cytidine deaminase contributes more than 5 kcal/mol to stabilization of the altered substrate in the transition state while providing no additional energy to substrate binding, despite being removed from the bonds directly involved in catalysis (Carlow & Wolfenden, 1998).

In order to provide 23 kcal/mol of enthalpic stabilization energy in the transition state, it is likely that interaction between all components of the altered substrate in the

transition state and MR must contribute to the free energy of stabilization. Mandelate is a small molecule with few groups available for hydrogen bonding or electrostatic interactions. It has been proposed that the carboxyl group of mandelate can reduce the free energy of activation by as much as 20 kcal/mol through formation of a short, strong hydrogen bond (SSHB) with Glu 317 (Gerlt & Gassman, 1993a, b), though no experimental evidence has yet been presented to support this hypothesis and replacing the proposed SSHB with a "normal" hydrogen bond by mutagenesis reveals only a 5 kcal/mol difference in transition state stabilization (Mitra et al., 1995). The α-hydroxyl group of the substrate has also been implicated as an important binding determinant in the transition state (St. Maurice & Bearne, 2000). It is not surprising, therefore, that further transition state discrimination could originate from interactions with the phenyl moiety of the altered substrate, at a location remote from the bonds directly involved in catalysis. An enzyme accelerates a chemical reaction by preferentially stabilizing the altered substrate in the transition state over the substrate in the ground state. This preferential stabilization is realized through a stronger apparent binding affinity for the altered substrate in the transition state relative to the substrate in the ground state. To achieve these higher binding affinities in the transition state, an enzyme takes advantage of multiple interactions, including those that are remote from the site of chemistry (Wolfenden, 1999). An investigation of the contribution to catalysis by cytidine deaminase from various substrate pieces has revealed that enzyme–substrate interactions remote from the site of chemistry have a significant effect in reducing both the k_{cat}/K_m for the enzyme–catalyzed reaction and the binding affinities for the corresponding transition state analogues (Carlow & Wolfenden, 1998). Modified transition state analogues for the enzymes adenosine deaminase and orotodine 5'-monophosphate decarboxylase

demonstrate that *all* components of a transition state analogue, including those distant from the site of chemistry, are critically important in binding (Kati *et al.*, 1992; Miller *et al.*, 1998).

5.4.3 Enzyme–Catalyzed Racemization of 2-Naphthylglycolate

To further investigate the role of the hydrophobic cavity in MR catalysis, the kinetic parameters for the bulky alternative substrate 2-naphthylglycolate were determined. The K_m values for both (R)- and (S)-2-naphthylglycolate are slightly less than those for (R)- and (S)-mandelate while the k_{cat} values are approximately 6% of the k_{cat} values observed for (R)- and (S)-mandelate. Because $K_m \approx K_s$ for MR (St. Maurice & Bearne, 2002), it is clear that the enzyme binds 2-naphthylglycolate and mandelate with equal affinity and that, contrary to the prediction by Felfer *et al.* (2001), no major steric restrictions are imposed on the binding of the bulkier substrate. Thus, the 10-fold decrease in k_{cat}/K_m for 2-naphthylglycolate relative to mandelate must result from an increase in the free energy barrier for the chemical step (**figure 5.6**). Because the extended π-system of 2-naphthylglycolate should stabilize a negative charge on the α-carbon through resonance as effectively as the phenyl group, it is unlikely that changes in electron delocalization are responsible for the increased free energy of activation. The most reasonable explanation for the decreased catalytic efficiency is that increased steric constraints on the transition state cause reduced stabilization of the altered substrate in the transition state. If this is the case, then it follows from the Hammond postulate (Hammond, 1955) that the binding affinity of the intermediate and intermediate analogues bearing the naphthyl group would also be reduced relative to BHA. Indeed, the change in free energy for binding of the
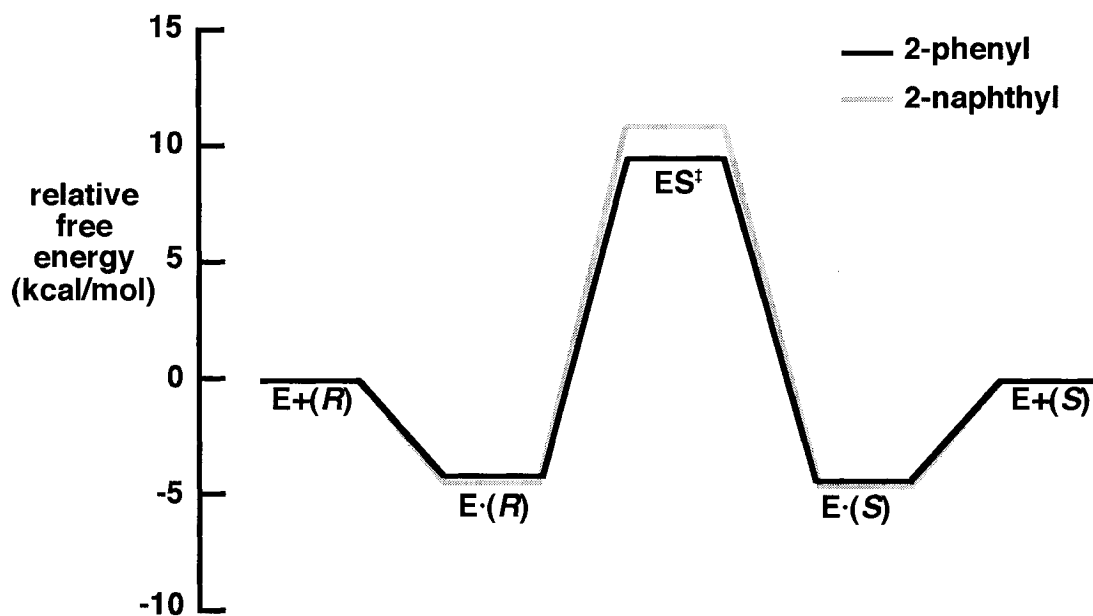
Figure 5.6 Free energy profile (25 °C, pH 7.5) for the racemization of (*R*)- and (*S*)-mandelate and (*R*)- and (*S*)-2-naphthylglycolate by wild-type MR. The *R* and *S* substrate enantiomers are denoted (*R*) and (*S*), respectively. The profiles are derived from the kinetic parameters in **table 5.2**. ES‡ represents the enzyme-substrate complex in the transition state.

intermediate analogue, 2-naphthohydroxamate ($\Delta G = -5.9$ kcal/mol), is 0.8 kcal/mol *less* favourable than the free energy for binding BHA ($\Delta G = -6.7$ kcal/mol). This difference in free energies of binding can account for a significant portion of the difference in transition state stabilization ($\Delta\Delta G = -1.3$ kcal/mol) afforded to mandelate and 2-naphthylglycolate in the transition state. These observations further support the conclusion that the hydrophobic cavity of mandelate racemase imposes constraints that discriminate between the substrate in the ground state and the altered substrate in the transition state.

5.4.4 Plasticity of the Hydrophobic Cavity

Several bulky ground state analogues of mandelate were investigated for their ability to inhibit MR. Both (R,S)-1- and (R,S)-2-naphthylglycolate are competitive inhibitors of MR and are bound with an an apparent affinity similar to mandelate. The inhibition constant for (R,S)-2-naphthylglycolate is in agreement with the K_m values determined from enzyme assays with the alternative substrates (R)- and (S)-2-naphthylglycolate, further confirming that K_m is equal to K_s for this alternative substrate. While both 1- and 2-naphthylglycolate bind with affinities similar to that of the substrate, 1-naphthylglycolate binds with slightly less affinity than would be predicted based on its π value or van der Waals surface area (**figure 5.4**), indicating that, for 1-naphthylglycolate, a slight steric constraint exists for binding. Benzilate is a diphenyl analogue of mandelate and may be regarded as a substrate/product analogue because it contains the phenyl moieties of both (R)- and (S)-mandelate. Because MR bindsbenzilate as a competitive inhibitor with an affinity that is slightly greater than mandelate, the

hydrophobic cavity appears to be capable of simultaneously accomodating two aromatic rings. Molecular mechanics simulations of benzilate in the active site of MR reveal both aromatic rings bound within the active site (**figure 5.3**) and provide, for the first time, an indication of where the phenyl ring of (R)-mandelate resides within the active site. Weak inhibition of MR by another diphenyl analogue, diphenylacetic acid, has also been reported (Hegeman *et al.*, 1970). The promiscuity of the MR hydrophobic cavity is also apparent from the ability of several *para-* and *meta*-substituted mandelate derivatives to act as alternative substrates for the enzyme (Felfer *et al.*, 2001; Hegeman *et al.*, 1970; St. Maurice & Bearne, 2002) and it is further reinforced by the competitive inhibition of MR by (S)-cyclohexylphenylglycolate.

5.4.5 Substrate Dynamics During MR Catalysis

Hydrogen bonding and electrostatic interactions between the α-hydroxyl and carboxylate groups of the substrate and Glu 317, Lys 164, Asn 197 and Mg^{2+} within the active site contribute significantly to substrate binding and transition state stabilization and make it very likely that the α-hydroxyl and carboxylate groups remain fixed in space as enzyme–catalyzed racemization proceeds. Because the interconversion of enantiomers by MR necessitates that two groups attached to the α-carbon of the substrate must physically switch positions, it follows that racemization involves movement of the aromatic ring to the position in space that was previously occupied by the α-hydrogen of the substrate (**figure 5.7**). The observed plasticity of the hydrophobic cavity should be compatible with a wide range of ligand conformations and the binding of benzilate in the

(i)   **(ii)**   **(iii)**
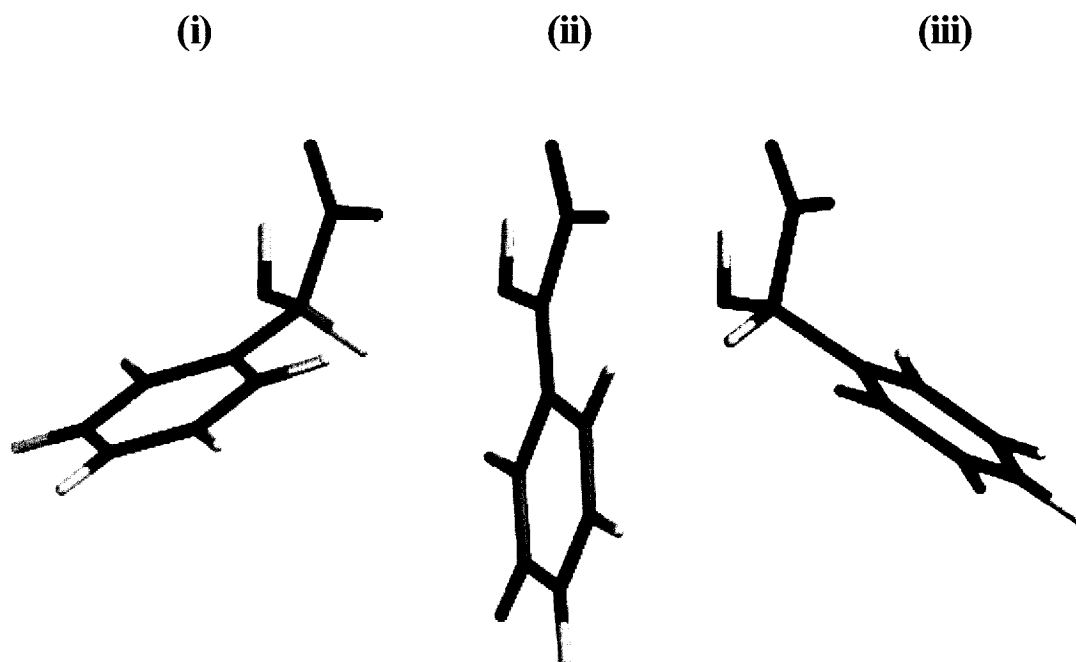
Figure 5.7 Proposed motion of (R)- and (S)-mandelate ((i) and (iii)) and the (aci)-carboxylate intermediate (ii) within the active site of MR. Assuming a rigid orientation for the substrate α-hydroxyl and carboxylate groups, the aromatic ring must "swing" through the hydrophobic cavity as catalysis proceeds. The conformation of the molecules were calculated for the gas phase and do not represent the exact orientation within the active site.

enzyme active site indicates that MR can certainly accomodate an aromatic ring on both "sides" of the hydrophobic cavity. Because nonpolar interactions between the hydrophobic cavity and the phenyl group are weak relative to the sum of the hydrogen bonding and electrostatic interactions with the α-hydroxyl and carboxylate functions (i.e., compare the K_i values for benzene and glycolate; **table 5.1**), movement of the phenyl ring may provide a mechanism by which MR discriminates between the substrate in the ground state and the altered substrate in the transition state. The observation that analogues of the planar *aci*-carboxylate intermediate are bound with greater affinity *only* if a phenyl group is present, rather than bulky alkyl groups, supports this notion.

While examples of the role of dynamic protein motions in enzyme catalysis are numerous (Hayward, 1999; Rajagopalan & Benkovic, 2002), there are few examples of substantial *substrate* motion through an enzyme active site during catalysis. The classic example of swinging motions of lipoic acid and biotin through multifunctional enzyme complexes has been well documented (Perham, 2000), but these motions involve a combination of active sites. Epimerases such as UDP-galactose-4-epimerase and 1-ribulose-5-phosphate 4-epimerase also appear to require substrate "rotation" in the active site in order to effect catalysis (see reviews by Allard *et al.*, 2001; Tanner, 2002).

If transition state stabilization by MR is based, in part, on strengthened interactions with a planar aromatic intermediate in a favoured position within the hydrophobic cavity, it is troubling that inhibition of MR by benzoylformate, a substrate analogue of mandelate with an sp^2-hybridized α-carbon, yields no improvement in binding affinity over substrate analogues with tetrahedrally arranged α-carbons (St. Maurice & Bearne, 2000). It has been suggested that a hydrogen bond *donor* is required at the α-OH position of the

substrate (St. Maurice & Bearne, 2000). Donation of a hydrogen bond from the α-OH in the planar intermediate may serve to lock both the enzyme and intermediate in a position that further strengthens interactions in the hydrophobic cavity. The significant role played by such a chelate effect (Page & Jencks, 1971) in transition state stabilization has been discussed (Wolfenden, 1999). Thus, the hydrogen bond donating potential of BHA may allow this intermediate analogue to more closely mimic the true position of the aromatic ring in the hydrophobic cavity of the enzyme–intermediate complex.

It appears that nonpolar interactions in the hydrophobic cavity of MR contribute to stabilization of the planar intermediate. Since the structure of the altered substrate in the transition state is similar in structure to the high energy intermediate (Hammond, 1955), the same forces are expected to apply to transition state stabilization. In general, discussions on the role of transition state stabilization in enzyme catalysis have focussed on contributions from hydrogen bonding and electrostatic interactions but have often overlooked the potential for seemingly small and distant interactions to contribute significantly to transition state stabilization (Bruice & Benkovic, 2000). Because of the limited number of polar functional groups present on mandelate, sites for hydrogen bonding and electrostatic interactions with the enzyme are sparse. It is, therefore, not surprising that MR might also take advantage of differences in spatial orientation of the substrate in the ground state and the altered substrate in the transition state to bind the latter with greater affinity.

CHAPTER 6

GROUND STATE AND TRANSITION STATE BINDING DETERMINANTS: ASSESSING BHA AS A TRANSITION STATE ANALOGUE

6.1 Introduction

BHA and α-HBP are potent, reversible inhibitors of MR (St. Maurice & Bearne, 2000). These inhibitors were designed to mimic the *aci*-carboxylate intermediate and serve as stable probes of the enzyme–transition state complex. Since the structure of the transition state is expected to resemble the structure of the intermediate (Hammond, 1955), a very good mimic of the *aci*-carboxylate intermediate should also be a good mimic of the transition state. Both α-HBP and BHA are bound with affinities approximately 100-fold greater than the substrate, indicating that both inhibitors may be reasonably good transition state analogues. The degree to which these inhibitors mimic the altered substrate in the transition state, however, has not yet been determined.

From the published crystal structures of MR with bound substrate and substrate analogues, it is apparent that Glu 317, Lys 164, and Asn 197 are in close proximity to the bound ligand (Kallarakal *et al.*, 1995; Landro *et al.*, 1994; Mitra *et al.*, 1995; Schafer *et al.*, 1996) (**figure 6.1**). The carboxamide group of Asn 197 is within hydrogen bonding distance of the substrate's α-OH, the carboxylate group of Glu 317 is 2.7 Å from one of the substrate's carboxylate oxygens while the amino group of Lys 164 is 2.7 Å from the second substrate carboxylate oxygen. Glu 317 functions as a general acid catalyst to facilitate proton abstraction from the α-carbon of the substrate and provides significant stabilization to the intermediate, perhaps through the formation of a short, strong hydrogen bond (SSHB) (Gerlt & Gassman, 1993a, b; Mitra *et al.*, 1995). The contribution from Lys 164 and Asn 197 to transition state stabilization is not known. The hydrophobic cavity also plays a significant role in ligand binding (Chapter 5). Val 29 resides on the
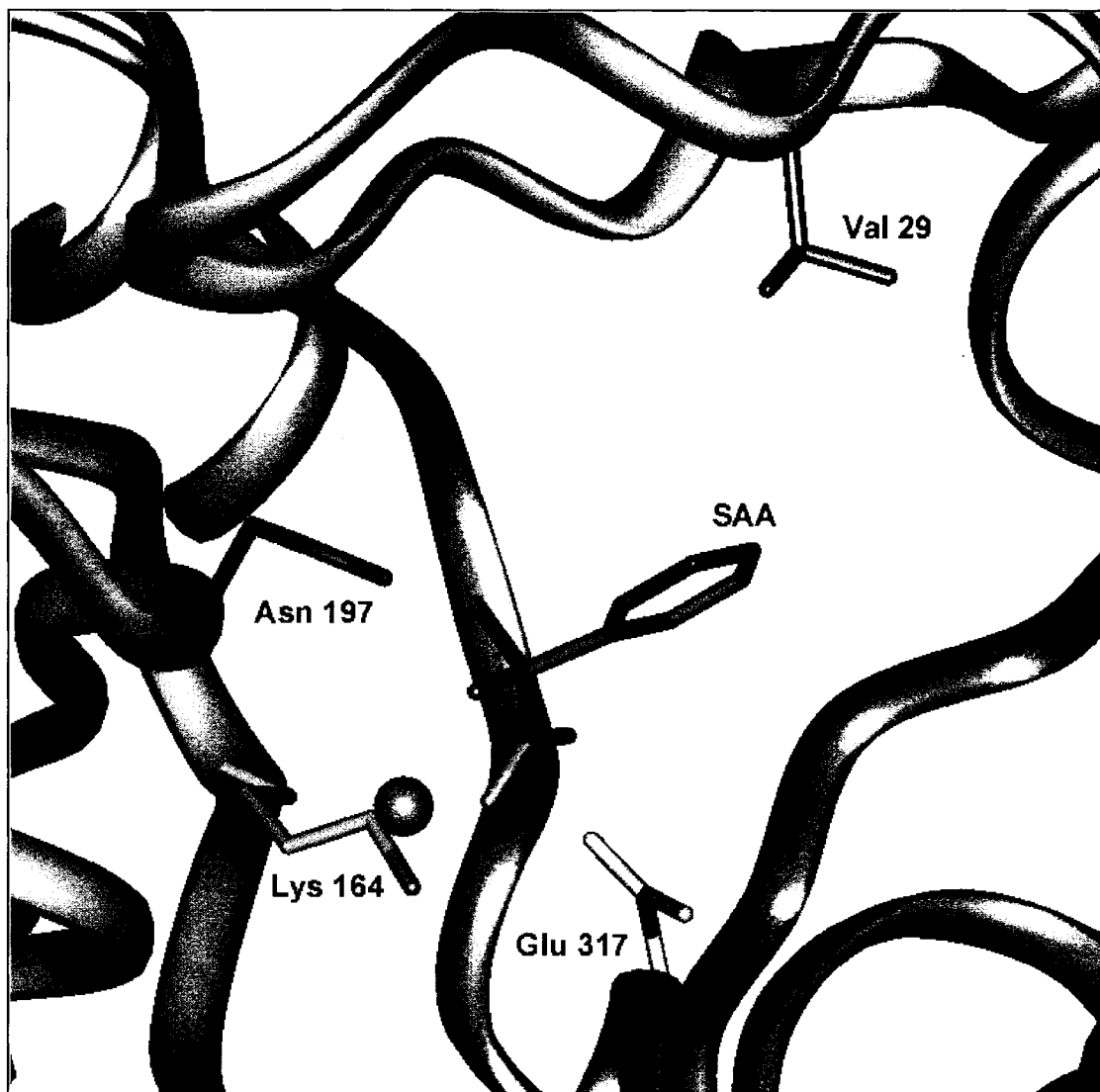
Figure 6.1 X-Ray crystal structure of the active site of wild-type MR with bound (S)-atrolactate (SAA) (pdb key = 1MDR; (Landro *et al.*, 1994)). Asn 197, Lys 164, Glu 317 and Val 29 are shown and the Mg^{2+} ion is highlighted in purple. The assignment of the position of the C=O and –NH$_2$ within the plane of the carboxamide of Asn 197 is completely arbitrary at the resolution of the crystal structure (Gregory A. Petsko, personal communication). Oxygen, nitrogen, and carbon atoms are red, blue, and green respectively. The α-carbon backbone is gold except for the flexible loop which is highlighted in yellow.

flexible loop of the hydrophobic cavity with its side chain extended inward towards the *para* position of the substrate's aromatic ring. In the present chapter, the N197A, E317Q, K164R and V29D mutants of MR are constructed and characterized in order to investigate the contribution made by these various binding determinants to both ground state and transition state stabilization. These mutants also permit the assessment of BHA as a transition state analogue. Each of the binding determinants interacts with the substrate but also plays an important role in stabilizing the altered substrate in the transition state. BHA appears to be a reasonable mimic of the altered substrate in the transition state but also does display a degree of ground state mimicry.

6.2 Materials and Methods

6.2.1 General

Benzohydroxamic acid, and (R)- and (S)-mandelic acid were purchased from Sigma–Aldrich Canada Ltd. (Oakville, ON). (R)-Atrolactate was purchased from Lancaster Synthesis Inc. (Windham, NH, USA). (R,S)-α-HBP was synthesized as described previously (section 4.2.2). Synthetic oligonucleotide primers used for site–directed mutagenesis and DNA sequencing were purchased from ID Labs (London, ON). Standard techniques were used for DNA isolation, cloning, and protein and DNA gel electrophoresis (Sambrook et al., 1989).

6.2.2 Site–Directed Mutagenesis

The pET-15b plasmid containing the recombinant mandelate racemase gene was used as the template for polymerase chain reaction–based site–directed mutagenesis (QuickChange Site–Directed Mutagenesis Kit, Stratagene, La Jolla, CA, USA). The procedure followed was that described by the manufacturer. The synthetic primers used to construct the mutants were as follows: N197A: 5'-dGGCATCATGGTCGACTAC GCCCAGAGTTTGGATGTACC-3' and 5'-dGGTACATCCAAACTCTGGGCGTA GTCGACCATGATGCC-3'; E317Q: 5'-dCCCAACTGCGCATTGGCTGCAGCGTTT GGATCTCGCC-3' and 5'-dGGCGAGATCCAAACGCTGCAGCCAATGCGCAGTT GGG-3'; K164R: 5'-dCGGATTCCGGGCGGTTAGGACCAAGATCGGCTATCCG-3' and 5'-dCGGATAGCCGATCTTGGTCCTAACCGCCCGGAATCCG-3'; V29D: 5'- dCCGCTGTTGGAACTGACGGCACAGCGCCTCTTGTTC-3' and 5'-dGAACAAGA GGCGCTGTGCCGTCAGTTCCAACAGCGG-3', where the positions of the mismatches are indicated by the underlined bases. Each of the mutant genes was completely sequenced to verify that no other alterations in the nucleotide sequence had been introduced. Automated sequencing was performed for wild–type, N197A, E317Q and K164R MR at the National Research Council Institute for Marine Biosciences (Halifax,

NS) and for V29D at the Robarts Research Institute (London, ON). The mutant enzymes, bearing a histidine tag, were purified using the same procedure as described for the wild-type enzyme (section 2.2.2). Once eluted from the Ni^{2+} affinity columns, the enzyme solutions were dialyzed into HEPES buffer (0.1 M, pH 7.5) containing $MgCl_2$ (3.3 mM) and NaCl (0.2 M).

The K_m value for Mg^{2+} was determined for both wild–type and N197A enzymes using the method described by Fee *et al.* (1974b). The enzyme, freed of Mg^{2+} by dialysis, was first incubated with the desired concentration of $MgCl_2$ for 5 min (wild–type) or 10 min (N197A), and then the reaction was initiated by addition of (*R*)-mandelate (final concentration = 10 mM).

6.2.3 Protein CD Spectra

The protein CD spectra were recorded in sodium phosphate buffer (25 mM, pH 7.5) containing $MgSO_4$ (10 mM) in a quartz cuvette with a 0.1 cm light path over a range from 185 nm to 260 nm. Enzyme solutions were dialyzed into sodium phosphate buffer (25 mM, pH 7.5) containing $MgSO_4$ (10 mM) and protein concentrations were subsequently determined using the Bio-Rad protein assay (Bio-Rad Laboratories, Mississauga, ON) with BSA standards in sodium phosphate buffer (25 mM, pH 7.5) containing $MgSO_4$ (10 mM). The enzyme concentrations used were 75.8 µg/mL for wild–type MR, 63.5 µg/mL for N197A MR, 71.0 µg/mL for E317Q MR, 61.8 µg/mL for K164R MR, and 71.0 µg/mL for V29D MR. Deconvolutions of the CD spectra were performed using *CDNN CD Spectra Deconvolution* v. 2.1 developed by G. Böhm (Bohm *et al.*, 1992).

6.2.4 Enzyme Assays

MR activity was assayed using the CD assay described by Sharp *et al.* (1979). All kinetic enzyme assays were conducted at 25 °C in Na^+-HEPES buffer (0.1 M, pH 7.5) containing $MgCl_2$ (3.3 mM) and BSA (0.1%). Assays were performed as described for the wild–type enzyme in section 4.2.7. The final enzyme concentration in the assays ranged from 2 to 10 μg/mL for N197A, 0.5 to 2.1 mg/mL for E317Q, 180 to 480 μg/mL for V29D, and 730 μg/mL for K164R.

6.2.5 Molecular Electrostatic Potential Surfaces

Geometry optimizations and electrostatic potential surfaces were calculated for (*R*)-mandelate, benzoylformate, the putative *aci*-carboxylate intermediate, the (*S*)-α-hydroxy benzylphosphonate monoanion, and the conjugate base of *trans*–BHA (*O*-deprotonated) by performing self–consistent–field calculations at the 6-31G* level using *MacSpartan Plus* (Wavefunction, Inc.; Irvine, CA). Geometry optimizations and electrostatic potential surfaces for benzoylformate were calculated with free rotation of the carboxylate group restricted so that the carboxylate function was co-planar with the carbonyl group. This was done so that the resulting planar geometry was in agreement with that predicted using the semi-empirical AM1 method contained within the *MacSpartan Plus* software.

6.3 Results

Several residues at the active site of MR were altered by site–directed mutagenesis. To verify that the mutations did not cause any significant perturbations to the overall protein structure, the CD spectra of histidine–tagged wild–type and mutant enzymes were measured. The molar ellipticities of wild–type, N197A, E317Q, K164R, and V29D MR all overlapped (**figure 6.2**), indicating that no significant structural perturbations were introduced by the mutations. (However, it must be noted that minor perturbations in structure can not be ruled out.) The secondary structure content of the wild–type and mutant enzymes were determined by deconvolution of the CD spectra and were in good agreement with the X-ray crystal structures for wild–type and E317Q MR (**table 6.1**).

6.3.1 Kinetics of the N197A Mutant

Site–directed mutagenesis was used to replace Asn 197 with alanine (N197A). The introduction of alanine did not significantly perturb the K_m value for Mg^{2+} relative to the wild–type enzyme (**table 6.2**). However, a marked effect on catalysis was observed. The value of k_{cat} was reduced 30-fold and 179-fold for catalysis in the $R \rightarrow S$ and $S \rightarrow R$ directions, respectively. Interestingly, the mutation had little effect on substrate binding with K_m increasing only 7-fold and 2-fold for (R)- and (S)-mandelate. Thus, interaction of Asn 197 with the α-hydroxyl of the substrate stabilizes the altered substrate in the transition state by 3.2–3.7 kcal/mol. Binding of α-HBP and BHA by the N197A mutant was reduced 51- and 18-fold, respectively, relative to the wild–type enzyme.

6.3.2 Kinetics of the E317Q Mutant

Mitra *et al.* identified Glu 317 as the general acid catalyst in MR and constructed and characterized the E317Q mutant (Mitra *et al.*, 1995). However, assay limitations prevented the K_m for (S)-mandelate from being directly determined. The complete kinetic
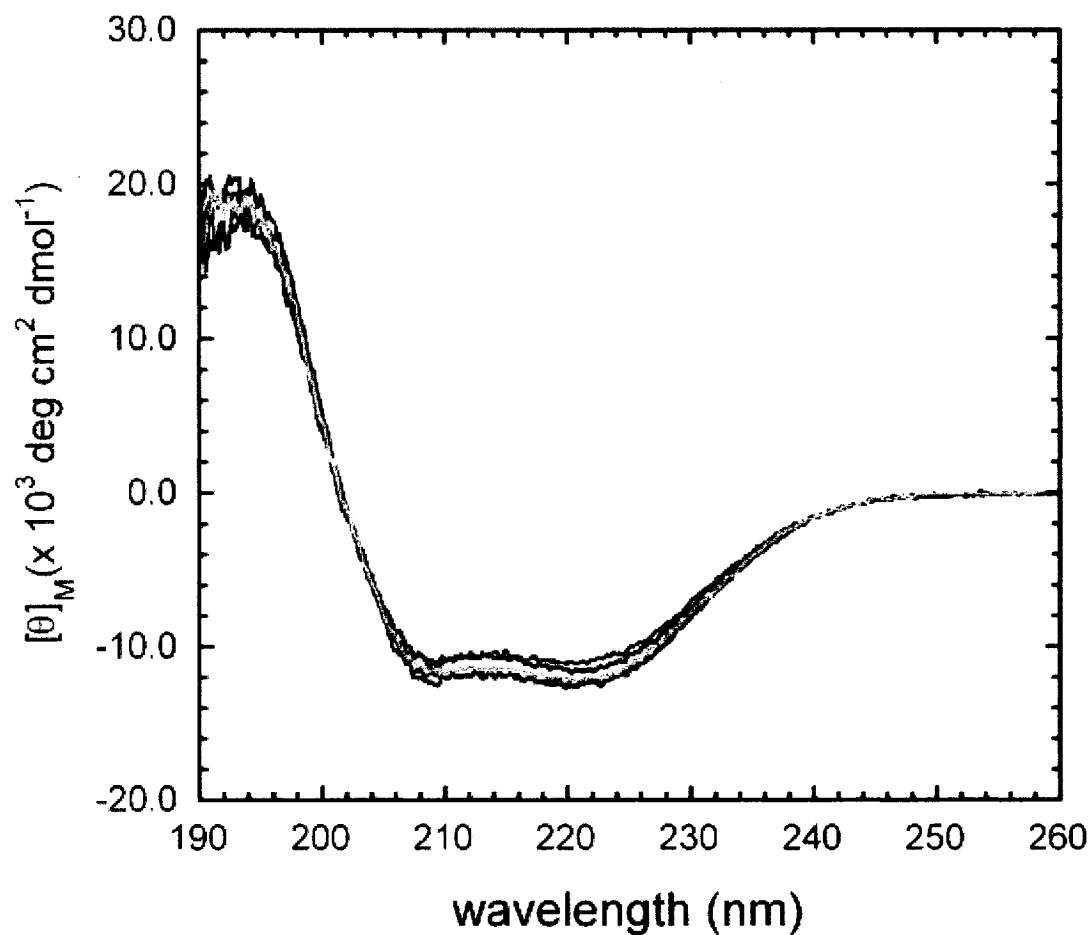
Figure 6.2 CD spectra for wild-type and mutant MR enzymes. Molar ellipticities as a function of wavelength are plotted for wild-type MR (75.8 µg/ml; black), N197A MR (63.5 µg/mL; red), E317Q MR (71.0 µg/mL; blue), K164R MR (61.8 µg/mL; green) and V29D MR (71.0 µg/mL; orange) at 25 °C, in Na^+-phosphate buffer (25 mM; pH 7.5) containing $MgSO_4$ (10 mM).

Table 6.1 Secondary structure content of wild–type and mutant MR enzymes predicted by CD spectra deconvolution [a] and X-ray crystallography.

Enzyme	% α content	% β content
wild–type	36.6 (40.4)[b]	30.2 (19.5)[b]
N197A	36.8	30.2
E317Q	38.0 (39.6)[c]	28.9 (20.9)[c]
K164R	35.4	31.5
V29D	35.5	31.2

[a] Values determined in the present work are for the wild–type and mutant enzymes bearing the histidine tag.

[b] Secondary structure content reported for the X-ray crystal structure of wild–type MR complexed with (S)-atrolactate (Landro et al., 1994) is shown in the brackets.

[c] Secondary structure content reported for the X-ray crystal structure of E317Q MR complexed with (S)-atrolactate (Mitra et al., 1995) is shown in the brackets.

Table 6.2 Kinetic Parameters and Inhibition Constants for N197A MR

Parameter	wild–type	N197A	N197A/ wild–type
K_m (Mg^{2+}), mM	0.65 ($\pm$ 0.06)	0.34 ($\pm$ 0.08)	–
k_{cat} $(R) \rightarrow (S)$, s^{-1}	514 ($\pm$ 48)	16.9 ($\pm$ 3.5)	0.033 ($\pm$ 0.007)
K_m ((R)-mandelate), mM	0.81 ($\pm$ 0.12)	5.40 ($\pm$ 0.66)	6.67 ($\pm$ 1.28)
k_{cat}/K_m $(R) \rightarrow (S)$, $M^{-1}s^{-1}$	6.4 ($\pm$ 1.1) $\times 10^5$	3.1 ($\pm$ 0.7) $\times 10^3$	4.8 ($\pm$ 1.4) $\times 10^{-3}$
k_{cat} $(S) \rightarrow (R)$, s^{-1}	447 ($\pm$ 12)	2.5 ($\pm$ 0.6)	5.6 ($\pm$ 1.4) $\times 10^{-3}$
K_m ((S)-mandelate), mM	0.62 ($\pm$ 0.04)	1.40 ($\pm$ 0.43)	2.3 ($\pm$ 0.71)
k_{cat}/K_m $(S) \rightarrow (R)$, $M^{-1}s^{-1}$ [a]	7.2 ($\pm$0.5) $\times 10^5$	1.3 ($\pm$0.5) $\times 10^3$	1.8 ($\pm$ 0.7) $\times 10^{-3}$
K_i ((R,S)-α-HBP), mM	0.0047 ($\pm$ 0.0007)	0.238 ($\pm$ 0.064)	51 ($\pm$ 16)
K_i (BHA), mM	0.0117 ($\pm$ 0.0012)	0.216 ($\pm$ 0.006)	18 ($\pm$ 2)
K_i ((R)-atrolactate), mM	0.95 ($\pm$ 0.33)	3.30 ($\pm$ 0.33)	3.5 ($\pm$ 0.4)

[a] For a racemase, the equilibrium constant (K_{eq}) for the reaction is unity. Thus for MR, the Haldane relationship (Segel, 1993a) requires that $(k_{cat}/K_m)^{(R)\rightarrow(S)}/(k_{cat}/K_m)^{(S)\rightarrow(R)} = K_{eq} = 1$. For wild–type MR, K_{eq} = 0.9 ($\pm$0.2), however, for N197A, K_{eq} = 2.4 ($\pm$1.1). The large error in K_{eq} for N197A reflects the difficulty in measuring the kinetic parameters where K_m is increased and k_{cat} is markedly reduced relative to the wild–type enzyme.

characterization of the E317Q mutant relative to wild–type MR is presented in **table 6.3**. Deconvolution of the CD spectrum of E317Q indicated no significant alteration of the secondary structure of the E317Q protein relative to the wild–type enzyme, in agreement with the previously determined X-ray crystal structure (Mitra *et al.*, 1995). The value of k_{cat} was reduced 4- and 5-orders of magnitude for catalysis in the $R{\to}S$ and $S{\to}R$ directions, respectively. The mutation had no effect on substrate binding for (*R*)- and (*S*)-mandelate. Thus, replacing the carboxylic acid functional group of Glu 317 with a carboxamide group has no effect on substrate binding but results in a reduction in transition state stabilization free energy equivalent to 4.9–5.5 kcal/mol. The binding affinity for BHA by the E317Q mutant was reduced 65-fold relative to the wild–type enzyme.

6.3.3 Kinetics of the K164R Mutant

Structural characterization of MR reveals that the ε-ammonium of Lys 164 is in close proximity to the carboxyl group of the bound ligand (Kallarakal *et al.*, 1995; Landro *et al.*, 1994; Mitra *et al.*, 1995). This residue has been implicated both in binding the substrate and in perturbing the pK_a of the general base catalysts Lys 166 and His 297 (Neidhart *et al.*, 1991; Schafer *et al.*, 1996). To probe the importance of Lys 164 in substrate binding and in transition state stabilization, the K164R mutant was constructed. The kinetics for the K164R mutant relative to wild–type MR are presented in **table 6.4**. Surprisingly, in the $S{\to}R$ direction, substrate inhibition was observed (**figure 6.3**). The kinetic data for (*S*)-mandelate as the substrate were fit to equation 6.1 which describes substrate inhibition as shown in **scheme 6.1**. This fit yielded a k_{cat} value of 0.154 s^{-1}, a K_s value of 0.38 mM and a K_s' value of 11.3 mM.

$$\frac{v_i}{[E]_T} = \frac{k_{cat}[S]}{[S] + K_s + \dfrac{[S]^2}{K_s'}}$$

(6.1)

Table 6.3 Kinetic Parameters and Inhibition Constants for E317Q MR

Parameter	wild–type	E317Q	E317Q/ wild–type
k_{cat} $(R) \rightarrow (S)$, s^{-1}	559 ($\pm$ 51)	0.18 ($\pm$ 0.05)	3.3 ($\pm$ 1.0) $\times$ 10^{-4}
K_m ((R)-mandelate), mM	0.81 ($\pm$ 0.12)	1.10 ($\pm$ 0.07)	1.4 ($\pm$ 0.2)
k_{cat}/K_m $(R) \rightarrow (S)$, $M^{-1}s^{-1}$	6.9 ($\pm$ 1.2) $\times$ 10^5	1.6 ($\pm$ 0.5) $\times$ 10^2	2.3 ($\pm$ 0.8) $\times$ 10^{-4}
k_{cat} $(S) \rightarrow (R)$, s^{-1}	510 ($\pm$ 13)	0.024 ($\pm$ 0.001)	4.7 ($\pm$ 0.1) $\times$ 10^{-5}
K_m ((S)-mandelate), mM	0.63 ($\pm$ 0.02)	0.32 ($\pm$ 0.08)	0.51 ($\pm$ 0.13)
k_{cat}/K_m $(S) \rightarrow (R)$, $M^{-1}s^{-1}$ [a]	8.1 ($\pm$ 0.3) $\times$ 10^5	0.76 ($\pm$ 0.19) $\times$ 10^2	9.4 ($\pm$ 4.2) $\times$ 10^{-5}
K_i (BHA), mM	0.0117 ($\pm$ 0.0012)	0.76 ($\pm$ 0.31)	65 ($\pm$ 4)

[a] For wild–type MR, K_{eq} = 0.9 ($\pm$0.2), however, for E317Q, K_{eq} = 2.1 ($\pm$0.8). The large error in K_{eq} for E317Q reflects the difficulty in measuring the kinetic parameters where k_{cat} is markedly reduced relative to the wild–type enzyme.

Table 6.4 Kinetic Parameters and Inhibition Constants for K164R MR

Parameter	wild–type	K164R	K164R/ wild–type
k_{cat} $(R) \rightarrow (S)$, s^{-1}	559 ($\pm$ 51)	0.27 ($\pm$ 0.02)	4.8 ($\pm$ 1.0) $\times$ 10^{-4}
K_m ((R)-mandelate), mM	0.81 ($\pm$ 0.12)	0.48 ($\pm$ 0.07)	0.59 ($\pm$ 0.12)
k_{cat}/K_m $(R) \rightarrow (S)$, $M^{-1}s^{-1}$	6.9 ($\pm$ 1.2) $\times$ 10^5	5.6 ($\pm$ 0.9) $\times$ 10^2	8.2 ($\pm$ 1.9) $\times$ 10^{-4}
k_{cat} $(S) \rightarrow (R)$, s^{-1}	510 ($\pm$ 13)	0.154 ($\pm$ 0.003)	3.1 ($\pm$ 0.1) $\times$ 10^{-4}
K_s ((S)-mandelate), mM	0.63 ($\pm$ 0.02)	0.38 ($\pm$ 0.03)	0.63 ($\pm$ 0.12)
K_s' ((S)-mandelate), mM	–	11.3 ($\pm$ 1.1)	–
k_{cat}/K_m $(S) \rightarrow (R)$, $M^{-1}s^{-1}$	8.1 ($\pm$ 0.3) $\times$ 10^5	4.0 ($\pm$ 0.3) $\times$ 10^2	4.9 ($\pm$ 0.4) $\times$ 10^{-4}
K_i (BHA), mM	0.0117 ($\pm$ 0.0012)	0.0062 ($\pm$ 0.0013)	0.53 ($\pm$ 0.12)
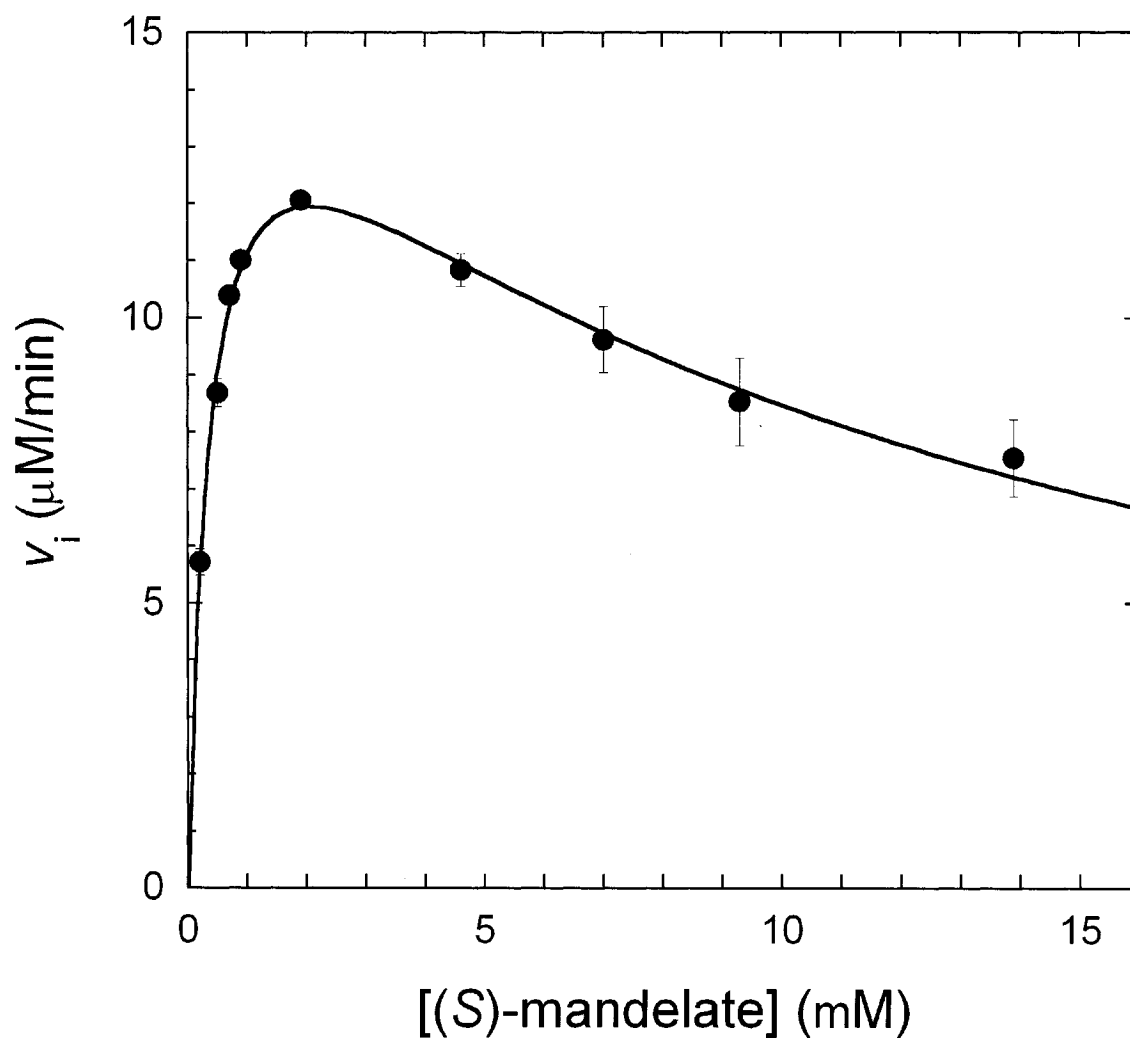
Figure 6.3   Initial velocity as a function of (S)-mandelate concentration for the K164R mutant. The decrease in initial velocity at substrate concentrations exceeding 3 mM is characteristic of substrate inhibition. Each data point is the mean of three determinations. Error bars are the standard deviations.   From a fit of the data to equation 6.1, values of k_{cat}, K_s and K_s' were determined to be 0.154 s^{-1}, 0.38 mM and 11.3 mM, respectively.

Scheme 6.1 A kinetic scheme describing substrate inhibition.

$$E + S \overset{K_S}{\rightleftharpoons} ES \xrightarrow{k_{cat}} E + P$$

$$+ S$$

$$\updownarrow K_S'$$

$$ES_2$$

The value of k_{cat} was reduced by 4-orders of magnitude in both reaction directions. The mutation resulted in a slight decrease in the K_m values for both (R)- and (S)-mandelate. Thus, replacing the ε-ammonium of Lys 164 with a guanidinium group yields a slight increase in substrate binding affinity but results in a reduction in transition state stabilization free energy equal to 4.2–4.5 kcal/mol. Interestingly, the K_i of BHA for the K164R mutant was decreased two–fold relative to the K_i determined using the wild–type enzyme.

6.3.4 Kinetics of the V29D Mutant

The role of the active site hydrophobic cavity in catalysis by MR has been discussed (Chapter 5). A major component of this cavity is a mobile, β-meander flap that extends over the active site substrate binding pocket (Neidhart *et al.*, 1991). The consequence of replacing a hydrophobic residue with a charged residue on this mobile flap in close proximity to the substrate was investigated by constructing and characterizing the V29D mutant. The kinetics for the V29D mutant relative to wild–type MR are presented in **table 6.5**. The value of k_{cat} was reduced 30- and 60-fold for catalysis in the $R{\rightarrow}S$ and $S{\rightarrow}R$ directions, respectively. The mutation also had a significant effect on substrate binding, reducing the binding affinity 80- and 50-fold for (R)- and (S)-mandelate, respectively, relative to the wild–type enzyme. Thus, introducing a charged functional group in the hydrophobic cavity resulted in a reduction in both ground state and transition state stabilization free energy equal to 2.3–2.6 and 4.6–4.7 kcal/mol, respectively, at 25 °C. The K_i for BHA with the V29D mutant was 250-fold greater than the K_i for BHA with the wild–type enzyme.

Table 6.5 Kinetic Parameters and Inhibition Constants for V29D MR

Parameter	wild–type	V29D	V29D/ wild–type
k_{cat} $(R) \rightarrow (S)$, s^{-1}	559 ($\pm$ 51)	19 ($\pm$ 2)	0.034 ($\pm$ 0.005)
K_m ((R)-mandelate), mM	0.81 ($\pm$ 0.12)	63 ($\pm$ 6)	78 ($\pm$ 14)
k_{cat}/K_m $(R) \rightarrow (S)$, $M^{-1}s^{-1}$	6.9 ($\pm$ 1.2) $\times$ 10^5	3.1 ($\pm$ 0.4) $\times$ 10^2	4.4 ($\pm$ 1.0) $\times$ 10^{-4}
k_{cat} $(S) \rightarrow (R)$, s^{-1}	510 ($\pm$ 13)	8.3 ($\pm$ 1.9)	0.016 ($\pm$ 0.004)
K_m ((S)-mandelate), mM	0.63 ($\pm$ 0.02)	32 ($\pm$ 10)	51 ($\pm$ 16)
k_{cat}/K_m $(S) \rightarrow (R)$, $M^{-1}s^{-1}$	8.1 ($\pm$ 0.3) $\times$ 10^5	2.6 ($\pm$ 1.0) $\times$ 10^2	3.2 ($\pm$ 1.2) $\times$ 10^{-4}
K_i (BHA), mM	0.0117 ($\pm$ 0.0012)	2.9 ($\pm$ 0.7)	250 ($\pm$ 70)

6.3.5 Electrostatic Potential Surfaces

Geometry optimizations and electrostatic potential surfaces were calculated for (R)-mandelate, the putative aci-carboxylate intermediate, the (S)-α-HBP monoanion, the conjugate base of $trans$-BHA (O-deprotonated), and benzoylformate by performing self–consistent–field calculations at the 6-31G* level. The color–coded electrostatic potential surfaces for each of these ligands are displayed in **figure 6.4**. The geometries of these species were optimized in the gas phase and are not intended to represent the conformation assumed by the bound ligand at the active site.

Figure 6.4 Molecular electrostatic potential surface at the van der Waals radii for (R)-mandelate (A), the putative *aci*-carboxylate intermediate (B), the (S)-α-HBP monoanion (C), the conjugate base of *trans*-BHA (O-deprotonated) (D), and benzoylformate (E). Color–coded electrostatic potential surfaces are shown for each of these ligands with an electron density isosurface displayed at a density of 0.002 e/a_0^3 which encompasses approximately 95% of the van der Waals radii (Sjoberg & Politzer, 1990). The red regions are the most negative potentials and the blue regions are the most positive on the electrostatic potential surfaces. The energy difference from the red to blue regions is approximately 131 kcal/mol. The stick models in the upper right corner of each panel have the same orientation as the electrostatic potential surface models while those in the lower right corner have been rotated to more clearly display the plane of the phenyl ring. The stick models use the colors red, blue, green, white, and yellow to represent oxygen, nitrogen, carbon, hydrogen, and phosphorus, respectively.
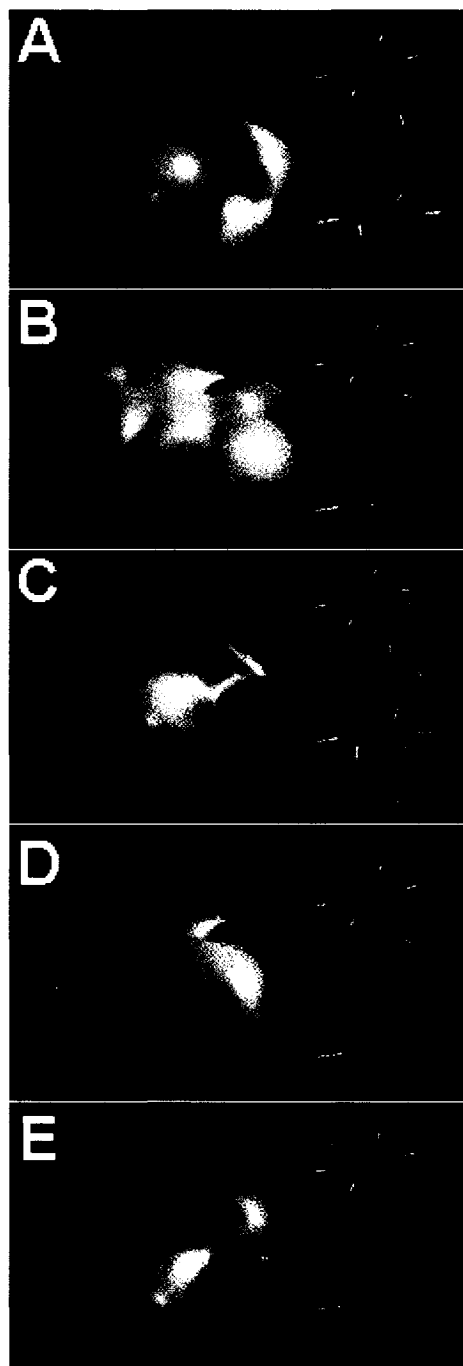
Figure 6.4

6.4 Discussion

The application of transition state theory to enzyme–catalyzed reactions led Pauling (1948) to propose that enzymes accelerate the rates of chemical reactions by selectively stabilizing the altered substrate in the transition state relative to the ground state. This idea was further developed by Jencks (Jencks, 1966), Wolfenden (Wolfenden, 1969, 1972), and Lienhard (Lienhard, 1973). In order to preferentially stabilize the transition state, an enzyme must provide new and/or strengthened interactions with the altered substrate as the reaction approaches the transition state. These strengthened interactions with the transition state are typically derived from hydrogen bonding and/or electrostatic interactions (Shan & Herschlag, 1996; Warshel, 1998; Wolfenden *et al.*, 1999) and, as discussed in Chapter 5, may also include strengthened van der Waals contacts and hydrophobic interactions.

Because of the paucity of functional groups on mandelate, MR appears to utilize only a few residues to directly provide hydrogen bonding and electrostatic interactions with the ligand, including Asn 197, Glu 317 and Lys 164. Thus, during catalysis, as the substrate approaches the transition state, new or strengthened interactions can originate from only a limited number of sources. In this chapter, site–directed mutagenesis has been used to investigate the role of several binding determinants on both ground state and transition state stabilization by MR. Since $K_m \approx K_s$ for wild–type MR (Chapter 3), K_m and k_{cat}/K_m serve to relate the effect of individual mutations on the affinity of the enzyme for both the substrate in the ground state and the altered substrate in the transition state. In addition, if BHA is a reasonable mimic of the reaction intermediate, its binding affinity may be used to probe the effect of mutations on intermediate stabilization. The extent to which BHA mimics the altered substrate in the transition state is discussed in detail in section 6.4.5.

The free energy diagrams for wild–type, N197A, E317Q, K164R, and V29D MR are overlaid in **figure 6.5**. Despite being centered in different regions of the active site
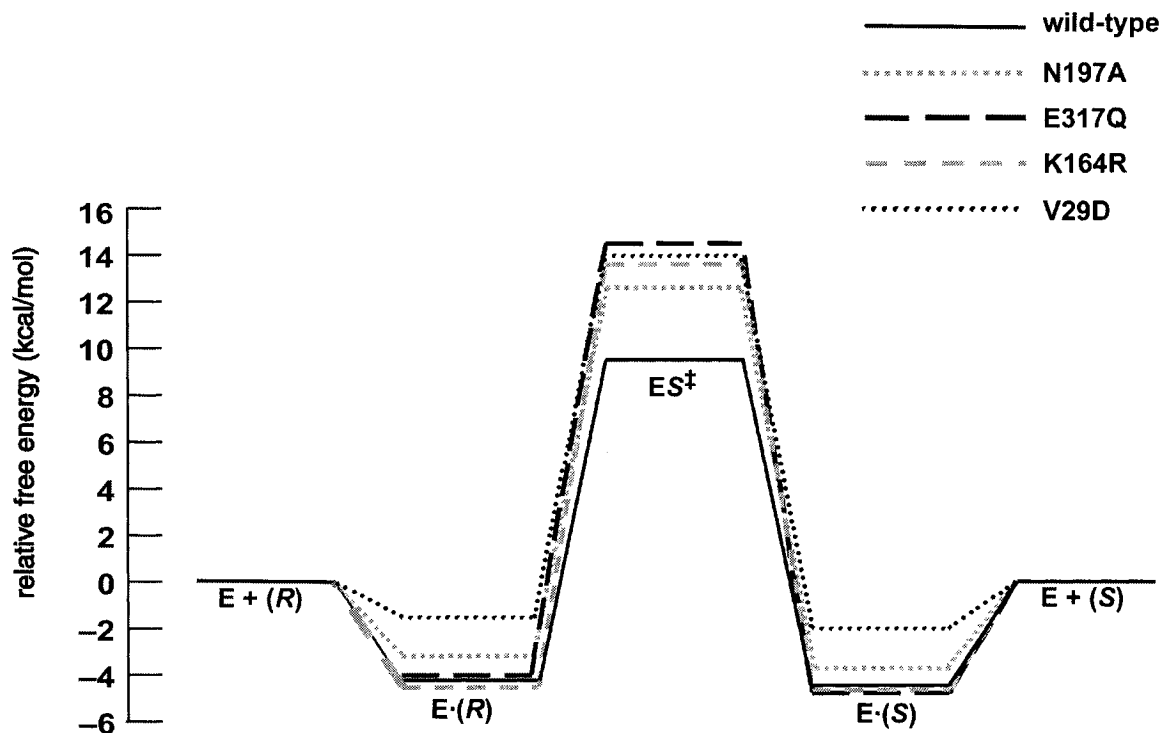
Figure 6.5   Free energy profiles (pH 7.5, 25 °C) for the racemization of (R)-mandelate ((R)) and (S)-mandelate ((S)) by wild-type and mutant mandelate racemases. The profiles are derived from the kinetic parameters in tables 6.2, 6.3, 6.4 and 6.5. ES‡ represents the enzyme-substrate complex in the transition state.

(figure 6.1), each of these mutations results in a substantial decrease in catalytic proficiency relative to the wild–type enzyme, with corresponding $\Delta\Delta G_{Tx}$ values ranging from +3.2 (N197A) to +5.5 kcal/mol (E317Q). Conversely, the ground state binding energies are much less affected by these same mutations with $\Delta\Delta G$ values ranging from –0.3 (K164R) to +2.3 kcal/mol (V29D). It appears from this initial survey that MR preferentially stabilizes the transition state relative to the ground state using *many* interactions with the altered substrate in the transition state. A more detailed discussion on the effects of each individual mutation follows.

6.4.1 The N197A Mutant

The sensitivity of MR to the presence of an α-hydroxyl function on the phosphonate analogues (Chapter 4) prompted the investigation of the contribution of Asn 197 to catalysis. In all published crystal structures of wild–type and mutant forms of MR, the carboxamide of this residue is within hydrogen bonding distance of the α-hydroxyl function of bound ligands as shown in **figure 6.1** (Kallarakal *et al.*, 1995; Landro *et al.*, 1994; Mitra *et al.*, 1995; Neidhart *et al.*, 1991; Schafer *et al.*, 1996). The γ-carboxylate of Glu 247 is also within hydrogen bonding distance of the α-hydroxyl group but is involved in coordinating the magnesium ion (Neidhart *et al.*, 1991).

The transition state stabilization free energy provided by the interaction between Asn 197 and the α-hydroxyl function of mandelate is 3.2–3.7 kcal/mol. This agrees well with the additional 3.5 kcal/mol that the α-hydroxyl contributes to the binding of α-HBP relative to benzylphosphonate (Chapter 4) and fits into the range of values expected for residues participating in neutral hydrogen bond pairs (Fersht, 1999; Street *et al.*, 1986; Wilkinson *et al.*, 1984; Wilkinson *et al.*, 1983). For example, Roth *et al.* (1998) have reported that His 357 of *E. coli* β-galactosidase interacts with the C3 hydroxyl of the ligand and stabilizes the transition state by approximately 3.5 kcal/mol. Since Asn 197 stabilizes the altered substrate in the transition state more than it stabilizes the substrate in

the ground state (differential binding (Albery & Knowles, 1976, 1977)), the binding affinity of intermediate analogue inhibitors to the N197A mutant would be expected to be reduced relative to the wild–type enzyme while the binding affinity of ground state analogues would not be significantly affected. Indeed, binding of both α-HBP and BHA by the N197A mutant is much more severely affected than is the binding of (R)-mandelate, (S)-mandelate, or (R)-atrolactate (**table 6.2**). The free energy profiles for racemization catalyzed by both the wild–type and N197A enzymes, shown in **figure 6.5**, illustrate the preferential binding of the altered substrate in the transition state relative to the ground state.

What is the structural basis for Asn 197's apparent discrimination between the substrate in the ground state and the altered substrate in the transition state? **Figure 6.1** reveals that the carboxamide of Asn 197 lies within hydrogen bonding distance of the ligand's α-hydroxyl function. The weak inhibition observed for benzoylformate and benzoylphosphonate may indicate a preference by MR for ligands with a hydrogen bond donor at the α-position (Chapter 4). Therefore, it is likely that the carboxamide oxygen of Asn 197 acts as the hydrogen bond *acceptor* (i.e., the carboxamide function is rotated 180° from the orientation shown in **figure 6.1**). As the intermediate is formed, the pK_a of the α-hydroxyl would be expected to decrease as the oxygen becomes enolic in the intermediate. For example, the pK_a of 2-propanol is 18 (McEwen, 1936) while the pK_a of enolic acetone is 10.9 (Chiang & Kresge, 1991). These alterations in pK_a values may account for some of the strengthening of the interaction between the hydrogen–bonding partners on formation of the intermediate. In addition, a hydrogen bond between the enzyme and the substrate could strengthen as a result of conformational changes in the enzyme–intermediate complex, contributing to increased enzyme–intermediate complementarity. Indeed, enhanced interactions between enzymes and intermediates or altered substrates in the transition state are a common theme in catalysis, even for binding

determinants on the ligand which appear to be remote from the site of chemistry (Fersht, 1999; Miller *et al.*, 2000; Roth *et al.*, 1998; Shan *et al.*, 1996; Wolfenden, 1999).

6.4.2 The E317Q Mutant

Concerted general acid–general base catalysis in MR leads to the formation of the stabilized enol tautomer of mandelic acid (Gerlt & Gassman, 1993a, b; Mitra *et al.*, 1995). The transfer of a proton from the general acid catalyst toward the carboxylic acid oxygen of the substrate facilitates concerted proton abstraction from the α-carbon of the substrate. Thus, the general acid catalyst allows the enzyme to overcome the significant kinetic and thermodynamic barriers associated with proton abstraction from a weakly acidic α-carbon acid using a weakly basic general base catalyst (Gerlt & Gassman, 1993a, b). Gerlt and Gassman have argued that proton abstraction by the general base catalyst of MR is rendered most effective when the pK_a of the general acid catalyst matches the pK_a of the enolic intermediate, leading to the formation of a short, strong hydrogen bond (SSHB) (Gerlt & Gassman, 1993a, b). To investigate the role of the proposed SSHB in catalysis, Mitra *et al.* (1995) identified Glu 317 as the general acid catalyst and constructed and characterized the E317Q mutant. While still capable of hydrogen bonding interactions, the carboxamide group of Gln has a substantially higher pK_a than the carboxylate group of Glu (Bordwell, 1988; Mitra *et al.*, 1995), preventing the matching of pK_a values between the general acid catalyst and the enolic intermediate and precluding the formation of a SSHB. In the present work, the E317Q mutant was used to probe the interaction of Glu 317 with BHA. Because of the requirement for a general acid catalyst in MR catalysis, it is very likely that only a very limited number of mutations at the Glu 317 position would retain sufficient activity to allow K_i values to be determined. Thus, the weakened acidity of the E317Q mutant allows the sensitivity of the binding interaction between the general acid catalyst and the intermediate analogue inhibitor, BHA, to be investigated.

The crystal structure of E317Q reported by Mitra *et al.* reveals that no significant structural perturbations are introduced by the substitution of Glu with Gln and that the substrate analogue, (*S*)-atrolactate, binds in the same orientation as it does with the wild–type enzyme (Mitra *et al.*, 1995). The CD spectra reported in **figure 6.2** and the deconvolution results reported in **table 6.1** also indicate that no structural perturbations are introduced by the Glu to Gln mutation. The kinetic values reported in **table 6.3** are in excellent agreement with the values reported by Mitra *et al.* for E317Q MR (Mitra *et al.*, 1995).

The decrease in k_{cat}/K_m for E317Q relative to the wild–type enzyme has been attributed to the increased pK_a value of the carboxamide group relative to the carboxyl group, resulting in a decreased strength of the hydrogen bond between Gln and the enol tautomer of mandelic acid (Mitra *et al.*, 1995). Although no direct evidence for a SSHB in MR has yet been reported, the E317Q mutation results in a significant reduction in transition state stabilization equivalent to 4.9–5.5 kcal/mol. Ground state stabilization, meanwhile, is unperturbed. The E317Q mutant binds the substrates (*R*)- and (*S*)-mandelate with an affinity equal to that of the wild–type enzyme. Thus, the decrease in the apparent affinity for the altered substrate in the transition state confirms the importance of the general acid catalyst in transition state stabilization. The strengthened interaction with Glu 317 in the transition state relative to the ground state results from the increased pK_a of the enolic intermediate relative to the substrate (Gerlt & Gassman, 1993a, b; Mitra *et al.*, 1995). The pK_a of the intermediate more closely matches the pK_a of the general acid catalyst, increasing the strength of their interaction. This is an excellent example of a mechanism by which an enzyme provides greater stabilization energy to the reactive species than it does to the ground state by taking advantage of unique features of the altered substrate in the transition state. In this case, MR takes advantage of the higher pK_a of the enol tautomer of mandelic acid to provide greater stabilization energy to the transition states and the intermediate.

Binding of BHA by the E317Q mutant is reduced 65-fold ($\Delta\Delta G$ = 2.5 kcal/mol) relative to the wild–type enzyme. While this reduction in free energy is only half the reduction observed for the free energy of activation ($\Delta\Delta G^{\ddagger}$), it reinforces the notion that the binding of BHA is sensitive to perturbations of the enzyme–transition state complex.

6.4.3 The K164R Mutant

Two roles have been suggested for Lys 164. First, the positive charge of Lys 164 is believed to influence the pK_as of the general acid/base catalysts (Neidhart et al., 1991; Schafer et al., 1996). Second, Lys 164 in combination with the active site Mg^{2+} ion, plays a role in permitting the substrate to react as a carboxylic acid rather than a carboxylate anion in the active site of MR thereby reducing the thermodynamic barrier for proton abstraction by concerted general acid–general base catalysis (Gerlt & Gassman, 1993a, b). Guthrie and Kluger (1993), however, have argued that the energies of the O-protonated acid, the enol and the enolate are all similar, and, therefore, that concerted general acid–general base catalysis is not sufficient to achieve catalysis. They propose that electrostatic stabilization of the intermediate enolate anion is sufficient to lower the thermodynamic barrier to proton abstraction and achieve the observed rates of catalysis by MR. In both proposals, Lys 164 is implicated as an important determinant in MR catalysis.

To assess the role of Lys 164 in both ground state and transition state stabilization by MR, the K164R mutant was constructed and characterized. A conservative mutation of Lys to Arg at position 164 was constructed in order to maintain a sufficient level of catalytic activity to allow characterization of the inhibition by BHA. This conservative mutation maintains a positive charge at position 164 and is less likely to disrupt the influence on the pK_as of the catalytic residues. An earlier report on the role of the general acid/base catalyst Lys 166 in MR catalysis revealed that substitution of Lys 166 with Ala, Gln and Met resulted in structural perturbations of the enzyme (Kallarakal et al., 1995).

Only the mutation of Lys to Arg at position 166 retained the wild–type enzyme structure (Kallarakal *et al.*, 1995). Lys 164 is in close proximity to Lys 166 (~5 Å) and the structural integrity of the enzyme could, therefore, also be sensitive to mutations at this position. The K164R mutation was constructed, therefore, in order to minimize structural perturbations to the enzyme while directly assessing the sensitivity of both ground state and transition state stabilization to a relatively subtle change at position 164 of MR. Indeed, the CD spectrum of K164R MR reveals no significant structural perturbations relative to the wild–type enzyme (**figure 6.2**).

The value of k_{cat} for the K164R mutant in both the $R{\rightarrow}S$ and $S{\rightarrow}R$ directions is reduced by four orders of magnitude relative to the wild–type enzyme. The K_m values for both (R)- and (S)-mandelate are also slightly reduced relative to the wild–type enzyme. This results in a decrease in k_{cat}/K_m equal to four orders of magnitude in both reaction directions for the K164R mutant relative to the wild–type enzyme; the equivalent of 4.2–4.5 kcal/mol of free energy. Surprisingly, the substitution of lysine with a bulkier arginine residue at position 164 results in a slight *increase* in the affinity of the enzyme for both substrates. The substantial decrease in k_{cat}/K_m, however, indicates that transition state stabilization is sensitive to a relatively subtle perturbation at Lys 164, suggesting that, in agreement with Guthrie and Kluger (1993), electrostatic stabilization assisted by Lys 164 is an important factor in catalysis. However, these results do not obviate the possibility that Lys 164 functions to promote the formation of a *neutral* enolic intermediate as suggested by Gerlt and Gassman (1993a; 1993b). If neutralization of the substrate's negative charge involves partial proton transfer from Lys 164, then the increased pK_a of arginine relative to lysine may afford less stabilization of the enolic intermediate. In their analysis of the reaction catalyzed by MR, Gerlt and Gassman do not invoke a proton transfer from Lys 164 to the substrate's carboxylate group but, rather, suggest that the negative charge of the substrate is neutralized by the proximity of the positively charged Lys 164 residue and the Mg^{2+} ion (Gerlt & Gassman, 1992, 1993a, b).

Thus, Gerlt and Gassman also implicate electrostatic stabilization from Lys 164 in the overall stabilization of the intermediate. If the contribution to transition state stabilization by Lys 164 is exclusively electrostatic, the reduction in transition state stabilization observed with the K164R mutant might result from improper positioning of the positively charged guanidinium group of arginine adjacent to the negative charge of the transition state. In this scenario, the difference in positioning does not adversely affect the binding of the substrates and, in fact, may allow for increased ground state binding affinity in the mutant enzyme. Combined with the E317Q mutant discussed above, it appears that transition state stabilization is quite sensitive to relatively subtle changes to enzyme residues surrounding the substrate carboxyl group whereas ground state stabilization is virtually unaffected by these same perturbations.

In the $S{\rightarrow}R$ direction, substrate inhibition was observed (**figure 6.3**). The data was fit to equation 6.1 describing substrate inhibition, yielding two binding constants: K_s = 0.38 mM and K_s' = 11.3 mM, where K_s is the dissociation constant for the enzyme–substrate complex and K_s' is the dissociation constant for a second bound substrate from an inactive enzyme–bisubstrate complex (**scheme 6.1**). Substrate inhibition at substrate concentrations of 30 mM has been reported previously for wild–type MR (Kenyon & Hegeman, 1970). The K_s value for (S)-mandelate with the K164R mutant is 1.6-fold less than it is with the wild–type enzyme indicating that the mutant enzyme binds (S)-mandelate with slightly greater affinity than does the wild–type enzyme. Substrate inhibition of the K164R mutant could result from the increased affinity of K164R for (S)-mandelate combined with the significantly reduced catalytic rate. These two effects will result in a slowly racemized, tightly bound enzyme–substrate complex that makes K164R more susceptible than the wild–type enzyme to substrate inhibition at low substrate concentrations. No other characterized mutant of MR has a substrate binding affinity greater than the wild–type enzyme and few assays of MR activity have been conducted at substrate concentrations exceeding 10 mM. This could explain why substrate inhibition

has not typically been reported for MR. However, the X-ray crystal structure of K166R MR co-crystallized with (R)-mandelate reveals both (R)- and (S)-mandelate in the active site of the enzyme (Kallarakal *et al.*, 1995), indicating that, at saturating concentrations, more than one molecule of substrate and/or product can be bound at sites proximal to the active site.

In addition to the simple substrate inhibition of **scheme 6.1**, other kinetic schemes can also give rise to substrate inhibition. Notably, substrate inhibition can be observed in kinetic schemes involving an activating metal ion (**scheme 6.2**) (Segel, 1993b). At fixed concentrations of activator (i.e., Mg^{2+}), the shape of the initial velocity curve as a function of substrate concentration will depend on the relative values of K_S, K_{EA} and K_{SA} from **scheme 6.2**, and is described by equation 6.2.

$$v = \frac{V_{max}}{\dfrac{K_0 K_{SA}}{[Mg^{2+}][S]}\left(1 + \dfrac{[S]}{K_S} + \dfrac{[Mg^{2+}]}{K_{EA}}\right) + 1}$$

(6.2)

The following scenario could explain the observed substrate inhibition: The wild–type enzyme preferentially binds the mandelate–Mg^{2+} complex and binds the substrate poorly in the absence of Mg^{2+} (i.e. $K_S > K_{EA}$, $K_{SA} < K_{EA}$). This will give rise to a typical hyperbolic curve that reaches saturation at high substrate concentrations (Segel, 1993b). Lys 164, however, is in close proximity to the metal ion binding site and its mutation to Arg could decrease the Mg^{2+} binding affinity. If this reduction in Mg^{2+} binding affinity results in increased values of K_{EA} and K_{SA} relative to K_S (i.e. $K_S < K_{EA}$, $K_{SA} < K_{EA}$) then formation of the unproductive ES complex becomes kinetically significant and gives rise to substrate inhibition (Segel, 1993b). In **scheme 6.2** the apparent substrate inhibition would likely be observed in both reaction directions. However, substrate inhibition was

Scheme 6.2 Kinetic scheme for the enzyme–catalyzed conversion of substrate to product in the presence of an essential activator.

$$
\begin{array}{ccc}
& K_S & \\
E + S & \rightleftharpoons & ES \\
+ A \;\searrow K_0 & & + A \\
& SA & \\
\Big\updownarrow K_{EA} & \searrow K_{SA} \;\Big\updownarrow \alpha K_{EA} & \\
& \alpha K_S & \\
EA & \rightleftharpoons & ESA \xrightarrow{\;k_{cat}\;} E + A + P
\end{array}
$$
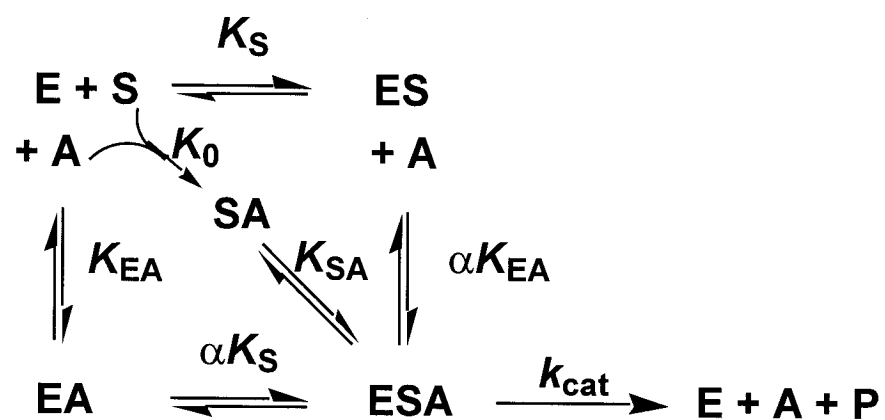
observed only with (S)-mandelate, making it unlikely that decreased binding of the activating Mg^{2+} is responsible for the observed substrate inhibition.

The inhibition constant for BHA with K164R MR was 6.2 ± 1.3 μM, nearly two–fold *less* than the K_i for BHA with the wild–type enzyme. The implications of this result are discussed in section 6.4.5.

6.4.4 The V29D Mutant

The hydrophobic cavity of MR contributes to catalysis by preferentially binding the aromatic ring of the planar intermediate (Chapter 5). This cavity is composed, in part, of a flexible, amphipathic hinged loop (residues 19–30) which closes down over the top of the active site (Neidhart *et al.*, 1991). Increasing evidence is emerging that the dynamic motions of flexible, active–site loops make significant contributions to enzyme catalysis. Recently characterized examples include triosephosphate isomerase (Rozovsky *et al.*, 2001; Rozovsky & McDermott, 2001), fructose-1,6-bisphosphate aldolase (Zgiby *et al.*, 2002), lactate dehydrogenase (Gulotta *et al.*, 2002), acetylcholinesterase (Shi *et al.*, 2001), glutathione transferase (Codreanu *et al.*, 2002), and dihydrofolate reductase (Osborne *et al.*, 2001). To evaluate the sensitivity of the hydrophobic pocket and the flexible hinged loop to disruption by a charged, polar residue, the V29D mutant was constructed and characterized.

Introducing a negative charge in close proximity to the *para* position of the substrate's aromatic ring results in a dramatic reduction in the substrate binding affinity, increasing the K_m value for (R)- and (S)-mandelate by 80- and 50-fold, respectively. The V29D mutant also exhibits a substantial decrease in the rate of catalysis, with k_{cat} reduced for (R)- and (S)-mandelate by 30- and 60-fold, respectively, relative to the wild–type enzyme. These effects combine to decrease k_{cat}/K_m in both reaction directions by four orders of magnitude. Thus, in agreement with the conclusions from Chapter 5, the hydrophobic cavity provides stabilizing interactions to the substrate both in the ground

state and in the transition state. The negative charge introduced into the flexible loop of the hydrophobic cavity may interfere with loop function by disrupting hydrophobic interactions within the cavity. Consistent with the discussion in Chapter 5, transition state stabilization is more significantly affected than ground state stabilization by disruptions to interactions within the hydrophobic cavity. Thus, the hinged lid may indeed clamp down over the active site to form a tight fit with the planar intermediate, providing a mechanism for preferential transition state stabilization originating from within the hydrophobic cavity. The inhibition of V29D MR by BHA was reduced 250-fold relative to the wild–type enzyme. Again, the reduced affinity of the mutant enzyme for BHA does not approach that predicted based on the four orders of magnitude reduction in k_{cat}/K_m but it is greater than the reduction in affinity for the substrate.

6.4.5 Assessment of BHA as a Transition State Analogue Inhibitor

Much of the analysis presented in Chapters 4 and 5 relied on the assumption that BHA was a reasonable mimic of the altered substrate in the transition state. While some attempts were made to justify this assumption in Chapter 4, a more thorough discussion of the transition state analogue nature of BHA and α-HBP is warranted in light of the mutagenesis experiments that have been presented in this chapter.

Enzymes affect chemistry by inducing changes in electron distribution in substrates (Schramm, 1998; Schramm *et al.*, 1994). Generation of differential charge distribution between the substrate and the altered substrate in the transition state permits electrostatic interactions between the enzyme and its ligand to selectively stabilize the altered substrate in the transition state (Warshel, 1991). Elegant studies conducted by Schramm and co-workers have focused on calculating the electrostatic potential surfaces of enzyme–bound transition state structures deduced from kinetic isotope effects (Horenstein *et al.*, 1991; Horenstein & Schramm, 1993a, b). These studies have revealed that, as the structure of the substrate is altered to that of the transition state, there are changes in the electrostatic

potential surface which an enzyme may utilize to selectively bind and stabilize the transition state relative to the ground state. Although the detailed geometric and electronic characteristics are not yet available for the MR–bound transition state, the electrostatic potential surface of the putative *aci*-carboxylate intermediate in the gas phase has been calculated so that its electrostatic potential surface can be compared to the intermediate analogue inhibitors α-HBP and BHA.

The electrostatic potential surface for (*R*)-mandelate (**figure 6.4A**) indicates that the negative potential is primarily localized on the carboxylate function of the substrate. On the other hand, the *aci*-carboxylate intermediate (**figure 6.4B**) has the negative charge delocalized over the entire molecule. The optimized geometry and calculated electrostatic potential surfaces for the conjugate base of (*S*)-α-HBP and *trans*–BHA (*O*-deprotonated) are shown in **figures 6.4C** and **6.4D**, respectively. Although the electrostatic potential surface of (*S*)-α-HBP appears to resemble aspects of both the substrate and the *aci*-carboxylate intermediate, the oxygen atoms of the phosphonate function may be oriented so that the negative charge is almost co-planar with the phenyl ring thereby mimicking the *aci*-carboxylate as indicated in the stick diagrams (**figure 6.4C**). While several different forms of BHA are theoretically possible, either the *cis*- or *trans*-BHA (*O*-deprotonated) most closely resembles the *aci*-carboxylate intermediate (Chapter 4). The *O*-deprotonated *trans*-BHA is planar and has an electrostatic potential surface which closely mimics the *aci*-carboxylate intermediate. The optimized geometry (with restrictions imposed on the rotation of carboxylate group) and calculated electrostatic potential surfaces for the carboxylate–containing analogue, benzoylformate, is shown in **figure 6.4E**. Because of its sp^2-hybridized α-carbon, benzoylformate has an electrostatic potential surface very similar to the planar *aci*-carboxylate intermediate. The fact that benzoylformate is a poor inhibitor of the enzyme emphasizes the important role that the α-hydroxyl function plays in the binding of intermediate analogues.

Often, transition state analogues are classified conceptually as a rationalization for the high binding affinity of inhibitors and are based on the structural and electronic mimicry of the transition state. The electrostatic surface potential of BHA and α-HBP provide a rationale for why these inhibitors might be reasonable mimics of the *aci*-carboxylate intermediate. However, these arguments are qualitative and are based on the calculated structures of these molecules in the gas phase. They cannot account for modified charge distributions or skewed binding orientations in the active site of the enzyme. The high binding affinity of both BHA and α-HBP relative to the substrate is also not sufficient to classify these inhibitors as transition state analogs. For example, the high affinity binding of methotrexate to dihydrofolate reductase caused it to initially be classified as a transition state analogue, but it was ultimately shown that this inhibitor is bound by the enzyme in a manner very different from that expected for the transition state (Oefner *et al.*, 1988).

Several criteria may be evaluated in order to establish whether an inhibitor is a transition state analogue. One of these criteria is that the inhibitors must exhibit slow–binding kinetics (Frieden *et al.*, 1980). The slow–binding kinetics observed for many transition state analogues are proposed to result from structural rearrangements of the enzyme. These rearrangements are necessary to achieve complementarity between with the enzyme and the transition state analogue just as structural changes are required to form the tightly bound enzyme–transition state complex (Frieden *et al.*, 1980). The initial velocity kinetics in the presence of either α-HBP or BHA show no evidence of slow binding inhibition. However, a transition state analogue need not necessarily be a slow binding inhibitor. The slow binding kinetics typical of many transition state analogues may simply result from the low inhibitor concentrations that are typically necessary to measure the K_i values of very high affinity inhibitors (Mader & Bartlett, 1997).

A more rigorous characterization of transition state analogy is based on the relationship between K_{Tx} and k_{cat}/K_S described in equation 1.7. If the binding of a

transition state analogue mimics that of the transition state, then K_i for the analogue inhibitor should be proportional to K_{Tx} for all reactions which proceed through a common non-enzymatic transition state. An ideal transition state mimic, therefore, will give a slope equal to one in a plot of the log K_i against log (K_m/k_{cat}) for a series of mutant enzymes catalyzing the same reaction (Mader & Bartlett, 1997). A plot of log (K_m/k_{cat}) against log K_i was constructed for BHA (**figure 6.6**) using the values reported in tables 5.2, 6.2, 6.3, 6.4 and 6.5. The linear regression line has a slope equal to 1.6 (r^2=0.92 excluding the K164R data point as discussed below). The series of mutants included in this plot were designed to probe the transition state mimicry over a complete cross–section of the active site, including the hydrophobic cavity. The kinetic parameters for the alternative substrate 2-naphthylglycolate and the inhibitor 2-naphthohydroxamate were also included in this plot as a means to further assess transition state mimicry of the hydroxamate in the hydrophobic cavity. (The inclusion of this point requires the not unreasonable assumption that the non-enzymatic rate for the racemization of 2-naphthylglycolate is very similar to the non-enzymatic rate for the racemization of mandelate.) A plot of log K_m against log K_i was also constructed (**figure 6.7**) to determine the degree to which BHA mimics the substrate in the ground state. In the $R{\rightarrow}S$ direction, the slope of the linear regression line was 0.62 (r^2=0.62) while in the $S{\rightarrow}R$ direction, the slope was 0.48 (r^2 =0.43). Thus, from the slopes of the lines and the qualities of the fits (coefficient of determination; r^2), BHA appears to be a better mimic of the transition state than of the substrate. Mader and Bartlett have noted that the slope of the line from this free energy relationship should not be interpreted as a measure of the degree of mimicry of the transition state analogue and that only a slope equal to one can validate an inhibitor as a transition state analogue (Mader & Bartlett, 1997). Withers and coworkers, however, disagree that a slope of 1.0 is *required* to indicate transition state mimicry (Mosi *et al.*, 1998). In their assessment of acarbose as a transition state analogue inhibitor of cyclodextrin glycosyltransferase, Mosi *et al.* (1998) observed a slope of 1.61

Figure 6.6   Linear free energy relationship between the K_i values for the competitive inhibition of MR by BHA and 2-naphthohydroxamate and the reciprocal of the second order rate constant (k_{cat}/K_m; $s^{-1}M^{-1}$) for the racemization of the substrates (R)-mandelate and (R)-2-naphthylglycolate. The curve shown is the linear regression line for all MR variants except K164R.

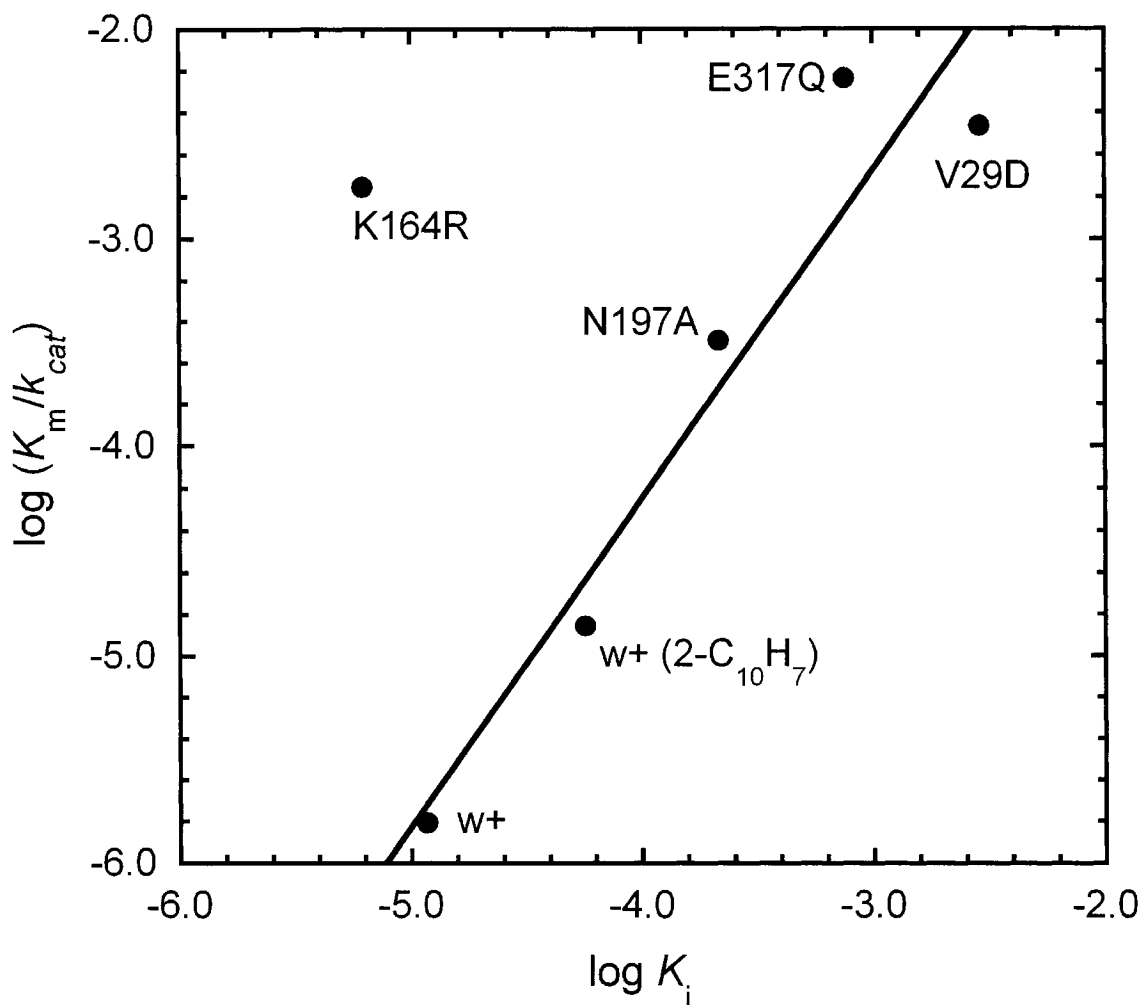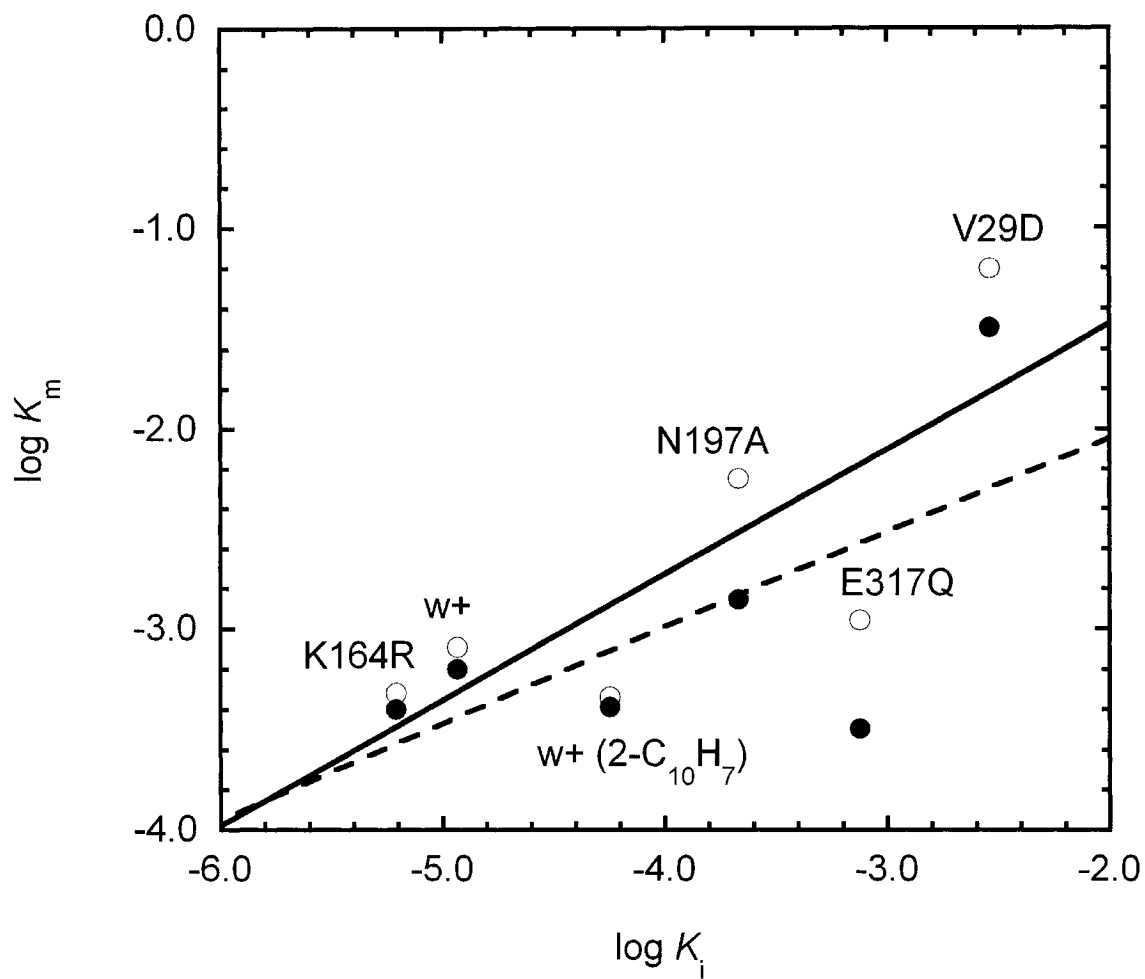**Figure 6.7** **Linear free energy relationship between the K_i values (M) for the competitive inhibition of MR by BHA and 2-naphthohydroxamate and K_m (M) for the substrates (R)-mandelate and (R)-2-naphthylglycolate (open circles; solid line) and the substrates (S)-mandelate and (S)-2-naphthylglycolate (closed circles; dashed line).** The plot is for all variants of MR.

for a plot of log (K_m/k_{cat}) against log K_i and a slope of 0.47 for a plot of log K_m against log K_i. From these data, they concluded that acarbose displayed approximately equal mimicry of both the ground state and the transition state. The slopes observed for the plots of the log K_i of BHA are similar to those reported for the inhibition of cyclodextrin glycosyltransferase by acarbose. Thus, BHA mimics aspects of the substrate in the ground state and in the transition state, though it appears to be a slightly better mimic of the altered substrate in the transition state.

K164R appears graphically to be an outlier in **figure 6.6**. There are many possible explanations for why K164R might be anomalous and one must be careful not to over–interpret these results. The complexity of enzyme systems often makes it particularly difficult to unambiguously interpret the significance of mutation experiments. For example, the effect of mutating Asp 32 in subtilisin has been interpreted as an electrostatic effect, a hydrogen bonding effect and an entropic effect (Warshel, 1998 and references therein). In the case of MR, the absence of structural data with bound BHA makes a precise interpretation of mutagenesis results difficult. The preceding discussion on the role of Lys 164 in transition state stabilization (section 6.4.3) relied on the assumption that the pK_a value of the general base catalyst, Lys 166, was not affected by the Lys to Arg mutation. Although the mutant was designed to minimize this possibility, a complete kinetic characterization of the K164R mutant lies beyond the scope of the present work and, as such, no direct evidence to support this assumption has been presented. With this assumption in mind, a few interpretations are presented to explain the anomalous behaviour of K164R in the linear free energy relationship.

It is possible that BHA does not interact significantly with Lys 164 and, therefore, its binding affinity is unaffected by a conservative substitution at this position. However, the binding affinity of BHA with the K164R enzyme is increased two–fold relative to the wild–type enzyme, implying that there is some interaction between BHA and Arg 164 in the K164R mutant. A potential role for Lys 164 in transition state stabilization was

discussed in section 6.4.3. Perhaps Lys 164 plays a significant role in lowering the intrinsic kinetic barrier ($\Delta G^{\ddagger}_{int}$) for the reaction. The intrinsic kinetic barrier can be lowered by neutralizing the negative charge on the carbonyl carbon as it develops during the concerted abstraction of the α-proton (Gerlt & Gassman, 1993a). While the general acid catalyst Glu 317 is believed to be principally responsible for this task (Gerlt & Gassman, 1992, 1993a, b), a positive charge from Lys 164 in close proximity to the developing negative charge may also assist in lowering the intrinsic kinetic barrier. The substantial reduction in k_{cat} for the K164R mutant may result from a less effective neutralization of the developing negative charge on the carboxyl oxygen by the guanidinium group of arginine. If, indeed, Lys 164 makes a substantial contribution to lowering the intrinsic activation barrier, then the binding interactions with Lys 164, even for a very good intermediate analogue inhibitor, may never fully capture the equivalent to the transition state stabilization free energy contributed by Lys 164.

BHA is not a perfect analogue of the transition state for several reasons. First, obviously, the electrostatic potential surface is not a perfect mimic of the intermediate. Second, Gerlt and Gassman (1993b) have suggested that the most effective transition state analog inhibitors for MR will have pK_a values that match that of the intermediate. According to Gerlt and Gassman, the pK_a of the neutral intermediate is critical to the formation of a SSHB between the general acid catalyst, Glu 317, and the intermediate, which lowers the thermodynamic barrier for the reaction. The pK_a of the neutral enolic intermediate is 6.6 (Chiang et al., 1990). The pK_a of BHA is 8.8 (Exner et al., 1993; Farkas et al., 2000), several units removed from the pK_a of Glu 317 (estimated to be ~6 in MR) (Gerlt & Gassman, 1993a, b). If, indeed, formation of a SSHB with Glu 317 dominates the stabilization of the intermediate, a SSHB is unlikely to form with BHA in the enzyme active site, severely limiting the extent to which BHA mimics the intermediate and transition states.

The stereoelectronic features of α-HBP make it difficult to explain its high binding affinity (Chapter 4) but the pK_{a2} of α-HBP may provide an explanation for the surprisingly high affinity of this inhibitor. The pK_{a2} of α-HBP is 6.9 (Chapter 4) and is very close to that of the enolic intermediate. This may allow a strong interaction to develop between the α-HBP monoanion and the general acid catalyst, Glu 317, resulting in the relatively high inhibitor binding affinity of α-HBP. Finally, Gerlt and Gassman have proposed, using Marcus formalism, that the general acid catalyst reduces the overall activation free energy of the enzyme by lowering the intrinsic kinetic barrier for proton abstraction (Gerlt & Gassman, 1993a, b). This is a kinetic rather than a thermodynamic effect which limits the ability of either α-HBP or BHA to fully mimic the interactions with the altered substrate in the transition state.

Based on its relatively high binding affinity, its mimicry of the electrostatic surface potential of the intermediate and the relatively good correlation observed in the linear free energy relationship with log (K_m/ k_{cat}) (**figure 6.6**), BHA may be considered to be a reasonable mimic of the intermediate in the reaction catalyzed by MR. BHA is far from an ideal transition state analogue and displays a degree of ground state mimicry, particularly in its interaction with Lys 164. This analysis validates the treatment of BHA as an intermediate analogue but also emphasizes the caveat that BHA is not an exact mimic of the reaction intermediate. Of course, the interpretation of the inhibition of MR by BHA will be greatly assisted by knowing precisely the orientation of BHA in the active site of MR when the X-ray crystal structure with BHA bound in the active site of MR becomes available.

CHAPTER 7

CONCLUSIONS

The remarkably high catalytic proficiency of MR prompted this investigation into the factors contributing to ground state, transition state and intermediate stabilization by MR. The intention of this study was to better describe *how* the enzyme discriminates between these species and preferentially binds the intermediate and transition states over the substrate. Since mandelic acid is a molecule with relatively few functional groups available for relatively localized interactions such as hydrogen–bonding and electrostatic interactions, it would seem that, in order for differential binding to occur, MR must take full advantage of relatively small structural and electronic changes in the substrate as it is enolized to the intermediate. It is clear that MR *must* stabilize the intermediate and transition states in order to achieve its large rate enhancement (Gerlt & Gassman, 1993a, b), but the exact mechanism by which it provides this stabilization is a matter of some debate (Guthrie & Kluger, 1993). This thesis has provided a thermodynamic description of catalysis by MR and has described the role of several binding determinants in ground state and transition state stabilization.

A novel HPLC assay for MR activity has been developed. This fixed–time assay involves the direct separation of underivatized enantiomers of mandelic acid on a chiral stationary phase. While this assay is more laborious and time–consuming than the CD assay, it is more sensitive than the existing CD and polarimetric assays. In addition, the HPLC assay allows the reaction kinetics to be followed in both the $R{\rightarrow}S$ and $S{\rightarrow}R$ directions, an inherent limitation of the coupled assay. The time–consuming nature of the HPLC assay has resulted in a preference for the CD assay for many of the routine kinetics

described in this thesis. However, the HPLC assay remains extremely useful in cases where high absorbance or a very slow rate of enzyme–catalyzed turnover prevent continuous assay on the CD spectrophotometer.

The temperature dependence of the MR catalyzed reaction has revealed the enthalpic and entropic contributions to the binding of substrate in the ground state, to the activation free energy for the chemical step, and to the free energy of transition state stabilization. It has also been shown that $K_m \approx K_s$ and that MR exhibits a partial viscosity dependence in both k_{cat} and k_{cat}/K_m, indicating that the physical steps to catalysis are partially rate–determining. The free energy of transition state stabilization is largely enthalpy–based (~23 kcal/mol at 25 °C) indicating that MR stabilizes the transition state by providing specific interactions with the altered substrate in the transition state.

Investigation of the molecular origins of these interactions required the identification of a high affinity, intermediate analogue inhibitor to act as a stable probe for the enzyme–transition state complex. Two competitive inhibitors, α-HBP and BHA, were bound by the enzyme with affinities 100-fold greater than that for the substrate, representing the most potent reversible inhibitors yet reported for MR. Both inhibitors were bound preferentially in the monoanion ionization state. The high affinity of α-HBP relative to several other phosphonate inhibitors revealed a preference for a hydrogen bond *donor* at the α-hydroxyl position of the intermediate analogues for effective binding. The electrostatic potential surfaces calculated for α-HBP and BHA are similar to that of the *aci*-carboxylate intermediate, providing a rationale for their high binding affinity. By comparing the binding of BHA (log K_i) to the reciprocal of the enzyme efficiency (log

K_m/k_{cat}), it was shown that BHA is a reasonable analogue of the transition state although it also exhibits a degree of ground state mimicry.

The contributions of several active site residues to both ground state and transition state stabilization by MR were investigated. Asn 197, a previously unrecognized residue within hydrogen–bonding distance to the substrate's α-hydroxyl group, provides +3.5 kcal/mol of free energy to stabilize the altered substrate in the transition state, the equivalent in energy to that of a typical hydrogen bond. Glu 317, the general acid catalyst, also contributes to the transition state stabilization free energy. The hydrogen bond from Glu 317 to the substrate provides $\geq$5 kcal/mol of free energy to stabilize the altered substrate in the transition state. Both Asn 197 and Glu 317 are required for effective binding of the transition state analogue, BHA. Lys 164 also makes a significant contribution to catalysis by MR although interpretation of the kinetics of the K164R mutant are complicated by the potential disruption of neighbouring residues. Assuming the pK_a of the general base catalyst is unperturbed by the K164R mutation, Lys 164 provides $\geq$4 kcal/mol to stabilize the altered substrate in the transition state. While the sum of these estimates fall well short of the estimated 26 kcal/mol of transition state stabilization afforded by MR, the conservative nature of the mutations described in this study make it likely that the values ascribed to Glu 317 and Lys 164 are substantially less than their total contribution to transition state stabilization. Additional stabilization of the intermediate and transition states originates from the hydrophobic cavity at the active site of the enzyme.

Interactions within the hydrophobic cavity of MR appear to selectively stabilize the altered substrate as it changes its hybridization state from sp^3 in the substrate to sp^2 in the

intermediate. Interactions with the intermediate's aromatic ring provide ≥4.6 kcal/mol to the stabilization of the planar intermediate. In addition, the surprisingly high affinity of MR for benzilate, a substrate/product analogue, has lead to a proposal for substrate motion through the hydrophobic cavity during catalysis. The aromatic ring of the substrate likely "swings" from one position in the cavity to the other as it is racemized. This mechanism might allow the planar intermediate to be preferentially stabilized, in part, by its location relative to an interacting enzyme residue (or residues) in the hydrophobic pocket.

With relatively few polar groups available on the substrate to provide strengthened interactions in the transition state, it might be argued that it is not possible for MR to provide an estimated 23 kcal/mol of enthalpic energy to stabilize the altered substrate in the transition state while providing only 9 kcal/mol of enthalpy to stabilize the substrate in the ground state (Bruice & Benkovic, 2000; Cannon *et al.*, 1996). However, the stabilizing interactions originating from within the hydrophobic cavity of MR offer an example of transition state stabilization that might often be overlooked upon preliminary inspection of available enzyme and substrate functional groups. The work in this thesis has led to the identification of *several* previously unrecognized binding determinants which contribute to preferential binding of the altered substrate in the transition state by MR. Thus MR, which serves as an excellent paradigm for enzymes that catalyze co-factor independent proton abstraction from carbon acids, has evolved to exquisitely match features of the altered substrate in the transition state.

CHAPTER 8

RECOMMENDATIONS FOR FUTURE WORK

Several approaches will help to further clarify issues which have been raised in this thesis. First, my studies implicate Lys 164 as an important residue in catalysis. It is unclear, however, whether this effect is related to the loss of transition state stabilization energy in the K164R mutant or whether it is due to other effects such as an altered Mg^{2+} binding constant or modified pK_a values of the general base catalysts relative to the wild–type enzyme. Clearly, the K164R mutant requires further study, particularly with regard to its pH–rate profile and its Mg^{2+} binding constant. A series of additional mutations at this position might further clarify the role of this residue in MR catalysis. In addition X-ray crystal structures of both wild–type and K164R co-crystallized with bound BHA would provide a more detailed perspective on how this intermediate analogue binds at the active site.

Given the proposal for dynamic motion of the substrate aromatic ring during catalysis, it would be of interest to impede ring motion of MR by "blocking" its swinging motion using bulky amino acid residues in the hydrophobic cavity. The contribution of the flexible hinged loop to catalysis might also be investigated using a MR mutant with a deletion in the loop region. Although I have constructed this mutant, its characterization awaits the development of an improved soluble protein expression system for MR.

What is the contribution to transition state stabilization by the essential magnesium ion? By analogy to site-directed mutagenesis experiments, the Mg^{2+} ion may be replaced by alternative divalent metal ions (i.e., Co^{2+}, Ni^{2+} and Mn^{2+}) and the effects on substrate binding, transition state stabilization and intermediate analogue binding could be

226

measured. It would be interesting to determine the extent to which both K_S and K_{Tx} correlate with the formation constants for the metal ion complexes.

A more accurate measure of the degree of transition state mimicry afforded by BHA (or α-HBP) with respect to each particular residue in the active site would be desirable. For example, a measure of the degree to which BHA mimics the interaction of the intermediate with Asn 197 is obtained by measuring k_{cat}/K_m and K_i for a series of mutants of Asn 197. A plot of the logarithms of these values against each other will give an indication of the degree to which this particular interaction mimics the interaction in the transition state and is more useful than a similar plot for mutations across a series of residues (Mader and Bartlett, 1997).

Are there additional residues that contribute directly to transition state stabilization in MR? The crystal structures of MR with bound ligands reveal some intriguing candidates, including Tyr 137 and Ser 139. As the number of fully sequenced genomes continues to grow, it is likely that genes encoding functional mandelate racemases will be discovered in a growing number of organisms. Indeed, putative MR genes have already been identified in *Solfolobus solfataricus* (Genbank A.N.: NC 2754), *Streptomyces coelicolor* A3(2) (Genbank A.N.: NC 3888) and *Mesorhizobium loti* (Genbank A.N.: NC 2678). Sequence alignments might provide a powerful tool to pinpoint additional conserved residues involved in MR catalysis.

One of the ultimate goals in studying catalysis by MR is to understand its mechanism so thoroughly as to allow its rational redesign to catalyze reactions with alternative substrates. For example, MR has recently been used to conduct dynamic kinetic resolutions (Strauss and Faber, 1999). A complete understanding of the role of

binding determinants in catalysis will aid attempts to re-engineer the substrate specificity

of MR for the preparation of compounds of pharmaceutical interest.

REFERENCES

Abraham, M. H., Grellier, P. L., Prior, D. V., Morris, J. J., and Taylor, P. J. (1990) Hydrogen bonding. Part 10. A scale of solute hydrogen-bond basicity using log K values for complexation in tetrachloromethane, *J. Chem. Soc. Perkin Trans. 2*, 521.

Abramov, V. S. (1950) Reaction of dialkyl phosphites with aldehydes and ketones (a new method of synthesis of esters of hydroxyalkanephosphonic acids), *Doklady Akad. Nauk. S.S.S.R. 73*.

Adams, J. A., and Taylor, S. S. (1992) Energetic limits of phosphotransfer in the catalytic subunit of cAMP- dependent protein kinase as measured by viscosity experiments, *Biochemistry 31*, 8516-8522.

Alagano, G., Ghio, C., and Kollman, P. A. (1997) Ab initio explorative survey of the mechanism catalyzed by mandelate racemase, *J. Mol. Struct. 390*, 217-223.

Alberty, R. A., and Hammes, G. G. (1958) Application of the theory of diffusion-controlled reactions to enzyme kinetics, *J. Am. Chem. Soc. 62*, 154-159.

Albery, W. J., and Knowles, J. R. (1976) Evolution of enzyme function and the development of catalytic efficiency, *Biochemistry 15*, 5631-5640.

Albery, W. J., and Knowles, J. R. (1977) Efficiency and Evolution in Enzyme Catalysis, *Angew. Chem. Int. Ed. Engl. 16*, 285-293.

Allard, S. T. M., Giraud, M.-F., and Naismith, J. H. (2001) Epimerases: structure, function and mechanism, *Cell. Mol. Life Sci. 58*, 1650-1665.

Amar, D., North, P., Miskiniene, V., Cenas, N., and Lederer, F. (2002) Hydroxamates as substrates and inhibitors for FMN-dependent 2-hydroxy acid dehydrogenases, *Bioorg. Chem. 30*, 145-162.

Anderson, P. M. (1983) CTP synthetase from *Escherichia coli*: an improved purification procedure and characterization of hysteretic and enzyme concentration effects on kinetic properties, *Biochemistry 22*, 3285-3292.

Anderson, V. E., Weiss, P. M., and Cleland, W. W. (1984) Reaction intermediate analogues for enolase, *Biochemistry 23*, 2779-2786.

Appleby, C. A., and Morton, R. K. (1959) Lactic dehydrogenase and cytochrome *b2* of baker's yeast, *Biochem J. 71*, 492-499.

Armstrong, D. W., Han, Y. I., and Han, S. M. (1988) Liquid chromatographic resolution of enantiomers containing single aromatic rings with β-cyclodextrin-bonded phases, *Anal. Chim. Acta 208*, 275-281.

Ash, E. L., Sudmeier, J. L., De Fabo, E. C., and Bachovchin, W. W. (1997) A low-barrier hydrogen bond in the catalytic triad of serine proteases? Theory versus experiment, *Science 278*, 1128-1132.

Babbitt, P. C., and Gerlt, J. A. (1997) Understanding enzyme superfamilies. Chemistry as the fundamental determinant in the evolution of new catalytic activities, *J. Biol. Chem. 272*, 30591-30594.

Babbitt, P. C., Hasson, M. S., Wedekind, J. E., Palmer, D. R., Barrett, W. C., Reed, G. H., Rayment, I., Ringe, D., Kenyon, G. L., and Gerlt, J. A. (1996) The enolase

superfamily: a general strategy for enzyme-catalyzed abstraction of the alpha-protons of carboxylic acids, *Biochemistry 35*, 16489-16501.

Babu, U. M., Johnston, R. B., and McNeef, L. C. (1975) A general NMR method for the assay of racemase activity with optically active or optically inactive substrates, *Anal. Biochem. 63*, 208-213.

Bagno, A., Comuzzi, C., and Scorrano, G. (1994) Site of ionization of hydroxamic acids probed by heteronucleur NMR relaxation rate and NOE measurements. An experimental and theoretical study, *J. Am. Chem. Soc. 116*, 916-924.

Banner, D. W., Bloomer, A. C., Petsko, G. A., Phillips, D. C., Pogson, C. I., and Wilson, I. A. (1975) Structure of chicken muscle triose phosphate isomerase determined crystallographically at 2.5 angstrom resolution using amino acid sequence data, *Nature 255*, 609-614.

Bartlett, P. A., and Marlowe, C. K. (1987) Possible role for water dissociation in the slow binding of phosphorus-containing transition-state-analogue inhibitors of thermolysin, *Biochemistry 26*, 8553-8561.

Bazelyansky, M., Robey, E., and Kirsch, J. F. (1986) Fractional diffusion-limited component of reactions catalyzed by acetylcholinesterase, *Biochemistry 25*, 125-130.

Bearne, S. L., and Kluger, R. (1992) Phosphoenol acetylphosphonates: substrate analogs as inhibitors of phosphoenolpyruvate enzymes, *Bioorg. Chem. 20*, 135-147.

Bearne, S. L., St. Maurice, M., and Vaughan, M. D. (1999) An assay for mandelate racemase using high-performance liquid chromatography, *Anal. Biochem. 269*, 332-336.

Bearne, S. L., and Wolfenden, R. (1995) Enzymatic Hydration of an Olefin: The Burden Borne by Fumarase, *J. Am. Chem. Soc. 117*, 9588-9589.

Bearne, S. L., and Wolfenden, R. (1997) Mandelate racemase in pieces: effective concentrations of enzyme functional groups in the transition state, *Biochemistry 36*, 1646-1656.

Berndt, D. C., and Shechter, H. (1964) Substituent effects in the lossen rearrangement of benzoyl acylhydroxamates, *J. Org. Chem. 29*, 916-918.

Blackburn, G. M., and Kent, D. E. (1986) Synthesis of α- and γ-fluoroalkylphosphonates, *J. Chem. Soc. Perkin Trans. 1*, 913-917.

Blacklow, S. C., Raines, R. T., Lim, W. A., Zamore, P. D., and Knowles, J. R. (1988) Triosephosphate isomerase catalysis is diffusion controlled. Appendix: Analysis of triose phosphate equilibria in aqueous solution by 31P NMR, *Biochemistry 27*, 1158-1167.

Bohm, G., Muhr, R., and Jaenicke, R. (1992) Quantitative analysis of protein far UV circular dichroism spectra by neural networks, *Protein Eng. 5*, 191-195.

Bojarski, A. J., and Mokrosz, M. J. (1999) 1,2,3,4-Tetrahydroisoquinoline derivatives; lipophilicity evaluation vs. 5-HT$_{1A}$ receptor affinity, *Pharmazie 54*, 828-830.

Bordwell, F. G. (1988) Equilibrium acidities in dimethyl sulfoxide solution, *Acc. Chem. Res. 21*, 456-463.

Breslow, E., Mombouyran, V., Deeb, R., Zheng, C., Rose, J. P., Wang, B.-C., and Haschemeyer, R. H. (1999) Structural basis of neurophysin hormone specificity: geometry, polarity and polarizability in aromatic ring interactions, *Protein Sci. 8*, 820-831.

Britt, B. M. (1993) A shifting specificity model for enzyme catalysis, *J. Theor. Biol. 164*, 181-190.

Brouwer, A. C., and Kirsch, J. F. (1982) Investigation of diffusion-limited rates of chymotrypsin reactions by viscosity variation, *Biochemistry 21*, 1302-1307.

Bruice, T. C., and Benkovic, S. J. (2000) Chemical basis for enzyme catalysis, *Biochemistry 39*, 6267-6274.

Bruice, T. C., and Lightsone, F. C. (1999) Ground state and transition state contributions to the rates of intramolecular and enzyme catalyzed reactions, *Acc. Chem. Res. 32*, 127-136.

Bubnik, Z., Kadlec, P., Urban, D., and Bruhns, M. (1995) in *Sugar Technologists Manual: Chemical and Physical Data for Sugar Manufacturers and Users* pp 164, Bartens, Berlin.

Burbaum, J. J., Raines, R. T., Albery, W. J., and Knowles, J. R. (1989) Evolutionary optimization of the catalytic effectiveness of an enzyme, *Biochemistry 28*, 9293-9305.

Burkhard, P., Taylor, P., and Walkinshaw, M. D. (2000) X-ray structures of small ligand-FKBP complexes provide an estimate for hydrophobic interaction energies, *J. Mol. Biol. 295*, 953-962.

Burley, S. K., and Petsko, G. A. (1988) Weakly polar interactions in proteins, *Adv. Protein Chem. 39*, 125-189.

Byers, L. D. (1978) Binding of reactive intermediate analogs to enzymes, *J. Theor. Biol. 74*, 501-512.

Caldwell, S. R., Newcomb, J. R., Schlecht, K. A., and Raushel, F. M. (1991) Limits of diffusion in the hydrolysis of substrates by the phosphotriesterase from Pseudomonas diminuta, *Biochemistry 30*, 7438-7444.

Campbell, R. E., Mosimann, S. C., Tanner, M. E., and Strynadka, N. C. J. (2000) The structure of UDP-*N*-acetylglucosamine 2-epimerase reveals homology to phosphoglycosyl transferases, *Biochemistry 39*, 14993-15001.

Cannon, W. R., Singleton, S. F., and Benkovic, S. J. (1996) A perspective on biological catalysis, *Nat. Struct. Biol. 3*, 821-833.

Carlow, D., and Wolfenden, R. (1998) Substrate connectivity effects in the transition state for cytidine deaminase, *Biochemistry 37*, 11873-11878.

Che, T. M., and Kustin, K. (1981) Complexation kinetics and equilibria of nickel(II) with vanillomandelic, mandelic and thiolactic acid ligands, *Inorg. Chem. 20*, 509-513.

Chiang, Y., and Kresge, A. J. (1991) Enols and other reactive species, *Science 253*, 395-400.

Chiang, Y., Kresge, A. J., Popik, V. V., and Schepp, N. P. (1997) The mandelic acid keto-enol system in aqueous solution. Generation of the enol by hydration of phenylhydroxyketene and phenylcarboxycarbene, *J. Am. Chem. Soc. 119*, 10203-10212.

Chiang, Y., Kresge, A. J., Pruszynski, P., Schepp, N. P., and Wirz, J. (1990) The enol of mandelic acid, detection, acidity in aqueous solution, and estimation of the keto-enol equilibrium constant and carbon acidity of mandelic acid, *Angew. Chem. Int. Ed. Engl. 29*, 792-794.

Chothia, C., and Janin, J. (1975) Principles of protein-protein recognition, *Nature 256*, 705-708.

Christensen, H., Martin, M. T., and Waley, S. G. (1990) Beta-lactamases as fully efficient enzymes. Determination of all the rate constants in the acyl-enzyme mechanism, *Biochem. J. 266*, 853-861.

Cleland, W. W. (2000) Low-barrier hydrogen bonds and enzymatic catalysis, *Arch. Biochem. Biophys. 382*, 1-5.

Cleland, W. W., and Kreevoy, M. M. (1994) Low-barrier hydrogen bonds and enzymic catalysis, *Science 264*, 1887-1890.

Codreanu, S. G., Ladner, J. E., Xiao, G., Stourman, N. V., Hachey, D. L., Gilliland, G. L., and Armstrong, R. N. (2002) Local protein dynamics and catalysis: detection of segmental motion associated with rate-limiting product release by a glutathione transferase, *Biochemistry 41*, 15161-15172.

Compere Jr., E. L. (1968) Synthesis of α-hydroxyarylacetic acids from bromoform, arylaldehydes, and potassium hydroxide, with lithium chloride catalyst, *J. Org. Chem. 33*, 2565-2566.

Dale, M. P., Kopfler, W. P., Chait, I., and Byers, L. D. (1986) Beta-glucosidase: substrate, solvent, and viscosity variation as probes of the rate-limiting steps, *Biochemistry 25*, 2522-2529.

Derreumaux, P., and Schlick, T. (1998) The loop opening/closing motion of the enzyme triosephosphate isomerase, *Biophys J 74*, 72-81.

Deupree, J. D., and Wood, W. A. (1972) L-Ribulose 5-phosphate 4-epimerase from *Aerobacter aerogenes*, *J. Biol. Chem. 247*, 3093-3097.

Dixon, H., and Webb, E. C. (1964) *Enzymes*, 2 ed., Academic Press.

Dougherty, D. A. (1996) Cation-π interactions in chemistry and biology: a new view of Benzene, Phe, Tyr, and Trp, *Science 271*, 163-168.

Drummond, L., Caldwell, J., and Wilson, H. K. (1989) The metabolism of ethylbenzene and styrene to mandelic acid: stereochemical considerations, *Xenobiotica 19*, 199-207.

El Gihani, M. T., and Williams, J. M. (1999) Dynamic kinetic resolution, *Curr. Opin. Chem. Biol. 3*, 11-15.

Esposito, A., Lukas, A., Meany, J. E., and Pocker, Y. (1999) The reversible enolization and hydration of pyruvate: possible roles of keto, enol, and hydrated pyruvate in lactate dehydrogenase catalysis, *Can. J. Chem. 77*, 1108-1117.

Exner, O., Hradil, M., and Mollin, J. (1993) Dissociation constants of hydroxamic acids: solvent effects, *Collect. Czech. Chem. Commun. 58*, 1109-1121.

Falzone, C. J., Wright, P. E., and Benkovic, S. J. (1994) Dynamics of a flexible loop in dihydrofolate reductase from Escherichia coli and its implication for catalysis, *Biochemistry 33*, 439-442.

Farkas, E., Enyedy, E. A., and Csoka, H. (2000) Some factors affecting metal ion-monohydroxamate interactions in aqueous solution, *J. Inorg. Biochem. 79*, 205-211.

Fastrez, J., and Fersht, A. R. (1973) Mechanism of chymotrypsin. Structure, reactivity, and nonproductive binding relationships, *Biochemistry 12*, 1067-1074.

Fee, J. A., Hegeman, G. D., and Kenyon, G. L. (1974a) Mandelate racemase from Pseudomonas putida. Affinity labeling of the enzyme by D,L-alpha-phenylglycidate in the presence of magnesium ion, *Biochemistry 13*, 2533-2538.

Fee, J. A., Hegeman, G. D., and Kenyon, G. L. (1974b) Mandelate racemase from Pseudomonas putida. Subunit composition and absolute divalent metal ion requirement, Biochemistry 13, 2528-2532.

Felfer, U., Strauss, U. T., Kroutil, W., Fabian, W. M. F., and Faber, K. (2001) Substrate spectrum of mandelate racemase: Part 2. (Hetero)-aryl-substituted mandelate derivatives and modulation of activity, J. Mol. Catal. B: Enzym. 15, 213-222.

Fersht, A. (1985) Enzyme structure and mechanism, 2 ed., W.H. Freeman and Company, New York.

Fersht, A. (1999) in Structure and mechanism in protein science pp 169-182, 329-331, and 428-438, Freeman, New York.

Fishbein, W. N., Daly, J., and Streeter, C. L. (1969) Preparation and some properties of stable and carbon-14 and tritium-labeled short-chain aliphatic hydroxamic acids, Anal. Biochem. 28, 13-24.

Fisher, L. M., Albery, W. J., and Knowles, J. R. (1986) Energetics of proline racemase: racemization of unlabeled proline in the unsaturated, saturated, and oversaturated regimes, Biochemistry 25, 2529-2537.

Flint, D. H. (1994) Initial kinetic and mechanistic characterization of Escherichia coli fumarase A, Arch. Biochem. Biophys. 311, 509-516.

Freeman, S., Irwin, W. J., and Schwalbe, C. H. (1991) Synthesis and hydrolysis studies of phosphonopyruvate, J. Chem. Soc. Perkin Trans. 2, 263-267.

Frey, P. A. (1996) The Leloir pathway: a mechanistic imperative for three enzymes to change the stereochemical configuration of a single carbon in galactose, FASEB J. 10, 461-470.

Frey, P. A., Whitt, S. A., and Tobin, J. B. (1994) A low-barrier hydrogen bond in the catalytic triad of serine proteases, Science 264, 1927-1930.

Frick, L., Yang, C., Marquez, V. E., and Wolfenden, R. (1989) Binding of pyrimidin-2-one ribonucleoside by cytidine deaminase as the transition-state analogue 3,4-dihydrouridine and the contribution of the 4-hydroxyl group to its binding affinity, Biochemistry 28, 9423-9430.

Frieden, C., Kurz, L. C., and Gilbert, H. R. (1980) Adenosine deaminase and adenylate deaminase: comparative kinetic studies with transition state and ground state analogue inhibitors, Biochemistry 19, 5303-5309.

Gallo, K. A., Tanner, M. A., and Knowles, J. R. (1993) Mechanism of the reaction catalyzed by glutamate racemase, Biochemistry 32, 3991-3997.

Garcia-Viloca, M., Gonzalez-Lafont, A., and Lluch, J. M. (2001) A QM/MM study of the racemization of vinylglycolate catalyzed by mandelate racemase enzyme, J. Am. Chem. Soc. 123, 709-721.

Genet, R., and Lederer, F. (1990) The carbanion of nitroethane is an inhibitor of, and not a substrate for, flavocytochrome 1.2 [L-(+)-lactate dehydrogenase], Biochem. J. 266, 301-304.

Gerlt, J. A. (1994) "Understanding the mechanism and rates of enzyme-catalyzed proton transfer reactions to and from carbon" in Bioorganic chemistry: peptides and proteins (S. M. Hecht, Ed.) pp 279-311, Oxford University Press, New York.

Gerlt, J. A., and Babbitt, P. C. (1998) Mechanistically diverse enzyme superfamilies: the importance of chemistry in the evolution of catalysis, Curr. Opin. Chem. Biol. 2, 607-612.

Gerlt, J. A., and Gassman, P. G. (1992) Understanding enzyme-catalyzed proton abstraction from carbon acids: details of stepwise mechanisms for β-elimination reactions, *J. Am. Chem. Soc. 114*, 5928-5934.

Gerlt, J. A., and Gassman, P. G. (1993a) An explanation for rapid enzyme-catalyzed proton abstraction from carbon acids: importance of late transition states in concerted mechanisms, *J. Am. Chem. Soc. 115*, 11552-11568.

Gerlt, J. A., and Gassman, P. G. (1993b) Understanding the rates of certain enzyme-catalyzed reactions: proton abstraction from carbon acids, acyl-transfer reactions, and displacement reactions of phosphodiesters, *Biochemistry 32*, 11943-11952.

Gerlt, J. A., Kozarich, J. W., Kenyon, G. L., and Gassman, P. G. (1991) Electrophilic catalysis can explain the unexpected acidity of carbon acids in enzyme-catalyzed reactions, *J. Am. Chem. Soc. 113*, 9667-9669.

Glavas, S., and Tanner, M. A. (2001) Active site residues of glutamate racemase, *Biochemistry 40*, 6199-6204.

Goldberg, J. M., and Kirsch, J. F. (1996) The reaction catalyzed by *Escherichia coli* aspartate aminotransferase has multiple partially rate-determining steps, while that catalyzed by the Y225F mutant is dominated by ketimine hydrolysis, *Biochemistry 35*, 5280-5291.

Gopalan, V., Daniels, L. B., Glew, R. H., and Claeyssens, M. (1989) Kinetic analysis of the interaction of alkyl glycosides with two human β-glucosidases, *Biochem. J. 262*, 541-548.

Gulick, A. M., Hubbard, B. K., Gerlt, J. A., and Rayment, I. (2000) Evolution of enzymatic activities in the enolase superfamily: crystallographic and mutagenesis studies of the reaction catalyzed by D-glucarate dehydratase from *Escherichia coli*, *Biochemistry 39*, 4590-4602.

Gulotta, M., Deng, H., Deng, H., Dyer, R. B., and Callender, R. H. (2002) Toward an understanding of the role of dynamics on enzymatic catalysis in lactate dehydrogenase, *Biochemistry 41*, 3353-3363.

Gunsalus, C. F., Stanier, R. Y., and Gunsalus, I. C. (1953a) The enzymatic conversion of mandelic acid to benzoic acid III. Fractionation and properties of the soluble enzymes, *J. Bacteriol. 66*, 548-553.

Gunsalus, I. C., Gunsalus, C. F., and Stanier, R. Y. (1953b) The enzymatic conversion of mandelic acid to benzoic acid I. Gross fractionation of the system into soluble and particulate components, *J. Bacteriol. 66*, 538-542.

Guthrie, J. P. (1996) Short strong hydrogen bonds: can they explain enzymic catalysis?, *Chem. Biol. 3*, 163-170.

Guthrie, J. P., and Kluger, R. (1993) Electrostatic stabilization can explain the unexpected acidity of carbon acids in enzyme-catalyzed reactions, *J. Am. Chem. Soc. 1993*, 11569-11572.

Hale, S. P., Poole, L. B., and Gerlt, J. A. (1993) Mechanism of the reaction catalyzed by staphylococcal nuclease: identification of the rate-determining step, *Biochemistry 32*, 7479-7487.

Hammond, G. S. (1955) A correlation of reaction rates, *J. Am. Chem. Soc. 77*, 334-338.

Hansch, C., and Leo, A. (1979) *Substituent Constants for Correlation Analysis in Chemistry and Biology*, Wiley, New York.

Hardy, L. W., and Kirsch, J. F. (1984) Diffusion-limited component of reactions catalyzed by *Bacillus cereus* beta-lactamase I, *Biochemistry 23*, 1275-1282.

Harris, T. K., Abeygunawardana, C., and Mildvan, A. S. (1997) NMR studies of the role of hydrogen bonding in the mechanism of triose phosphate isomerase, *Biochemistry 36*, 14661-14675.

Hasinoff, B. B. (1984) Kinetics of carbonic anhydrase catalysis in solvents of increased viscosity: a partially diffusion-controlled reaction, *Arch Biochem Biophys 233*, 676-681.

Hayward, S. (1999) Structural principles governing domain motions in proteins, *Proteins 36*, 425-435.

Hegeman, G. D. (1966a) Synthesis of the enzymes in the mandelate pathway by *Pseudomonas putida* I. Synthesis of enzymes by the wild type, *J. Bacteriol. 91*, 1140-1154.

Hegeman, G. D. (1966b) Synthesis of the enzymes in the mandelate pathway by *Pseudomonas putida* II. Isolation and properties of blocked mutants, *J. Bacteriol. 91*, 1155-1160.

Hegeman, G. D. (1966c) Synthesis of the enzymes in the mandelate pathway by *Pseudomonas putida* III. Isolation and properties of constitutive mutants, *J. Bacteriol. 91*, 1161-1167.

Hegeman, G. D. (1970) Mandelate racemase (*Pseudomonas putida*), *Methods Enzymol. 17*, 670-674.

Hegeman, G. D., Rosenberg, E. Y., and Kenyon, G. L. (1970) Mandelic acid racemase from *Pseudomonas putida*. Purification and properties of the enzyme, *Biochemistry 9*, 4029-4036.

Henriksen, A., Schuller, D. J., Meno, K., Welinder, K. G., Smith, A. T., and Gajhede, M. (1998) Structural interactions between horseradish peroxidase c and the substrate benzhydroxamic acid determined by X-ray crystallography, *Biochemistry 37*, 8054-8060.

Hiratake, J., Irie, T., Tokutake, N., and Oda, J. (2002) Recognition of a cysteine substrate by *E. coli* γ-glutamylcysteine synthetase probed by sulfoximine-based transition-state analogue inhibitors, *Biosci. Biotechnol. Biochem. 66*, 1500-1514.

Hoffmann, M. (1985) Diphenylmethyl as a phosphorous protecting group in the synthesis of P-terminal phosphonodidepsipeptides, *Pol. J. Chem. 59*, 395-404.

Hoffmann, M. (1988) A simple, efficient synthesis of dibenzyl and bis(p-nitrobenzyl) 1-hydroxyalkanephosphonates, *Synthesis*, 62-64.

Hoggett, J. G., and Kellett, G. L. (1976) Yeast hexokinase. A fluorescence temperature-jump study of the kinetics of the binding of glucose to the monomer forms of hexokinases P-I and P- II, *Eur J Biochem 68*, 347-353.

Horenstein, B. A., Parkin, D. W., Estupinan, B., and Schramm, V. L. (1991) Transition-state analysis of nucleoside hydrolase from *Crithidia fasciculata*, *Biochemistry 30*, 10788-10795.

Horenstein, B. A., and Schramm, V. L. (1993a) Correlation of the molecular electrostatic potential surface of an enzymatic transition state with novel transition-state inhibitors, *Biochemistry 32*, 9917-9925.

Horenstein, B. A., and Schramm, V. L. (1993b) Electronic nature of the transition state for nucleoside hydrolase. A blueprint for inhibitor design, *Biochemistry 32*, 7089-7097.

Howe, R., Moore, R. H., and Rao, B. S. (1973) Beta-adrenergic blocking agents. 14. Microbiological reduction of isopropylaminomethyl 2-naphthyl ketone to (R)-(−)-2-isopropylamino-1-(2-naphthyl)ethanol and related reductions, *J. Med. Chem. 16*, 1020.

Ibba, M., Kast, P., and Hennecke, H. (1994) Substrate specificity is determined by amino acid binding pocket size in *Escherichia coli* phenylalanyl-tRNA synthetase, *Biochemistry 33*, 7107-7112.

Jencks, W. P. (1966) in *Current aspects of biochemical energetics* (N. O. Kaplan, and E. P. Kennedy, Eds.) pp 273, Academic Press, New York.

Jencks, W. P. (1975) Binding energy, specificity and catalysis - the Circe effect, *Adv. Enzymol. Relat. Areas Mol. Biol. 43*, 219-410.

Jencks, W. P. (1987) in *Catalysis in Chemistry and Enzymology* pp 243-281, Dover Publications, Inc., New York.

Jencks, W. P., and Regenstein, J. (1968) "Ionization Constants of Acids and Bases" in *Handbook of Biochemistry* (H. A. Sober, Ed.) pp J150-J189, The Chemical Rubber Co., Cleveland, OH.

Johnson, J. E., Ghafouripour, A., Haug, Y. K., Cordes, A. W., Pennington, W. T., and Exner, O. (1985) Synthesis and configurations of *O*-substituted hydroximoyl chlorides. Stereochemistry and mechanism of alkoxide ion substitution at the carbon-nitrogen double bond, *J. Org. Chem. 50*, 993-997.

Johnson, J. E., and Tanner, M. E. (1998) Epimerization via carbon-carbon bond cleavage. L-Ribulose 5-phosphate 4-epimerase as a masked class II aldolase, *Biochemistry 37*, 5746-5754.

Johnston, H. S. (1966) *Gas phase reaction rate theory*, Ronald, New York.

Juszczak, L. J., Zhang, Z. Y., Wu, L., Gottfried, D. S., and Eads, D. D. (1997) Rapid loop dynamics of *Yersinia* protein tyrosine phosphatases, *Biochemistry 36*, 2227-2236.

Kallarakal, A. T., Mitra, B., Kozarich, J. W., Gerlt, J. A., Clifton, J. G., Petsko, G. A., and Kenyon, G. L. (1995) Mechanism of the reaction catalyzed by mandelate racemase: structure and mechanistic properties of the K166R mutant, *Biochemistry 34*, 2788-2797.

Kati, W. M., Acheson, S. A., and Wolfenden, R. (1992) A transition state in pieces: major contributions of entropic effects to ligand binding by adenosine deaminase, *Biochemistry 31*, 7356-7366.

Kati, W. M., and Wolfenden, R. (1989) Contribution of a single hydroxyl group to transition-state discrimination by adenosine deaminase: evidence for an "entropy trap" mechanism, *Biochemistry 28*, 7919-7927.

Kato, Y., Toledo, L. M., and Rebek Jr., J. (1996) Energetics of a low barrier hydrogen bond in nonpolar solvents, *J. Am. Chem. Soc. 118*, 8575-8579.

Kenyon, G. L., Gerlt, J. A., Petsko, G. A., and Kozarich, J. W. (1995) Mandelate Racemase: Structure-Function Studies of a Pseudosymmetric Enzyme, *Acc. Chem. Res. 28*, 178-186.

Kenyon, G. L., and Hegeman, G. D. (1970) Mandelic acid racemase from *Pseudomonas putida*. Evidence favoring a carbanion intermediate in the mechanism of action, *Biochemistry 9*, 4036-4043.

Kenyon, G. L., and Hegeman, G. D. (1979) Mandelate racemase, *Adv. Enzymol. Relat. Areas Mol. Biol. 50*, 325-360.

Kinbara, K., Harada, Y., and Saigo, K. (2000) A high-performance, tailor-made resolving agent: remarkable enhancement of resolution ability by introducing a naphthyl group into the fundamental skeleton, *J. Chem. Soc., Perkin Trans. 2*, 1339-1347.

Kluger, R., and Chin, J. (1978) Rates of formation and decomposition of tetrahedral intermediates in the hydrolysis of dimethyl aroylphosphonates. Substituent effects on a model for carboxylate ester hydrolysis., *J. Am. Chem. Soc. 100*, 7382-7388.

Kluger, R., Nakaoka, K., and Tsui, W.-C. (1978) Substrate analog studies of the specificity and catalytic mechanism of D-3-hydroxybutyrate dehydrogenase, *J. Am. Chem. Soc. 100*, 7388-7391.

Kolthoff, I. M., and Stenger, V. A. (1942) in *Volumetric Analysis. I: Theoretical Fundamentals* pp 65, Interscience, New York.

Kotoris, C., Wen, W., Lough, A., and Taylor, S. D. (2000) Preparation of chiral α-monofluoroalkylphosphonic acids and their evaluation as inhibitors of protein tyrosine phosphatase 1B, *J. Chem. Soc. Perkin Trans. 1*, 1271-1281.

Kraut, J. (1988) How do enzymes work?, *Science 242*, 533-540.

Kresge, A. J. (1991) Generation and study of enols and other reactive species, *Pure Appl. Chem 63*, 213-221.

Kubala, G., and Martell, A. E. (1982) Proton association and metal stability constants of 2-oxalopropionic, α-ketobutyric and acetoacetic acids., *Inorg. Chem. 21*, 3007-3013.

Kurz, J. L. (1963) Transition state characterization for catalyzed reactions, *J. Am. Chem. Soc. 85*, 987-991.

Kurz, L. C., Weitkamp, E., and Frieden, C. (1987) Adenosine deaminase: viscosity studies and the mechanism of binding of substrate and of ground- and transition-state analogue inhibitors, *Biochemistry 26*, 3027-3032.

Laidler, K. J., and Peterman, B. F. (1979) Temperature effects in enzyme kinetics, *Methods Enzymol. 63*, 234-257.

Landro, J. A., Gerlt, J. A., Kozarich, J. W., Koo, C. W., Shah, V. J., Kenyon, G. L., Neidhart, D. J., Fujita, S., and Petsko, G. A. (1994) The role of lysine 166 in the mechanism of mandelate racemase from *Pseudomonas putida*: mechanistic and crystallographic evidence for stereospecific alkylation by (*R*)-α-phenylglycidate, *Biochemistry 33*, 635-643.

Landro, J. A., Kallarakal, A. T., Ransom, S. C., Gerlt, J. A., Kozarich, J. W., Neidhart, D. J., and Kenyon, G. L. (1991) Mechanism of the reaction catalyzed by mandelate racemase. 3. Asymmetry in reactions catalyzed by the H297N mutant, *Biochemistry 30*, 9274-9281.

Landro, J. A., Kenyon, G. L., and Kozarich, J. W. (1992) Mechanism-based inactivation of mandelate racemase by propargylglycolate, *Bioorg. Med. Chem. Lett. 2*, 1411-1418.

Larsen, K., Sjoberg, B.-M., and Thelander, L. (1982) Characterization of the active site of ribonucleotide reductase of *Escherichia coli*, bacteriophage T4 and mammalian

cells by inhibition studies with hydroxyurea analogues, *Eur. J. Biochem. 125*, 75-81.

Lee, L. V., Vu, M. V., and Cleland, W. W. (2000) ^{13}C and deuterium isotope effects suggest an aldol cleavage mechanism for L-ribulose-5-phosphate 4-epimerase, *Biochemistry 39*, 4808-4820.

Leo, A., Hansch, C., and Elkins, D. (1971) Partition coefficients and their uses, *Chem. Rev. 71*, 525-616.

Leo, A., Jow, P. Y. C., Silipo, C., and Hansch, C. (1975) Calculation of hydrophobic constant (log P) from π and *f* constants, *J. Med. Chem. 18*, 865-868.

Li, R., Powers, V. M., Kozarich, J. W., and Kenyon, G. L. (1995) Racemization of vinylglycolate catalyzed by mandelate racemase, *J. Org. Chem. 60*, 3347-3351.

Li, S., and Purdy, W. C. (1992) Direct separation of enantiomers using multiple-interaction chiral stationary phases based on the modified β-cyclodextrin-bonded stationary phase, *J. Chromatogr. 625*, 109-120.

Li, Y., Feng, L., and Kirsch, J. F. (1997) Kinetic and spectroscopic investigations of wild-type and mutant forms of apple 1-aminocyclopropane-1-carboxylate synthase, *Biochemistry 36*, 15477-15488.

Lienhard, G. E. (1973) Enzymatic catalysis and transition-state theory, *Science 180*, 149-154.

Lightsone, F. C., and Bruice, T. C. (1996) Ground state conformations and entropic and enthalpic factors in the efficiency of intramolecular reactions. 1. Cyclic anhydride formation by substituted glutarates, succinate and 3,6-endoxo-Δ^4-tetrahydrophthalate monophenyl esters, *J. Am. Chem. Soc. 118*, 2595-2605.

Lin, D. T., Powers, V. M., Reynolds, L. J., Whitman, C. P., Kozarich, J. W., and Kenyon, G. L. (1988) Evidence for the generation of α-carboxy-α-hydroxy-*p*-xylylene from *p*-(bromomethyl)mandelate by mandelate racemase, *J. Am. Chem. Soc. 110*, 323-324.

Loh, S. N., and Markley, J. L. (1994) Hydrogen bonding in proteins as studied by amide hydrogen D/H fractionation factors: Application to staphylococcal nuclease, *Biochemistry 33*, 1029-1036.

Mader, M. M., and Bartlett, P. A. (1997) Binding energy and catalysis: the implications for transition-state analogs and catalytic antibodies, *Chem. Rev. 97*, 1281-1301.

Maggio, E. T., Kenyon, G. L., Mildvan, A. S., and Hegeman, G. D. (1975) Mandelate racemase from *Pseudomonas putida*. Magnetic resonance and kinetic studies of the mechanism of catalysis, *Biochemistry 14*, 1131-1139.

Manchester, K. L. (1980) Determination of magnesium and potassium binding constants to phosphoenolpyruvate, 2- and 3-phosphoglycerate and a number of other anions, *Biochim. Biophys. Acta 630*, 225-231.

Martin, D. J., and Griffin, C. E. (1965) Determination of polar substituent constants for the dialkoxy- and diarylphosphono and trialkyl- and triaryl-phosphonium groups, *J. Org. Chem. 30*, 4034-4038.

Mattei, P., Kast, P., and Hilvert, D. (1999) *Bacillus subtilis* chorismate mutase is partially diffusion-controlled, *Eur. J. Biochem. 261*, 25-32.

McEwen, W. K. (1936) A further study of extremely weak acids, *J. Am. Chem. Soc. 58*, 1124-1129.

Menger, F. M. (1992) Analysis of ground state and transition state effects in enzyme catalysis, *Biochemistry 31*, 5368-5373.

Miller, B., Snider, M. J., Short, S. A., and Wolfenden, R. (2000) Contribution of enzyme-phosphoribosyl contacts to catalysis by orotidine 5'-phosphate decarboxylase, *Biochemistry 39*, 8113-8118.

Miller, B. G., Traut, T. W., and Wolfenden, R. (1998) Effects of substrate binding determinants in the transition state for ortodine 5'-monophosphate decarboxylase, *Bioorg. Chem. 26*, 283-288.

Mitra, B., Kallarakal, A. T., Kozarich, J. W., Gerlt, J. A., Clifton, J. G., Petsko, G. A., and Kenyon, G. L. (1995) Mechanism of the reaction catalyzed by mandelate racemase: importance of electrophilic catalysis by glutamic acid 317, *Biochemistry 34*, 2777-2787.

Morrison, J. F., and Walsh, C. T. (1988) The behavior and significanceof slow-binding enzyme inhibitors, *Adv. Enzymol. Relat. Areas Mol. Biol. 61*, 201-301.

Mosi, R., Sham, H., Uitdehaag, J. C. M., Ruiterkamp, R., Dijkstra, B. W., and Withers, S. G. (1998) Reassessment of acarbose as a transition state analogue inhibitor of cyclodextrin glycosyltransferase, *Biochemistry 37*, 17192-17198.

Murphy, D. J. (1995) Revisiting ground-state and transition-state effects, the split-site model, and the "fundamentalist position" of enzyme catalysis, *Biochemistry 34*, 4507-4510.

Nagarajan, K., Rajappa, S., Rajagopalan, P., and Talwalkar, P. K. (1991) Hydroxamic acid derivatives with potential antiinflammatory activity, *Ind. J. Chem. 30B*, 222-229.

Neidhart, D. J., Howell, P. L., Petsko, G. A., Powers, V. M., Li, R. S., Kenyon, G. L., and Gerlt, J. A. (1991) Mechanism of the reaction catalyzed by mandelate racemase. 2. Crystal structure of mandelate racemase at 2.5-Å resolution: identification of the active site and possible catalytic residues, *Biochemistry 30*, 9264-9273.

Neidhart, D. J., Powers, V. M., Kenyon, G. L., Tsou, A. Y., Ransom, S. C., Gerlt, J. A., and Petsko, G. A. (1988) Preliminary X-ray data on crystals of mandelate racemase, *J. Biol. Chem. 263*, 9268-9270.

Newman, P. (1981) in *Optical resolution procedures for chemical compounds* pp 299-300, Optical Resolution Information Center, Riverdale, N.Y.

Northrop, D. B. (1975) Steady-state analysis of kinetic isotope effects in enzymic reactions, *Biochemistry 14*, 2644-2651.

Novagen (1995) *pET System Manual*, 6 ed.

O'Brien, T. A., Kluger, R., Pike, D. C., and Gennis, R. B. (1980) Phosphonate analogs of pyruvate. Probes of substrate binding to pyruvate oxidase and other thiamin pyrophosphate-dependent decarboxylases, *Biochim. Biophys. Acta 613*, 10-17.

Oefner, C., D'Arcy, A., and Winkler, F. K. (1988) Crystal structure of human dihydrofolate reductase complexed with folate, *Eur. J. Biochem. 174*, 377-385.

Ornston, L. N., and Stanier, R. Y. (1966) The conversion of catechol and protocatechuate to beta-ketoadipate by *Pseudomonas putida*, *J. Biol. Chem. 241*, 3776-3786.

Osborne, M. J., Schnell, J., Benkovic, S. J., Dyson, H. J., and Wright, P. E. (2001) Backbone dynamics in dihydrofolate reductase complexes: role of loop flexibility in the catalytic mechanism, *Biochemistry 40*, 9846-9859.

Page, M. I., and Jencks, W. P. (1971) Entropic contributions to rate accelerations in enzymic and intramolecular reactions and the chelate effect, *Proc. Natl. Acad. Sci., USA 68*, 1678-1683.

Pauling, L. (1948) Chemical achievement and hope for the future, *Am. Sci. 36*, 50-58.

Perham, R. N. (2000) Swinging arms and swinging domains in multifunctional enzymes: catalytic machines for multistep reactions, *Annu. Rev. Biochem. 69*, 961-1004.

Perrin, C. L., and Nielsen, J. B. (1997) "Strong" hydrogen bonds, *Annu. Rev. Phys. Chem. 48*, 511-544.

Pirrung, M. C., and Chau, J. H.-L. (1995) A convenient procedure for the preparation of amino acid hydroxamates from esters, *J. Org. Chem. 60*, 8084-8085.

Pocker, Y., and Janjic, N. (1987) Enzyme kinetics in solvents of increased viscosity. Dynamic aspects of carbonic anhydrase catalysis, *Biochemistry 26*, 2597-2606.

Polanyi, M. (1921) *Z. Elektrochem. 27*, 143-150.

Porter, D. J. T., and Bright, H. J. (1980) 3-Carbanionic substrate analogues bind very tightly to fumarase and aspartase, *J. Biol. Chem. 255*, 4772-4780.

Porter, D. J. T., Rudie, N. G., and Bright, H. J. (1983) Nitro analogs of substrates for adenylosuccinate synthase and adenylosuccinate lyase, *Arch. Biochem. Biophys. 225*, 157-163.

Powers, V. M., Koo, C. W., Kenyon, G. L., Gerlt, J. A., and Kozarich, J. W. (1991) Mechanism of the reaction catalyzed by mandelate racemase. 1. Chemical and kinetic evidence for a two-base mechanism, *Biochemistry 30*, 9255-9263.

Radzicka, A., and Wolfenden, R. (1995) A proficient enzyme, *Science 267*, 90-93.

Rajagopalan, P. T. R., and Benkovic, S. J. (2002) Preorganization and protein dynamics in enzyme catalysis, *Chem. Rec. 2*, 24-36.

Ransom, S. C., Gerlt, J. A., Powers, V. M., and Kenyon, G. L. (1988) Cloning, DNA sequence analysis, and expression in *Escherichia coli* of the gene for mandelate racemase from Pseudomonas putida, *Biochemistry 27*, 540-545.

Raushel, F. M. (1984) Nitro analogues of substrates for argininosuccinate synthetase and argininosuccinate lyase, *Arch. Biochem. Biophys. 232*, 520-525.

Rose, I. A. (1966) *Annu. Rev. Biochem. 35*, 23-57.

Roth, N. J., Rob, B., and Huber, R. E. (1998) His-357 of beta-galactosidase (Escherichia coli) interacts with the C3 hydroxyl in the transition state and helps to mediate catalysis, *Biochemistry 37*, 10099-10107.

Rozovsky, S., Jogl, G., Tong, L., and McDermott, A. E. (2001) Solution-state NMR investigations of triosephosphate isomerase active site loop motion: ligand release in relation to active site loop dynamics, *J. Mol. Biol. 310*, 271-280.

Rozovsky, S., and McDermott, A. E. (2001) The time scale of the catalytic loop motion in triosephosphate isomerase, *J. Mol. Biol. 310*, 259-270.

Sala, R. F., Morgan, P. M., and Tanner, M. E. (1996) Enzymatic formation and release of a stable glycal intermediate: The mechanism of the reaction catalyzed by UDP-*N*-acetylglucosamine 2-epimerase, *J. Am. Chem. Soc. 118*, 3033-3034.

Sambrook, J., Fritsch, E. F., and Maniatis, T. (1989) *Molecular Cloning: A laboratory manual*, Cold Spring Harbor Laboratory Press, Plainview, NY.

Sampson, N. S., and Knowles, J. R. (1992) Segmental motion in catalysis: investigation of a hydrogen bond critical for loop closure in the reaction of triosephosphate isomerase, *Biochemistry 31*, 8488-8494.

Schafer, S. L., Barrett, W. C., Kallarakal, A. T., Mitra, B., Kozarich, J. W., Gerlt, J. A., Clifton, J. G., Petsko, G. A., and Kenyon, G. L. (1996) Mechanism of the reaction catalyzed by mandelate racemase: structure and mechanistic properties of the D270N mutant, *Biochemistry 35*, 5662-5669.

Schloss, J. V., and Cleland, W. W. (1982) Inhibition of isocitrate lyase by 3-nitropropionate, a reaction-intermediate analogue, *Biochemistry 21*, 4420-4427.

Schloss, J. V., Porter, D. J. T., Bright, H. J., and Cleland, W. W. (1980) Nitro analogues of citrate and isocitrate as transition-state analogues for aconitase, *Biochemistry 19*, 2358-2362.

Schonbaum, G. R. (1973) New complexes of peroxidases with hydroxamic acids, hydrazides, and amides, *J. Biol. Chem. 248*, 502-511.

Schowen, R. L. (1978) "Catalytic power and transition-state stabilization" in *Transition states of biological processes* (R. D. Gandour, and R. L. Schowen, Eds.) pp 77-114, Plenum Press, New York.

Schramm, V. L. (1998) Enzymatic transition states and transition state analog design, *Annu. Rev. Biochem. 67*, 693-720.

Schramm, V. L., Horenstein, B. A., and Kline, P. C. (1994) Transition state analysis and inhibitor design for enzymatic reactions, *J. Biol. Chem. 269*, 18259-18262.

Segel, I. H. (1993a) in *Enzyme kinetics* pp 34-37, John Wiley & Sons, New York.

Segel, I. H. (1993b) in *Enzyme kinetics* pp 242-271, John Wiley & Sons, New York.

Sekine, M., Futatsugi, T., Yamada, K., and Hata, T. (1982) Silyl phosphites. Part 20. A facile synthesis of phosphoenolpyruvate and its analog utilizing in situ generated trimethylsilyl bromide, *J. Chem. Soc. Perkin Trans. 1*, 2509-2513.

Shan, S., Loh, S., and Herschlag, D. (1996) The energetics of hydrogen bonds in model systems: implications for enzymatic catalysis, *Science 272*, 97-101 and references therein.

Shan, S. O., and Herschlag, D. (1996) The change in hydrogen bond strength accompanying charge rearrangement: implications for enzymatic catalysis, *Proc. Natl. Acad. Sci. U S A 93*, 14474-14479.

Sharp, T. R., Hegeman, G. D., and Kenyon, G. L. (1977) Mandelate racemase from *Pseudomonas putida*. Absence of detectable intermolecular proton transfer accompanying racemization, *Biochemistry 16*, 1123-1128.

Sharp, T. R., Hegeman, G. D., and Kenyon, G. L. (1979) A direct kinetic assay for mandelate racemase using circular dichroic measurements, *Anal. Biochem. 94*, 329-334.

Shaw, J. P., Petsko, G. A., and Ringe, D. (1997) Determination of the structure of alanine racemase from *Bacillus sterothermophilus* at 1.9-Å resolution, *Biochemistry 36*, 1329-1342.

Shi, J., Boyd, A. E., Radic, Z., and Taylor, P. (2001) Reversibly bound and covalently attached ligands induce conformational changes in the omega loop, Cys69-Cys96, of mouse acetylcholinesterase, *J. Biol. Chem. 276*, 42196-42204.

Shibaev, V. N., Elisseva, G. I., and HKochetkov, N. K. (1975) Interaction of uridine diphosphate glucose analogs with calf liver diphosphate glucose dehydrogenase. Influence of substituents at C-5 of pyrimidine nucleus, *Biochim. Biophys. Acta 403*, 9-16.

Shortle, D., Stites, W. E., and Meeker, A. K. (1990) Contributions of the large hydrophobic amino acids to the stability of staphylococcal nuclease, *Biochemistry* *29*, 8033-8041.

Simopoulos, T. T., and Jencks, W. P. (1994) Alkaline phosphatase is an almost perfect enzyme, *Biochemistry* *33*, 10375-10380.

Sjoberg, P., and Politzer, P. (1990) Use of the electrostatic potential at the molecular surface to interpret and predict nucleophilic processes, *J. Phys. Chem.* *94*, 3959-3961.

Smaardijk, A. A., Noorda, S., Bolhuis, F., and Wynberg, H. (1985) The absolute configuration of α-hydroxyphosphonates, *Tetrahedron Lett.* *26*, 493-496.

Smyth, M. S., Ford, H. J., and Burke, T. R. J. (1992) A general method for the preparation of benzylic α,α-difluorophosphonic acids; non-hydrolizable mimetics of phosphotyrosine, *Tetrahedron Lett.* *33*, 4137-4140.

Snider, M. J., Gaunitz, S., Ridgway, C., Short, S. A., and Wolfenden, R. (2000) Temperature effects on the catalytic efficiency, rate enhancement, and transition state affinity of cytidine deaminase, and the thermodynamic consequences for catalysis of removing a substrate "anchor", *Biochemistry* *39*, 9746-9753.

Snider, M. J., and Wolfenden, R. (2000) The rate of spontaneous decarboxylation of amino acids, *J. Am. Chem. Soc.* *122*, 11507-11508.

Snider, M. J., and Wolfenden, R. (2001) Site-bound water and the shortcomings of a less than perfect transition state analogue, *Biochemistry* *40*, 11364-11371.

Sosnovsky, L., and Krogh, L. (1980) A new method for the preparation of aliphatic hydroxamic acids; reaction of primary nitroalkanes with selenium dioxide in the presence of triethylamine, *Synthesis*, 654-656.

St. Maurice, M., and Bearne, S. L. (2000) Reaction intermediate analogues for mandelate racemase: interaction between Asn 197 and the α-hydroxyl of the substrate promotes catalysis, *Biochemistry* *39*, 13324-13335.

St. Maurice, M., and Bearne, S. L. (2002) Kinetics and thermodynamics of mandelate racemase catalysis, *Biochemistry* *41*, 4048-4058.

Stecher, H., Hermetter, A., and Faber, K. (1998) Mandelate racemase assayed by polarimetry, *Biotechnol. Tech.* *12*, 257-261.

Steyaert, J., Wyns, L., and Stanssens, P. (1991) Subsite interactions of ribonuclease T1: viscosity effects indicate that the rate-limiting step of GpN transesterification depends on the nature of N, *Biochemistry* *30*, 8661-8665.

Stone, S. R., and Morrison, J. F. (1988) Dihydrofolate reductase from *Escherichia coli*: the kinetic mechanism with NADPH and reduced acetylpyridine adenine dinucleotide phosphate as substrates, *Biochemistry* *27*, 5493-5499.

Stratton, J. R., Pelton, J. G., and Kirsch, J. F. (2001) A novel engineered subtilisin BPN' lacking a low-barrier hydrogen bond in the catalytic triad, *Biochemistry* *40*, 10411-10416.

Strauss, U. T., and Faber, K. (1999) Deracemization of (±)-mandelic acid using a lipase-mandelate racemase two-enzyme system, *Tetrahedron: Asymmetry* *10*, 4079-4081.

Street, I. P., Armstrong, C. R., and Withers, S. G. (1986) Hydrogen bonding and specificity. Fluorodeoxy sugars as probes of hydrogen bonding in the glycogen phosphorylase-glucose complex, *Biochemistry* *25*, 6021-6027.

Summers, J. B., Mazdiyasni, H., Holms, J. H., Ratajczyk, J. D., Dyer, R. D., and Carter, G. W. (1987) Hydroxamic acid inhibitors of 5-lipoxygenase, *J. Med. Chem. 30*, 574-580.

Syed, S. E. H. (1993) in *Enzyme Assays* (R. Eisenthal, and M. J. Danson, Eds.) pp 123-166, Oxford Univ. Press Inc., New York.

Takahashi, E., Nakamichi, K., Furui, M., and Mori, T. (1995) *R*-(−)-mandelic acid production from racemic mandelic acids by *Pseudomonas polycolor* with asymmetric degrading activity, *J. Ferment. Bioeng. 79*, 349-442.

Tanner, M. A. (2002) Understanding nature's strategies for enzyme-catalyzed racemization and epimerization, *Acc. Chem. Res. 35*, 237-246.

Taylor, S. D., Dinaut, A. N., Thadini, A., and Huang, Z. (1996) Synthesis of benzylic mono(α,α-difluoromethylphosphonates) and benzylic bis(α,α-difluoromethylphosphonates) via electrophilic fluorination, *Tetrahedron Lett. 45*, 8089-8092.

Thibblin, A., and Jencks, W. P. (1979) Unstable carbanions. General acid catalysis of the cleavage of 1-phenylcyclopropanol and 1-phenyl-2-arylcyclopropanol anions, *J. Am. Chem. Soc. 101*, 4963-4973.

Thompson, T. B., Garrett, J. B., Taylor, E. A., Meganathan, R., Gerlt, J. A., and Rayment, I. (2000) Evolution of enzymatic activity in the enolase superfamily: structure of *o*-succinylbenzoate synthase from *Escherichia coli* in complex with Mg^{2+} and *o*-succinylbenzoate, *Biochemistry 39*, 10662-10676.

Thornton, E. K., and Thornton, E. R. (1978) "Scope and limitations of the concept of the transition state" in *Transition states of biochemical processes* (R. D. Gandour, and R. L. Schowen, Eds.) pp 3-76, Plenum Press, New York.

Tipton, K. F., and Dixon, H. B. F. (1979) Effects of pH on enzymes, *Methods Enzymol. 63*, 183-234.

Truhlar, D. G., Hase, W. L., and Hynes, J. T. (1983) Current status of transition-state theory, *J. Phys. Chem. 87*, 2664-2682.

Van Kuilenburg, A. B., Elzinga, A. B., Van den Berg, A. A., Slingerland, R. J., and Van Gennip, A. H. (1994) A fast and novel assay of CTP synthetase. Evidence for hysteretic properties of the mammalian enzyme, *Anticancer Res. 14*, 411-415.

Ventura, O. N., Rama, J. B., Turi, L., and Dannenberg, J. J. (1993) Acidity of hydroxamic acids: an *ab initio* and semi-empirical study, *J. Am. Chem. Soc. 115*, 5754-5761.

Villa, J., Strajbl, M., Glennon, T. M., Sham, Y. Y., Chu, Z. T., and Warshel, A. (2000) How important are entropic contributions to enzyme catalysis?, *Proc. Natl. Acad. Sci. U S A 97*, 11899-11904.

Wang, G. P., Cahill, S. M., Liu, X., Girvin, M. E., and Grubmeyer, C. (1999a) Motional dynamics of the catalytic loop in OMP synthase, *Biochemistry 38*, 284-295.

Wang, G. P., Lundegaard, C., Jensen, K. F., and Grubmeyer, C. (1999b) Kinetic mechanism of OMP synthase: a slow physical step following group transfer limits catalytic rate, *Biochemistry 38*, 275-283.

Warshel, A. (1991) *Computer modeling of chemical reactions in enzyme and solutions*, John Wiley & Sons, New York.

Warshel, A. (1998) Electrostatic origin of the catalytic power of enzymes and the role of preorganized active sites, *J. Biol. Chem. 273*, 27035-27038.

Warshel, A., Papazyan, A., and Kollman, P. A. (1995) On low-barrier hydrogen bonds and enzyme catalysis, *Science 269*, 102-106.

Wedekind, J. E., Poyner, R. R., Reed, G. H., and Rayment, I. (1994) Chelation of serine 39 to Mg^{2+} latches a gate at the active site of enolase: structure of the bis(Mg^{2+}) complex of yeast enolase and the intermediate analog phosphonoacetohydroxamate at 2.1-Å resolution, *Biochemistry 33*, 9333-9342.

Weil-Malherbe, H. (1966) Some properties of mandelate racemase from Pseudomonas fluorescens, *Biochem J. 101*, 169-175.

Welsh, J. T. (1987) Advances in the preparation of biologically active organofluorine compounds, *Tetrahedron 43*, 3123-3197.

Westkaemper, R. B., and Hanzlik, R. P. (1981) Mechanistic studies of epoxide hydrolase utilizing a continuous spectophotometric assay, *Arch. Biochem. Biophys. 208*, 195-204.

Whitman, C. P., Hegeman, G. D., Cleland, W. W., and Kenyon, G. L. (1985) Symmetry and asymmetry in mandelate racemase catalysis, *Biochemistry 24*, 3936-3942.

Wilkinson, A. J., Fersht, A., Blow, D. M., Carter, P., and Winter, G. (1984) A large increase in enzyme-substrate affinity by protein engineering, *Nature 307*, 187-188.

Wilkinson, A. J., Fersht, A., Blow, D. M., and Winter, G. (1983) Site-directed mutagenesis as a probe of enzyme structure and catalysis: tyrosyl-tRNA synthetase cysteine-35 to glycine-35 mutation, *Biochemistry 22*, 3581-3586.

Williams, J. C., and McDermott, A. E. (1995) Dynamics of the flexible loop of triosephosphate isomerase: the loop motion is not ligand gated, *Biochemistry 34*, 8309-8319.

Wolfenden, R. (1969) Transition state analogues for enzyme catalysis, *Nature 223*, 704-705.

Wolfenden, R. (1972) Analog Approaches to the Structure of the Transition State in Enzyme Reactions, *Acc. Chem. Res. 5*, 10-18.

Wolfenden, R. (1974) Enzyme catalysis: conflicting requirements of substrate access and transition state affinity, *Mol Cell Biochem 3*, 207-211.

Wolfenden, R. (1976) Transition state analog inhibitors and enzyme catalysis, *Annu. Rev. Biophys. Bioeng. 5*, 271-306.

Wolfenden, R. (1999) Conformational aspects of inhibitor design: enzyme-substrate interactions in the transition state, *Bioorg. Med. Chem. 7*, 647-652.

Wolfenden, R., and Frick, L. (1987) "Transition State Affinity and the Design of Enzyme Inhibitors" in *Enzyme Mechanisms* (M. I. Page, and A. Williams, Eds.) pp 97-122, Royal Society of Chemistry, London.

Wolfenden, R., and Snider, M. J. (2001) The depth of chemical time and the power of enzymes as catalysts, *Acc. Chem. Res. 34*, 938-945.

Wolfenden, R., Snider, M. J., Ridgway, C., and Miller, B. (1999) The temperature dependence of enzyme rate enhancements, *J. Am. Chem. Soc. 121*, 7419-7420.

Zgiby, S., Plater, A. R., Bates, M. A., Thomson, G. J., and Berry, A. (2002) A functional role for a flexible loop containing Glu182 in the class II fructose-1,6-bisphosphate aldolase from *Escherichia coli*, *J. Mol. Biol. 315*, 131-140.